THE UNIVERSITY OF QUEENSLAND

AUSTRALIA

Automated injury segmentation to assist in the treatment of children with cerebral palsy

Alex Michael Pagnozzi

Bachelors of Electrical and Electronic Engineering (Hons)/ Bachelor of Science (Biochemistry)

A thesis submitted for the degree of Doctor of Philosophy at

The University of Queensland in 2017

School of Information Technology and Electrical Engineering

Abstract

Cerebral palsy (CP) describes a group of permanent disorders of posture and movement caused by disturbances in the developing brain. It is the most common physical disability of children worldwide and can lead to a wide range of functional impairments. Accurate diagnosis and prognosis, in terms of the type and severity of functional impairment, is difficult due to the wide range of injuries that may occur and the variable effect of plasticity; which leads to inconsistency in the clinical outcomes of children with CP. The use of Magnetic resonance imaging (MRI) to identify and locate brain lesions has facilitated the diagnosis and qualitative classification of children with CP.

Currently, the quantification of image findings from structural MRIs is not automated and remains labour intensive, hence is not widely performed for clinical assessment. Automated brain image segmentation techniques could reduce the clinical time required to provide an accurate and reproducible quantification of injury. Although such approaches have been used to study other neurological disorders, the heterogeneous appearance of injury and the large anatomical distortion that occurs in CP require modification of existing algorithms to be sufficiently reliable. As a result, they have not been widely applied to MRIs of children with CP.

In this thesis, a series of automated image quantification techniques are presented for analysing the MRI data obtained from children with CP. These techniques identify and quantify the severity of the three main types of injury observed in children with CP; including ventricular enlargement, cortical malformations and white and grey matter injury. The developed automated pipeline involves a number of technical developments and contributions to the automated analysis of CP MRI data. A brain tissue segmentation approach based on the Expectation Maximisation (EM)/Markov Random Field (MRF) approach was developed, with a modified MRF implementation that expects different tissue labels within a given neighbourhood to have a corresponding intensity gradient. Following this segmentation step, three different approaches were used to identify and quantify the three distinct types of injury observed from children with CP, which are all important for clinical assessment. Biomarkers from each type of injury obtained from these approaches were used as independent variables in a devised statistical methodology designed to elucidate significant and generalisable correlations between image-derived measures of injury and patient function.

Ventricular enlargement was quantified using a model of lateral ventricular shape that encapsulates healthy variation observed in ventricular shape. The residual of this model to a target shape reveals a volume of injury, allowing a measure of involvement of critical adjacent anatomies, such as the thalamus, caudate nucleus and lenticular nucleus, to be computed. This measure of involvement was devised as a way to translate the indirect injury of ventricular enlargement to the direct injury to the surrounding tissue leading to impairment. With this approach, injury was strongly linked to subcortical grey matter structures to multiple clinical measures of patient function.

Cortical malformations were investigated using an encompassing set of shape measures, calculated at labelled regions on the cortical grey matter. The use of all several combined shape measures, including cortical thickness, sulcal depth and curvature, ensured that the range of cortical malformations would be detected. Anomalous shapes were identified compared to the healthy population in the corresponding cortical regions, and with this approach a succinct set of cortical biomarkers were linked to patient function.

White and grey matter injuries were identified as outliers to the tissue models in the EM-MRF segmentation, additionally using registered tissue probability maps and T2-weighted MRIs, where this injury appears hyperintense, to aid lesion detection. Following lesion segmentation refinement using the EM algorithm, specific classes of white matter, grey matter and internal capsule lesions were identified. This approach was shown to outperform the state of the art lesion detection approach. Significant and generalisable correlations to multiple clinical outcomes were identified using this method, which highlighted the importance of additionally considering grey matter lesions in addition to white mater lesions.

These automated approaches tailored to CP related injury highlight (1) the reliance on atlas priors should be minimised and instead rely on adaptive approaches and data-driven modifications to enhance segmentations in regions of severe injury, which deviate significantly from healthy atlases, (2) utilise unsupervised approaches for lesion segmentation with dedicated WM and GM lesion classes, (3) the use of multiple shape measures to fully parameterise cortical topology, and (4) the construction of shape models of injury should be avoided, and instead measure residual volumes from the closest healthy shape from the model manifold.

The combination of these automated methods provides a framework for a decision support tool to assist clinicians tasked at analysing the MRI of children with CP. Using these combined approaches, a moderate to strong correlation between brain injury and patient function was observed (Pearson's r between 0.545 and 0.795, $p < 0.008$) on an unseen test set. Furthermore, these automated methods can repeatedly and automatically provide a delineation of lesions, and through the statistical models, estimate patient outcome, which can help guide treatment and therapy decisions. This has the potential to benefit the wider scientific community, where the translation of structural MR-derived biomarkers to functional outcomes can help to understand of the aetiology of CP, as well as children with CP, where the prediction of functional outcomes can help tailor patient-specific intervention strategies in order to promote greater improvements in function.

Declaration by author

This thesis is composed of my original work, and contains no material previously published or written by another person except where due reference has been made in the text. I have clearly stated the contribution by others to jointly-authored works that I have included in my thesis.

I have clearly stated the contribution of others to my thesis as a whole, including statistical assistance, survey design, data analysis, significant technical procedures, professional editorial advice, and any other original research work used or reported in my thesis. The content of my thesis is the result of work I have carried out since the commencement of my research higher degree candidature and does not include a substantial part of work that has been submitted to qualify for the award of any other degree or diploma in any university or other tertiary institution. I have clearly stated which parts of my thesis, if any, have been submitted to qualify for another award.

I acknowledge that an electronic copy of my thesis must be lodged with the University Library and, subject to the policy and procedures of The University of Queensland, the thesis be made available for research and study in accordance with the Copyright Act 1968 unless a period of embargo has been approved by the Dean of the Graduate School.

I acknowledge that copyright of all material contained in my thesis resides with the copyright holder(s) of that material. Where appropriate I have obtained copyright permission from the copyright holder to reproduce material in this thesis.

Publications during candidature

Peer-reviewed Journal Papers

1. **Alex M. Pagnozzi**, Yaniv Gal, Roslyn N. Boyd, Simona Fiori, Jurgen Fripp, Stephen Rose and Nicholas Dowson. The need for improved lesion segmentation techniques to optimise rehabilitation strategies for children with cerebral palsy: A review. *International Journal of Developmental Neuroscience* 47 (2015): 229-246.
2. **Alex M. Pagnozzi**, Simona Fiori, Rosyln N. Boyd, Andrea Guzzetta, James Doecke, Yaniv Gal, Stephen Rose and Nicholas Dowson. Optimization of MRI-based scoring scales of brain injury severity in children with unilateral cerebral palsy. *Pediatric radiology* 46 (2016): 270-279.
3. **Alex M. Pagnozzi**, Nicholas Dowson, Pierrick Bourgeat, Andrew P. Bradley, Roslyn N. Boyd and Stephen Rose, “Expectation-maximization with image-weighted Markov Random Fields to handle severe pathology,” *Digital Image Computing: Techniques and Applications (DICTA)*, Adelaide, SA, November 2015.
4. **Alex M Pagnozzi**, Kaikai Shen, James D Doecke, Roslyn N Boyd, Andrew P Bradley, Stephen Rose, Nicholas Dowson. Using ventricular modeling to robustly probe significant deep gray matter pathologies: Application to cerebral palsy. *Human Brain Mapping 37* (2016): 3795-3809.
5. **Alex M Pagnozzi**, Nicholas Dowson, Simona Fiori, James Doecke, Andrew P Bradley, Roslyn N Boyd, Stephen Rose. Alterations in regional shape on ipsilateral and contralateral cortex contrast in children with unilateral cerebral palsy and are predictive of multiple outcomes. *Human Brain Mapping 37* (2016): 3588-3603.
6. **Alex M Pagnozzi**, Nicholas Dowson, James Doecke, Simona Fiori, Andrew P Bradley, Roslyn N Boyd, Stephen Rose. Automated, quantitative measures of grey and white matter lesion burden correlates with motor and cognitive function in children with unilateral cerebral palsy. *NeuroImage: Clinical* 11 (2016): 751-759.

Conference Abstracts

1. **Alex M. Pagnozzi**, Nicholas Dowson, James Doecke, Simona Fiori, Andrea Guzzetta, Roslyn N. Boyd and Stephen Rose, “Combining lesion burden with cortical malformation morphology strongly predicts motor outcomes in children with

cerebral palsy," *International Society for Magnetic Resonance in Medicine (ISMRM),* Singapore, May 2016.

Publications included in this thesis

Alex M. Pagnozzi, Yaniv Gal, Roslyn N. Boyd, Simona Fiori, Jurgen Fripp, Stephen Rose and Nicholas Dowson. The need for improved lesion segmentation techniques to optimise rehabilitation strategies for children with cerebral palsy: A review. *International Journal of Developmental Neuroscience* 47 (2015): 229-246.

This publication constitutes most of Chapter 2 of this thesis, and is available at the following URL doi:10.1016/j.ijdevneu.2015.08.004. This review compares multiple image-processing algorithms, formulating the methodologies implemented in Chapters 4 to 7. It additionally outlines the unique challenges specific to the CP setting, advancing automated injury detection for this condition.

Contributor	Statement of contribution
Alex M. Pagnozzi	Conception and design (20%) Conducted review (100%) Developed inclusion/exclusion criteria (100%) Analysed and compared studies (100%) Interpretation of results (50%) Drafted and edited the article (100%)
Yaniv Gal	Interpretation of results (10%) Critical revision on draft article (20%)
Roslyn N. Boyd	Critical revision on draft article (10%)
Simona Fiori	Critical revision on draft article (20%)
Jurgen Fripp	Interpretation of results (10%) Critical revision on draft article (20%)
Stephen Rose	Conception and design (50%) Interpretation of results (10%) Critical revision on draft article (10%)
Nicholas Dowson	Conception and design (30%) Interpretation of results (20%)

	Critical revision on draft article (20%)

Alex M. Pagnozzi, Simona Fiori, Roslyn N. Boyd, Andrea Guzzetta, James Doecke, Yaniv Gal, Stephen Rose and Nicholas Dowson. Optimization of MRI-based scoring scales of brain injury severity in children with unilateral cerebral palsy. *Pediatric Radiology 46* (2015): 270-279.

This publication constitutes most of Chapter 3. The final publication is available at Springer via http://dx.doi.org/10.1007/s00247-015-3473-y. This publication outlines and tests the statistical methodology used throughout Chapters 4 to 8 in order to achieve Aim 2 of this thesis. The contribution of this work is that is aids the translation of technical image-processing algorithms into clinically useful measures.

Contributor	Statement of contribution
Alex Pagnozzi	Conception and design (30%) Designed experiments (50%) Performed the analyses (100%) Drafted and edited the article (100%) Interpreted results (50%)
Simona Fiori	Manually scored MR data (100%) Critical revision on draft article (10%)
Roslyn N. Boyd	Conception and design (30%) Collection of data (100%) Critical revision on draft article (10%)
Andrea Guzzetta	Critical revision on draft article (10%)
James D. Doecke	Designed experiments (25%) Interpreted results (15%) Critical revision on draft article (20%)
Yaniv Gal	Critical revision on draft article (10%)
Stephen Rose	Conception and design (20%)

	Interpreted results (10%) Critical revision on draft article (20%)
Nicholas Dowson	Conception and design (20%) Designed experiments (25%) Interpreted results (25%) Critical revision on draft article (20%)

Alex Pagnozzi, Kaikai Shen, James D. Doecke, Roslyn N. Boyd, Andrew P. Bradley, Stephen Rose and Nicholas Dowson. Using ventricular modelling to robustly probe significant deep grey matter pathologies: application to cerebral palsy. Submitted to Human Brain Mapping on 20/05/2015.

This publication constitutes most of Chapter 5. This publication constitutes most of Chapter 3. The final publication is available at Wiley Online via DOI:10.1002/hbm.23276. This publication links to the methodology outlined in Chapter 2, and the challenges of point-wise correspondence in cases of severe injury. The proposed method helps advance the field of shape modelling in such settings, as well as presenting a robust biomarker of deep grey matter injury in the CP setting.

Contributor	Statement of contribution
Alex Pagnozzi	Conception and design (70%) Designed experiments (50%) Performed the analyses (100%) Drafted and edited the article (100%) Interpreted results (50%)
Kaikai Shen	Designed experiments (20%) Developed software (100%) Wrote and edited paper (30%) Critical revision on draft article (20%)

James D. Doecke	Critical revision on draft article (20%)
Roslyn N. Boyd	Collection of data (100%) Critical revision on draft article (20%)
Andrew P. Bradley	Critical revision on draft article (20%)
Stephen Rose	Designed experiments (25%) Interpreted results (25%) Critical revision on draft article (20%)
Nicholas Dowson	Conception and design (30%) Designed experiments (30%) Interpreted results (25%) Critical revision on draft article (20%)

Alex Pagnozzi, Nicolas Dowson, Simona Fiori, James Doecke, Andrew P. Bradley, Roslyn N. Boyd and Stephen Rose. Alterations in regional shape on ipsilateral and contralateral cortex contrast in children with unilateral cerebral palsy and are predictive of multiple outcomes. *Human Brain Mapping 37* (2015): 3588-3603.

This publication constitutes parts of Chapters 4 and 6. The final publication is available at Wiley Online via DOI:10.1002/hbm.23262. This publication links to the methodology outlined in Chapter 2, and the limitation of registration-based surface approaches for measuring cortical shape. This study helps to advance image-processing fields, in the use of Laplace's equation and level sets to avoid registration techniques, and the CP field by presenting morphological measures from both hemispheres of children with unilateral injury.

Contributor	Statement of contribution
Alex Pagnozzi	Conception and design (50%) Designed experiments (50%) Performed the analyses (100%)

	Developed software (100%) Drafted and edited the article (100%) Interpreted results (30%)
Nicholas Dowson	Conception and design (30%) Designed experiments (20%) Interpreted results (30%) Critical revision on draft article (20%)
Simona Fiori	Critical revision on draft article (20%)
James Doecke	Designed experiments (20%) Critical revision on draft article (20%) Interpreted results (10%)
Andrew P. Bradley	Critical revision on draft article (10%)
Roslyn N. Boyd	Collection of data (100%) Critical revision on draft article (10%)
Stephen Rose	Conception and design (20%) Designed experiments (30%) Interpreted results (30%) Critical revision on draft article (20%)

Alex M. Pagnozzi, Nicholas Dowson, James Doecke, Simona Fiori, Andrew P. Bradley, Roslyn N. Boyd and Stephen Rose. Automated white and grey matter lesion segmentations linked to outcomes in children with unilateral cerebral palsy. *NeuroImage: Clinical* 11 (2016): 751-759.

This publication constitutes most of Chapter 7. The final publication is available at Elsevier via doi:10.1016/j.nicl.2016.05.018. This publication links to the methodology outlined in Chapter 2, and presents a segmentation method that outperforms the state of the art on CP data. This work presents the first published quantitative assessment of functional impairment caused by GM lesion involvement in children with CP, helping to advance the understanding of the brain.

Contributor	Statement of contribution
Alex M. Pagnozzi	Conception and design (60%) Designed experiments (50%) Performed the analyses (100%) Developed software (100%) Drafted and edited the article (100%) Interpreted results (30%)
Nicholas Dowson	Conception and design (30%) Designed experiments (10%) Interpreted results (30%) Critical revision on draft article (20%)
James D. Doecke	Designed experiments (40%) Critical revision on draft article (20%) Interpreted results (10%)
Simona Fiori	Critical revision on draft article (20%)
Andrew P. Bradley	Critical revision on draft article (10%)
Roslyn N. Boyd	Collection of data (100%) Critical revision on draft article (10%)
Stephen Rose	Interpreted results (30%) Critical revision on draft article (20%)

Alex M. Pagnozzi, Nicholas Dowson, James Doecke, Simona Fiori, Andrew P. Bradley, Roslyn N. Boyd and Stephen Rose. Assessment of injury prevalence and MRI predictors in a cohort of children with unilateral cerebral palsy.

This publication constitutes most of Chapter 8. A draft manuscript has been prepared, has been submitted to PLOS ONE. This work combines the image processing methods from previous chapters to present the prevalence of brain injury in our cohort of children with

CP, and determines which biomarkers were most predictive of functional outcomes, helping radiologists identify important clinical characteristics.

Contributor	Statement of contribution
Alex M. Pagnozzi	Conception and design (60%) Designed experiments (50%) Performed the analyses (100%) Developed software (100%) Drafted and edited the article (100%) Interpreted results (30%)
Nicholas Dowson	Conception and design (30%) Designed experiments (10%) Interpreted results (30%) Critical revision on draft article (20%)
James D. Doecke	Designed experiments (40%) Critical revision on draft article (20%) Interpreted results (10%)
Simona Fiori	Critical revision on draft article (20%)
Andrew P. Bradley	Critical revision on draft article (10%)
Roslyn N. Boyd	Collection of data (100%) Critical revision on draft article (10%)
Stephen Rose	Interpreted results (30%) Critical revision on draft article (20%)

Contributions by others to the thesis

A/Prof Stephen Rose (primary supervisor), Dr Nicholas Dowson (associate supervisor), Dr Andrew Bradley (associate supervisor), Prof Roslyn Boyd, Mrs Simona Fiori, Dr Andrea Guzzetta, Dr Yaniv Gal, Dr James Doecke, Dr Kaikai Shen and Dr Pierrick Bourgeat have all made contributions towards research ideas, experimental design, data collection and interpretation of results. This thesis contains work that has been published (Chapters 2, 3, 4, 5, 6 and 7). The individual contributions of all authors are detailed in the previous section.

Statement of parts of the thesis submitted to qualify for the award of another degree

None.

Acknowledgements

I would like to thank my PhD supervisors Stephen Rose and Nicholas Dowson who made this project possible. Thanks to Stephen Rose for his guidance over the course of this project, and for providing the bridge between technical work and clinical implementation that allowed this research to develop. Thanks to Nicholas Dowson for his frequent support and advice regarding all the nerdy techniques used throughout this PhD, and his many edits to the research manuscripts that I produced. Thanks to Yaniv Gal and Andrew Bradley for providing their sanity checks of our methods, and their pattern recognition and machine learning experience that has improved this research.

Thanks also to Roslyn Boyd, Simona Fiori and Andrea Guzzetta for their frequent advice from the clinical perspective, which has helped put this research in perspective and helped us to focus on the real world impact of this research. Special thanks to both Roslyn Boyd and Simona Fiori for the provision of a great number of MRI scans, which I have used frequently over the course of this PhD. Thanks also to my review panel, Stephen Wilson, Paul Colditz and Andrew Janke, for their incisive comments of this PhD project. Their advice was invaluable in identifying changes and inclusions for this research that highlighted the key novelties of this PhD.

Thanks to many people in the CSIRO Imaging Team for their technical help, including Kaikai Shen for his help with the statistical shape models, James Doecke for his help with the statistical analyses, David Rivest-Henault for his knowledge on medical image registration, and Pierrick Bourgeat for his help with several brain analysis and segmentation methods. Thanks to the many people involved in the study design, recruitment and data collection for the children with CP MiTii study, that provided the MRI data used in my thesis: Roslyn Boyd, Simona Fiori, Andrea Guzzetta, nurses, and staff at the Department of Medical Imaging at the Royal Brisbane and Women's Hospital.

Thanks to Jeeva Kanesarajah for supporting me, advising me, and inspiring me to achieve my best. I am so glad that I have gone through this journey with you. And also to my parents and sister, for their words of encouragement from across the country (and the world).

This research was funded by the Australian Postgraduate Award scholarship and a CSIRO stipend.

Keywords

structural magnetic resonance imaging, image segmentation, brain injury, paediatrics

Australian and New Zealand Standard Research Classifications (ANZSRC)

ANZSRC code: 080106, Image Processing	34%
ANZSRC code: 110999, Neurosciences	33%
ANZSRC code: 111403, Paediatrics	33%

Fields of Research (FoR) Classification

FoR code: 0801, Artificial Intelligence and Image Processing	34%
FoR code: 1109, Neurosciences	33%
FoR code: 1114, Paediatrics and Reproductive Medicine	33%

Table of Contents

List of Figures

List of Tables

List of Abbreviations

AAL	Automated Anatomical Labelling
AAM	Active appearance model
AD	Alzheimer's Disease
AHA	Assisting Hand Assessment
AIC	Akaike Information Criterion
ALIC	Anterior limb of the internal capsule
ANOVA	Analysis of Variance
ANTs	Advanced Normalization Tools
AUC	Area Under the Curve
BRIEF	Behaviour Rating Inventory of Executive Function
CDGM	Cortical and deep grey matter
CFCS	Communication Function Classification System
CIMT	Constraint Induced Movement Therapy
CP	Cerebral palsy
CRF	Conditional random field
CRUISE	Cortical Reconstruction Using Implicit Surface Evolution
CSF	Cerebrospinal fluid
DEHSI	Diffuse Excessive High Signal Intensity
DSC	Dice Similarity Coefficient
EER	Equal Error Rate
EM	Expectation maximisation
EM-ICP	Expectation Maximisation – Iterative Closest Point
FAST	fMRIB's Automated Segmentation Tool
FCM	Fuzzy c-means

FDA	Food and Drug Administration
FLAIR	Fluid-attenuated inversion recovery
FSL	fMRIB Software Library
GM	Grey matter
GMFCS	Gross Motor Function Classification System
HASTE	Half-Fourier Acquisition Single-Shot Turbo Spin-Echo
HMC	Hidden Markov chain
IC	Internal capsule
IQ	Intelligence Quotient
ITK	Insight Toolkit
kNN	k-Nearest Neighbours
LASSO	Least Absolute Shrinkage and Selection Operator
LST	Lesion Segmentation Toolbox
MACS	Manual Ability Classification System
MMSR	Multi-contrast multi-scale surface registration
MPRAGE	Magnetisation-Prepared Rapid Acquisition with Gradient Echo
MRF	Markov random field
MRI	Magnetic resonance imaging
MS	Multiple Sclerosis
NPV	Negative Predictive Value
PCA	Principal Component Analysis
PLIC	Posterior limb of the internal capsule
PPV	Positive Predictive Value
PVL	Periventricular Leukomalacia
PWM	Periventricular white matter
QCPRRC	Queensland Cerebral Palsy and Research Rehabilitation Centre

ROC	Receiver Operator Characteristic
SDQ	Strengths and Difficulties Questionnaire
SE	Standard Error
SOM	Self-organising map
SPM	Statistical Parametric Mapping
SSD	Sum of Square Distances
SSM	Statistical shape model
SVM	Support vector machine
TDC	Typically Developing Children
TE	Time to echo
TLE	Trimmed likelihood estimation
TIRM	Turbo Inversion Recovery Magnitude
TPM	Tissue Probability Map
TR	Repetition time
TVPS	Test of Visual Perception Skills
VBM	Voxel-based morphometry
VLBW	Very Low Birth Weight
VOC	Vocabulary
VTK	Visualization Toolkit
WM	White matter
WPPSI	Wechsler Preschool and Primary Scale of Intelligence
WR	Word Reasoning
WS	Williams Syndrome

1. Introduction

1.1 Cerebral palsy and early brain development

Cerebral palsy (CP) is the most prevalent cause of physical disability in children worldwide, occurring in around 2 children per 1000 live births [Kuban and Leviton, 1994]. It describes a heterogeneous group of permanent disorders of posture and movement caused by non-progressive disturbances in the brain during fetal development [Rosenbaum et al 2007]. These pathogenic disturbances lead to a heterogeneous range of injuries, depending on the stage of brain development the disturbance occurs. During the 1st and 2nd trimesters, when proliferation, migration and organisation of neuronal cells are the predominant activities, disturbances most commonly lead to brain malformations (e.g. cortical malformations). In contrast, during the 3rd trimester when the architecture of the brain is established and key structures are formed, disturbances most often result in lesions in the white matter (WM) and grey matter (GM) of the brain. The periventricular white matter (PWM) is particularly susceptible to injury in the early stages of the 3rd trimester, leading to necrosis and gliosis in the WM, and is typically accompanied by loss of tissue, which may result in the enlargement of the ventricles. During the latter stages of the 3rd trimester, the cortical and deep GM is more susceptible to disturbances, leading to focal cortical GM or more selective deep GM involvement. Depending on the location of these disturbances, this may lead to various functional and motor impairments, as well as cognitive, linguistic, behavioural, and sensory problems [Himmelmann and Uvebrant, 2011; Pueyo et al., 2009; Venkateswaran and Shevell, 2008].

Current diagnosis of CP is based on clinical observations and qualitative assessment of delays in motor development, abnormal muscle tone and unusual posture [Krigger, 2006] in the first 12-18 months of life. There are three main types of CP [Rosenbaum et al., 2007], the most common type being spastic CP where muscle tone is stiff and typically arises from damage in the corticospinal tract. Other types include dyskinetic CP, which is characterised by involuntary muscle contractions arising from injury in the basal ganglia, and ataxic CP which is characterised by shaky movements caused by injury in the cerebellum. Qualitative classification of motor impairment in different types of CP is performed by applying the Gross Motor Function Classification System (GMFCS), and a number of functional scales can be applied for specific functional impairments, such as the

Manual Ability Classification System (MACS) to test hand function in children with CP or the Communication Function Classification System (CFCS) to test the effectiveness of communication. These scales allow for treatment strategies, which typically encompass physical therapy, medication, and surgery in severe cases [Krigger, 2006; Rosenbaum, 2003], to be tailored to individual children with the aim of increasing the efficacy of rehabilitation. However, determining the most appropriate treatment for individual cases remains challenging due to difficulties in obtaining consistent diagnoses, and the variable influence of neuroplasticity [Belsky and Pluess, 2009; Chapman et al., 2003], which introduces complexity when predicting functional impairments [Accardo et al., 2004]. Standardising clinical assessment is essential to improve the consistency of diagnoses, help elucidate the relationship between cerebral structure and functional outcome and assist the optimisation of treatment strategies for individual children.

1.2 Imaging of brain injury

Assessments of motor impairment can be confirmed by non-invasive medical imaging. This allows clinicians to qualitatively classify injury into brain malformations, WM and GM lesions and ventricular enlargement, based on known classification systems [Krägeloh-Mann and Horber, 2007], which is utilised to predict functional impairment and adjust treatment strategies accordingly. Medical imaging is crucial in improving individualisation of treatment [Bax et al., 2006; Ment et al., 2009], as well as increasing consistency in the diagnosis of CP. Several imaging technologies are used to assess CP [Accardo et al., 2004; Bosanquet et al., 2013], including computed tomography, cranial ultrasonography and magnetic resonance imaging (MRI). Of these modalities, MRI is favoured as ultrasound is limited by acoustic windows, computed tomography involves ionising radiation, and both lack soft tissue contrast important for brain imaging [Hoon and Vasconcellos Faria, 2010]. Although alternate modalities, including functional and diffusion MRI, can provide complementary information on brain structure and function [Heeger and Ress, 2002; Madden et al., 2009], structural MRI remains most widely used in clinical practice, detecting injury in approximately 85% of children with CP [Korzeniewski et al., 2008; Krägeloh-Mann and Horber, 2007]. The role of neuroimaging has been emphasised by the American Academy of Neurology who recommend all children with CP have an MRI at 2 years of age. This will facilitate injury detection in young children and neonates who might not show visible signs of motor or cognitive impairment, and enables interventions to

be implemented earlier in life. Studies in the literature have found qualitative MR findings to be a strong predictor of the pathogenesis of CP [Palmer, 2004; de Vries et al., 2011] that can be used to assess neuro-developmental risk [Ashwal et al., 2004; Mathur and Inder, 2009], and predict neurological deficits [Arnfield et al., 2013; Hoon and Vasconcellos Faria, 2010; Krägeloh-Mann and Horber, 2007].

Although qualitative classifications of injury into brain malformations, WM and GM lesions, and ventricular enlargement is the standard practice in the radiological assessment of children with CP, they are not sufficient to describe the large variability within each injury category [Feys et al., 2010]. Furthermore, the aetiology of CP in individual cases is often difficult to precisely establish [Paneth et al., 2006], and the variability in the cerebral injury covered by the term CP means that outcomes predicted by current diagnosis can be inconsistent [Bartlett and Palisano, 2002]. Multiple semi-quantitative scoring systems have been developed to address these issues and to standardise the assessment of MRIs [Cioni et al., 1997; Fiori et al., 2014; Inder et al., 2003; Kidokoro et al., 2013; Miller et al., 2005; Shiran et al., 2014; Sie et al., 2005; Skiöld et al., 2013]. In these methods, specific criteria of brain injury are graded based on their severity, or anatomical regions are given a discrete score based on whether the region contained injury or was healthy, and then summed to provide a total measure of injury. Although such techniques allow for comparisons of injury between children, these methods still require manual work, and still only broadly classify the extent and location of injury in order to reduce the amount of manual effort required.

Utilizing medical imaging in a *quantitative* manner, e.g. performing image segmentation to measure the extent, location and type of injury, is likely to be more revealing than the broad qualitative classifications of injury currently used in the assessment of CP [de Vries et al., 2011]. Quantitative assessment has the potential to assist diagnosis [Bax et al., 2005], and also elucidate the underlying physiological relationship between the extent of brain injury and function [Arnfield et al., 2013; Krägeloh-Mann and Horber, 2007]. This quantitative assessment will assist in developing image-derived biomarkers predictive of functional outcomes, which has an important role in developing models linking image findings to patient outcomes. These models can be used to predict patient impairment from the image alone, acting as a decision-support tool that can guide clinical decisions and help tailor patient specific treatment strategies. Furthermore, these models can

potentially provide an insight into the complex relationship between structure and function in the brain [Arnfield et al., 2013; Krägeloh-Mann and Horber, 2007]. The link between imaging findings and functional outcomes is an important area of investigation in the CP setting [Arnfield et al., 2013], however this quantitative assessment is hampered by the current need for time intensive manual or semi-automated assessment.

Automated approaches can alleviate manual effort and additionally benefit from repeatability, allowing for clinicians to instead focus on the interpretation of image findings and the decision of optimal treatment interventions. However, as yet, no automated tools are being used in the clinical assessment of children with CP. Although a number of U.S. Food and Drug Administration (FDA) approved medical device tools for the quantification of biomarkers of interest exist, such as NeuroQuant (CorTechs, Inc., La Jolla, CA, USA), they are mainly related to neurodegenerative disease, and not paediatric disorders. There is need for similar automated tools which are tailored to the specific challenges of children with CP, particularly the potential heterogeneity and severity of brain injury, to provide these benefits at the time of clinical assessment.

1.3 Pathophysiology of lesions

The disturbances in the developing brain indicative of CP manifest in a variety of characteristic ways in structural MRIs, depending on the aetiology and the presumed timing of the insult. Primary pathological entities include brain maldevelopments (particularly cortical malformations), that had occurred in the 1st and 2nd trimester of pregnancy, and WM and GM lesions that occur in the early and late 3rd trimester respectively. Ventricular enlargement and volume related changes are usually assumed to be secondary entities related to primary pathologies. These categories are based on their appearance in MRI scans, and from known classification schemes for CP [Krägeloh-Mann and Horber, 2007], and are shown in Figure 1.1 below.

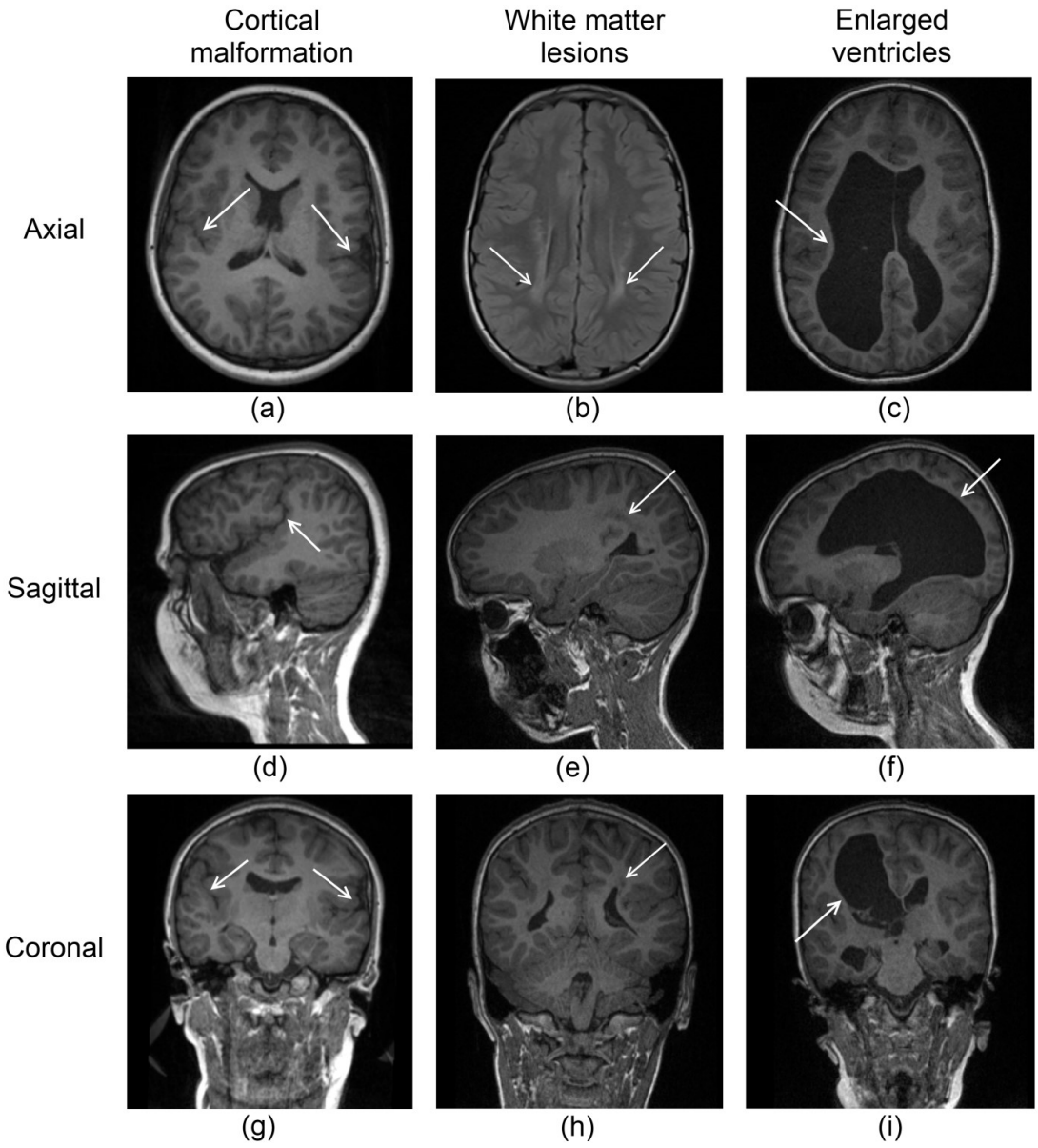

Fig. 1.1 Illustration of three types of disturbances indicative of CP that are visible in structural MRI. Each column shows a different subject. All images are T1-weighted MRI, except for (b) which is T2-weighted FLAIR. The axial plane (a-c) of each subject is shown in the top row, sagittal plane (d-f) in the second and coronal plane (g-i) in the bottom row. In each case, disturbances are indicated by arrows on the MRI slices. Cortical malformations, specifically bilateral perisylvian polymicrogyria, are visible as excessive numbers of small gyri in (a, d, g). WM lesions resulting from PVL are shown as local regions of high intensity in (b), and regions of lower intensity in (e, h). In (c, f, g), periventricular hemorrhagic infarction leading to a severe loss of WM and secondary enlargement of the lateral ventricles, particularly on the left side of the image, is shown.

1.3.1 Brain malformations

During the 1st and 2nd trimesters, the proliferation and migration of neuronal cells and the organisation of cortical sulci and gyri on the surface of the brain during development is controlled by several factors [Barkovich et al., 2012]. Malformations occur when this process is disrupted, either by genetic factors, physical or biochemical insults [Grant and Barkovich, 1997]. Brain maldevelopments represent a wide range of injury, including abnormalities of the cortical surface which constitute a large portion of brain malformations that commonly lead to CP. Disorders of cortical organisation can result in reduced cortical folding (lissencephaly), excessive numbers of small gyri (polymicrogyria), abnormally thick folds (pachygyria) and abnormal clefts (schizencephaly) [Barkovich et al., 2012; Legault et al., 2011]. Disorders of cortical migrations, termed dysplasia, is further subdivided into architectural dysplasia, cytoarchitectural dysplasia, Taylor-type cortical dysplasia [Tassi et al., 2002] and neuronal heterotopia [Hannan et al., 1999]. The clinical assessment of these malformations is typically performed with T1-weighted MRI, although the detection of cortical dysplasia was observed to be between 40-60% [Tassi et al., 2002]. An illustration of polymicrogyria is provided in Figure 1.1(a). Both polymicrogyria [Barkovich and Kjos, 1992a] and schizencephaly [Barkovich and Kjos, 1992b] have been found to correlate with motor impairment in children with CP. The assessment of these injuries is performed in Chapter 6.

1.3.2 White and grey matter lesions

During the 3rd trimester when the architecture of the brain is established and key structures are formed, disturbances including hypoxic-ischemia and intraventricular haemorrhage most often result in lesions in the WM or GM, which are common in children with CP [Bax et al., 2006; Cioni et al., 1999]. These lesions represent a heterogeneous group, and include PWM lesions, occurring early in the 3rd trimester when the immature oligodendrocytes are more vulnerable, and cortical and deep grey matter (CDGM) lesions, occurring late in the 3rd trimester or around birth when CDGM areas are more susceptible to disturbances. PWM lesions are characterised on brain MRI by focal abnormal WM signal intensities [Argyropoulou, 2010], and were found to be the most common form of lesion in children with CP [Bax et al., 2006; Krägeloh-Mann and Horber, 2007]. Less common WM lesions, including Diffuse Excessive High Signal Intensity (DEHSI) lesions [Counsell et al., 2003] and punctuate WM lesions, have been found to have a possible

impact on clinical outcomes [Rutherford et al., 2010]. Although CDGM lesions were also found to be less common [Bax et al., 2006], severe motor impairment was observed in children with this kind of lesion [Krägeloh-Mann and Horber, 2007; Martinez-Biarge et al., 2010], reflecting the physiological importance of the deep GM structures. Both lesion types appear hypointense in T1-weighted MRI, and hyperintense in T2-weighted MRI. Commonly, both T1- and T2-weighted MRI are used in clinical assessment of WM and CDGM lesions, specifically Fluid Attenuated Inversion Recovery (FLAIR) which provides a better contrast of PWM injury. Focal lesions indicative of CP are shown in Figure 1.1(b). The timing and extent of MRI lesions has been found to correlate with the severity of neurological defects [Bax et al., 2006; Krägeloh-Mann et al., 2002; Yin et al., 2000]. The assessment of these lesions is detailed in Chapter 7 of this thesis.

1.3.3 Ventricular enlargement

The PWM is particularly susceptible to injury in the early stages of the 3rd trimester, which is typically accompanied by tissue loss [Melhem et al., 2000; Palmer, 2004] and the enlargement of the ventricles. Excessive ventricular enlargement, termed ventriculomegaly, is defined as the atrial width of the ventricles exceeding 10 mm [Glenn, 2009]. Ventriculomegaly is typified by the irregular angular appearance of the trigone and body of the lateral ventricle, often appearing asymmetric. T1-weighted MRI is sufficient for clinically assessing this type of lesion. Although FLAIR is commonly used to identify the underlying WM loss, in some cases ventricular enlargement may not have associated periventricular signal abnormalities. An example of ventricular enlargement is illustrated in Figure 1.1(c). There is a marked increase in lateral ventricle volume amongst children with CP [Grant and Barkovich, 1997; Sööt et al., 2008]. Enlarged ventricles are an indirect measure for loss in WM due to brain injury [Hoon and Vasconcellos Faria, 2010], and has been correlated with motor and cognitive impairment [Melhem et al., 2000]. The assessment of this secondary lesion is described in Chapter 5 of this thesis.

1.4 Thesis aims and format

In this thesis, new methods tailored to CP are developed to meet these challenges. This doctorate aims to:

1. to develop several automated segmentation approaches to delineate the three main classes of injury observed in children with CP; cortical malformations, WM and GM injury and ventricular enlargement;
2. to establish a statistical methodology for modelling the relationship between brain injury, as measured by the image-derived measures of injury severity, and patient outcomes;
3. to compare the automated results against a manual gold standard, as well as the current state of the art automated segmentation methods.

Chapters 2 to 7 of this thesis is presented as a series of papers that have been published in international peer reviewed journals, while Chapter 8 is presented as yet unpublished results that are under peer review. All works are included in this thesis with permission from the publishing journals. The links between these publications as part of this thesis are outlined in Figure 1.2.

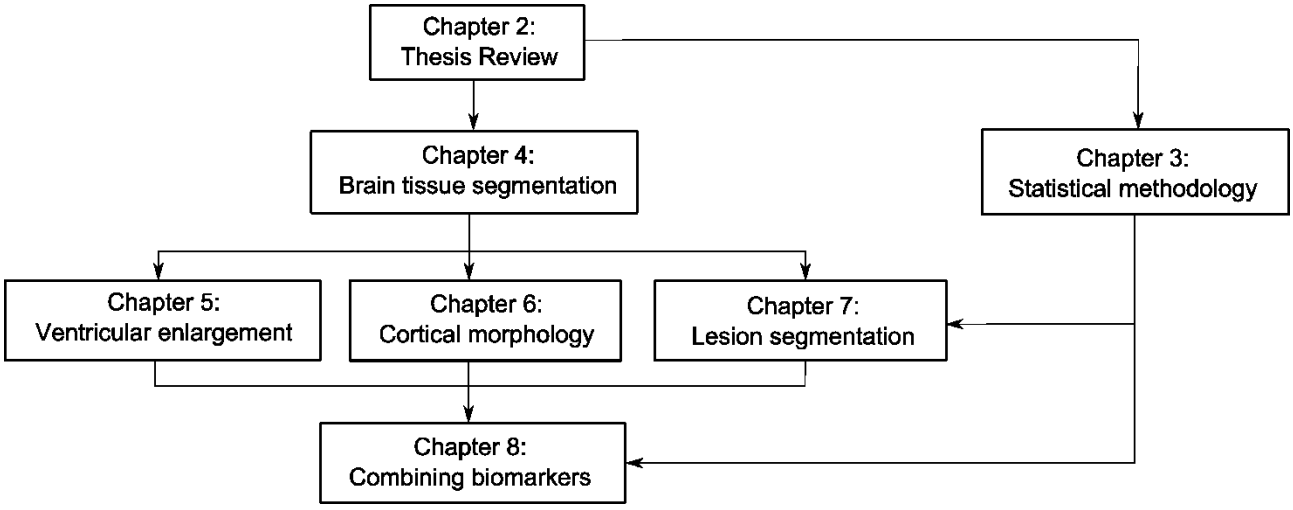

Fig. 1.2 A schematic outlining how the chapters of this thesis are linked together.

Chapter 2 presents a systematic review of automated segmentation studies that identifies the main classes of lesions observed in children with CP. This review describes the current dearth of literature specific to the automated injury segmentation of children with CP, and details the current state of the art automated techniques used in other applications that could be modified for application to the CP setting. This review highlights the importance of obtaining measures for all lesion types, requiring the use of multiple methods, and the potential clinical utility of modelling the link between brain injury to patient outcome.

Chapter 3 is an original article that describes the statistical procedure used to model the extent to which image-derived measures of injury correlate with patient function. This method uses standard linear regression models, with a data-driven variable selection approach to maximise model generalisability and elucidate the key links between brain structure and function. The proposed approach was applied to measures of injury obtained from a manual template-derived scoring approach [Fiori et al., 2014] in this chapter, and then applied to the measures of injury obtained from automated methods in the subsequent chapters.

Chapter 4, 5, 6 and 7 are original articles addressing Aims 1, 2 and 3, which detail the automated methods for detecting three main classes of injury observed in children with CP. Chapter 4 outlines an automated brain tissue segmentation approach robust to the presence of severe injury. Chapter 5 describes a method for measuring ventricular enlargement using a healthy ventricular shape model, and using the residual volume from this corresponded model to estimate the extent that critical adjacent anatomies are impacted. Chapter 6 details the process for analysing the shape of the cerebral cortex using a set of shape measures to detect a heterogeneous range of cortical malformations. Chapter 7 describes the methodology for segmenting WM and GM lesions as outlier classes to the healthy tissue distributions, using T2-weighted MRI to weight the healthy and lesion classes respectively, and computing lesion involvement into specific GM anatomies and WM tracts. Aim 3 has been addressed throughout these chapters by validating the performance of the methods against a ground truth assessment obtained from a manual expert, as well as comparing the methods against current gold standard techniques where applicable.

These three automated methods are combined in Chapter 8 to characterise the extent of injury present in this cohort of children with CP. These measures of injury will be hereon referred to as “biomarkers”, as they are structural characteristics that can be objectively measures and evaluated as an indicator of normal biological processes, pathogenic disturbances related to CP, and potential responses to therapeutic intervention, which is consistent with previous definitions [Anon, 2001]. The biomarkers from all injury types were incorporated into the statistical methodology developed in Chapter 3, in order to test if they are independent predictors of function, and to identify the most predictive features for multiple types of clinical outcomes.

In Chapter 9, a review of the findings from the above chapters is given, and discusses the limitations and areas of future research. Specifically, it details the framework for producing a decision support tool that can acts as a second, independent reader in the future, which can guide clinical decision making and additionally build models of the brain that can predict outcomes, and tailor patient-specific treatment interventions.

2. Review of automated injury detection techniques in the CP setting

2.1 Introduction

In Chapter 1, it was highlighted that utilising medical imaging in a quantitative manner can facilitate in identifying the relationship between characteristics of brain injury and patient function. Through the use of automated algorithms, these quantitative models can be developed without the need for manual labelling. Although extensive automated quantitative image analysis methods exist to analyse structural MRI data, which have been applied to numerous diseases, including Alzheimer's Disease (AD) [Ferrarini et al., 2008a], Schizophrenia [White et al., 2003], and Multiple Sclerosis (MS) [Van Leemput et al., 2001], none of these have been validated specifically on children with CP. The development of automated image segmentation techniques for CP would reduce the need for manual delineation of injuries, giving a finer assessment of injury by including characterisation of the location and extent of lesions. Furthermore the ability to measure the extent of anatomical injury and repeatability could enable correlations between injury and motor function impairment across very large cohorts, as has been performed for AD [Adaszewski et al., 2013; Villemagne et al., 2013].

The dearth of automated approaches applied specifically to CP may be explained by the significant technical challenges present in this clinical setting. Firstly, all three major types of injury; including ventricular enlargement, focal WM and GM lesions, and malformations have different appearances, however all injury types need to be considered during assessment [Krägeloh-Mann and Horber, 2007; Sööt et al., 2008], necessitating the use of multiple segmentation techniques. The heterogeneity in lesion appearance within each class is also an important factor. For instance, injury may appear as subtle malformations, requiring algorithms highly sensitive to changes to cortical shape and robust to partial volume effects, or as excessive ventricular enlargement extending to the cortex, invalidating structural *a priori* assumptions on the brain, which are challenging for atlas based techniques to resolve [Northam et al., 2011]. The severity of injury is a significant challenge in the CP setting, requiring the exclusion of up to a quarter of data as the commonly used segmentation approaches remain error prone, and require substantial manual intervention. Segmentations obtained from three approaches commonly used in

neurological settings are illustrated in Figure 2.1. As shown, all the segmentation results degrade as the extent of malformations increases, with even the best method showing substantial mislabelled regions even for moderate malformations. Finally, as the MR images of children with CP may be taken between birth to 18 years of age, specific challenges relating to reduced contrast between WM and GM due to reduced myelination and higher levels of noise in neonates [Mewes et al., 2006; Prastawa et al., 2005], and the temporal development of complex structures, particularly the cortical surface [Dubois et al., 2008a], need to be considered.

The remainder of the chapter is organised as follows. In Section 2.2, a review of the strengths and limitations of the automated techniques for performing tissue segmentation is provided, as well as the segmentation of several lesion types observed in children with CP, providing focus on the challenges that exist in the CP setting. A discussion of future trends is made in Section 2.4, which highlights the current technical challenges in this area, proposes several developments to these methods which will be incorporated into the developed methods detailed in Chapters 4 to 6, and provides a focus on using these methods to develop quantitative biomarkers of injury that are predictive of patient outcome. This addresses Aim 1 of this thesis, as to “develop several automated segmentation approaches to delineate the three main classes of injury observed in children with CP; cortical malformations, WM injury and ventricular enlargement”, existing methods with potential application to CP must first be identified. This review has been published, and is available at doi:10.1016/j.ijdevneu.2015.08.004.

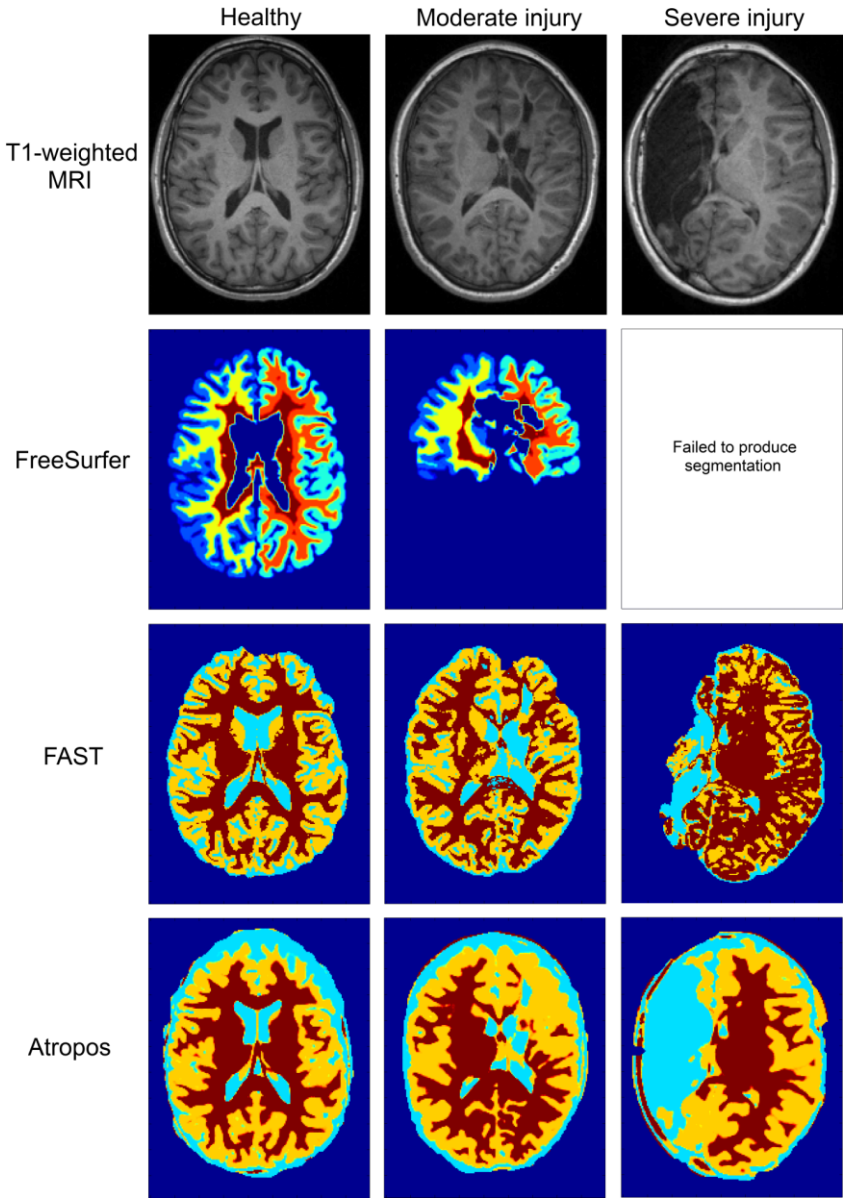

Fig 2.1 Illustration of the robustness of three software packages commonly used for neurological assessment: FreeSurfer, fMRIB's Automated Segmentation Tool (FAST), and Advanced Normalisation Tools (ANTs) Atropos, in brains of increasing injury severity. The cortical surface mesh deformation performed in FreeSurfer progressively deteriorates with increasing injury severity, failing to deform to the severely injured cortex in the most severe case. FAST achieves an accurate segmentation in the first two cases, however the severity of injury led to incorrect initial estimates of GM and WM, and hence incorrect tissue segmentation. Atropos, while providing the greater robustness to injury severity among all three methods, over segments the GM in the more injured cases, and under segments the WM in the second case.

2.2 Review of image lesion segmentation algorithms

In this section, a review of the current automatic image segmentation techniques that can be used to segment injury related to CP is provided. This review is separated into four sections; first the fundamental problem of segmenting cerebral tissues in the presence of structural abnormalities is discussed in Section 2.2.1. These methods provide a basis for the review of techniques which segment local tissue injury, in Section 2.2.2, surface based analyses for identifying cortical malformations in Section 2.2.3, and shape based analyses for identifying morphological shape abnormalities, in Section 2.2.4. These later methods typically involve the tissue segmentation methods discussed in Section 2.2.1, either modified to incorporate lesion classes, or to provide preliminary segmentations for subsequent analyses.

2.2.1 Tissue segmentation in the presence of structural abnormalities

Robust automated tissue segmentation is a fundamental challenge, particularly in the application of CP. The segmentation of the GM, WM and cerebrospinal fluid (CSF), allow for measures of tissue volume to be computed, and can be used to detect abnormalities related to CP as well as preterm birth [Chou et al., 2012; Northam et al., 2011]. These segmentation approaches facilitate subsequent lesion and anatomical shape analyses to better identify injury, which are detailed in Section 2.2.2 to Section 2.2.4. Although several brain MRI segmentation reviews exist [Balafar et al., 2010; Bezdek, 1993], this review considers the technical challenges and the potential application of these techniques specifically in the CP setting. A summary of the studies reviewed in this section is provided in Table 2.1.

Clustering algorithms are techniques that aim to identify natural groupings in unlabelled data, and do not rely on *a priori* information. Soft clustering techniques such as fuzzy c-means (FCM) clustering [Bezdek et al., 1984], which associates each voxel with a membership probability to each tissue class [Brandt and Kharas, 1993; Pham and Prince, 1999]. This approach finds groupings in the data without *a priori* knowledge, however often has reduced performance compared to supervised approaches, and may be more susceptible to noise, inhomogeneities and artefacts in the image, which is a major drawback in the CP setting. These approaches do have utility as robust, fast initialisation mechanisms for adaptive algorithms [Greenspan et al., 2006; Xue et al., 2007].

Supervised methods utilise *a priori* information to assist in tissue classification. The k-nearest neighbours (kNN) algorithm [Duda and Hart, 1973], have been frequently used to non-parametrically model tissue distributions [Hüppi et al., 1998; Inder et al., 1999], often utilizing labelled training data from atlas priors [Cocosco et al., 2003; Vrooman et al., 2007; Warfield et al., 2000] to assign a tissue class based on the most frequent label observed amongst a voxels kNN in the low dimensional space. Multiple MR modalities are often used to improve tissue classification, and to minimise the impact of noise. Robustness of supervised approaches to severe injury is dependent on the variability of injury in the training data, and may require semi-supervised selection of priors [Cocosco et al., 2003].

Several studies have proposed automated segmentation of the cerebral tissues using the Expectation Maximisation (EM) [Dempster et al., 1977] algorithm [Van Leemput et al., 1999; Mortamet et al., 2005; Wells et al., 1996], which interleaves classifying each voxel to a specific distribution in the Expectation Step, and updating the distribution parameters based on the new clustering of the data in the Maximisation Step. Tissue distribution parameters are frequently initialised using registered *a priori* atlases [Weisenfeld and Warfield, 2009; Wells et al., 1996]. As the accuracy of registration may be affected by severe injury, this could lead to irrecoverable estimates of tissue distributions. This highlights the value of robust mechanisms, such as FCM or Otsu thresholding [Otsu, 1975], to initialise EM [Avants et al., 2011; Greenspan et al., 2006; Xue et al., 2007]. Modelling of myelinated and unmyelinated WM separately has been performed for neonatal applications [Prastawa et al., 2005; Xue et al., 2007]. Robustness to parameter initialisation can be achieved by interleaving the EM method with Markov Random Field (MRF) models [Kindermann and Snell, 1980] to incorporate spatial information [Ashburner and Friston, 2005; Bricq et al., 2008b; Chai et al., 2015; Habas et al., 2010; Marroquin et al., 2002; Melbourne et al., 2012; Murgasova et al., 2006; Zhang et al., 2001]. Markov modelling has been performed for tissue segmentation without the EM assumptions, instead using non-parametric estimates of neighbourhood tissue distributions [Awate et al., 2006].

Atlas-based image segmentation allows for the delineation of cerebral tissues and subcortical anatomies, using registered probabilistic atlases of tissue type [Fischl et al., 2002; van der Lijn et al., 2008], and atlases with discrete anatomical labels [Ciofolo and Barillot, 2009; Klein and Hirsch, 2005]. As atlas-driven label propagation is sensitive to the

accuracy of registration, anatomical variability is accounted for by propagating labels from multiple atlases [Artaechevarria et al., 2009; Heckemann et al., 2006; Sabuncu et al., 2010; Sanroma et al., 2015]. Multi-atlas segmentation approaches benefit from an efficient atlas selection strategy, choosing atlases that meet a threshold similarity metric to the target image [Aljabar et al., 2009] or nearby atlases in a lower dimensional projection [Li et al., 2015b; Wolz et al., 2010]. Further refinement of segmentations have been performed with incorporated EM approaches [Lötjönen et al., 2010; Rajchl et al., 2015], while relaxation of atlas priors was performed to better accommodate cerebral injury [Cardoso et al., 2009; Ledig et al., 2015], which could potentially account for the severe distortion, or absence, of brain tissue commonly observed in children with CP. Alternatively, approaches such as Large Deformation Diffeomorphic Metric Mapping (LDDMM) would allow for more significant deformations, and have been complemented with semi-automated segmentations of the ventricle to improve registration accuracy in children with ventriculomegaly [Djamanakova et al., 2013]. Atlas-based anatomical parcellation has been performed in the CP setting for tracking anatomical volumes and diffusion tensor measures during healthy development [Faria et al., 2010; Oishi et al., 2011] and also for quantifying anatomical injury [Faria et al., 2011; Oishi et al., 2013; Yoshida et al., 2013].

Voxel based morphometry (VBM) [Ashburner and Friston, 2000] has been used to perform tissue segmentation and compare regional tissue volumes [Giménez et al., 2006; Soria-Pastor et al., 2008]. This approach performs voxel-wise statistical analyses using general linear models, allowing for comparisons between (healthy and unhealthy) sub-populations [Smith et al., 2007] or correlations with clinical outcomes. VBM software is supplied in the Statistical Parametric Mapping (SPM) package (Wellcome Trust Centre for Neuroimaging, UK) which utilises *a priori* information to perform tissue segmentation prior to VBM analysis [Chou et al., 2012; Giménez et al., 2006; Hutton et al., 2008; Soria-Pastor et al., 2008]. As *a priori* constraints typically do not represent extensive injury, a Hidden Markov Model (HMM) was used to relax these constraints [Northam et al., 2011] and yield more accurate segmentations in the presence of gross disturbances. The VBM approach, however, has been found to be susceptible to false positive findings, particularly in the neocortex [Scarpazza et al., 2015].

Table 2.1 Overview of tissue segmentation studies. Green cells represent methods strengths that are suitable for application to CP, while red cells represent challenges that preclude these methods from this application. References highlighted in purple have applied these methods to children with CP or infants born preterm.

Article	Method	Strengths	Challenges	Application
Unsupervised methods				
Brandt and Kharas, 1993; Pham and Prince, 1999	Fuzzy c-means	No a priori information required Simple implementation	Reduced accuracy Susceptible to image artefacts	Segment cerebral tissues
Supervised methods				
Hüppi et al., 1998; Inder et al., 1999; Warfield et al., 2000; Cocosco et al., 2003; Vrooman et al., 2007	K-nearest neighbours	Multiple prior selection strategies possible No assumptions on tissue distribution	Require a priori information Registration of prior information critical	Segment cerebral tissues
Expectation-maximisation				
Mortamet et al., 2005	EM segmentation	Fast, robust clustering method	Susceptible to noise Registering atlas priors may fail in severe injury	Segment cerebral tissues
Van Leemput et al., 1999; Wells et al., 1996; Weisenfeld and Warfield, 2009; Prastawa et al., 2005; Xue et al., 2007; Ashburner and Friston, 2005; Bricq et al., 2008; Habas et al., 2010; Marroquin et al., 2002; Melbourne et al., 2012; Murgasova et al., 2006; Zhang et al., 2001; Greenspan et al., 2006; Chai et al., 2015	EM-MRF segmentation	Fast, robust clustering method Can incorporate robust initialisation mechanism Robust to noise	Registering atlas priors may fail in severe injury	Segment cerebral tissues
Markov modelling				
Awate et al., 2006	Nonparametric density estimation	Robust to noise and inhomogeneity No assumptions on tissue distribution	Require a priori information Uncommon neighbourhoods	Segment cerebral tissues

			poorly segmented	
Atlas-based methods				
Van der Lijn et al., 2008; Fischl et al., 2002; Cardoso et al., 2009	Probabilistic atlas propagation	Can perform GM anatomy and WM tract parcellation Only requires alignment of 1 atlas Suitable for moderate anatomical variability	Dependent on atlas selection and registration accuracy Complex model estimation	Segment sub-cortical anatomies
Djamanakova et al., 2013; Ciofolo et al., 2009; Klein and Hirsch, 2005; Faria et al., 2010; Faria et al., 2011; Yoshida et al., 2013	Label propagation	Can perform GM anatomy and WM tract parcellation Only requires alignment of 1 atlas Intuitive model segmentation	Dependent on atlas selection and registration accuracy Only tolerates limited amounts of anatomical variability	Segment cortical and sub-cortical anatomies Quantify developmental injury Classify CP type
Sabuncu et al., 2010; Artaechevarria et al., 2009; Heckermann et al., 2006; Aljabar et al., 2009; Wolz et al., 2010; Lötjönen et al., 2010; Rajchl et al., 2015; Ledig et al., 2015; Oishi et al., 2011; Oishi et al., 2013; Sanroma et al., 2015; Li et al., 2015	Multi-atlas propagation	Can perform GM anatomy and WM tract parcellation Suitable for anatomical variability Can be refined with EM	Require multiple registrations Atlas selection and label fusion challenging	Segment cortical and sub-cortical anatomies Construct neonatal atlases Quantify developmental injury
Voxel based morphometry				
Giménez et al., 2006; Soria-Pastor et al., 2008; Smith et al., 2007; Chou et al., 2012; Northam et al., 2011; Scarpazza et al., 2015	VBM	Can identify significant difference between sub-populations Can correlate image markers with outcome	Susceptible to registration errors Confounded by anatomical variability Susceptible to false positives	Identify local tissue volume differences between healthy and impaired or preterm cohorts

2.2.2 Segmentation of localised tissue injury

Although the field of lesion detection is well-researched, there is no published work on the automatic segmentation of focal lesions related specifically to CP. Techniques that can be used to detect lesions from pathologies such as AD and MS can be modified for the detection of lesions in CP. One property of all reviewed methods is their use of intensity as a feature to discriminate lesions from healthy tissue. Due to the overlapping intensities between injured and healthy tissues, lesion segmentation techniques utilise multiple MRI modalities. While the detection of GM lesions requires specialised sequences [Nelson et al., 2007], T2-FLAIR images offer improved contrast of WM lesions [Herskovits et al., 2001; Tan et al., 2002]. Consequently, correctly aligning multi-modal images is critical [He and Narayana, 2002].

Lesion detection techniques can be classified either as a modelled tissue class separate to WM, GM and CSF, or simply as outliers to these classes. This distinction can have implications for performance; a modelled lesion class may not be general enough, while lesion-as-outlier formulations may include many examples of non-lesions which must be filtered out as a post-process. Lesion outliers have been identified using FCM clustering, with T2-weighted MRI for refining lesion outliers [Boudraa et al., 2000; Shen et al., 2010]. The efficacy of unsupervised approaches depends on the availability of MR modalities to distinguish lesions that appear as another tissue type (e.g. WM lesions appearing as GM in T1-weighted MRI, or hyperintense in T2-weighted MRI). Supervised methods overcome this limitation using training data to identify lesions in the WM as voxels incorrectly labelled as GM [de Boer et al., 2009; Schmidt et al., 2012]. Supervised kNN classification is commonly used for lesion classification of multi-spectral data [Anbeek et al., 2004; Cárdenes et al., 2003; Wu et al., 2006]. Supervised artificial neural network have also been used to identify WM lesions [Zijdenbos et al., 2002]. However the variability of lesion appearance and location observed in children with CP requires that supervised approaches have large cohorts of training data containing many examples of injury.

Models of healthy brain tissue intensities provided by the EM algorithm can be used to identify lesions, either based on aligned *a priori* tissue classes [Jain et al., 2015; Warfield et al., 1995], or as voxels with a high Mahalanobis distance from their assigned class [Dugas-Phocion et al., 2004]. An alternative to EM, called the Trimmed-Likelihood Estimation (TLE), was used for WM lesion segmentation [García-Lorenzo et al., 2011;

Souplet, 2009]. In another approach [Zacharaki and Bezerianos, 2012] use low-dimensional statistical models of normality for image patches to delineate multiple abnormalities. The EM approach has significant potential for lesion detection in the CP setting, however its performance would crucially rely on the availability of multiple, specific MR modalities or prior information.

Several studies utilise MRFs to smooth the tissue and lesion segmentations obtained using the EM method [Van Leemput et al., 2001; Sajja et al., 2006]. To avoid computing likelihood functions for MRFs, a Conditional Random Field (CRF) was implemented for lesion detection [Karimaghaloo et al., 2012], while a simplification of the MRF, called the Hidden Markov Chain (HMC) [Baum and Petrie, 1966], was used to classify outliers as lesion [Bricq et al., 2008a]. Alternatively, the Graph Cuts algorithm was then used to refine the MS lesion segmentations [García-Lorenzo et al., 2009], while a stochastic spatial approach was utilised to identify WM lesions as voxels sufficiently different to surrounding voxel intensities [Cheng et al., 2015]. Spatial priors that encode tissue transitions in a conditional transition probability matrix can play a pivotal role in achieving robustness in heterogeneous lesion segmentation.

Atlas-based methods commonly utilise topological and statistical *a priori* information to classify outlier voxels as lesion [Lindemer et al., 2015; Prastawa and Guido, 2008; Shiee et al., 2008; Shiee et al., 2010]. Atlases have been applied to more extensive space-occupying lesions, typically tumour delineation and simultaneous brain segmentation using lesion growth models [Bach Cuadra et al., 2006; Pollo et al., 2005], biomechanical models [Zacharaki et al., 2009] or graphical models [Njeh et al., 2015; Parisot et al., 2012; Parisot et al., 2014]. The ability to accommodate high deformation extends the use of these methods to cases of severe CP-related injury. For this purpose however, these methods need to segment brain tissue types within highly deformed regions as well as healthy regions of the brain, without misclassifying severely malformed regions as a separate tumour entity. A summary of these reviewed lesion segmentation studies is provided in Table 2.2.

Table 2.2 Overview of lesion detection studies. Green cells represent methods strengths that are suitable for application to CP, while red cells represent challenges that preclude these methods from this application. References highlighted in purple have applied these methods to children with CP or infants born preterm.

Article	Method	Strengths	Challenges	Application
Unsupervised methods				
Boudraa et al., 2000; Shen et al., 2010	Fuzzy c-means	Lesion-as-outlier, or as separate class, definitions possible Simple implementation	Requires multiple MR modalities Susceptible to image artefacts	WM lesion detection
Supervised methods				
De Boer et al., 2009; Schmidt et al., 2012; Anbeek et al., 2004; Cárdenes et al., 2003; Wu et al., 2006	K-nearest neighbours	Lesion as separate class definition *A priori* information enhance lesion specificity	Requires *a priori* information from multiple modalities Lesion detection dependent on trained injury	WM lesion detection in MS patients
Zijdenbos et al., 2002	Artificial neural networks	Can estimate non-linear relationships	Lesion detection dependent on trained injury Model relationship hidden	WM lesion detection
Expectation-maximisation				
Warfield et al., 1995; Dugas-Phocion et al., 2004	EM segmentation	Lesion-as-outlier definition Robust to image noise and inhomogeneity Fast, robust clustering method	Requires *a priori* information Requires multiple MR modalities	WM lesion detection in MS patients
Garcia-Lorenzo et al., 2011; Souplet et al., 2009	Trimmed-likelihood estimation	Less likely to converge to local optima Less sensitive to outliers	Requires *a priori* information for initialisation Requires multiple MR modalities	WM lesion detection in MS patients
Zacharaki et al., 2012	Distribution estimation	Lesion-as-outlier definition Can detect broad range of lesions No *a priori* information needed	Lower specificity than models of pathology	Segment multiple brain abnormalities
Markov modelling				

Sajja et al., 2006; Van Leemput et al., 2001; Jain et al., 2015	EM-MRF	Lesion-as-outlier, or as separate class, definitions possible Robust to image noise and inhomogeneity	Requires multiple MR modalities Sensitive to registration errors	WM lesion detection in MS patients
Karimaghaloo et al., 2012	CRF	Avoids likelihood computations *A priori* information enhance lesion specificity	Training data required for parameter learning Requires multiple MR modalities	WM lesion detection in MS patients
Bricq et al., 2008	HMC	Lesions as outliers definition Less computationally intensive	Requires multiple MR modalities Simpler neighbourhood model Required *a priori* atlas	WM lesion detection in MS patients
Garcia-Lorenzo et al., 2009	Graph cuts	Lesions as outliers definition Robust to image noise and inhomogeneity	Requires multiple MR modalities Automated sink/source allocation challenging	WM lesion detection in MS patients
Cheng et al., 2015	Stochastic process	Lesions as outliers definition No assumptions on tissue distribution	Requires *a prior* information or atlas alignment to compute tissue segmentations Assumes lesion characteristics	WM injury detection in preterm infants
Atlas-based methods				
Shiee et al., 2010; Shiee et al., 2011; Prastawa and Gerig, 2008; Lindemer et al., 2015	Focal WM lesion detection	Lesions as outliers definition Suitable for anatomical and pathological variability	Requires multiple MR modalities Requires *a priori* statistical and topological atlases	WM lesion detection in MS and AD patients
Bach Cuadra et al., 2006; Pollo et al., 2002; Zacharaki et al., 2009; Parisot et al., 2012; Parisot et al., 2014; Njeh et al., 2015	Space-occupying lesion detection	Lesions as separate class/model Only requires alignment of 1 atlas Suitable for anatomical and pathological variability	Regions of deformation mislabelled as tumour Dependent on atlas selection and registration accuracy Lesion modelling challenging	Segment tumour, cortical and sub-cortical anatomies

2.2.3 Cortical surface based analysis

The assessment of cortical malformations is essential, but delineating this type of injury remains technically challenging. Cortical GM segmentation can be performed using the methods described in Section 2.2.1, using parametric deformable models [MacDonald et al., 2000; Xu et al., 1999], or geometric deformable models [Malladi et al., 1995; Zeng et al., 1999] to delineate cortical surfaces. Parametric deformable models, including snakes [Kass et al., 1988], explicitly represent surfaces, while geometric deformable models implicitly represent this surface as the zero level set of a higher dimensional "level set function" [Osher and Sethian, 1988]. Both methods allow for relatively simple correspondences between surfaces, whereas mesh segmentations may require mapping the surface into a standard parameterisable surface, usually a sphere, to allow for point-wise correspondences between subjects [Dale et al., 1999; Fischl et al., 1999], with exceptions such as CIVET. Although these comparisons can be used to measure deviations from normal anatomy [Thompson and Toga, 1997], point-wise correspondence and spherical transformations are difficult to obtain for children with severe cortical malformations. More recently, 4D regression models have been developed to track shape evolution of the cortex [Rekik et al., 2015], however this has only been demonstrated for children with healthy development.

Although cortical volume measures can detect several malformations on a global scale, more advanced techniques that extract multiple shape measures of the cortical surface are needed to detect the spectrum of malformations observed in children with CP. Cortical thickness is an important developmental quantification of neural architecture [Chen et al., 2008]. It has multiple definitions in the literature, including geometric distances [MacDonald et al., 2000; Martinussen et al., 2005], geodesic distances from the level set function [Tosun et al., 2004; Xue et al., 2007; Zeng et al., 1999], diffeomorphic distances [Das et al., 2009] and parametric correspondence distances [Lerch et al., 2005]. In contrast to these mesh-based measures, voxel-based measures of cortical thickness have been obtained with the Laplacian approach [Hutton et al., 2008; Jones et al., 2000], which computes topologically smooth streamlines across the cortex. FreeSurfer (Laboratory for Computational Imaging, US) [Fischl, 2012] has frequently been used to measure cortical thickness [Dierker et al., 2015; Fischl and Dale, 2000; Hatfield et al., 2011], and has been applied in the CP setting [Pannek et al., 2014; Rose et al., 2011]. Although it has been

found to be reliable when applied to relatively healthy data [Han et al., 2006; Iscan et al., 2015], segmentation accuracy is significantly reduced for children with severe cortical malformations, as illustrated in Figure 2.1, and often requires manual correction. Unlike FreeSurfer, CIVET performs mesh segmentations initialised from the same polyhedron, allowing surface topology and point-wise correspondence to be inherently obtained [Ad-Dab'bagh et al., 2006]. This software has been used to measure cortical thickness in children learning a second language [Klein et al., 2014]. As cortical thickness has been investigated in the context of cortical thinning due to AD [Haidar and Soul, 2006], it can be readily applied to the detection of pachygyria in children with CP.

Cortical curvature, or folding, is an important developmental measure as the brain forms sulci and gyri to increase cortical volume. Cortical folding anomalies have commonly been investigated in infants born preterm [Dubois et al., 2008a; Dubois et al., 2008b; Rodriguez-Carranza et al., 2008; Zhang et al., 2015]. Local curvature measures have been computed from cortical meshes [Chung et al., 2003; Joshi et al., 1999b; Schaer et al., 2008; Tosun et al., 2006; White et al., 2003], and from level set function topology [Han et al., 2004; Xue et al., 2007; Zeng et al., 1999]. Measures of local curvature, compared to the spatially corresponding cortical regions of controls, have the potential to quantify several malformations, including lissencephaly and polymicrogyria.

Alternate parameterisations of the cortical surface, including the sulcal depth [Dierker et al., 2015; van Essen, 2005; van Essen et al., 2006; Nordahl et al., 2007; Zhang et al., 2015], and geodesic depth [Rettmann et al., 2002; Tosun et al., 2004], have been used to quantify the Euclidean distance between sulci and gyri to corresponding points on a smooth template brain, and the geodesic distances from sulci to gyri following the cortical surface, respectively. Maps of sulcal depth [Alhazmi et al., 2015] have been computed using the BrainVoyager software (Brain Innovation, Netherlands) [Goebel, 2012]. Although these methods often require substantial manual input to correct errors in cortical segmentation, they capture critical information on sulcal depth that can identify schizencephaly.

A cortical shape measure closely related to both curvature and sulcal depth is the surface area of the cortex. It has been investigated in the context of schizophrenia [Rimol et al., 2012], AD [Dickerson et al., 2009] and twin studies [Panizzon et al., 2009], which compare mappings of surface area provided by FreeSurfer between two populations. This measure could be extended to CP in order to identify several malformations, including lissencephaly and schizencephaly.

Analyses of cortical shape has also been performed using statistical shape models (SSM), which represent a sample of shapes as a mean shape and estimates of shape variability provided by dimensionality reduction approaches [van der Maaten et al., 2009]. These methods have been used to characterise cortical shape [Caunce and Taylor, 2001; Joshi et al., 1997; Lohmann and von Cramon, 2000; Yu et al., 2007], however the need for dimensionality reduction may limit the modelling of fine topology, reducing the sensitivity of malformation detection using SSM approaches. A summary of the cortical modelling studies reviewed in this section is provided in Table 2.3.

Table 2.3 Overview of cortical surface analyses. Green cells represent methods strengths that are suitable for application to CP, while red cells represent challenges that preclude these methods from this application. References highlighted in purple have applied these methods to children with CP or infants born preterm.

Articles	Method	Strengths	Challenges	Application
Cortical grey matter surface representation				
MacDonald et al., 2000; Xu et al., 1999	Parametric deformable model	Computationally efficient Simple correspondence between models	Additional snake forces required to fit convoluted shapes Manual intervention of force weights Initialisation of surface critical	Segmentation of cortical GM
Malladi et al., 1995; Zeng et al., 1999	Geometric deformable model	Robust to topological changes Suited to boundary representation Robust to initialisation Level set function can compute	Computationally intensive Sensitive to partial volume effects	Shape modelling Segmentation of cortical GM

		volume, surface area, curvature and thickness		
Rekik et al., 2015	4D current representation of the cortex	Current representation avoids requirement for point-to-point correspondence Can track thickness and gyrification longitudinally	Only developed for healthy developmental trajectories	Construction of spatiotemporal atlases of the cortex Predict temporal evolution of test subject cortices
Cortical Thickness				
MacDonald et al., 2000; Martinussen et al., 2005	Geometric definition of cortical thickness	Simple measures	Sensitive to segmentation errors Correspondence require surface inflation Not a topology preserving measure	Measure cortical thickness in healthy children and in very low birth weight children
Tosun et al., 2004; Zeng et al., 1999; Xue et al., 2007	Geodesic definition of cortical thickness	Simple topologic measure Topology preserving measure	Correspondence require surface inflation Computationally intensive	Measure cortical thickness
Das et al., 2009	Diffeomorphic registration definition of cortical thickness	Topology preserving measure Sub-voxel estimate of thickness Accurately resolve subtle sulci	Utilises thickness priors Requires registration normalisation	Measure thickness on 3D phantoms and cortical GM Track thickness longitudinally in dementia patients
Lerch et al., 2005	Parametric definition of cortical thickness	Simple measure Simple inter-patient correspondence	Dependent on parametric surface representation	Measure cortical thickness in AD and healthy controls
Hutton et al., 2008; Jones et al., 2000; Haidar and Soul, 2006	Cortical thickness using Laplacian approach	Robust and reliable measure Provide topology preserving, one-to-one mapping Robust to scanning parameters	Sensitive to segmentation errors Complex inter-patient correspondence Sensitive to partial volume effects	Measure cortical thickness in healthy patients and patients with AD
Han et al., 2006; Hatfield et al., 2011; Dierker et al., 2015	Cortical thickness using FreeSurfer	Robust to scanning parameters Simple geometric measure	Correspondence require surface inflation	Measure cortical thickness and perform regression with diagnosis of

				infection
Curvature/sulcation				
Dubois et al., 2008a; Zhang et al., 2015	Sulcation index measure of curvature	Simple measure Correlates with functional outcomes	Global measure of curvature Sensitive to partial volume effects and segmentation accuracy	Correlate cortical surface measures with neurological outcomes
Dubois et al, 2008b; Rodriguez-Carranza et al., 2008; Chung et al., 2003; Joshi et al., 1999; Schaer et al., 2008; Tosun et al., 2006; White et al., 2003	Mesh-based measure of curvature	Simple measure Correlates with gestational age Measure independent of global size	Sensitive to segmentation accuracy May require manual editing Complex inter-patient correspondence	Correlate curvature measure to gestational age Compare curvature between healthy children and children with disease, Williams syndrome (WS) or developmental disorders
Han et al., 2004; Zeng et al., 1999; Xue et al., 2007	Geodesic measure of curvature	Topologically preserving measure Robust measure	Sensitive to segmentation accuracy Complex inter-patient correspondence	Compute curvature measure
Sulcal/geodesic depth				
Van Essen et al., 2006; Nordahl et al., 20007; Van Essen et al., 2005; Alhazmi et al., 2015; Dierker et al., 2015; Zhang et al., 2015	Sulcal depth	Unique morphological measure Correlates with neurological outcome	Sensitive to segmentation accuracy Complex inter-patient correspondence	Compare sulcal depth asymmetry between controls and children with WS, autism and Asberger's syndrome
Rettman et al., 2002; Tosun et al., 2004;	Geodesic depth	Unique morphological measure	Complex inter-patient correspondence	Classification of sulci
Surface area				
Rimol et al., 2012	Surface area using FreeSurfer	Simple measure Correlates with gestational age	Sensitive to segmentation errors Complex inter-patient correspondence	Compare surface area between healthy patients and patients with schizophrenia, bipolar disorder,

			Sensitive to partial volume effects	AD, and across twins
Statistical shape models				
Yu et al., 2007; Caunce and Taylor, 2001; Lohmann and von Cramon, 2000; Joshi et al., 1997	Statistical shape model	Harmonic shape model suited to cortical shape Low dimensional shape representation can construct healthy manifold Correlates with neurological outcome	Sensitive to segmentation accuracy Correspondence sensitive to initial alignment	Characterise cortical development Classification of sulci Compare shape between healthy patients and patients with schizophrenia

2.3.4 Shape analysis of subcortical structures

The shape analysis of anatomies is an important facet of lesion detection in children with CP, as developmental disturbances typically impact the shape of cerebral structures. A common instance of shape variation is the enlargement of the ventricles as a result of periventricular injury, which is present in up to 70% of children with CP [Sööt et al., 2008]. Unlike other lesion types, this does not manifest as an intensity change, but as a morphological change. As the ventricle borders critical deep WM and GM structures, which have a significant influence on outcome, this motivates the characterisation of shape. A summary of these shape modelling studies reviewed in this section is provided in Table 2.4. Additionally a summary of freely available software used by studies in this review is provided in Table 2.5.

Measurements of ventricular enlargement have been used in investigations of several cerebral diseases such as AD and schizophrenia. In these studies, variation in ventricle shape is frequently modelled using SSMs, with shape being represented either as landmarks on the ventricular surface [Graham et al., 2006; Narr et al., 2001], as multiple central points and surface-to-core radial measurements [Chou et al., 2007; Thompson et al., 2004], or as spherical harmonics [Gerig et al., 2001; Styner et al., 2003]. Typically, these studies construct separate models of healthy and enlarged ventricular shape [Ferrarini et al., 2006; Ferrarini et al., 2008a], in order to identify significant shape differences. However this requires machine learning approaches, such as the Self-Organised Map (SOM) [Kohonen, 1990] and Support Vector Machines (SVM) [Cortes and Vapnik, 1995], to find point correspondence between the two models, and to classify ventricles based on trained shape features, respectively. This is not feasible for CP, where

although more recent methods for estimating correspondence exist [Ravikumar et al., 2015], the variability in ventricular enlargement complicates finding the correspondences between enlarged ventricle surfaces, necessary to construct a model of injury, as well as point-wise correspondences from ventricular surfaces to this model of injury. Furthermore, it is of interest in CP to quantify the severity of enlargement and the impingement of periventricular anatomies.

Shape modelling can also be used to identify morphological changes to subcortical anatomies, which are secondary lesions arising from various developmental disturbances. Shape models have also been used to segment deep GM structures, such as the hippocampus [Hong et al., 2015; Kelemen et al., 1998; Shen et al., 2012a; Styner et al., 2004] and the thalamus [Patenaude et al., 2011], by transforming an SSM constructed from training segmentations to a registered image volume [Heimann and Meinzer, 2009]. An extension of SSMs that incorporates the texture on the surface boundary into the model, called the Active Appearance Model (AAM) [Cootes et al., 2001], was used to refine the segmentation of deep GM structures with adjacent boundaries [Babalola et al., 2008]. Although these techniques focus more on the segmentation of these structures, the shape model method additionally allows for the quantitative evaluation of morphological deformation, in comparison to healthy shapes. This has significant potential for detecting injury and for identifying biomarkers linked to the outcome of children with CP.

Table 2.4 Overview of anatomical shape analysis methods. Green cells represent methods strengths that are suitable for application to CP, while red cells represent challenges that preclude these methods from this application. References highlighted in purple have applied these methods to children with CP or infants born preterm.

Articles	Method	Strengths	Challenges	Application
Lateral ventricles				
Graham et al., 2006; Narr et al., 2001; Ferrarini et al., 2006; Ferrarini et al., 2008; Ravikumar et al., 2015	Statistical shape model - landmark representation	Clear ventricle boundary assists segmentation Can quantify extent of enlargement	Correspondence to model of injury	Comparison between healthy controls and patients with schizophrenia, AD

Chou et al., 2007; Thompson et al., 2004	Statistical shape model - medial representation	Clear ventricle boundary assists segmentation Quantify extent of enlargement Correlate enlargement to outcome	Correspondence to model of injury Only model ventricular horn	Compare shape between healthy and AD groups
Gerig et al., 2001; Styner et al., 2003	Statistical shape model - spherical harmonics representation	Clear ventricle boundary assists segmentation Robust shape alignment Can quantify distances between models	Correspondence to model of injury Non-intuitive shape descriptors	Compare shape between twins
Deep grey matter structures				
Kelemen et al., 1998; Styner et al., 2004	Statistical shape model - spherical harmonics representation	Robust shape alignment	Accurate segmentation challenging Correspondence to model of injury Non-intuitive shape descriptors	Segment deep GM structures with deformation of shape model Compare shape models between healthy and schizophrenia groups
Shen et al., 2012; Hong et al., 2015	Statistical shape model - landmark representation	Trained shape features based on training shapes May not require point-to-point correspondence	Hippocampus segmentation may require semi-automated approach Method relies on representative training set	Classify hippocampus shape as healthy or AD
Patenaude et al., 2011	Bayesian appearance model - landmark representation	Intensity information included Allow for correspondence to injury	Elastic registration and model optimisation computationally intensive Affected by MR contrast	Segment deep GM structures with elastic deformation of shape and intensity model
Babalola et al., 2008	Active appearance model	Intensity information included to refine segmentation	Affected by MR contrast	Segment deep GM structures with shape and intensity model

Table 2.5 List of software packages used by studies in this chapter.

Software	Website	Papers
ANTs	http://stnava.github.io/ANTs/	Avants et al., 2011; Das et al., 2009
BrainVISA	http://brainvisa.info/	Dubois et al., 2008a; Dubois et al., 2008b
BrainVoyager	http://www.brainvoyager.com/	Goebel, 2012; Alzhami et al., 2015
CIVET	http://mcin-cnim.ca/neuroimagingtechnologies/civet/	Ad-Dab'bagh et al., 2006; Klein et al., 2014
CRUISE	https://www.nitrc.org/projects/toads-cruise/	Xue et al., 2007; Han et al., 2004
FreeSurfer	http://surfer.nmr.mgh.harvard.edu/	Hatfield et al., 2011; Rose et al., 2011; Pannek et al., 2014
FSL	http://fsl.fmrib.ox.ac.uk/fsl/fslwiki/	Zhang et al., 2001; Patenaude et al., 2011
ITK	http://www.itk.org/	Avants et al., 2011; Prastawa et al., 2005; Garcia-Lorenzo et al., 2009; Cabezas et al., 2011; Mortamet et al., 2005
NifTK	http://cmic.cs.ucl.ac.uk/home/software/	Cardoso et al., 2011; Melbourne et al., 2012; Rajchl et al., 2015
SPM	http://www.fil.ion.ucl.ac.uk/spm/	Ashburner and Friston, 2005; Schmidt et al., 2012; Sajja et al., 2006; Soria-Pastor et al., 2008; Gimenez et al., 2006; Hutton et al., 2008
VBM	http://dbm.neuro.uni-jena.de/vbm/	Northam et al., 2012
VTK	http://www.vtk.org/	Avants et al., 2011; Rajchl et al., 2015

2.3 Future trends

Although most of the techniques covered in the review were applied to other cerebral pathologies, they have utility when assessing children with CP. However, the particular attributes of CP and its clinical assessment have associated technical challenges that need to be surmounted. Firstly, the severity of lesions in CP is heterogeneous in appearance, requiring techniques that can identify subtle and extensive lesions. Additionally, it is important to delineate all of the types of injury involved in clinical assessment, which will require multiple segmentation techniques. This is essential for examining the link between changes in anatomical structure and patient outcome. To frame the following discussion of recommended approaches for lesion segmentation in CP, Table 2.6 summarises the reviewed studies that have been applied to children with CP, or children born preterm, which is an intrinsically linked condition that leads to CP in almost half of all cases [Beaino et al., 2010].

Table 2.6 Summary of reviewed lesion segmentation approaches using structural MRIs that have been applied to children with CP or infants born preterm. Studies with (n > 25) images and using a scanner strength 3T of above has been bolded.

Articles	Description	Data	Result
Tissue segmentation in the presence of structural abnormalities			
Weisenfeld and Warfield, 2009	Automatically segment brain tissue volumes of preterm infants	10 T1- and T2-weighted MRI 1.5T	Tissue Dice similarity coefficients ~0.9 compared to manual segmentation.
Prastawa et al., 2005	Automatically segment brain tissue volumes	4 T1- and T2-weighted MRI 3T	Tissue Dice similarity coefficients ~0.7 compared to manual segmentation.
Faria et al., 2010	Quantify healthy brain development and CP-related injury	13 T2-weighted MRI 1.5T	Identify volumetric measures discrepancy from healthy development in a cohort of children with CP
Oishi et al., 2011	Quantify healthy brain development	14 T1- and 20 T2-weighted MRI 3T	Anatomical parcellation achieved greater than 0.75 Dice similarity for all anatomies.
Faria et al., 2011	Quantify healthy brain development and CP-related injury	13 T2-weighted MRI 1.5T	Identify volumetric measure discrepancy from healthy development in a cohort of children with CP
Oishi et al., 2013	Quantify healthy brain development and CP-related injury	13 T1- and T2-weighted MRI 3T	Identify volumetric measure discrepancy from healthy development in a cohort of children with CP
Yoshida et al., 2013	Quantify anatomical differences between CP sub-types	38 T1- and T2-weighted MRI 1.5T	Identify volumetric measures that are reflected in functional findings for two CP types.
Giménez et al., 2006	Track WM density and volume during development.	50 T2-weighted MRI 1.5T	Regional WM density significantly correlated with gestation age and weight (p < 0.0001).
Soria-Pastor et al., 2008	Automatically segment brain tissue volumes of preterm infants	68 T1-weighted MRI 1.5T	WM volume correlated with intelligence quotient (r = 0.32, p = 0.036).
Northam et al., 2011	Automatically segment brain tissue volumes of preterm infants	49 T2-weighted MRI 1.5T	WM and corpus callosum significant predictors of intelligence quotient (adjusted r^2 = 0.7, p < 0.001).

Segmentation of localised tissue injury			
Cheng et al., 2015	Automatically segment WM injury in preterm neonates	177 T1-weighted MRI 1.5T	Automatic segmentation difference from ground truth < $0.2cm^2$
Cortical surface based analyses			
Martinussen et al., 2005	Identify disruptions to cortical development in preterm infants	157 T1-weighted MRI 1.5T	Identified regions of significant differences in cortical thickness between healthy and preterm infants. Obtain significant correlations between cortical measure and intelligence quotient (r = 0.30-0.48, $p < 0.05$).
Xue et al., 2007	Automatically segment brain tissue volumes and characterise healthy cortical development	25 T1- and T2-weighted MRI 3T	Tissue Dice similarity coefficients ~0.75 compared to manual segmentation. Identify linear relationship between cortical measures and gestational age.
Dubois et al., 2008a	Quantify healthy cortical development	45 T1- and T2-weighted MRI 1.5T	Obtain significant correlations between cortical surface measure and volume at term equivalent age (r^2 = 0.48-0.49). Obtain significant correlations between cortical surface measure and multiple neurological outcomes (r^2 = 0.33-0.38).
Dubois et al., 2008b	Quantify healthy cortical development, and development when lesions were present	35 T1- and T2-weighted MRI 1.5T	Obtained significant correlations between cortical surface and tissue volume measures with gestational age (r^2 = 0.60-0.97).
Rodriguez-Carranza et al., 2008	Quantify healthy cortical development	15 T1-weighted MRI 1.5T	Quantify several cortical folding measures, all significantly correlated with age.
Zhang et al., 2015	Compared cortical shape measures between healthy term-born children and children born preterm	249 T1- and T2-weighted MRI 3T	Identified significant cortical shape differences between the two cohorts.
Shape analysis of subcortical structures			
No studies found.			

The classification of cerebral tissue types is a fundamental problem in the analysis of disturbances observed in children with CP. Utilizing *a priori* information is critical for achieving accurate anatomical segmentations [Ledig et al., 2012; Sabuncu et al., 2010; Wolz et al., 2010] or overcoming contrast limitations in the newborn brain [Prastawa et al., 2005]. To accommodate the severity of injury typical of CP, atlas-based approaches should incorporate *a priori* relaxation [Cardoso et al., 2009], or alternatively (or in addition) implement registration approaches that allow for more significant deformations [Djamanakova et al., 2013; Faria et al., 2011], an approach that has been applied to CP setting. Furthermore these segmentation approaches should incorporate adaptive EM approaches [Chai et al., 2015; Van Leemput et al., 1999; Lötjönen et al., 2010; Rajchl et al., 2015; Weisenfeld and Warfield, 2009; Wells et al., 1996], augmented with spatial MRF models [Zhang et al., 2001], an approach which has been validated on challenging neonatal and newborn MRIs [Prastawa et al., 2005; Weisenfeld and Warfield, 2009]. Initialising this EM approach with robust estimates of tissue distributions using FCM [Bezdek et al., 1984] or Otsu thresholding [Otsu, 1975] is recommended. In support of this proposal, these initialisation approaches which are implemented in Atropos [Avants et al., 2011], provided greater robustness to injury illustrated in Figure 2.1 compared to FreeSurfer and FAST, as the latter rely to a greater extent on prior information. Additional modifications are required to further reduce reliance on prior information and better accommodate injury, for instance by modifying spatial clique potentials based on certain tissue or spatial characteristics, in order to enhance segmentation accuracy in cases such as those presented in Figure 2.1. Although measures of tissue volume can be computed from the tissue segmentations obtained using this approach, [Chou et al., 2007; Dubois et al., 2008b; Northam et al., 2011], volume alone is not sufficient for identifying the heterogeneous range of injury observed in children with CP. Furthermore, although several studies use anatomical parcellation to track measures from diffusion MRI throughout healthy development [Faria et al., 2010; Faria et al., 2011; Oishi et al., 2011; Oishi et al., 2013; Yoshida et al., 2013], the long scanning times for diffusion MRI complicate the imaging of young children, and are currently not the standard for clinical assessment [Saunders et al., 2007]. Instead it is advantageous to assess individual focal lesions from structural MRI.

Statistical models that identify lesions as outliers to healthy tissue classes [Dugas-Phocion et al., 2004; Zacharaki and Bezerianos, 2012] may be best suited for identifying the heterogeneous range of lesions, and can be readily extended onto EM-based segmentation approaches [Van Leemput et al., 2001]. For the CP setting, detection of both WM and GM lesions are important, the latter of which remains a particular challenge [Pannek et al., 2014]. Lesions-as-outliers detection should be complemented with additional MR modalities where lesions appear as hyper-intense regions [Herskovits et al., 2001; Jain et al., 2015; Nelson et al., 2007; Tan et al., 2002], to avoid false negatives when lesion voxels resemble healthy tissue distributions. Spatial information should again be incorporated using spatial models [Bricq et al., 2008a; Karimaghaloo et al., 2012; Van Leemput et al., 2001; Sajja et al., 2004], or with matrices of expected tissue transitions within neighbourhoods that has been applied to lesion detection in preterm neonates [Cheng et al., 2015], which can enhance the specificity of lesion detection. For lesion detection in neonatal images, it is likely necessary to include healthy tissue models of myelinated and unmyelinated WM, which often have ambiguous contrast in MR images [Prastawa et al., 2005].

Analysis of cortical shape is necessary to identify the range of cortical malformations observed in children with CP. While several shape parameterisations exist, they critically rely on an accurate segmentation of the cortex. This remains a non-trivial task, despite several software packages being freely available (Table 2.5). The complex structure of the cortical surface challenges cortical segmentation [Hatfield et al., 2011], and surface inflation [Fischl et al., 1999]. These difficulties are exacerbated for CP, which can be typified by highly abnormal anatomy. The relaxation of atlas priors using EM approaches and spatial models may yield a robust cortical segmentation, while deformable models such as snakes [Kass et al., 1988] or level sets [Osher and Sethian, 1988] assist in identifying topological correspondences between cortical surfaces [Han et al., 2004; Zeng et al., 1999]. If an accurate mesh of the cortical surface can be provided, multiple characteristics of shape can be obtained, including cortical thickness [Hutton et al., 2008; Jones et al., 2000; Lerch et al., 2008; Martinussen et al., 2005] to identify pachygyria, and cortical folding [Chung et al., 2003; Joshi et al., 1999a; Tosun et al., 2006; White et al., 2003] and sulcal depth [Dierker et al., 2015; van Essen et al., 2006] to quantify the extent of several malformations, including schizencephaly, lissencephaly and polymicrogyria. All

three of these cortical measures have been used to characterise healthy cortical development or quantify interrupted development in children born preterm [Dubois et al., 2008a; Dubois et al., 2008b; Martinussen et al., 2005; Rodriguez-Carranza et al., 2008; Xue et al., 2007; Zhang et al., 2015], illustrating the potential use of these measures in the CP setting. Comparison of these shape measures to the spatially corresponding regions of healthy brains may assist in the identification and quantification of cortical injury in children with CP.

Although no study has applied shape models to the CP setting, the analysis of anatomical shape is important for detecting the enlargement of the lateral ventricles. Reviewed studies use the SSM method to construct separate healthy and pathologic models to ascertain shape differences between the cohorts [Ferrarini et al., 2008a; Gerig et al., 2001; Thompson et al., 2004]. Unlike degenerative pathologies, developmental disturbances cause highly irregular changes in ventricular shape [Truwit et al., 1992]. Hence obtaining point-wise correspondences between injured ventricular shapes is challenging. The use of normative models, constructed solely from healthy shapes, in order to minimise correspondence errors, is recommended. As normative models contain information on the natural variability in anatomical shape, the location and the extent of enlargement may be characterised as either as large deformations from this healthy model, or as regions that are not described by the healthy manifold contained in shape model. Shape modelling of subcortical anatomies [Hong et al., 2015; Kelemen et al., 1998; Patenaude et al., 2011; Styner et al., 2004] could reveal morphological injury in these physiologically important structures, which profoundly impact functional impairment [Rose et al., 2011]. Heterogeneity in anatomical shape suggests an explicit model for injured anatomies should be eschewed in favour of characterizing the extent of abnormality relative to normative shape models [Yu et al., 2007].

The clinical value of the reviewed techniques is the identification and quantification of image-derived biomarkers of brain injury, which can be correlated with clinical measures of outcomes [Dubois et al., 2008a; Martinussen et al., 2005; Nordahl et al., 2007; Northam et al., 2011; Soria-Pastor et al., 2008]. This may help provide more refined prognoses and treatments for children with CP, by providing links between brain structure and patient function to reduce inconsistencies in observed outcomes. Future studies should look to provide correlations between image findings and clinical outcomes, specifically motor

outcomes, which are the main type of limitation in children with CP. This understanding will assist in the accurate prediction of functional outcomes, which can support clinical assessment and the tailoring of treatment to individual children.

2.4 Conclusion

A review of algorithms for segmenting brain injury observed in the MRIs of children with CP has been presented in this chapter. Due to the complexity of CP, it is crucial to assess all three types of brain injury, including ventricular enlargement, cortical malformations and WM and GM lesions, which requires the use of several segmentation algorithms that will be discussed in the following chapters. In this chapter, SSMs have been identified as a method to analyse anatomical shape and to detect morphological changes caused by injury, specifically ventricular enlargement. This proposed analysis of ventricular shape using healthy SSMs to detect injury in critical periventricular anatomies is provided in Chapter 5. Additionally, multiple geometric measures of cortical shape obtained from a mesh-based model of the cortical surface are recommended from this chapter to identify of the spectrum of possible developmental malformations of the GM, which have serious implications for outcome. Critical to this method is to have a robust segmentation algorithm, incorporating relaxation strategies of atlas-based priors, and instead relying on adaptive EM algorithms with interleaved contextual spatial information via MRFs to provide robustness to injury severity. The developed brain segmentation and cortical shape analysis as part of this thesis are in provided in Chapters 4 and 6 respectively. This review has also recommended the detection of heterogeneous lesions with lesion-as-outliers approaches using multiple MR modalities. The lesion detection strategy developed during this thesis is detailed in Chapter 7 in order to correlate lesion burden with patient impairment. These automated methods are combined in Chapter 8 to assess whether the different biomarkers of injury are independent. In order to elucidate the relationships between quantifications of injury and clinical function, statistical models are first required. Therefore, in Chapter 3, a potential statistical methodology for constructing these models is discussed. Crucially, such algorithms can assist clinicians in tailoring effective, patient-specific treatment for children with CP.

3. Statistical methodology to model the relationship between brain injury and patient motor outcomes

3.1 Introduction

The automated quantification of injury from MRI allows for the construction of statistical models relating biomarkers of injury to patient outcome. This allows such approaches to provide an estimate of patient function for motor, cognitive, visual or communication tasks, to name a few, guiding clinical decisions around what type of interventions may be needed, and how intensive these interventions should be, for individual children. However, the selection of the statistical methodology in this chapter was performed using manual measures of injury based on MRI assessment, instead of using automated quantifications of injury as described in Chapters 4-7, in order to focus on the methodology itself. The work in this chapter has been published, and is available at doi:10.1007/s00247-015-3473-y.

Several manual scoring systems have been developed to standardise the radiological assessment of MRIs [Fiori et al., 2014; Inder et al., 2003; Kidokoro et al., 2013; Miller et al., 2005; Shiran et al., 2014; Sie et al., 2005; Skiöld et al., 2013]. In these methods, specific criteria of brain injury are graded based on their severity [Inder et al., 2003; Kidokoro et al., 2013; Miller et al., 2005; Shiran et al., 2014; Sie et al., 2005; Skiöld et al., 2013], or anatomical regions are given a discrete score based on whether the region contained injury or was healthy [Fiori et al., 2014; Shiran et al., 2014]. The sum of these individual sub-scores of injury provides a total measure of injury. Such techniques allow for comparisons of injury between children, which can help elucidate links between brain injury and patient function, and facilitate the prediction of patient function from imaging findings.

Although several of these MRI scoring methods were compared with clinical scores of patient function [Shiran et al., 2014; Sie et al., 2005], they inherently weight the sub-scores through separate injury scales. As with automatically computed biomarkers, there is a need to optimise the weights of these manual clinical scores in order to account for the relative impact that different injuries have on patient function, which would provide a more accurate prediction of patient outcome. It is also important for any scoring system to

consist of a succinct set of the most relevant scores of injury for a particular neurological outcome. This can improve the clinical expediency of MRI scoring methods, while maintaining its value as a predictive tool.

In this chapter, standard linear regression models are used to optimise these scoring systems in two ways. The first of these developments was to weight the individual injury scores in order to minimise the residual variance between the predicted score of function with measures of bimanual coordination. These model weights take into account that the various parts of the brain have different degrees of impact on the overall neuro-cognitive and motor function of children with cerebral palsy. The second development was to reduce the number of individual injury scores in the scoring method. A major risk of using a large number of independent variables is overfitting, which while giving good results on training data will not generalise to unseen data. Reducing the number of injury scores minimises the risk of over-fitting the linear models, with the aim of improving both the accuracy of predicting impaired motor function in unseen data as well as the clinical expediency of injury quantification in children with CP. These developments are applied to the semi-quantitative scale for brain lesion severity introduced by Fiori et al. [Fiori et al., 2014], and relate these measures of injury to the AHA clinical score for bimanual hand function. However these developments can be applied on any quantitative radiological scoring scale, or extended to any correlation analyses between image-derived measures and patient outcome [Cioni, 2000; Kulak et al., 2007; Mercuri et al., 1999; de Vries et al., 1998; Yokochi et al., 2008]. This addresses Aim 2 of the thesis, “establish a statistical methodology that translates image-derived measures of injury severity to patient functional impairment, and thus determine the elucidated impact between brain injuries to patient outcomes”.

3.2 Materials and Methods

3.2.1 Study Participants

Image data used in this chapter, and throughout the rest of this thesis, were obtained from The University of Queensland Cerebral Palsy and Research Rehabilitation Centre (QCPRRC), Brisbane, Australia, and the Stella Maris Fondazione, Pisa, Italy. Study participants included children who were recruited as part of ongoing studies of children with unilateral CP [Boyd et al., 2013a; Boyd et al., 2013b]. For both studies, ethical

approval was granted from the appropriate ethics committees. Informed parental consent was obtained for all participants from both studies. Data were included based on the clinical phenotype of unilateral CP, diagnosed by the same experienced clinician. Children with the clinical phenotype of bilateral CP were excluded from this study.

Of the total children recruited in these ongoing studies, a total of 139 children were included for the studies constituting Chapters 3 through to 8 of this thesis. This includes 95 children with clinically diagnosed CP (50 male, 45 female, mean age 11.4, age range 5-17), and 44 typically developing children (TDC) with no observed diagnosis of injury (15 male, 29 female, mean age 10.7, age range 7-16). Chapters 5, 6 and 8 include this entire cohort, while only a subset of this data were used in the remaining chapters, which is defined within the specific chapters.

3.2.2 MRI acquisition

T1-weighted magnetisation-prepared rapid acquisition with gradient echo (MPRAGE) images for the whole cohort (*n* = 139) detailed in Section 3.2.1 were acquired from one of two scanners, and one of three sets of scanning parameters: including 106 images acquired with a 3T MR-system (Siemens, Germany) scanner (TR = 1900 ms, TE = 2.32 ms, flip angle = 9 degrees), 19 images acquired with a 1.5T system (General Electric, USA) scanner (TR = 12.36 ms, TE = 5.17 ms, flip angle = 13 degrees) and 14 images acquired with a 1.5T system (General Electric, USA) scanner (TR = 124.29 ms, TE = 4.37 ms, flip angle = 10 degrees).

A subset of recruited children (*n* = 125) also underwent either T2 Turbo Inversion Recovery Magnitude (TIRM) (TR = 7000 ms, TE = 79 ms, flip angle = 120 degrees, slice thickness = 4 mm, *n* = 116) or T2 Half-Fourier Acquisition Single-Shot Turbo Spin-Echo (HASTE) (TR = 1500 ms, TE = 81 ms, flip angle = 150 degrees, slice thickness = 4 mm, *n* = 112), acquired using a 3T Siemens' scanner.

3.2.3 Magnetic Resonance Imaging scoring technique

Out of the entire cohort described in Section 3.2.1, a subset of 76 children were scored using the semi-quantitative brain lesion severity scale by a single child neurologist [Fiori et al., 2014]. For each child, the MPRAGE and TIRM images were used for scoring injury. Both modalities are important for assessing the full range of injury observed in children with CP, to avoid incorrect estimates of injury severity. In this scoring technique, after

visually assessing the MRI scans, any observed tissue abnormality was manually drawn onto the closest of the six representative slices from the brain on the graphical template. The cerebral lobes (temporal, frontal, parietal and occipital) were traced according to the Talairach atlas [Talairach and Tournoux, 1988], on the graphical six-axial-slice template, and further divided into periventricular, middle and cortico/subcortical WM layers. Each of these regions were scored either '0' if the anatomy was not impacted on any slice, '0.5' if the anatomy was impacted on less than half of the axial slices it was present, '1' if the anatomy was impacted on more than half of the axial slices it was present. Subcortical structures (e.g. basal ganglia, thalami, brainstem and posterior limb of the internal capsule (PLIC)), corpus callosum and cerebellum were scored either ‘0’ or ‘1’ if not impacted or impacted respectively. Anatomical scores were added together to produce aggregated measures of hemispheric (contralateral or ipsilateral to the clinical side of hemiplegia) and of global injury. This scoring technique was found to be a reliable measure of injury, and both the intra-rater and inter-rater reliabilities exceed 0.85 observed from the global scores from 34 children [Fiori et al., 2014]. An example of a completed form is provided in Figure 3.1.

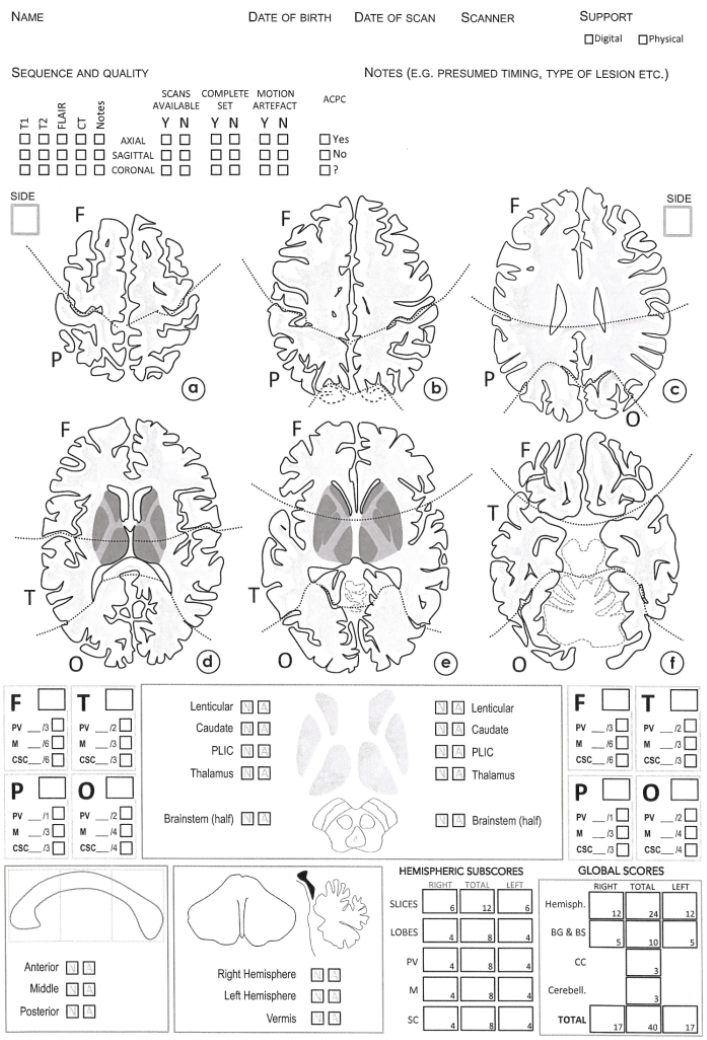
NAME
DATE OF BIRTH
DATE OF SCAN
SCANNER
SUPPORT
Digital
Physical
SEQUENCE AND QUALITY
NOTES (E.G. PRESUMED TIMING, TYPE OF LESION ETC.)
T1
T2
FLAIR
CT
Notes
SCANS AVAILABLE
COMPLETE SET
MOTION ARTEFACT
ACPC
AXIAL
SAGITTAL
CORONAL
Yes
No
SIDE
F
P
T
O
Lenticular
Caudate
PLIC
Thalamus
Brainstem (half)
Anterior
Middle
Posterior
Right Hemisphere
Left Hemisphere
Vermis
HEMISPHERIC SUBSCORES
GLOBAL SCORES
RIGHT
TOTAL
LEFT
SLICES
LOBES
PV
M
SC
Hemisph.
BG & BS
CC
Cerebell.
TOTAL

(a)

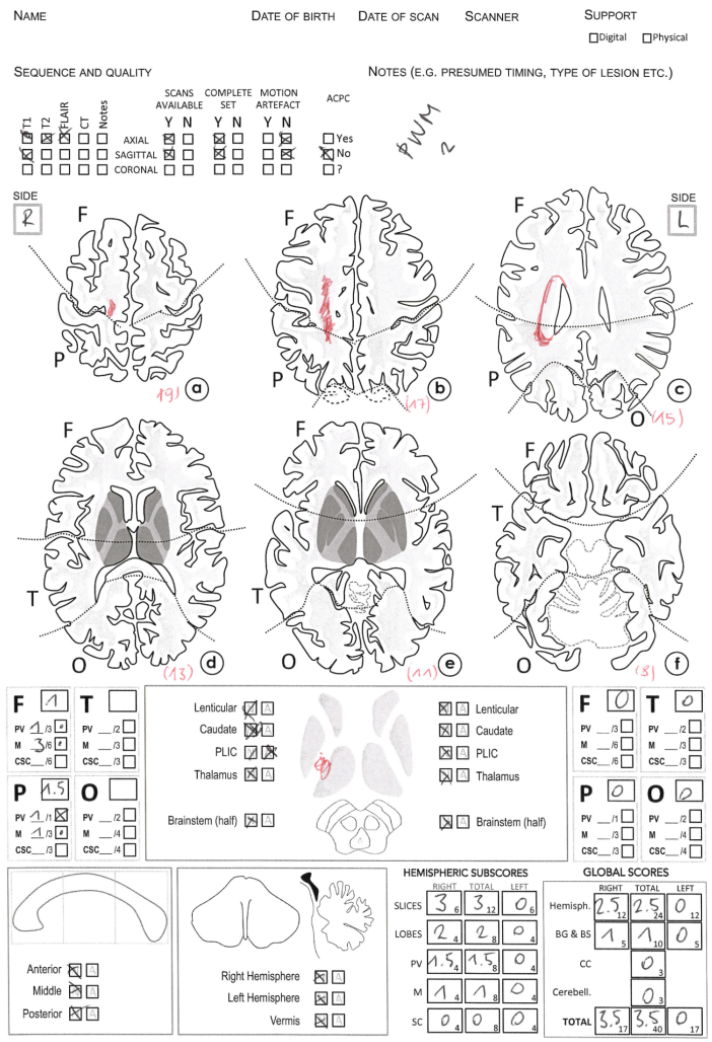
NAME
DATE OF BIRTH
DATE OF SCAN
SCANNER
SUPPORT
Digital
Physical
SEQUENCE AND QUALITY
NOTES (E.G. PRESUMED TIMING, TYPE OF LESION ETC.)
SCANS AVAILABLE
COMPLETE SET
MOTION ARTEFACT
ACPC
AXIAL
SAGITTAL
CORONAL
Yes
No
PWM
SIDE
F
P
T
O
Lenticular
Caudate
PLIC
Thalamus
Brainstem (half)
Anterior
Middle
Posterior
Right Hemisphere
Left Hemisphere
Vermis
HEMISPHERIC SUBSCORES
GLOBAL SCORES
RIGHT
TOTAL
LEFT
SLICES
LOBES
PV
M
SC
Hemisph.
BG & BS
CC
Cerebell.
TOTAL

(b)

Fig. 3.1 (a) The template used in the semi-quantitative scale for brain lesion severity introduced by Fiori et al. [Fiori et al., 2014]. Patient details and available MR-sequences are filled in at the top of the template. Six representative axial slices are portrayed below, to allow any observed injury from the MRI to be translated onto this form. This injury is quantified in the boxes below. Left and right hemispheres of the frontal (F), temporal (T), parietal (P) and occipital (O) lobes are split in to periventricular (PV), middle (M) and cortical/subcortical (CSC) regions. These regions are scored '0' if the region is uninjured on any of the axial slices that it is present, '0.5' if the region is affected in fewer than half of the axial slices that the region is present, or '1' if the region is affected in more than half of the axial slices that the region is present. The lenticular nucleus, caudate nucleus, PLIC, thalamus and brainstem are scored dichotomously, '0' if uninjured or '1' if injured. The corpus callosum is divided into three parts; anterior, middle and posterior, and the brainstem is divided into left and right hemispheres, and the cerebellar vermis, as shown at the bottom of the template. These scored regions are then added in the set of boxes on the lower right of the form, to give a total measure of injury that is out of 40 (the maximum score). (b) Shows an example of a completed template. Observed injury from the MRI is drawn in red, with filled in red regions showing PWM injury, and the red outline from the ventricle illustrating ventricular enlargement. The red numbers below the axial slices denote with axial slice of the image each slice corresponds to. Scores of '0' are left blank, scores of '0.5' are denoted with a dot and scores of '1' with a cross. The sum of these scores to produce a total injury score are shown in the bottom right of the template.

3.2.4 Patient function scoring

For most of the children involved in this study (*n* = 89), several clinical scores of patient function were measured 0-22 weeks after MRI scanning as part of the ongoing studies on children with CP [Boyd et al., 2013a; Boyd et al., 2013b], in order to provide an overview of patient function. In this thesis, six of those clinical scores were utilised to represent patient motor, cognitive, visual and communicative function. The Assisting Hand Assessment (AHA) was used to quantify the motor capabilities of children with CP, specifically the function of the impaired hand as an assisting hand in bimanual tasks. The AHA score ranges from 0 and 100, with larger scores indicating greater ability from the impaired hand during these tasks. Although not a measure of gross motor function, the Rasch measured AHA score was used for several reasons. Firstly, this score has a wide dynamic range (from 0 to 100) making it more suitable for regression analyses compared to the GMFCS, which only has five levels. Furthermore, most study participants had a GMFCS level of either I or II, making the measure of upper limb manual ability more relevant for this cohort. Additionally, this measure has been shown to be a reliable and responsive measure for children with unilateral CP [Krumlinde-Sundholm et al., 2007]. Finally, it does not contain information on laterality, referring solely to the assisting hand. In this chapter, the multiple correlation between the optimised MRI-based score and the AHA measure was used as a measure of goodness of fit of the model.

Other measures of patient function were also recorded, and are utilised in the following chapters of this thesis. Measures of patient cognition, although difficult to quantify, is measured in this study using two parent reported questionnaires scoring their child's behavioural and emotional function in daily life; the Behaviour Rating Inventory of Executive Function (BRIEF) [Gioia et al., 2002] and Strengths and Difficulties Questionnaire (SDQ) [Bourdon et al., 2005]. To quantify visual acuity in this study, the Test of Visual Perception Skills (TVPS) measure [Frostig et al., 1961] was utilised to assess the child's ability to discriminate and memorise visual cues. Communicative ability was quantified in this study using the vocabulary (VOC) and word reasoning (WR) subtests of the Wechsler Preschool and Primary Scale of Intelligence (WPPSI-III) [Wechsler, 1967], which assess the child's ability to express and comprehend language, respectively.

3.2.5 Template pre-processing

Since the cohort was recruited on the basis of unilateral symptoms, it was assumed that the contralateral/ipsilateral relationship was more relevant to motor function than left/right handedness, accounting for the brain's strong bilateral symmetry [Rickard et al., 2000]. Hence, prior to analysis, the anatomical scores on the template were left-right flipped to align the side of the brain with greater injury, termed the ipsilesional side. The anatomical regions on the side of less damage, termed the contralesional side, were removed from the subsequent analysis. Considering ipsilesional injury only makes the assumption that the more injured side is associated with the assisting hand, in line with current knowledge [Holmström et al., 2010], and hence is more predictive of performance. This step halves the number of features considered, increasing the power of the analysis to better support the conclusions, and reducing the risk of overfitting. Moreover, despite the cohort containing 20 children with bilateral injury, injury is relatively infrequent on the contralesional side. The extent of injury laterality is investigated in both cohorts using a laterality index, which was computed using the template-derived score of injury of the left hemisphere, S_L, and right hemisphere, S_R, as shown in the following equation.

$$Laterality\ index = \frac{S_L - S_R}{S_L + S_R} \qquad Eq\ 3.1$$

Children were divided into PWM and CDGM cohorts by a child neurologist according to the classification of pathogenesis [Krägeloh-Mann and Horber, 2007]. These classes of injury differ in both their aetiology and the presumed timing of the insult during development, and have different impacts on functional outcomes [Aisen et al., 2011].

3.2.6 Statistical Methodology

The relationship between anatomical measures of injury and patient outcomes were investigated using multivariable linear regression models. In these models, the injury scores for each anatomy are the independent (predictor) variables, and the AHA motor score is the dependent (criterion) variable. The partial regression coefficients of these regression models encode the optimal, relative weights of the individual template-derived anatomical injuries in impacting AHA. This analysis was performed using R statistical software Version 3.1.1 [The R Development Core Team, 2008]. To test the normality assumption of the linear models, a normal quantile plot is constructed for each regression model. This result is supplemented with the Shapiro-Wilk [Shapiro and Wilk, 1965] test of

normality for the normalised residuals of each model. This tests the null-hypothesis that the residuals are normally distributed.

As cerebral injury may impact adjacent areas, a data-driven analysis was performed using the 'stepAIC' package in R. Variables are successfully added and removed in a greedy fashion to minimize the Akaike Information Criterion (AIC) function. The number of variables is controlled by the regularization coefficient, leaving a parsimonious set of anatomical regions that best describe the variance in the AHA measure. For this work the default value of 2 was used for this penalty term. This method was chosen as feature selection can be robustly performed using AIC [Ronchetti, 1985], minimising the effect of model overfitting. In this approach, the default 'stepAIC' parameters were chosen. To limit sensitivity of the data-driven approach in both cohorts, anatomical regions that were impacted in five or fewer children were removed prior to constructing the linear model. Interaction effects, which describe when the simultaneous influence of two injury measures on the AHA measure is also multiplicative, were not included in these models due to the limited amount of data available relative to the large number of parameters needed to model them.

The bootstrapping approach was used to assess how well the model generalised, by measuring the extent of variance in the partial regression coefficients in response to selecting a different subset of data. This method repeatedly samples a random subset of the data from the linear model, and constructs a regression model with the corresponding predictor variable for each chosen subset. This yields a standard error for each partial regression coefficient. In this analysis, 1500 subsets were sampled for each linear model.

A power analyses was performed to quantify the risk of not detecting the relationship between injury score and patient outcome when such a relationship exists, given the available data (52 and 24 cases for each cohort). For these analyses, the desired significance level was chosen to be the standard P = 0.05. As an estimate of effect size, Cohen's f^2 formula for multivariable regression models was used, which depends on the squared multiple correlation of the linear model, R^2, and is defined as:

$$f^2 = \frac{R^2}{1 - R^2} \qquad Eq\ 3.2$$

Using a conservative multiple correlation value of 0.15, which is sufficient to detect small relationships between the anatomical scores and the AHA measure, gives an f^2 measure of 0.18. This measure represents the strength of the associations in the regression model, and falls within the small to medium range for the f^2 measure (0.1 - 0.25) [Cohen, 1988]. The chosen power for this analysis was also set to a conservative value of 0.8, which indicates that there is a 20% chance of committing a Type II error, i.e. a false negative.

3.3 Results

3.3.1 Cohort demographics

Seventy six T1-weighted and fluid-attenuated inversion recovery MRIs were obtained from 76 children. The demographics of the PWM, CDGM and combined cohorts are outlined in Table 3.1. A histogram characterizing the extent of laterality of injury in this combined cohorts is given in Figure 3.2.

Table 3.1. Demographic characteristics for the PWM, CDGM, and the total combined cohort of children with unilateral cerebral palsy.

Cohort	PWM	CDGM	Total
Total No. Samples	52	24	76
Gender			
Male	29	12	41
Female	23	12	35
Age at scan (years)			
Mean ± standard deviation	11.1 ± 3.3	12.3 ± 2.3	11.6 ± 2.8
Range (minimum - maximum)	5 - 17	7 - 17	5 - 17
Global brain injury severity score [Fiori et al., 2014]			
Mean ± standard deviation	7.7 ± 4.4	13.1 ± 4.1	9.4 ± 5.0
Range (minimum - maximum)	0 - 21	2 - 18.5	0 - 21
Number with bilateral lesions	18	2	20
Assisted Hand Assessment Score			
Mean ± standard deviation	68.5 ± 18.8	52.2 ± 23.5	63.4 ± 21.6
Range (minimum - maximum)	27 - 98	8 - 98.8	8 - 98.8

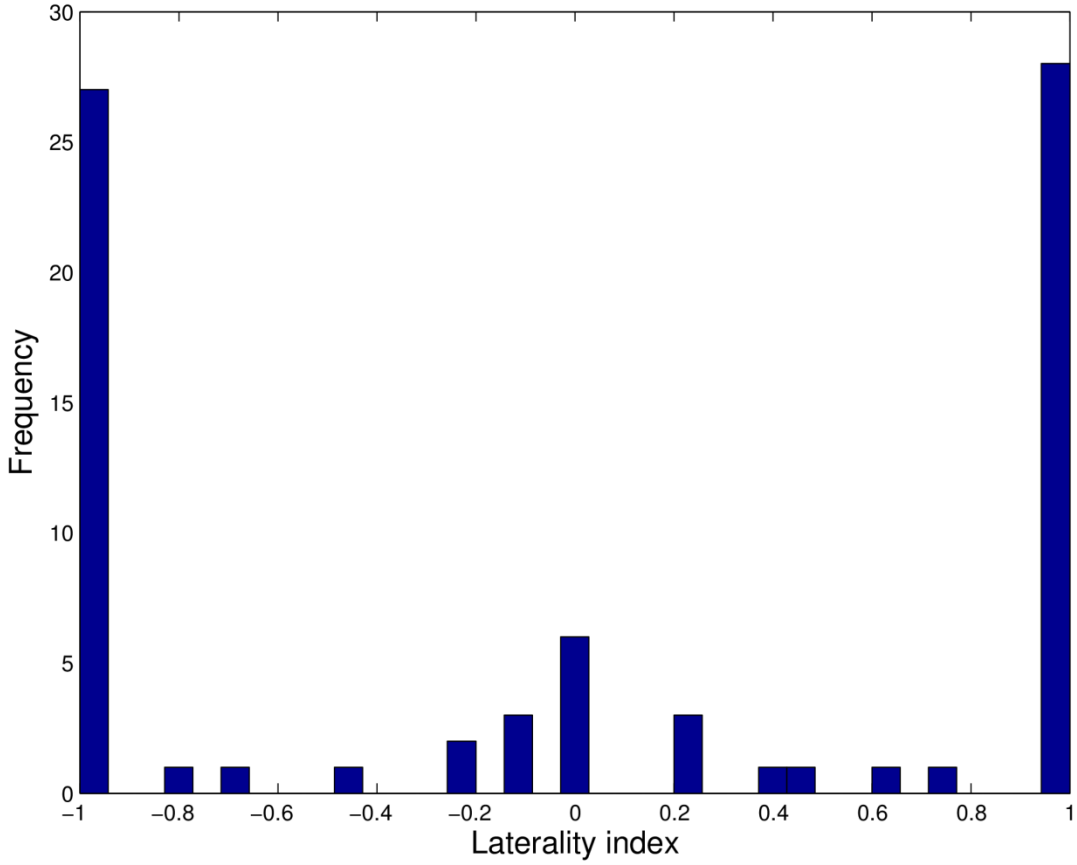

Fig. 3.2 A histogram of laterality indices, measuring the lateral asymmetry of injury in the children included in this analysis. A score of -1 indicates lesions were solely in the right hemisphere, +1 indicates lesions were solely in the left hemisphere. Measures close to 0 indicate symmetrical lesions.

3.3.2 PWM cohort findings

The data-driven approach identified six important regions, including the thalamus, the caudate nucleus, and the vermis of the cerebellum. Four of these variables were found to be statistically significant, including the cortical/subcortical region of the occipital lobe, caudate nucleus, thalamus, and the vermis of the cerebellum ($p < 0.05$). The full list of regions and the corresponding coefficients of this linear model are shown in Table 3.2. The standard errors of both the complete and bootstrapped models were comparable.

Table 3.2. Retained data-driven anatomical regions, and their respective weights, for the PWM phenotype. Statistically significant variables are shown in bold.

Brain region	Partial regression coefficient	Standard error	p-value	Bootstrap standard error
(Intercept)	69.95	6.92	<0.0001	6.88
Medial frontal lobe	25.30	12.66	0.0519	12.18
Cortical/subcortical frontal lobe	-37.04	18.69	0.0538	18.54
Cortical/subcortical occipital lobe	46.98	17.99	0.0123	18.17
Caudate	-15.68	6.69	0.0236	6.47
Thalamus	-19.10	4.77	0.0002	4.62
Cerebellum vermis	29.22	11.42	0.0140	11.04

The features obtained from the data-driven approach explained 45% of the variance seen in the AHA score ($p < 0.0001$), while less than 1% of the variance in the AHA score was explained by the unweighted score (R squared < 1%, $p = 0.9$).

3.3.3 CDGM cohort findings

The data-driven approaches identified seven important anatomical regions, which included the PLIC, the caudate nucleus and the brainstem. The complete list of variables retained by the data-driven approach, and the corresponding partial regression coefficients, are provided in Table 3.3. All features retained by the data-driven approach were significantly associated with the AHA measure ($p < 0.05$). Table 3.3 highlights the standard error for these coefficients, obtained from bootstrapping, which were comparable to the standard error of the data-driven model.

Table 3.3. Retained data-driven anatomical regions, and their corresponding weights, for the CDGM phenotype. Statistically significant variables are shown in bold.

Brain region	Partial regression coefficient	Standard error	p-value	Bootstrap standard error
(Intercept)	18.38	15.70	0.2588	7.63
Periventricular temporal lobe	-25.13	7.67	0.0047	11.07
Medial occipital lobe	-39.41	12.27	0.0054	18.82
Cortical/subcortical occipital lobe	53.60	14.86	0.0023	21.23
Caudate	-18.72	6.78	0.0139	10.22
Posterior limb of the internal capsule	67.72	15.34	0.0004	N/A
Brainstem	-27.24	7.63	0.0026	10.04
Middle corpus callosum	16.57	5.78	0.0112	8.85

The partial regression coefficients for the data-driven variables for the PWM and CDGM cohorts are visually portrayed in Figure 3.3. In this figure, the ipsilesional side is portrayed visually as the left side.

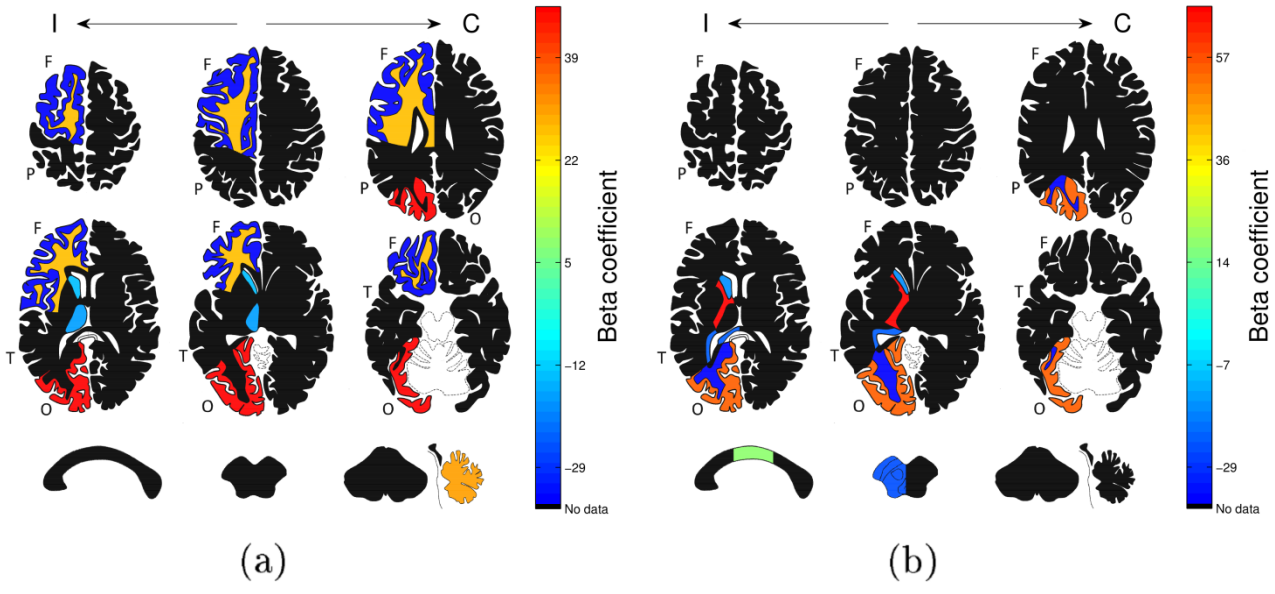

Fig. 3.3 An illustration of the partial regression coefficients obtained for the linear models fitted using the data-driven variables, for the (a) PWM and (b) CDGM cohort. Black colours represent a zero value.

Regions selected by the data-driven approach explained 84% of the variance in AHA (p < 0.0001), while the unweighted, complete template score explained 44% of the variance in AHA (p = 0.0004). A summary of the squared multiple correlations of both linear models for the PWM and CDGM cohorts are shown in Table 3.4.

Table 3.4. Summary of the squared multiple correlations between both the template-derived score and the optimised regression models with the AHA measure.

Cohort	**PWM**		**CDGM**	
	R squared	P Value	R squared	P Value
All anatomical regions, unweighted	<0.001	NS	0.44	<0.001
Subset of regions, weighted	0.45	<0.001	0.84	<0.001

NS not significant.

3.3.4 Assessment of normality

To assess the normality assumption of both linear models, a normalised quantile plot of the model residuals is presented in Figure 3.4. Normalised distributions visually appear in this plot close to the theoretical $y = x$ line. Both quantile plots appear visually close to this line. A Shapiro-Wilk normality test is also applied to these model residuals. For both PWM (W = 0.975, p = 0.352) and CDGM (W = 0.983, p = 0.947) cohorts, the lack of statistical significance implies that the null hypothesis is retained, i.e. that the residuals from both models are normally distributed. Both these results imply the normality assumption of the regression models is not violated, indicating the distributions of both dependent and independent variables are normally distributed.

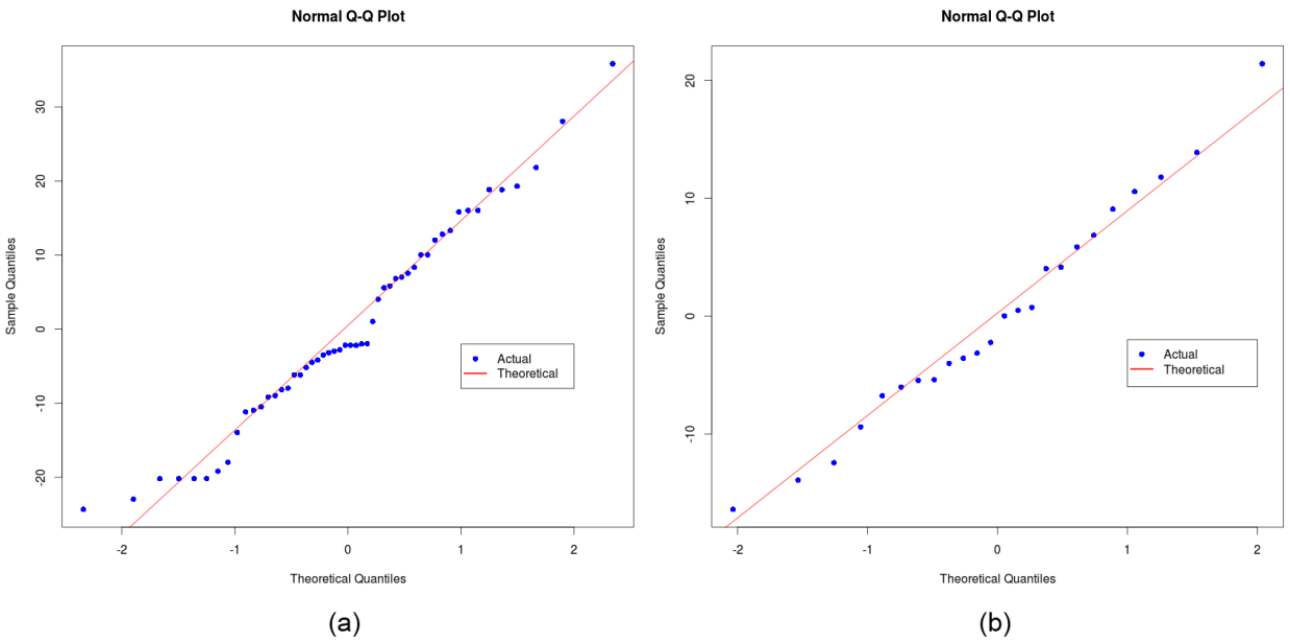

Fig. 3.4 Normal quantile plots of the regression model residual from the (a) PWM and (b) CDGM cohorts.

3.3.5 Model stability

For the linear models of both PWM and CDGM cohorts, the error associated with each partial regression coefficient was similar to the error of the bootstrapped model, as shown in Tables 3.2 and 3.3. The slightly larger discrepancy between these two errors observed in the CDGM cohort aligns with the fewer children in this clinical phenotype. Similarity in model and bootstrap errors demonstrates that the fitted models are an accurate representation of the structure-function relationship evident in this cohort, and hence should accurately predict impaired motor function in previously unseen MRI data.

3.3.6 Power analysis

Computing the statistical power of using all ipsilesional template anatomies, given the number of samples in both cohorts and a statistical significance of p = 0.05, was 0.18 and 0.06 for PWM and CDGM cohorts respectively. This indicates that there is an 84% and 94% chance of committing a Type II error. Performing the same power analysis for the optimised models which contained fewer anatomical regions, as well as a different f^2 measure based on the squared multiple correlations of the models (0.45 and 0.84, respectively), the model power was 0.85 and 0.79 for PWM and CDGM cohorts

respectively. The reduced number of anatomical regions (6 and 8, respectively) lowered the chance of a Type II error among these optimised models.

The power analysis revealed that a sample size of 141 is required for either cohort to produce a linear model able to correctly detect a relationship between all scored anatomies (when not discarding any regions on the template) and AHA score (corresponding to an overall R^2 of 0.15 for the model) with a power of 80% and a statistical significance of $p = 0.05$.

3.4 Discussion

In this chapter, two developments for the semi-quantitative MRI scale of brain injury severity for children with CP proposed by Fiori et al. [Fiori et al., 2014] were demonstrated, which will be used as the statistical methodology for the rest of this thesis. This methodology includes reducing the number of regions on the template for both PWM and CDGM phenotypes, which is desirable to avoid over-fitting the data, and weighting these regions using linear models, which allows the relative importance of anatomical regions to be accounted for. Although this weighting introduces additional work for clinicians using the template, it is offset by the reduced number of anatomical features considered. Since the two cohorts considered in this analysis had a clinical phenotype of hemiplegia, this initial reduction in variables was achieved by discarding regions on the contralesional side. The ability to report on children by hand also means that the modelling of interactions should be avoided, as the number of calculations would increase with the square of the number of features considered. Hence, care must be taken to select anatomical regions that are relatively independent of each other. The results shown here demonstrate that, using a small number of independent anatomical features, equal or better prediction of functional AHA score can be obtained.

The greater multiple correlation obtained for the data-driven selected variables was expected, as the step-wise selection method attempts to maximise the association by selecting a set of variables that best explain the variance in the AHA score. This set of anatomical regions for the PWM phenotype consisted of regions known to be important for motor function, including the caudate nucleus, thalamus and the cerebellar vermis [Doya, 2000; Herrero et al., 2002; Hikosaka et al., 1989]. These regions are consistent with the known clinical phenotype of periventricular leukomalacia (PVL), with both caudate nucleus

and thalamus being strongly associated to injury in the adjacent WM fibres. Additionally, this data-driven approach led to a large and significant increase in squared multiple correlations between the image-based score and the AHA score over the unweighted, complete template. This demonstrates the better predictive performance of the proposed approach, particularly for the PWM phenotype where the unweighted template score explained little of the variance in the AHA score. Furthermore, this approach suggests that the template can be reduced from 40 to 6 anatomical regions for this phenotype.

Similar to the PWM cohort, substantial co-dependence between anatomical regions exists in the CDGM cohort, enabling a substantial improvement in multiple correlation to be obtained. The data-driven approach indicated that the template can be simplified to 7 anatomical regions for the CDGM phenotype. The anatomical weightings were estimated with greater confidence than the PWM phenotype, and highlighted regions such as the caudate nucleus, brainstem and corpus callosum that are known to be important for motor function [Hikosaka et al., 1989; Takakusaki et al., 2004; Wahl et al., 2007]. Note that the PLIC was removed in the bootstrap method for this cohort as it was impacted in the majority of children with CDGM injury, preventing a standard error to be computed for many of the randomly chosen subsets. This highlights the importance of having data that contains a diverse range of injury for each anatomical region.

The linear models of both cohorts highlighted deep GM structures as significant, which highlights their known role in motor function. However the greater number of anatomical regions retained in the model for the CDGM cohort reflects the typically larger anatomical involvement of this phenotype, where injury arises from disturbances in cortical organisation and migration [Barkovich et al., 2012]. In addition, the wider extent of injury among this cohort and the understanding that this form of injury arises from migrational disturbances earlier in development, likely resulted in the inclusion of the corpus callosum and brainstem respectively [Hetts et al., 2006; Leong, 1997]. The involvement of the occipital lobe in both linear models suggests that the children's visual impairment may have impacted their bimanual tasks during motor assessment [Stoerig, 2006]. There are further differences in which cerebral lobes were retained from the data-driven approach between the cohorts, for instance the medial frontal lobe was retained the PWM cohort and the temporal lobe was retained in the CDGM cohort. While these regions do not have a solely motor role, they are associated with perception and recognition [Eichenbaum et

al., 2007; Owen et al., 1990], which may influence performance in the children's motor assessment and thus be retained in the linear models.

The data-driven method was unexpectedly found to discard anatomical regions that medical knowledge suggest as important for impacting upper limb motor function. This inconsistency arises from the presence of associated injuries occurring in multiple anatomical regions, and the efforts of the data-driven approach to select regions that explain a unique portion of variance in the AHA score. In the PWM cohort, this is illustrated in the exclusion of the PLIC capsule using the data-driven approach. Although the PLIC is known to be important for motor function, injury in this region was strongly correlated with injuries in the thalamus, so only one of these anatomical regions was selected. It has recently shown using diffusion weighted MRI and probabilistic tractography that sensorimotor thalamic WM pathways have more influence on motor function control of the paretic hand than does preservation of PLIC based corticospinal tracts [Rose et al., 2011], highlighting the role of injury to the thalamus in cerebral palsy.

A limitation of this analysis was the relatively low number of participants in each of the two clinical phenotypes. Despite the bootstrapping method illustrating comparable standard errors to the linear models fitted using all children for both PWM and CDGM cohorts, future studies should look to perform similar analyses on a greater set of data for both PWM and CDGM phenotypes. This will assist in identifying the relative importance of anatomical regions that are more representative of the structure-function relationships of all children with a specific CP phenotype, which would lead to improved predictions of clinical outcomes from image-derived measures. Another limitation of this proposed methodology is that it does not account for the effect of plasticity, the capability of the brain to reorganise and regain certain functions after injury through alternate WM pathways, which depends on a multitude of factors [Belsky and Pluess, 2009; Chapman et al., 2003]. The translation of specific patient functions to other spatial regions of the brain confuses the underlying structure-function relationship of the healthy brain, and will appear as noise within the linear model. This may also be overcome by utilizing diffusion MRI, which can elucidate altered WM connections arising from neuroplastic mechanisms. Structural and diffusion MRI was used in conjunction with the semi-quantitative brain lesion severity scale to explore the relationship between brain injury and motor and sensory function with insights into the mechanisms of plasticity [Fiori et al., 2015].

The results have several potential implications. Firstly, when the CP phenotype is known, the utilisation of weighting enables the number of anatomical regions scored during evaluation of MRIs to be reduced from more than 40 to 6-7. This has the effect of not only simplifying the clinical evaluation of children with CP, but substantially improving the squared multiple correlation between lesions observed on MRI images and the clinical assessments of motor function. The greater prediction of a clinical outcome using fewer scored anatomies motivates the clinical use of quantitative approaches as suggested by Fiori et al. [Fiori et al., 2014], and highlights the value that can be captured by quantifying injury in this manner. Future developments of this scoring method should focus on two areas. Firstly, this method may be optimised to any functional outcome of interest, such as Gross Motor Function Measure, a more general measure of overall motor function. Measures of cognitive function, communicative ability and vision acuity would also be of interest. Producing models which correlate scores of injury with multiple clinical scores allow for a more encompassing prediction of patient outcome. Secondly, the use of computer-based tools could further enable enhanced injury segmentation and volume assessment, allowing for large scale population analyses of MRIs. These enhanced characterisations of injury may help elucidate the relationship between brain lesion severity and functional correlates for each phenotype, which would enable better prediction of future outcomes and inform the tailoring of interventions.

3.6 Conclusion

This chapter has presented a statistical methodology for finding a succinct set of brain injuries strongly associated with motor outcome in children with CP. This method was applied to the standardised, semi-quantitative scale of brain lesion severity for assessing MRIs of specific CP injury phenotypes, weighting individual anatomical regions, allowing for a simplification of the scoring system, reducing the number of scored regions examined from 40 to fewer than 8. This led to an improved prediction of the clinical AHA measure, compared to the unweighted, complete template score (R squared 0.45 from <0.01 for the PWM cohort, 0.84 from 0.44 for the CDGM cohort). Optimisation of MRI scoring systems using this approach reduces the time taken to manually score each image, and can potentially provide important insights on the relationship between the topography of brain lesions and clinical function in children with CP. These developments provide a framework for the biomarkers of injury, computed using the automated approaches detailed in Chapters 4 to 8, to not just quantify injury but model the brain's structure-function relationship, and produce estimates of patient impairment and function. Consequently, these predictions of outcome has many implications for the selection of what interventions may be necessary, targeting motor, cognitive, communicative or visual function, unilateral or bilateral inventions, and how intensive these therapies should be.

4. Brain tissue segmentation in the presence of severe injury

4.1 Introduction

Brain tissue segmentation is an important preliminary step before the modelling of ventricle shape, measuring of cortical morphology or segmentations of lesions can be performed. For instance, an accurate segmentation of the GM is necessary to compute meaningful measures of the cortical surface that can be used to predict patient outcome and aid in implementing effective interventions. Automated segmentation methods are required in these instances, as a manual segmentation of this surface is infeasible on large data sets. Despite the wealth of automated techniques presented in Chapter 2, this remains a challenging task as the organization of the cortical surface or subcortical regions can be significantly different in children with severe developmental injury.

The EM algorithm [Dempster et al., 1977] has frequently been used for the automated segmentation of brain MRI data [Van Leemput et al., 1999; Wells et al., 1996]. This approach allows for iteratively interleaved image bias correction [Pohl et al., 2002], and a spatial consistency of labels through the MRF [Zhang et al., 2001]. It has been frequently applied to neonatal data sets [Cardoso et al., 2011; Makropoulos et al., 2012; Murgasova et al., 2006] due to the robustness of the segmentation in the presence of high noise, significant partial volume effects, lack of tissue contrast, and extensive anatomical variability typical of these data sets. Despite EM being an adaptive approach, these studies typically utilize atlases to initialize the EM parameters, or iteratively scale the tissue probability of each voxel by the expected tissue prior from an atlas. To deal with anatomical variability, a non-rigid registration is performed to align the atlas priors to the data, and the influence of the atlas is subsequently reduced with a relaxation parameter that allows for more data-driven segmentation in later iterations [Cardoso et al., 2011; Makropoulos et al., 2012]. However in cases of severe injury, non-rigid registration typically fails and even with partial relaxation of the atlas priors, the discrepancies between the anatomical assumptions of the normative atlases and children CP are too great to provide a robust initialization.

The limited relevance of atlas based priors for this application places more of the burden of accuracy on non-atlas priors defined by the clique potentials, which is a term that describes the relative cost on the frequency of tissue labels appearing in a small

neighbourhood of voxels. Hence, in this chapter, a modification to the formulation of the local clique potentials within the adaptive EM algorithm is proposed, to enable an improved segmentation of the cerebral cortex in the structural MRI of children with CP. Using 23 T1-weighted MRIs of children, of which 17 were children CP exhibiting severe cortical malformations, the proposed approach was compared to four widely used methods: FreeSurfer [Fischl, 2012], NiftySeg [Cardoso et al., 2011], FSL's FAST [Zhang et al., 2001]) and ANT's Atropos [Avants et al., 2011]. The FreeSurfer software uses a data-driven deformable surface approach, initialized by registration to an atlas, to detect the inner and outer surfaces of the cortical GM, while NiftySeg, FAST and Atropos use an EM segmentation algorithm with an incorporated MRF and interleaved bias correction. The proposed approach is demonstrated to be able to accurately model the cerebral cortex in the presence of large injury variability, in comparison to FreeSurfer, NiftySeg, FAST and Atropos. This work addresses Aim 1 of this thesis, "develop several automated segmentation approaches to delineate the three main classes of injury observed in children with CP; cortical malformations, WM injury and ventricular enlargement", as well as Aim 3, "[comparing] the automated results against a manual gold standard, as well as the current state of the art". The work in this chapter has been published, and is available at doi:10.1109/DICTA.2015.7371257.

4.2 Materials and methods

4.2.1 Study Participants

The entire cohort described in Section 3.2.1 was included in this chapter for brain tissue segmentation. Method validation was performed on a subset of this cohort, including 23 T1-weighted volumes, of which 17 were children with CP and severe alterations observed from the MRI. The mean age at the time of the scan was 12.04 ± 2.40 years (range 7-15 years), while the male to female ratio was 9/14. These images were manually segmented on the hemisphere of injury by two raters.

4.2.2 Image pre-processing

Several pre-processing steps for the T1- and T2-weighted MRIs were implemented to assist downstream methods. Bias correction was performed using the N4 algorithm [Tustison et al., 2010]. An affine transform was used to register the MRIs to the Colin 27 Average Brain Atlas [The McConnell Brain Imaging Centre, 2012] using a block-matching

registration approach [Rivest-Hénault et al., 2015]. Intensity normalisation and image de-noising, using anisotropic diffusion [Perona and Malik, 1990] with modified curvature diffusion equation [Yezzi, 1998], was performed with the Insight Toolkit (ITK) in order to minimise the effect of Rician-distributed noise in the MR image, while attempting to preserve high resolution features within the image. Skull stripping was performed using an in-house algorithm developed in MATLAB 2015a (Mathworks, Natick, MA). In this approach, intradural CSF was identified using thresholding and morphological operations, following which brain tissues were isolated. By identifying CSF internal to the skull boundary, this approach is capable of accurately segmenting the brain in cases of large lesions, which may be present in children with CP. An example of a MRI with a large injury is shown in Figure 4.1.

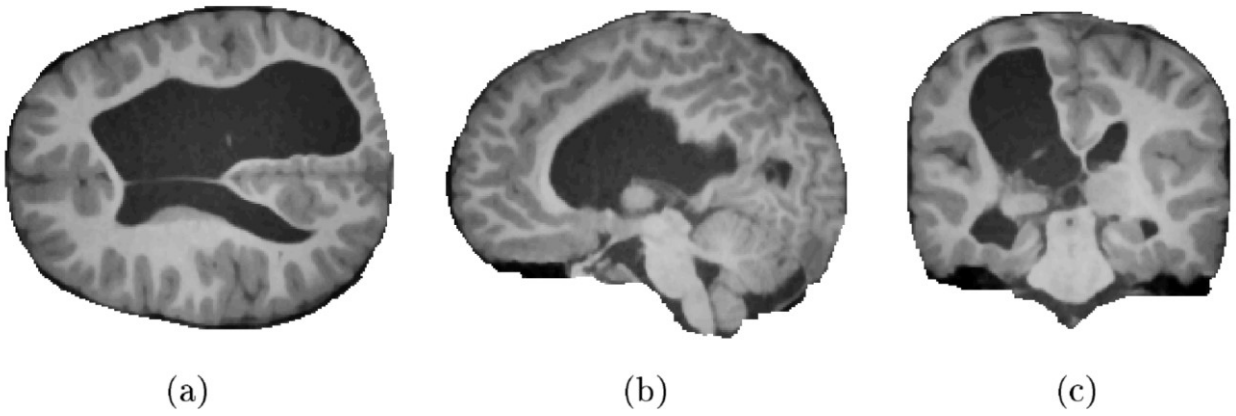

Fig. 4.1 The computed brain mask obtained from an MR image of a 5 year old male, clinically diagnosed with CP, using the in-house developed brain masking algorithm. This MRI shows severe ventricular enlargement, particularly in the right hemisphere. (a) Axial, (b) sagittal and (c) coronal views are shown.

Additionally, tissue probability maps (TPM) from the Colin 27 Atlas and the ICBM DTI-81 Atlas (International Consortium for Brain Mapping, CA) were registered to the T1-weighted MRIs of each patient using the fast free-form deformation registration algorithm [Modat et al., 2010] to assist the downstream lesion segmentation presented in Chapter 7.

4.2.3 Expectation Maximisation algorithm

The adaptive EM algorithm [Dempster et al., 1977] has frequently been used for the automated segmentation of brain MRI data [Van Leemput et al., 1999; Wells et al., 1996],

often with interleaved methods for enforcing spatial homogeneity using MRF [Zhang et al., 2001]. For neonatal data sets, EM provides robust segmentations even in the presence of high noise, significant partial volume effects, lack of tissue contrast, and extensive anatomical variability typical of these data sets [Cardoso et al., 2011; Makropoulos et al., 2012; Murgasova et al., 2006], highlighting its potential application to CP.

The limitation of the EM approach, particularly in the presence of severe injury, is its reliance on atlas priors during initialisation, and when iterative scaling voxel-wise tissue likelihoods based on the expected tissue type. Although non-rigid alignment of the atlas priors to the data is performed, non-rigid registration typically fails in cases of severe injury. Additionally, while a number of *a priori* relaxation strategies allow for more data-driven segmentation in later iterations [Cardoso et al., 2011; Makropoulos et al., 2012], the discrepancies between the anatomical assumptions of the normative atlases and CP patients are too great to provide a robust initialisation [Pagnozzi et al., 2015].

To avoid making assumptions about the volume of different tissues, the segmentation was initialised using an in-house developed, 1-dimensional peak finding algorithm that searches the smoothed intensity histogram for two sufficiently separated second derivative minima with an associated sign change in the first derivative, which are then labelled as GM or WM. The mean intensity of the CSF distribution was estimated by searching backwards from the GM mode, looking for a minima in either the first or second derivative. The standard deviation of each distribution is computed from the gradient of the Gaussian intensity histogram on either side of the respective maximum. An illustration of the initialisation provided by this peak-finding algorithm is given in Figure 4.2 below.

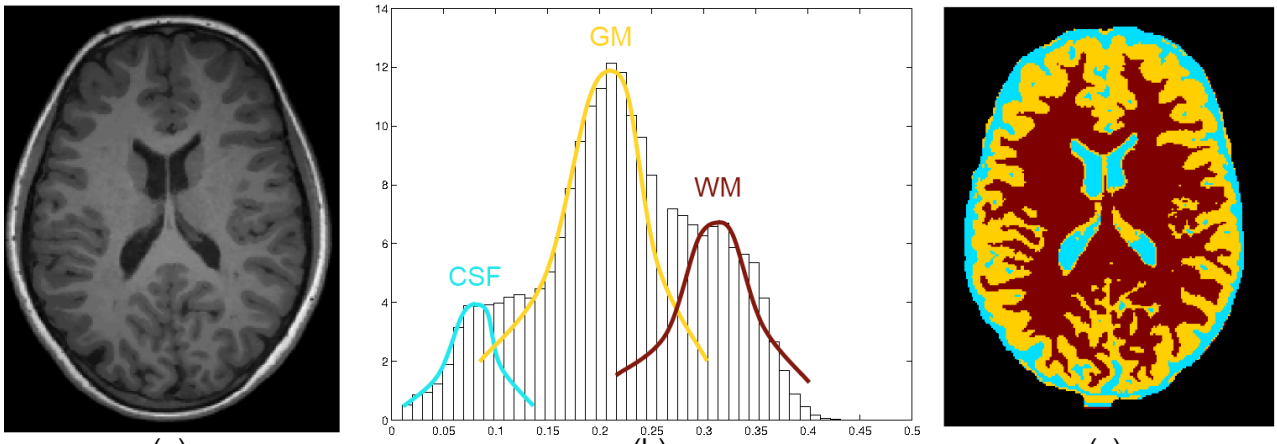

Fig. 4.2 Shows a structural MRI in (a), and the initialisation of CSF, GM and WM distributions obtained from the peak-finding algorithm on the intensity histogram of the image in (b). The resulting segmentation using this initialisation is shown in (c).

In the EM approach, the segmentation problem is formulated as an incomplete data problem where given the set of n voxel intensities in the image, $\boldsymbol{y} = \{y_i | i \, \epsilon \, [1;\, n]\}$, the algorithm attempts to compute a set of labels, $\boldsymbol{z} = \{z_i \, \epsilon \, [1; K]\}$, describing which of K tissue classes each voxel belongs to, with k denoting a specific tissue class $1 \leq k \leq K$. Voxels are indexed by i. Intensity distributions for each tissue class k are assumed to be normally distributed, with mean and standard deviation $\Phi_k = (\mu_k, \sigma_k)$. The estimation of the maximum likelihood parameters, $\hat{\Phi}$, is obtained by interleaving the estimation of the hidden segmentation, $\hat{\boldsymbol{z}}$, (E-step), followed by the update of the class distributions, Φ, based on the observed image y and segmentation $\boldsymbol{z}$ (M-step).

In the E-step, tissue labels at each voxel, i, were selected as the tissue class k that has the minimum posterior likelihood p_{ik}, which at iteration $m+1$ takes the form:

$$p_{ik}^{(m+1)} = \frac{\frac{1}{\sqrt{2\pi\sigma_k^2}} exp\left(-\frac{y_i - \mu_k}{2\sigma_k^2}\right) f(z|\Phi_z)}{\sum_{j=1}^{K}\left[\frac{1}{\sqrt{2\pi\sigma_k^2}} exp\left(-\frac{y_i - \mu_k}{2\sigma_k^2}\right) f(z|\Phi_z)\right]} \qquad Eq\ 4.1$$

Given a set of labels $\boldsymbol{z}$, the parameters were updated in the M-step as follows:

$$\mu_k^{(m+1)} = \frac{\sum_{\mathrm{i}}^{\mathrm{n}} {p_{ik}}^{(m+1)} y_i}{\sum_{\mathrm{i}}^{\mathrm{n}} {p_{ik}}^{(m+1)}} \qquad Eq\ 4.2$$

$$\left(\sigma_k^{(m+1)}\right)^2 = \frac{\sum_{\mathrm{i}}^{\mathrm{n}} p_{ik}^{(m+1)} \left(y_i - \mu_{\mathrm{k}}^{(\mathrm{m}+1)}\right)^2}{\sum_{\mathrm{i}}^{\mathrm{n}} p_{ik}^{(m+1)}} \qquad Eq\ 4.3$$

4.2.4 Gradient weighted Markov Random Fields

The form of $f(z|\Phi_{\mathrm{z}})$ in Eq 4.1, which is related to the MRF implementation, is critical to the performance of the algorithm. This modification is proposed in order to provide necessary robustness to the segmentation of MRI scans with extensive CP-related injuries. Commonly, the spatial relationship between a voxel and its six adjacent neighbours is assumed to be a random field following a Gibbs distribution:

$$f(z|\Phi_z) = Z(\Phi_{\mathrm{z}})^{-1}\exp\left(-U_{mrf}\right), \qquad Eq\ 4.4$$

where $Z(\Phi_{\mathrm{z}}) = \sum_{\mathrm{z}} \exp\left(-U_{mrf}\right)$ is called the partition function and U_{mrf} is the energy function. The energy function is the sum of clique potentials $V_c(\boldsymbol{z})$ over all possible cliques, C:

$$U_{mrf}(\boldsymbol{z}) = \sum_{c \in C} V_c(\boldsymbol{z})\,. \qquad Eq\ 4.5$$

Traditionally, clique potentials compute the sum of mismatched labels between the voxel x_i and its clique neighbours:

$$V_c\left(z_i, z_j\right) = \begin{cases} \frac{1}{2} & if\ z_i \neq \mathrm{z}_j \\ 0 & if\ z_i = z_j \end{cases}. \qquad Eq\ 4.6$$

This standard formulation of the clique potential is implemented in the Atropos software [Avants et al., 2011], although several other modulations of the MRF parameters have been proposed [Geman and Geman, 1984; Mumford and Shah, 1989]. These techniques modulate clique potentials based on gradients or smooth edges in the label field, $\boldsymbol{z}$. Both FSL's FAST and NiftySeg use a clique potential discretely weighted by gradients in the label field [Geman and Geman, 1984].

To compensate for the lack of an informative atlas-based prior, the proposed modification instead incorporates a new assumption in the model, that a mismatch of labels at a clique edge will have an associated mismatch of intensity at defined tissue boundaries. In comparison to previous studies, in the proposed modification the cost of neighbouring voxels with different labels is down scaled by the presence of intensity gradients between

the voxels in the image, $\boldsymbol{y}$. Correspondingly, the cost of neighbouring voxels with identical labels is up-scaled in the presence of intensity gradients between the voxels. Hence, in the modified MRF the cost of neighbouring labels is weighted by the gradient of intensity between the neighbouring voxels, which is congruous with the concept that different labels in a clique should have a different intensity, and vice versa. Therefore the cost of neighbouring voxels as follows:

$$V_c(z_i, z_j) = \begin{cases} \frac{1}{2}\left(\exp\left(-\frac{|y_i - y_j|}{w}\right)\right) & if\ z_i \neq z_j \\ \frac{1}{2}\left(1 - \exp\left(-\frac{|y_i - y_j|}{w}\right)\right) & if\ z_i = z_j \end{cases} \qquad Eq\ 4.7$$

In (7), w is a global parameter to control the influence of the gradient across tissue boundaries present in the MRI, typically based on the expected difference between classes y_i and y_j. In the experiments, this parameter was chosen to be half of the difference in intensity between WM and GM at initialisation, which was consistent due to intensity normalisation in MRI pre-processing. A practical illustration of this weighted MRF is provided in Figure 4.3 below.

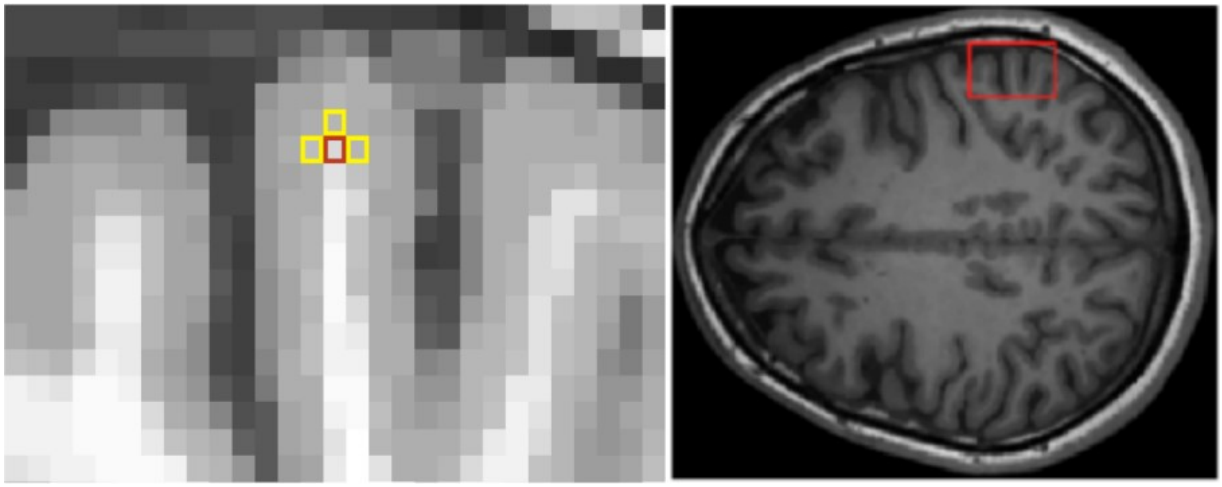

Fig. 4.3 An illustration of a WM voxel (highlighted in maroon), surround mostly by GM voxels (shown in yellow). Standard MRF's would impose a cost on the maroon voxel being classified as WM based on its neighbourhood, however the weighted MRF would down weight the cost of being associated with neighbouring GM voxels by the difference in intensity between WM and GM.

4.3 Results

To assess the accuracy of the cortical GM segmentations using the proposed EM approach with the gradient weight MRF, these segmentations were compared to the manual segmentations performed by two manual raters, one of whom was an expert experienced at assessing MRIs of children with CP, using the DSC metric [Dice, 1945]. Manual segmentations were obtained on 23 of the 139 T1-weighted MRIs, 17 of these were the MRIs of the children with severe cortical alterations, and the remaining 6 were from children with healthy development. Furthermore, these segmentations were compared to the segmentations obtained from several automated software packages. including FreeSurfer (Laboratory for Computational Neuroimaging, Massachusetts, USA) [Fischl, 2012], NiftySeg [Cardoso et al., 2011], FSL's FAST [Zhang et al., 2001] and ANT's Atropos [Avants et al., 2011]. FreeSurfer uses a data-driven deformable surface approach, initialized by registration to an atlas, to detect the inner and outer surfaces of the cortical GM. Many studies utilise FreeSurfer to measure cortical thickness [Ronan et al., 2011], which is computed from the deformable surface representation of both surfaces of the cortical GM [Fischl and Dale, 2000]. NiftySeg, FAST and Atropos all use an EM segmentation algorithm with an incorporated MRF and interleaved bias correction. In addition to these, the segmentations obtained from the EM approach with the standard MRF formulation of (6) were also compared to assess the difference of the proposed weighted MRF modification. The NiftySeg algorithm was run once using the default relaxation of the atlas priors, and once with the relaxation parameter set to its maximum. In this second implementation, atlas priors are still used to initialize tissue distributions, but the atlas priors were subsequently given zero weight during EM optimization.

The proposed approach gave the best DSC for both healthy (0.825) and injured data (0.783). Atropos obtained the second-best performance for both healthy data (0.814) and injured data (0.762). NiftySeg with 100% relaxation gave the third-highest performance in healthy and injured, consistently better than NiftySeg with default relaxation. FAST was among the best performing approaches in the healthy set, but had significantly reduced performance in the injured set. Neither FreeSurfer nor the classic MRF implementation demonstrated comparative performance. Overall, the proposed modified EM segmentation approach consistently had the best performance: in 14 of the 23 cases, versus 5 cases for Atropos, one case for NiftySeg with 100% relaxation and one case for FAST.

Table 4.1. Mean DSC results comparing the segmentations obtained from the proposed EM-weighted MRF approach, EM with the standard MRF, FreeSurfer, NiftySeg with default and 100% relaxation of atlas priors, FAST and Atropos with the manual segmentations obtained from two raters. Inter-rater reliability is provided based on the DSC overlap between the segmentations from the two raters. For each patient, the best DSC is in bold.

Patient ID	EM - weighted MRF	EM - standard MRF	Free-Surfer	NiftySeg	NiftySeg 100% relaxation	FSL's FAST	ANT's Atropos	Inter-rater reliability
Healthy cases								
1	**0.820**	0.818	0.750	0.761	0.795	0.798	0.812	0.772
2	0.783	0.724	0.767	0.772	0.785	0.790	**0.791**	0.837
3	0.807	0.766	0.776	0.769	0.796	0.796	**0.819**	0.821
4	**0.852**	0.843	0.794	0.794	0.835	0.822	0.834	0.869
5	**0.825**	0.720	0.790	0.779	0.811	0.771	0.783	0.820
6	**0.862**	0.810	0.781	0.823	0.835	0.828	0.845	0.865
Mean DSC	**0.825**	0.780	0.776	0.783	0.810	0.801	0.814	0.831
Cases with cortical injury								
7	**0.790**	0.712	0.589	0.631	0.677	0.657	0.730	0.765
8	0.772	**0.793**	NaN	0.693	0.729	0.706	0.746	0.810
9	0.834	**0.845**	0.709	0.759	0.771	0.745	0.827	0.842
10	**0.749**	0.650	NaN	0.663	0.735	0.240	0.746	0.714
11	0.766	0.675	0.649	0.741	0.765	0.720	**0.768**	0.788
12	0.726	0.733	0.689	0.742	0.761	0.761	**0.781**	0.811
13	0.735	0.635	0.680	0.709	0.733	0.717	**0.765**	0.766
14	**0.819**	0.794	0.751	0.761	0.791	0.798	0.755	0.837
15	0.763	0.705	0.363	0.747	**0.769**	0.685	0.740	0.803
16	**0.788**	0.725	0.691	0.712	0.737	0.701	0.776	0.783
17	**0.813**	0.673	0.686	0.725	0.751	0.744	0.794	0.796
18	**0.831**	0.739	NaN	0.763	0.776	0.779	0.782	0.820
19	0.715	0.767	0.474	0.765	0.793	**0.774**	0.759	0.810
20	**0.822**	0.780	NaN	0.726	0.778	0.624	0.720	0.805
21	**0.811**	0.679	NaN	0.763	0.777	0.699	0.777	0.802
22	**0.771**	0.726	NaN	0.723	0.745	0.658	0.696	0.800
23	**0.812**	0.756	0.668	0.727	0.747	0.732	0.797	0.801
Mean DSC	**0.783**	0.728	0.631	0.726	0.757	0.691	0.762	0.797

In all cases, the inter-rater reliability was greater than the DSC obtained for any of the methods. The agreement between the raters went as low as 0.714. The discrepancy between the two raters was largely due to local reductions in the contrast between the GM and WM, obscuring the tissue boundary, which was more prevalent in the injured data, as well as ambiguous partial volume voxels affecting the agreement between raters. This may account for the reduced reliability computed in the injured data (0.797) compared to the healthy data (0.831), and highlights the difficulty in obtaining an accurate segmentation in severely injured cases. An illustration of the segmentations obtained from the several methods from two images containing severe injury is shown in Figure 4.4.

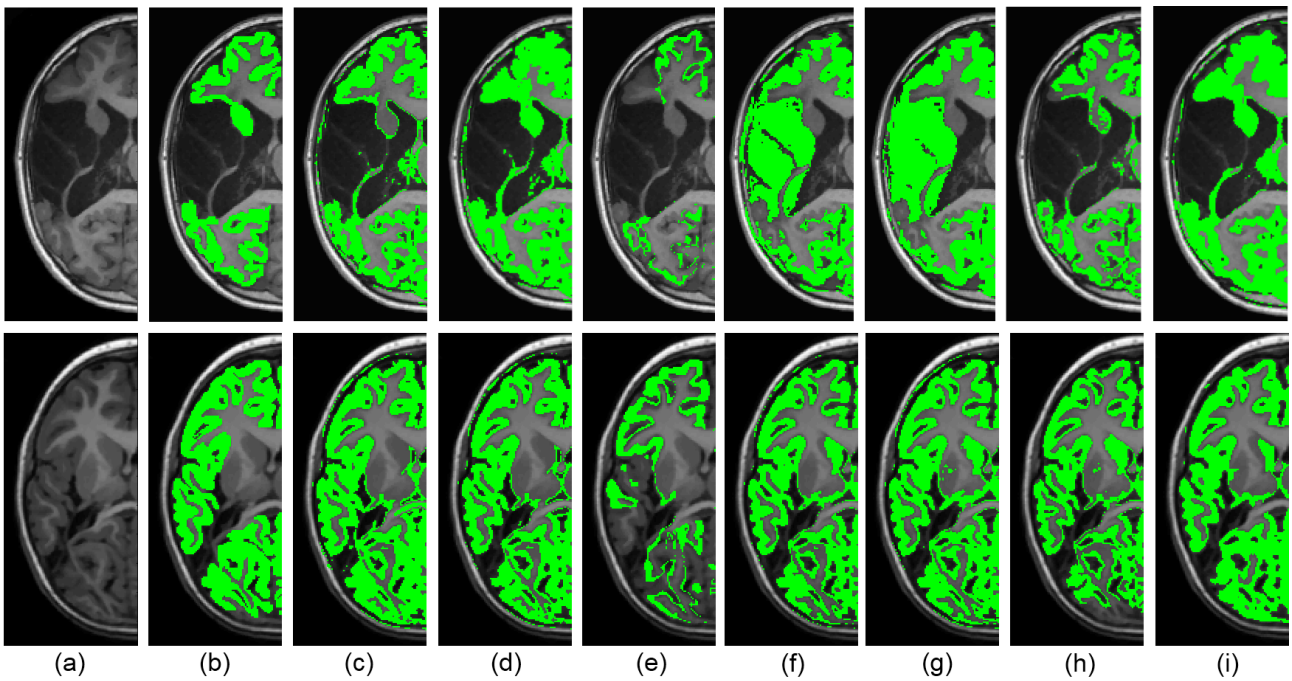

Fig. 4.4. (a) An axial slice of a patient with cortical injury, and the cortical GM segmentations obtained from the (b) manual rater, (c) EM-weighted MRF (proposed approach), (d) EM-standard MRF, (e) FreeSurfer software, (f) NiftySeg, (g) NiftySeg with fully relaxed priors, (h) FAST and (i) Atropos.

4.4 Discussion

The proposed segmentation approach outperformed all the other state-of-the-art EM methods with integrated atlas priors on the cases with cortical injury, demonstrating the potentially deleterious effect of incorporating atlas-based priors when segmenting scans with severe injury. A fraction of this improvement is the result of the weighted MRF, which

provides additional robustness by forcing the labelling to be consistent with intensity gradients in the image. The benefit of the modified MRF is demonstrated by the reduced DSC's obtained using the EM with the standard MRF, as this approach computes high neighbour costs at tissue boundaries. Consequently, thin extensions of WM or CSF are smoothed over and labelled as GM using this method, as is shown in Figure 4.4(d).

Although existing approaches exist, their reduced robustness of severe injury limits their efficacy in identifying structure-function relationships of the cortex, as illustrated in Figure 4.4(e-h). For instance, in Fig. 4.4(g, top row), due to the extreme anatomical malformations, much of the CSF was incorrectly labelled as GM during initialization, resulting in poor and irrecoverable initial estimates of distribution. The same limitation resulted in Case #10 where the DSC=0.240 was observed for FAST. FreeSurfer failed to produce a result (NA in Table 4.1) on six of the 23 MRI scans, corresponding to data sets exhibiting more severe injury causing failure in the deformation of the cortical surface. For the remaining scans, the presence of injury was observed to impact the deformation of the cortical surfaces, as illustrated in Figure 4.4(e). The most robust approaches were those that had reduced reliance on atlas priors, NiftySeg performed 100% relaxation of priors during the EM iteration, Atropos utilizes robust data-driven initialization approaches [Avants et al., 2011], such as Otsu thresholding [Otsu, 1975] or fuzzy c-means [Bezdek et al., 1984], and the proposed approach performs both of the above, initialized with a data-driven peak-finding algorithm and not weighted by atlas priors.

Although this highlights the limitation of atlases to initialize prior tissue distributions, many atlas-based segmentation algorithms accommodate pathologies using a local relaxation of atlas priors [Parisot et al., 2012; Parisot et al., 2014]. These approaches, while validated on data with brain tumours, have unique challenges in the CP setting, where the region of severe malformation may include GM that needs to be continuously segmented along with healthy regions of GM, and not as a separate tumour entity. In the proposed EM-weighted MRF implementation, a straightforward peak-finding algorithm was instead used to robustly estimate initial tissue distributions, assisting an accurate segmentation of cortical GM in injured cases. Alternative approaches, such as Otsu thresholding [Otsu, 1975] or fuzzy c-means [Bezdek et al., 1984], could similarly provide robust tissue distribution initializations. These methods are used for initialization in the Atropos software [Avants et

al., 2011], potentially accounting for its second-highest performance among the injured cases.

A limitation of this work is that the accurate segmentation of cortical GM remains challenging, even in healthy brains, with DSC's of ~0.8 reported in the few available references [Makropoulos et al., 2012; Melbourne et al., 2012; Murgasova et al., 2006], due to the narrow and complex morphology of cortical GM and partial volume effects. The extensive injuries typical of CP compound this, making the distinction between GM and WM ambiguous and impacting on the DSC. Finally, the proposed adaptive algorithm does trade off sensitivity in segmenting fine structures for robustness to injury (although the weighted MRF attempts to minimise the consequence of this trade-off). Another limitation of the proposed modification is that it has only been applied to the segmentation of tissue types, with specific focus on improving cortical GM segmentations. As shown in Figure 4.4(c), the proposed modification mislabels the caudate nucleus, and has been observed to mislabel partial volume voxels around the ventricles. Anatomical parcellation requires the use of *a priori* information provided by atlas-based methods, while errors caused by partial volumes can be addressed using *a priori* partial volume maps, or modification of the clique potential to down-weight WM to CSF transitions. Future work will investigate registering *a priori* partial volume maps to healthy regions of the brain, relaxing the prior constraints in regions of injury.

In summary, the results highlight the challenges of using atlas-based priors in cases of severe injury, as healthy atlases do not generalize to unhealthy cases and even sophisticated non-rigid registration algorithms like that used by NiftySeg, FAST or Atropos cannot compensate for severe changes in anatomy. This places the burden of obtaining robust segmentations on the design of the clique weighting function as opposed to dictating a need for more training data. Although relatively simple adaptive approaches such as the proposed modified MRF can yield a robustness to severe pathology or injury, additional approaches are still required to segment cortical regions in this setting, which will be addressed in a later chapter.

4.5 Conclusion

In this chapter, a modification to the EM-MRF approach tailored specifically for the automated cortical GM segmentation of MRI of children with CP has been described. The extensive anatomical malformations caused by injury related to CP limit the utility of atlas based priors. To impart robustness to the formulation of the posterior likelihood, and to compensate for the limited relevance of atlas priors, the clique potentials in the MRF were modified to include penalization for mismatched labels over low intensity gradients, and matched labels over high intensity gradients. The result is an improved segmentation at the boundary of cerebral tissues in a cohort of patients with severe CP-related injury (DSC 0.783 across 17 children with severe cortical injury) in comparison to four state-of-the-art segmentation methods: FreeSurfer (0.631), NiftySeg (0.757), FAST (0.691) and Atropos (0.762). This segmentation approach is utilised for the robust segmentation of the lateral ventricles and cortical GM in Chapters 5 and 6 respectively. Further modifications to this approach were then implemented to perform lesion segmentation in Chapter 7.

5. Quantifying ventricular enlargement using statistical shape models

5.1 Introduction

One class of injury discussed in the review of the literature in Chapter 2 is the enlargement of the ventricles. The challenge for implementing automated image analysis tools for detecting injuries observed in children with CP is the substantial heterogeneity in the appearance and location of injury. An advantage of the lateral ventricles is their clearly defined boundary, which assists the segmentation of these structures, even in cases of severe enlargement. Furthermore, their proximity to key deep GM structures, and the observations that ventricular enlargement occurs in up to 70% of CP cases [Kulakowski and Larroche, 1980; Sööt et al., 2008; Truwit et al., 1992], suggests that surrogate markers of deep GM injury based on ventricular enlargement are likely to be relevant to the clinical assessment of children with CP.

The ventricles are spaces filled with CSF in the centre of the brain that transport nutrients to the brain and act as a cushion to movement. They may enlarge due to an abnormal accumulation of CSF in the brain, or following a hypoxic-ischemic event in the periventricular WM or GM. As this expansion of the ventricles is caused by developmental disturbances, it is fundamentally different from degenerative pathologies like AD where there is a global expansion of the ventricular space [Gado et al., 1983]. Instead, this enlargement is typified by the local, irregular, or angular appearance of the lateral ventricles and ventricular trigones, and may impact one or both hemispheres of the brain [Truwit et al., 1992]. Expansion of the ventricles into the adjacent WM and key sub-cortical GM structures of the brain has been shown to provide an indirect measure of tissue loss [Hoon and Vasconcellos Faria, 2010], and has been shown to correlate with the degree of patient impairment [Maunu et al., 2011; Melhem et al., 2000].

Several techniques for assessing ventricular enlargement have been proposed, albeit in the context of degenerative diseases, rather than developmental ones, such AD [Horga et al., 2011; Nestor et al., 2008] and schizophrenia [Kempton et al., 2010]. Of these, global ventricular volume is the most common biomarker extracted from structural MRIs, which have been computed using automatic edge-detection [Shenton et al., 1991], fuzzy tissue segmentation [Barra et al., 2002] and region growing techniques [Nestor et al., 2008]. Less

frequently, this biomarker has also been measured in the setting of CP, [Melhem et al., 2000]. Although straight forward to measure, ventricular volume varies significantly amongst the healthy population [Wright et al., 2002], complicating the identification of subtle ventricular enlargement due to injury.

More complex biomarkers based on the shape of ventricles have been developed in other studies. Several studies have reported linear measures of ventricular dilation [Maunu et al., 2011; Northam et al., 2011]. The distance between the approximate centroid of the ventricle, to the surface, was found to be sensitive to local atrophy [Apostolova et al., 2012]. SSMs area a common technique used to model ventricular shape, as it provides a more detailed description of how the shape of ventricles varies. These models have been used to identify the pathological enlargement of ventricles due to AD [Chou et al., 2007; Ferrarini et al., 2006; Ferrarini et al., 2008a; Thompson et al., 2004] and schizophrenia [Graham et al., 2006; Narr et al., 2001; Styner et al., 2003]. The extent of atrophy can thus be identified as the distance of the ventricle surface from corresponding points on a healthy SSM. These measures were correlated to measures of cognition in the context of AD [Ferrarini et al., 2008b]. Although this local shape based analysis would allow for a more informative assessment of ventricular enlargement in children with CP, there has been little focus on applying these methods in this setting. This is due to the large variability in the appearance and severity of injury observed in children with CP, leading to technical difficulties obtaining vertex-wise correspondences between meshes of enlarged ventricles.

In this chapter a novel biomarker of deep GM injury is presented. This marker is extracted from an automated method for identifying and quantifying the extent of ventricular enlargement observed in structural MRIs of children with CP. The key contribution of this work is to use local deformation as a surrogate marker for ventricular impingement upon adjacent surrounding anatomy. The relationship between the proposed measure and several functional outcomes is examined to evaluate the extent to which the proposed method can assist clinicians in identifying injury indicative of CP, and hence guide the selection of treatment strategies. This work addresses Aim 1 of this thesis, “develop several automated segmentation approaches to delineate the three main classes of injury observed in children with CP; cortical malformations, WM injury and ventricular

enlargement", as well as Aim 3, "[comparing] the automated results against a manual gold standard". This work has been published, and is available at doi:10.1002/hbm.23276.

5.2 Materials and methods

5.2.1 Study Participants

All 139 children recruited as part of the studies detailed in Section 3.2.1 have been included in this chapter: 95 patients with clinically diagnosed CP (50 male, 45 female, mean age 11.4, age range 5-17), and 44 TDC with no observed diagnosis of injury (15 male, 29 female, mean age 10.4, age range 7-16). Of the 95 children with CP, 68 exhibited ventricular enlargement while the remaining 27 did not.

5.2.3 Overview of scoring method

The surrogate marker of injury is generated in two steps as outlined in Fig. 5.1. In the first step a set of impingement volumes are generated using a SSM, shown in Fig. 5.1(a). In the second step the impingement volumes are converted into a scalar estimate of clinical function using a linear regression model, shown in Fig. 5.1(b).

The SSM describes the typical shape and variability of the lateral ventricles in healthy children. The SSM was constructed from the available cohort of 44 healthy children. The constructed SSM was subsequently fitted to the ventricles of individual unhealthy patients to generate an estimate of the volume of (atypical) enlargement. The volume of enlargement is partitioned into a set of volumes associated with nearby anatomical regions, referred to as *impingement volumes*.

The regression model was constructed using the cohort of unhealthy patients. The impingement volumes, patient age and patient gender were used as the independent variables in the regression model, with the dependent variables consisting of the clinical scores. A separate regression model was constructed for each clinical score. Correlations between the estimated clinical function from the regression model and the actual clinical measures were measured to test the accuracy of the entire method.

Finally, for new data, ventricular enlargement is computed. After alignment with the normative atlas, impingement of subcortical GM structures is computed. The values are combined with age and gender and weighted by the coefficients of the regression model, to obtain a predictive image score, shown in Fig. 5.1(c).

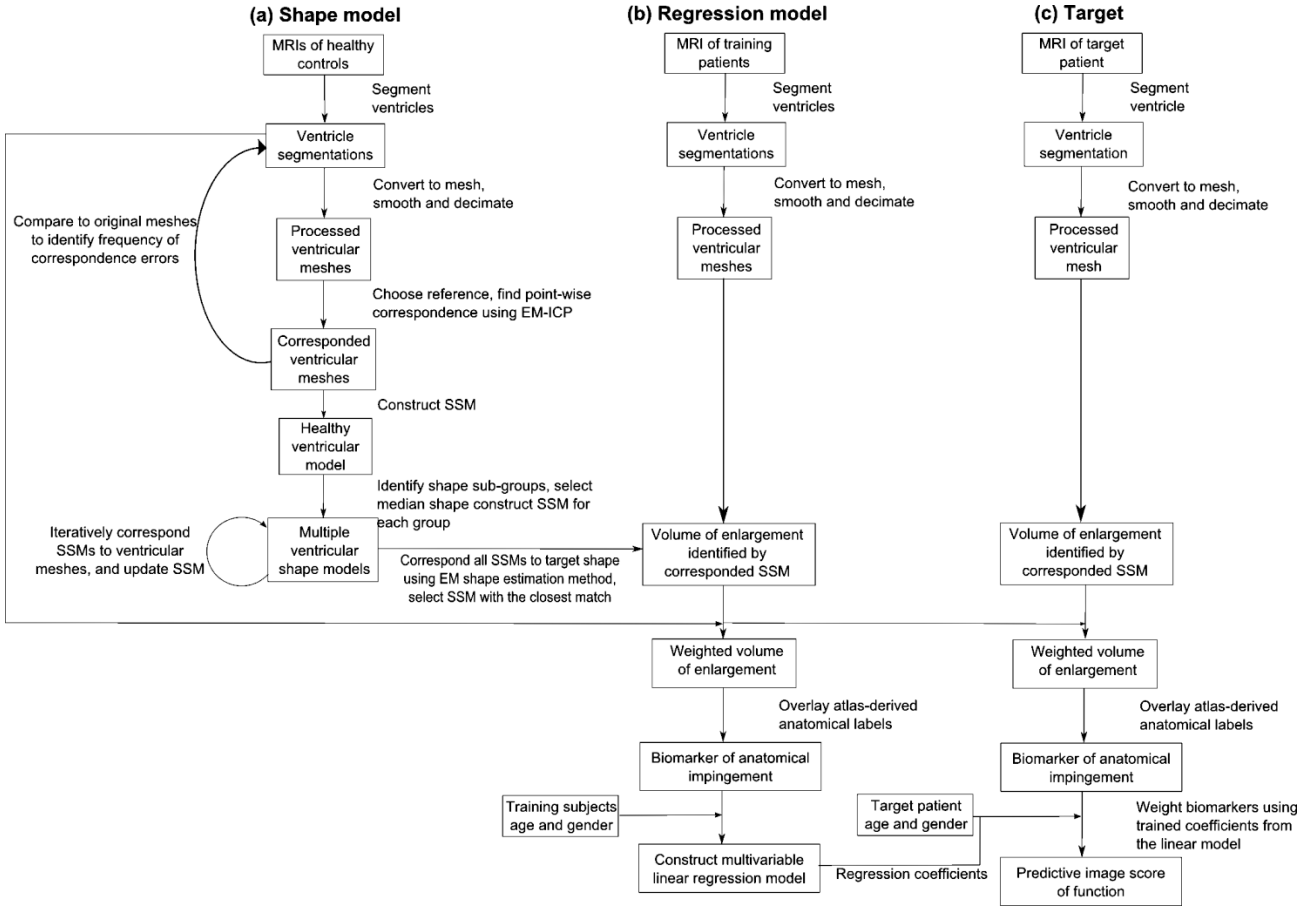

Fig. 5.1 The pipeline of the (a) healthy ventricular shape model construction, (b) multivariable linear regression model construction relating image-derived marker of injury to outcome, and (c) computing image derived measures of injury from a target image.

5.2.4 Ventricle segmentation

The automated segmentation of the ventricles was performed using the segmentation approach detailed in Chapter 4. This segmentation includes the third ventricle and the cerebral aqueduct, however only the lateral ventricles were retained for the subsequent analysis using several atlas-derived seed points, and morphological opening was utilised to ensure that any connections of ventricular CSF to the subarachnoid space due to injury were contained. Subsequent morphological closing operations were applied to ensure that internal gaps in the segmented ventricles that were left out due to partial volume effects were filled in, and to ensure that if a ventricle appeared as a number of disconnected pieces, they were connected into a single structure. All morphological operations were performed with a fixed radius across all subjects. The segmented ventricles were divided

into the left and right lateral ventricles based on the position of the third ventricle segmentation, and the right lateral ventricle was mirrored to align it to the left lateral ventricle yielding 88 (single) lateral ventricles for statistical analysis and training. The aligned lateral ventricles were used to generate a single SSM, which was flipped to test for enlargement in each lateral ventricle independently. This, as opposed to constructing two separate SSMs for each lateral ventricle, ensures the same statistical assessment of enlargement can be applied to either lateral ventricle, of which one or both may be enlarged.

5.2.5 Mesh point-correspondences

The segmented ventricles were converted to meshes using the marching cubes algorithm [Lorensen and Cline, 1987]. Decimation was then performed on the meshes, removing 65% of the triangles [Knapp, 2002]. Smoothing was subsequently performed on these meshes using a windowed sinc filter [Gabriel et al., 1996]. Each ventricle surface is represented by the coordinates of its n landmarks, concatenated into a $3n$-vector. Note that initially the number *n* of landmarks in each ventricle surface is not necessarily the same for each mesh. The median reference ventricle was selected from the subset of 88 healthy lateral ventricles by selecting the ventricle with the minimum row sum from the matrix of residuals between each mesh pair. This shape surface was then registered to the remaining 87 healthy lateral ventricles using the Expectation Maximisation – Iterative Closest Point (EM-ICP) method [Combès and Prima, 2010]. This method interleaves estimating the non-rigid transformation between two surfaces that minimises the sum of squared distance (SSD) between corresponding surface points, and updating the expected correspondence between surface points using the EM algorithm. A term enforcing symmetry of the forward and reverse transformations, and a regularisation term were included in the cost function to ensure inverse consistency and regularity of the transformation. This method allows the points corresponding to each vertex on the reference mesh to be located on every other mesh. The point correspondences allow the remaining meshes to be represented by vectors of the same size as the reference mesh.

5.2.6 Statistical shape model construction

The meshes of the registered healthy lateral ventricles with point correspondences were represented by concatenating the landmark points into vectors of equal length. The mean shape, $\bar{\boldsymbol{x}}$, and covariance matrix, Σ, were computed from the s shapes in the sample. A

Principal Component Analysis (PCA) [Joliffe, 2005] was performed to obtain eigenvectors ϕ_m, and their corresponding eigenvalues λ_m. The eigenvectors capture the principal modes of variation in the sample of shapes. Only the first c eigenvectors were used, such that the ranked c eigenvalues with largest magnitude eigenvalues described more than 90% of the total variance. As a result, the first six ranked eigenvectors were used in this shape modelling approach. Each individual shape $\boldsymbol{x}_i$ can be represented by both the mean shape $\bar{\boldsymbol{x}}$, and a c-length vector describing the projection of the shape along each of the main modes of variation using the shape descriptor b:

$$\boldsymbol{x}_i \approx \bar{\boldsymbol{x}} + \sum_{m=1}^{c} b_{i,m}\phi_m \qquad Eq\ 5.1$$

To accurately describe the high degree of healthy variation in shape of the ventricles, an iterative method was used to estimate the SSM [Hufnagel et al., 2009] in which the current estimated SSM was registered back to the original 87 healthy ventricles using the EM-ICP based shape estimation method [Shen et al., 2012b], which is formulated in the Bayesian setting. In this approach two parameters are iteratively updated, the vertex-wise correspondence between the SSM and the ventricular mesh in the E-step, and the transformation of the SSM constrained to its six eigenvectors to minimise the Euclidean distance between corresponding vertices in the M-step. This method produces an updated SSM at each iteration, for five iterations. In this Bayesian framework, Tikhonov regularisation was used on the estimator to penalise large deviations from the mean shape, i.e. the objective function included a regularisation term consisting of the weighted sum of square parameters. The default regularisation parameter $(\beta = 1)$, equivalent to a Bayesian estimation informed by the shape priors, was used here. Previous results show robustness of regularising the hippocampal shape parameters (provided it is non-zero) in estimating the shape of the hippocampus [Shen et al., 2012b]. The process of iteratively corresponding the SSM back to the original shapes reduces the residual error of the fit of the SSM to the original healthy shapes, making the computed eigenvectors more representative of the majority of the population.

The mean shape and the first three modes of variation (of the six eigenvectors contained in the SSM), within 2 standard deviations, of the final SSM are illustrated in Figure 5.2. The first three modes were illustrated as these modes explain the greatest amount of shape

variation. The first mode approximately describes variations along the lateral aspect of the ventricle, the second describes an anterior to posterior shifts, while the third defines changes in size of the anterior horn. Note that care should be taken not to assign too much meaning to the principle components by conflating them with physical effects.

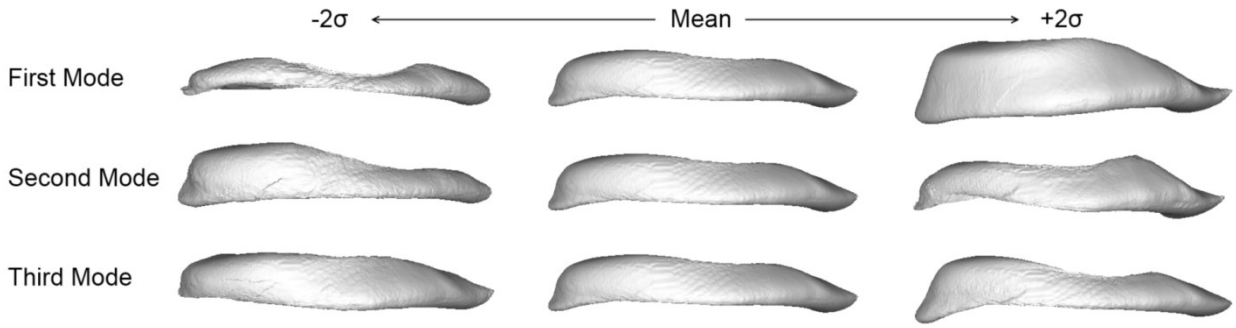

Fig. 5.2 Mean shape and first three modes of variation (+/- 2 S.D.) of the SSM.

5.2.7 Identifying age-related changes in ventricular shape

To identify any changes in ventricle shape due to patient age, and potentially account for this in the SSM, two groups of corresponding meshes were isolated, those belonging to patients between 5 and 9 years (n = 8, 4 male, 4 female), and between 12 to 17 years of age (n = 8, 5 male, 3 female) respectively. Following initial ICP matching, Procrustes analysis was performed [Gower, 1975], i.e. the ventricles were uniformly scaled to obtain an optimal match, followed by discriminant analysis between the ventricle shapes of both groups. From this analysis, a map of significance was generated which illustrates the statistical significance of the difference of each corresponding point between the two groups. In addition, the first three shape descriptors of the constructed SSM corresponding to these meshes were analysed using Hotelling's T-squared test [Styner et al., 2007], providing a shape descriptor comparison for each age group with a Hotelling's T-squared statistic [Shen et al., 2011].

5.2.8 Multiple statistical shape model construction

To account for the deviation of ventricle shapes observed from the healthy children, three additional SSMs were constructed, using subsets of the 88 cases, with the aim of using the most appropriate SSM to fit to a given unclassified ventricle. To identify the separate groups of shapes, the initially constructed SSM was transformed to fit the original healthy ventricles, providing a vector of shape descriptors. FCM [Bezdek et al., 1984] clustering

was performed on the first two shape descriptors, which combined describe the gross anatomical shape, identifying three shape groups. Individual SSMs were constructed for each of these groups, as detailed in Section 5.2.6.

To determine the differences between these three groups, the meshes were Procrustes aligned and discriminant analysis was performed between the three possible pairs. This generates a map of the statistical significance of the difference between the corresponding points between the compared groups. Additionally, the SSM constructed from all healthy ventricles was transformed to the remaining 87 ventricles, and the first three shape descriptors from the transformation were obtained and grouped based on the shape grouping of the target healthy ventricle. Shape descriptors were again analysed using the Hotelling's T-squared test between the different shape groups, correcting for multiple comparisons using Bonferroni correction.

5.2.9 Measuring SSM correspondence

The EM shape estimation method [Shen et al., 2012b] was further used to transform the iteratively improved single and multiple SSMs to the remaining ventricles obtained from the MRIs of the 95 children with CP. In this step, the SSM transforms along the six largest eigenvectors to best fit the target ventricle. Tikhonov regularisation was used to constrain the shape descriptors fitting the SSM to a given lateral ventricle, x_i, which can be described as:

$$\boldsymbol{x}_i = \overline{\boldsymbol{x}} + b\boldsymbol{\phi} + \epsilon = \overline{\boldsymbol{x}} + (b_{constrained} + b_{remainder})\boldsymbol{\phi} + \epsilon, \qquad Eq\ 5.2$$

where $\overline{\boldsymbol{x}}$ is the mean SSM shape, $\boldsymbol{\phi}$ contains the SSM eigenvectors, $b_{constrained}$ contains the constrained shape parameters obtained from the SSM fitting process, $b_{remainder}$ contains the difference between unconstrained and constrained shape descriptors, and ϵ contains the residual that cannot be described by the model. As a result, the SSM provides the closest healthy shape to a target (healthy or injured) ventricular shape, with regions of ventricular enlargement caused by injury not modelled by the SSM. Hence, for the function, $V(x)$, that converts a mesh model x into its volumetric representation, the enlarged volume mask, $V_{enlarged}$, is:

$$V_{enlarged} = V(\boldsymbol{x}_i) - V(\overline{\boldsymbol{x}} + b_{constrained}\boldsymbol{\phi}) = V(b_{remainder}\boldsymbol{\phi} + \epsilon) \qquad Eq\ 5.3$$

Here, the term $V(\bar{\boldsymbol{x}} + b_{constrained}\phi)$ represents the assumed maximum natural variation in ventricle shape. The remaining volume $V(b_{remainder}\phi + \epsilon)$ is assumed to represent the atypical shape variation arising from injury. The volume mask $V_{enlarged}$ was termed the *volume of enlargement*.

As the constrained SSM models the closest healthy shape, with a volume mask $V_{enlarged}$ representing the difference to the volume of the actual shape $V(\boldsymbol{x}_i)$, in cases of severe enlargement, as shown in Figure 5.3, the SSM can be up to 3.5cm away from the segmented ventricle.

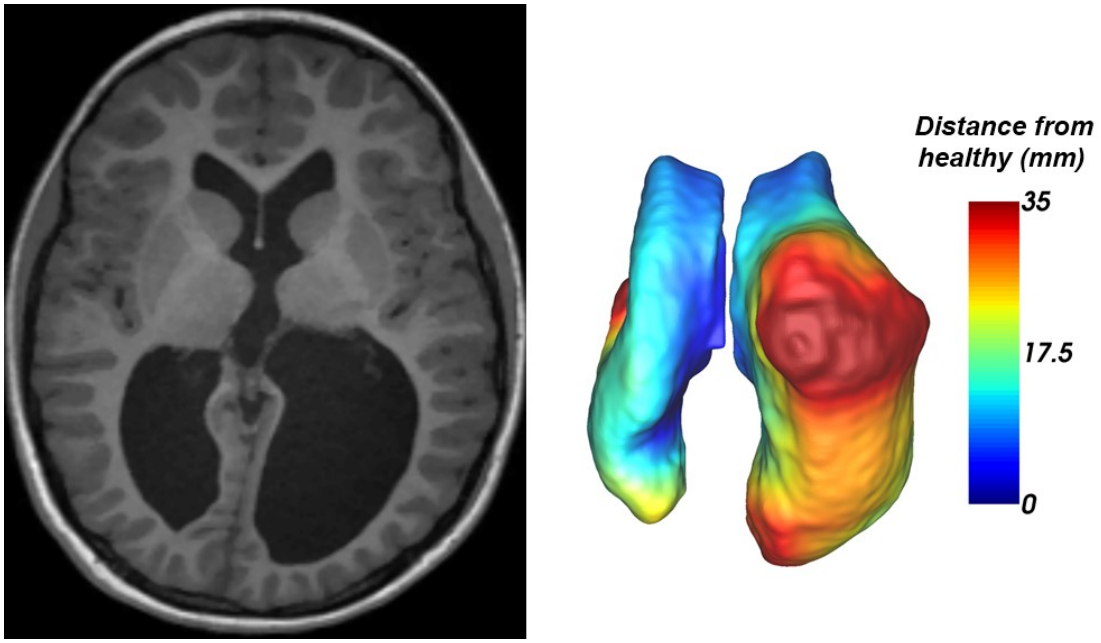

Fig. 5.3 A structural MRI displaying severely enlarged lateral ventricles, and the measured Euclidean distance between the transformed healthy SSM and the segmented ventricle displayed on the ventricle mesh. This distance revealed up to 3.5cm of enlargement due to injury, observed in the superior portion of the ventricle.

This approach, along with its inherent assumptions of healthy anatomy lying within the constraints of the eigenspace defined by the six components of the healthy SSM, was taken because the parameters obtained from fitting (i.e. $b_{constrained}$), which represent the distance of the transformed SSM from the mean shape, may not adequately describe the magnitude of injury. Although enlarged ventricles are generally larger than the mean, regions of enlargement may not be accurately described using the eigenvectors of the healthy SSM, and as such are not captured with the $b_{constrained}$ parameters. Even so, for

completeness, the utility of distance from the mean, $\sum b^2_{constrained}$ was tested as another potential measure of injury.

A Receiver Operator Characteristic (ROC) analysis was performed to determine the performance of both the volume of enlargement and sum of squares of the constrained shape parameters to correctly identify cases of ventricular enlargement caused by disturbances during development, compared to the gold standard diagnosis of ventricular enlargement obtained from a medical expert. From these ROC analyses for each measure of enlargement, the Area Under the Curve (AUC) and the Standard Error (SE) were computed using the trapezoidal integration approach [Bradley, 1997]. In addition, at the optimal location, the positive and negative predictive values were computed. ROC analyses were performed using a single SSM, constructed from all healthy ventricles, for correspondence, as well as for multiple SSMs, each representing a specific sub-group of ventricular shape in the healthy population. In the latter case, the SSM that most closely matched the target ventricle was used to obtain correspondence.

5.2.10 Measuring anatomical biomarkers of injury

From the ventricles classified as enlarged by the SSM, the volume of enlargement was identified from the correspondence of the SSM, and impingement volumes quantifying of the extent of deep WM and GM impact was measured. This was computed as the overlap of the enlarged ventricular volume, and the labelled deep GM structures obtained from the Automated Anatomical Labelling (AAL) atlas registered to the Colin 27 atlas. The overlap with the PLIC and the anterior limb of the internal capsule (ALIC) were also computed, which was achieved by manually labelling the respective limbs of the internal capsule on the Colin 27 atlas.

A voxel-wise weighting was applied to these labelled anatomies, to down-weight voxels in regions where correspondence errors were observed among the healthy ventricles. Figure 5.4(a) shows the frequency and location of correspondence errors among the set of healthy ventricles used to construct the SSM. Figure 5.4(b) shows the corresponding weights of this region in the atlas, illustrating the down weighted regions with high correspondence errors. This was performed by linearly scaling the correspondence errors shown in Figure 5.4(a) to have a maximum of 1, inverting this result, and reflecting the minimum value observed on either side of the medial line, in effect copying the greatest

correspondence error observed on either lateral ventricle to both hemispheres. Figure 5.4(c) shows a cumulative map of ventricular enlargement, identified from the set of children with CP having either healthy or enlarged ventricles, using the multiple healthy SSMs. This map shows the frequency of injury at locations in the adjacent deep WM and GM anatomies, scaled by the weights from Figure 5.4(b).

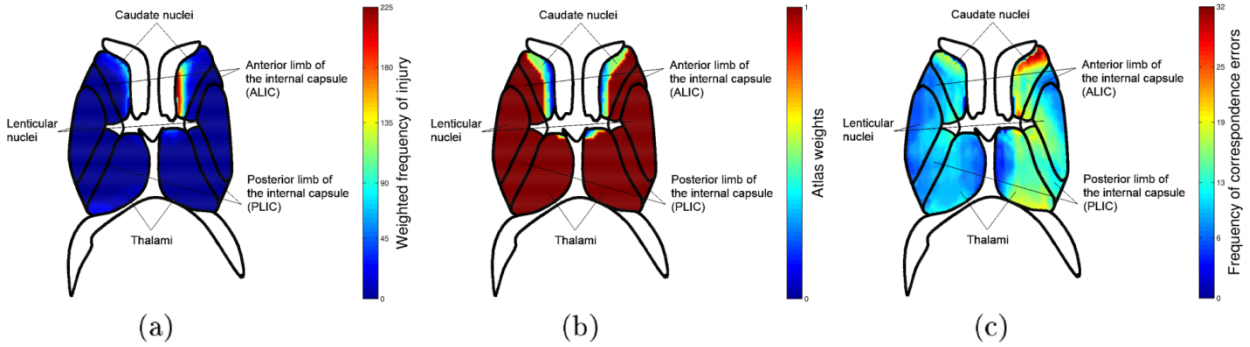

Fig. 5.4 (a) The frequency of correspondence errors observed among the healthy ventricles used to construct the SSM. (b) The corresponding atlas weights used to down weight regions with high correspondence errors. (c) The frequency of ventricular enlargement observed in the set of unclassified ventricles (containing both healthy and enlarged ventricles), weighted by the atlas weights in (b).

5.2.11 Statistical methodology

Statistical analysis was performed using R statistical software Version 3.1.1 [The R Development Core Team, 2008]. Multivariable linear regression was used to quantify the relationship between the computed impingement volumes into five key structures, as well as patient age and gender, to several clinical scores of function. The structures analysed comprised of the thalamus, lenticular nucleus, caudate nucleus, PLIC and ALIC. The regression coefficients for the independent variables were standardised to a variance of one to allow for more intuitive comparisons between coefficients. The covariance between the measured impingement volumes for each anatomy was also computed, to observe the extent to which these measures co-vary. Measures of statistical significance were corrected for multiple comparisons using Bonferroni correction, comparing the calculated p-values against the adjusted alpha (α=0.05/6, 0.008).

5.2.12 Comparison to direct measure of injury

To address concerns that the volume of local ventricular enlargement is an indirect measure of injury to sub-cortical anatomies, an additionally a set of regression models were computed using the volumes of these anatomies as a direct measure of possible injury to these structures, for comparison. Deep GM anatomies were segmented using FIRST [Patenaude et al., 2011], providing volumes of the lenticular nucleus, caudate nucleus and thalamus for 70 out of the 95 CP patients.

5.3 Results

5.3.1 Age Comparisons

The Hotelling's T-squared statistic, which quantifies the difference in the shape descriptors obtained from the two age groups, was 5.31 (p = 0.746). The low T-squared value implies that the effect of age was not a significant factor influencing ventricular shape. Hence subject age was not controlled for in the SSM.

5.3.2 Shape sub-population comparisons

Significant shape differences were observed between the three shape groups, with the significance map of the point-wise comparison between the first and second identified shape groups, as well as the first and third shape groups, is illustrated in Figure 5.5. These maps highlight extensive regions along the ventricle shape that are statistically significantly different between the three shape groups. Furthermore the Hotelling's T-squared statistic showed statistically significant differences between the first and second shape groups (T = 142.5, $p < 0.0001$), the second and third shape groups (T = 68.1, $p < 0.0001$), and then first and third groups (T = 56.6, $p < 0.0001$), motivating for the use of multiple SSMs. The three SSMs were observed to have a similar variation in healthy ventricle shape i.e. eigenvectors, including the global lateral widening, and anterior/posterior thickening, and mainly differed in their mean shape.

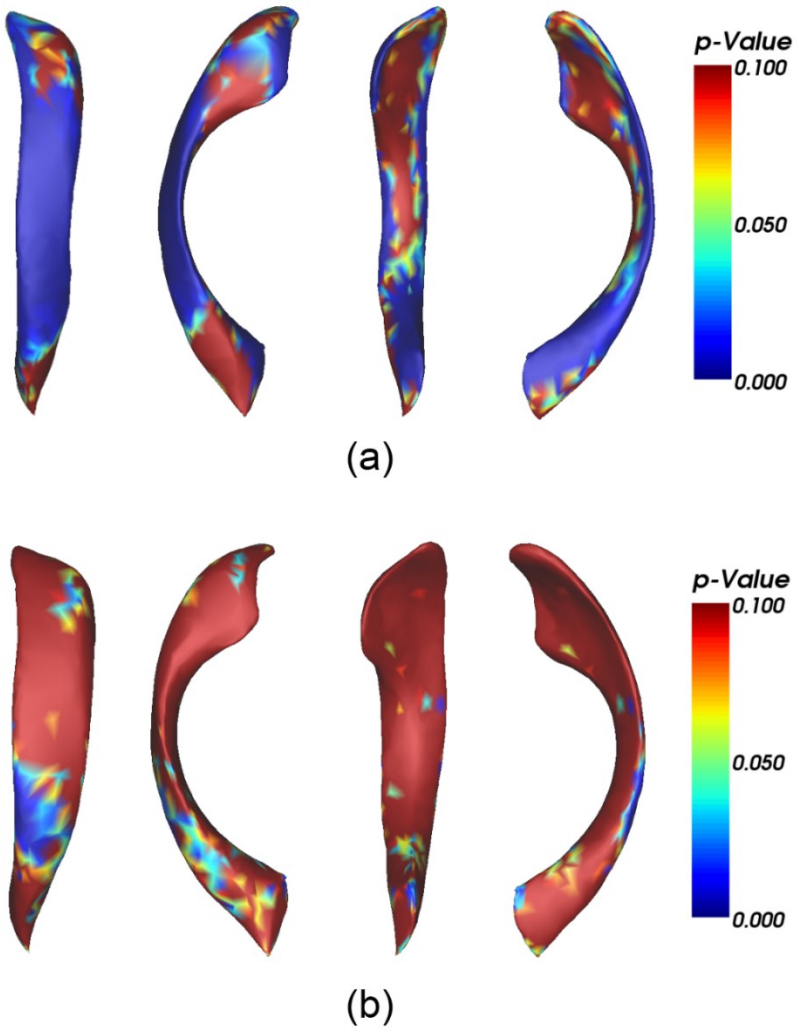

Fig. 5.5 The *p*-map of statistical significance between corresponding points between the (a) first and second shape, and (b) first and third shape groups, which were identified from fuzzy c-means clustering, obtained from the discriminant analysis. The comparison between the second and third shape groups is not shown.

5.3.3 ROC analysis

The results of the ROC analysis are illustrated in Table 5.1. Two measures of SSM correspondence were computed, the sum of squares of the shape descriptors and the volume of enlargement, in order to identify the optimal biomarker for the classification of ventricular enlargement compared to the manual gold standard. In this table, the top row shows the ROC results using measures computed from the single SSM transformed to the unclassified ventricles, and the bottom row shows the ROC results from using the three SSMs constructed from each shape group. In the latter case, only the SSM that was most

similar to the unclassified shape, as determined by the Dice overlap [Dice, 1945], and the correspondence measures obtained from this transformation were used. The computed performance measures include the AUC, SE, positive predictive value (PPV) and negative predictive value (NPV) for both measures. These performance measures quantify how closely the classification of ventricular enlargement by the SSM agrees with the gold standard classification obtained from a medical expert, with the AUC measure representing the probability of correctly classifying ventricles as healthy or enlarged. As expected, the SSM shape descriptors showed reduced performance compared to the volume of enlargement, hence only the volume of enlargement was used to measure the magnitude of injury in individual anatomical regions.

Table 5.1. The computed AUC, SE, PPV and negative predictive value NPV for each of the three measures of model correspondence, obtained from the ROC analysis.

ROC Measure		**Sum of squares of the shape descriptors**	**Volume of enlargement (mm^3)**
Single SSM	AUC ± SE	0.680 ± 0.050	0.889 ± 0.029
	PPV	0.629	0.798
	NPV	0.629	0.800
Multiple SSMs	AUC ± SE	0.545 ± 0.057	0.925 ± 0.023
	PPV	0.489	0.830
	NPV	0.486	0.829

5.3.4 Performance of biomarkers

The linear regression models of the impingement volumes in the periventricular WM and GM structures with the multiple clinical scores are detailed in Table 5.2. The variables incorporated into each regression mode, which include the impingement volumes into each labelled anatomy as well as subject age and gender, are shown in the rows of Table 5.2. Each column of this table describes the standardised regression coefficients of each variable with the AHA, BRIEF, SDQ, TVPS, WR or VOC clinical scores respectively. The amount of variation in each clinical measure explained by the regression models is described by the R-squared value. In addition, the amount of variation explained by the two covariates, age and gender, alone were computed from regression models constructed using only these variables. The likelihood of the regression coefficients being erroneously found to have a non-zero relationship with the outcome variable is shown by the associated *p*-value.

All deep WM and GM structures, except the caudate nucleus, were significantly associated with the AHA clinical score for motor function. The PLIC was significantly associated with both scores of executive function (BRIEF and SDQ), while the ALIC was also associated with the SDQ score. No significant anatomical associations were observed for the TVPS score for visual perception or the VOC score for vocabulary. The caudate nucleus, ALIC, and lenticular nucleus were strongly associated with the word reasoning (WR) score.

Table 5.2. The standardised regression coefficients and associated p-value for each of the linear models, which show the relationship between the volume biomarkers of enlargement into key structures surrounding the ventricle, and the AHA, BRIEF, SDQ, TVPS, WR and VOC clinical scores of outcome. The resulting r-squared of the complete linear models, as well as linear models of just the covariates (patient age, in years, and gender) are shown at the bottom.

	AHA	**BRIEF**	**SDQ**	**TVPS**	**VOC**	**WR**
Variable	Regression coefficient	Regression coefficient	Regression coefficient	Regression coefficient	Regression coefficient	Regression coefficient
Caudate nucleus	-0.20	0.14	0.49	0.20	-0.09	**0.59***
Thalamus	**1.15*****	0.40	-0.45	0.10	-0.08	0.18
PLIC	**-1.77*****	**-0.78***	**1.06***	0.02	0.59	-0.47
ALIC	**0.76***	0.19	**-1.13***	-0.32	0.03	**-0.99***
Lenticular nucleus	**-0.48***	0.03	-0.03	0.24	-0.42	**0.78****
Age	**0.25***	-0.06	**0.42****	-0.21	0.33	**0.49*****
Gender	-0.01	**0.49****	**0.46***	0.08	-0.08	-0.21
Multiple r-squared	**0.62*****	**0.33***	**0.55*****	0.09	0.20	**0.50*****
Multiple r-squared of covariates (age, gender)	0.08	**0.24****	**0.24***	0.05	0.10	**0.28*****

Asterisked correlations were found to be statistically significant: * $p < 0.008$; ** $p < 0.0016$, *** $p < 0.00016$. Correlations in bold have a statistical significance of $p < 0.08$.

Gender was observed to have a significant effect on both the BRIEF and SDQ measures of executive function ($p < 0.008$), while age was strongly associated with the AHA, SDQ and WR scores ($p < 0.008$). This latter observation of age being strongly associated with these functional scores is expected from the literature [Henry and Millar, 1991; Morris et

al., 1982], even though age was not found to be associated to lateral ventricle shape and hence not incorporated into the SSM. Overall, these covariates explained relatively less variation in the AHA score than the measured impingement volumes. However they explained most of the variance in the BRIEF measure, and explained roughly half of the variation in the SDQ, TVPS, VOC and WR measures.

Regression models explained between 9% of the variance in the clinical score (for the TVPS measure) to 62% (for the AHA measure). Four of the regression models (for the AHA, BRIEF, SDQ and WR scores) reached significance (p < 0.008). A visual representation of the regression coefficients from the regression models in Table 5.2 is illustrated in Figure 5.6. In this figure, the deep GM structures, and the ALIC and PLIC, are illustrated adjacent to the outlined lateral ventricles.

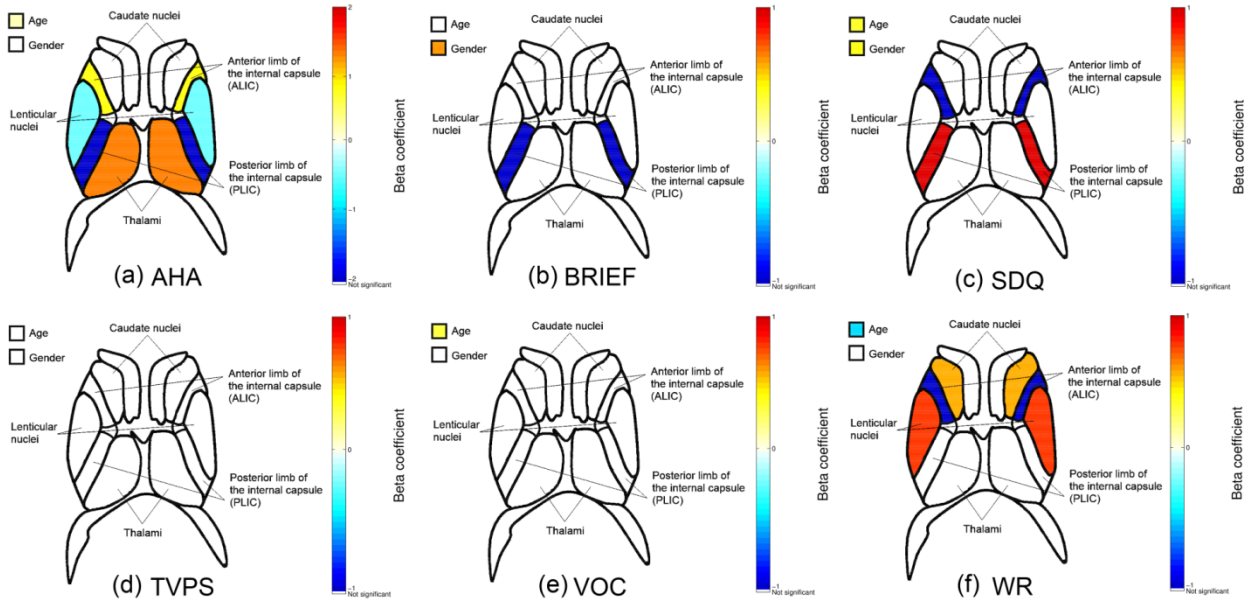

Fig. 5.6 A visual illustration of the regression coefficients of the linear models computed between the impingement volumes, and the (a) AHA, (b) BRIEF, (c) SDQ, (d) TVPS, (e) VOC and (f) WR. Blue colours indicate a larger negative regression coefficient, red represents a larger positive regression coefficient. Non-significant regression coefficients (p > 0.008) are indicated in white.

5.3.5 Performance of anatomical volumes

The regression models constructed with the deep GM anatomical volumes obtained from FIRST are detailed in Table 5.3. These regressions explained between 5 and 25% of the

variance in the six clinical measures, with only the regression model of the AHA score of motor function reaching clinical significance following Bonferroni correction. The thalamus and lenticular nucleus volumes were found to be significant in the BRIEF measure, however no other anatomical volumes were found to be significant in any of the other regression models. Patient age was found to be a significant factor for three of the six clinical scores. Overall, these regression models explained less of the variance in the clinical scores compared to the corresponding regression models containing the identified volume of local ventricular enlargement, shown in Table 5.2.

Table 5.3. The standardised regression coefficients and associated p-value for the linear models which show the relationship between the anatomical volumes and the AHA, BRIEF, SDQ, TVPS, WR and VOC clinical scores. The resulting r-squared of the model, and of the covariates (patient age and gender) alone are shown at the bottom.

	AHA	**BRIEF**	**SDQ**	**TVPS**	**VOC**	**WR**
Variable	Regression coefficient	Regression coefficient	Regression coefficient	Regression coefficient	Regression coefficient	Regression coefficient
Caudate nucleus	-0.18	-0.08	0.22	-0.28	-0.28	0.22
Thalamus	-0.30	**-0.95***	0.05	0.13	0.13	0.05
Lenticular nucleus	0.35	**1.07****	-0.46	0.29	0.29	-0.46
Age	**-0.43***	0.24	-0.43	0.47	**0.47***	**-0.43***
Gender	0.93	0.15	0.09	-0.08	-0.08	0.09
Multiple r-squared	**0.25***	0.16	0.13	0.05	0.15	0.13
Multiple r-squared of covariates (age, gender)	0.22	0.02	0.10	0.04	0.14	0.10

Asterisked correlations were found to be statistically significant: * $p < 0.008$; ** $p < 0.0016$, *** $p < 0.00016$. Correlations in bold have a statistical significance of $p < 0.08$.

5.4 Discussion

In this chapter, an automated tool to quantify ventricular enlargement and demonstrated its correlation to clinical function has been described. The proposed automated method uses SSMs to model the healthy variation in ventricular shape, which provide a surrogate marker of sub-cortical GM tissue damage that can be measured robustly. The robustness

of measuring ventricular enlargement was demonstrated with a ROC analysis, with showed the healthy SSM was frequently able to identify the regions of ventricular enlargement symptomatic of injury (AUC = 0.925). Additionally, significant correlations were observed between the computed anatomical impingement volumes and multiple clinical scores of function. This demonstrates the clinical utility of these predictive regression models of function using the proposed impingement volumes to predict patient outcome from MR images alone, and subsequently tailor patient-specific treatment. Furthermore, these regression models provide a tool to elucidate the relationship between observable injury and clinically observed symptoms, which can help improve the understanding of the brain's structure-function relationship.

The high variability in the shape of healthy ventricles presents a technical challenge in the modelling and correspondence of the SSM approach, so several additional steps were included in the methodology. Firstly, to avoid errors in obtaining correspondences between healthy ventricles and the highly variable shapes of enlarged ventricles, a healthy SSM was constructed, which allows injured areas to be identified as the volume of enlargement outlined by the transformed SSM. To further account for the high variability in shape of healthy ventricles, point correspondences between the constructed SSM and the training data were iteratively recomputed to further reduce the reconstruction error of the SSM, resulting in a better representation of these healthy ventricle shapes. Secondly, multiple diverse SSMs were generated, to describe sub-populations of healthy ventricle shapes. The utilisation of multiple SSMs led to improvements in the binary classification of ventricular enlargement compared to the manual gold standard from 0.889 to 0.925 (Table 5.1). Although using multiple SSMs requires greater computational resources, it minimises errors in the SSM construction and transformation processes, which critically rely on an accurate correspondence match between shapes.

The sum of squares of the shape descriptors was observed to not be predictive of enlargement whether one or multiple references were used (respective AUCs of 0.68 and 0.545). The greater than random classification performance of this measure reflects that enlarged ventricles are typically larger than the mean, however its reduced performance compared to enlargement arises as instances of ventricular enlargement do not lead to the ventricles extending significantly along healthy eigenmodes, but rather this enlargement typically occurs along eigenmodes not contained within the healthy SSM. For instance, in

cases where small ventricles were locally enlarged due to injury, appearing as a subtle irregularity, the computed shape descriptors would be small as the global ventricle size is small, however the subtle irregular enlargement is still captured by the volume mismatch measure. Furthermore, the drop in performance of the sum of squares descriptor on multiple SSMs compared to one SSM is the result of this descriptor relying on the "distance from the mean shape" to be indicative of enlargement. When multiple SSMs are used, each with their own mean shape, the closest mean to the target shape will be selected, in effect underestimating the $b_{constrained}$ parameters and leading to the poorer prediction of enlargement based on $b_{constrained}$ alone.

The impingement volumes quantifying the extent to which deep WM and GM structures adjacent to the ventricle were impacted by the change in shape were found to be significantly associated with four of the six measured clinical scores of functional outcomes. The known importance of the thalamus, PLIC and basal ganglia (which includes the putamen of the lenticular nucleus) in relaying motor information [Hoon Jr et al., 2009; Rose et al., 2011; Rutherford et al., 1996] is reflected in the strong association of all structures with the AHA score, and the explanation of over 60% of variance in the AHA score in the regression model. WM abnormalities in the PLIC and ALIC were strongly associated with both scores of executive function (BRIEF and SDQ), which is consistent with the literature [Edgin et al., 2008; Kurowski et al., 2009]. However the known role of the thalamus and caudate nucleus in executive function [Grahn et al., 2008; Van der Werf et al., 2003] has not been identified in these regression models. There were few significant associations between impacted periventricular anatomies and the clinical scores for visual perception and communication (TVPS and VOC respectively), which may be due to the larger role the cortical GM plays in both visual processing as well as the comprehension and production of language. Despite this, the second score for communication (WR) showed a significant association with the caudate nucleus, ALIC and lenticular nucleus. The association between these anatomies with language comprehension has been demonstrated in the literature [Giroud et al., 1997; Watkins et al., 2002]. Gender was observed to be a factor for both scores of executive function, indicating that females performed better than males in these tasks within the age range of 5-17, which was expected. Similarly age was found to have a positive association with several scores including AHA, SDQ and WR, indicating that older patients performed better in these

tasks. The strong relationship to several clinical outcomes highlights that the impact of ventricular enlargement on adjacent structures plays an important role in influencing patient outcome.

There was a positive covariance observed between the computed impingement volumes for all pairs of anatomical structures. This was expected as injury to one anatomy due to ventricular enlargement is likely to lead to greater impact to adjacent structures as well. These associations between anatomies explain why there are positive regression coefficients in the constructed regression models, as shown in Table 5.2. In all the regression models, the largest regression coefficient was negative, and the association of injury measures in adjacent regions caused other coefficients to have smaller positive values in order to maximise the fit to the clinical score. Including interaction effects into the regression was considered to help minimise this effect, and will produce regression models with better correlations to clinical outcomes, however the risk of over-fitting by including too many interaction terms was deemed to outweigh the potential benefit. Therefore although the positive regression coefficients imply that there is a positive relationship between extent of injury and patient function, it is important to note that these positive coefficients should be considered as part of the regression model, with all anatomies included, and not in isolation with the clinical score.

The volume of ventricular enlargement, identified using multiple SSMs, was found to explain a greater percentage of variance in all of the clinical scores compared to the computed volume of the entire sub-cortical structures obtained from FIRST. The regression models constructed using the volume of these anatomies was not strongly indicative of any measure of patient function, with patient age being the only significant variable identified across multiple regression models. This suggests either that anatomical volume does not represent injury or that the estimation of anatomical volumes is too error prone in the presence the large anatomical injuries typical of CP. As a result, the proposed method of identifying a volume of enlargement using healthy ventricular SSMs provides measures that are more representative of the underlying injury due to ventricular enlargement, and yields regression models that can more accurately predict patient function given this type of injury. This performance benefit stems directly from the method’s use of ventricle segmentations, lending it robustness in the face of extensive anatomical malformation.

The limitation of this work was that the proposed method only analyses the shape of the ventricles, so the measure is fundamentally a surrogate measure of injury, albeit one that can be reliably characterised. Although this is a common type of injury in children with CP, it does not consider lesions and cortical malformations that do not influence ventricular shape. Consequently, these forms of injury are investigated using different methods, which are detailed in the following chapters. Another limitation is that the areas labelled as deep WM and GM anatomies were only defined from the Colin 27 atlas, and not identified individually for each patient. Therefore there may be inaccuracy in the computed impingement volumes as it does not account for the translation of these anatomies due to ventricular enlargement.

The main strength of this proposed surrogate biomarker is that it avoids quantifying deep GM volumes directly, an error prone approach when injuries are large. This is an important consideration, as extreme anatomical variations which are commonly observed in children with CP are a critical limitation of atlas-based approaches for segmenting anatomical structures for subsequent estimations of volume. Additionally, the proposed method only requires one structural MR image, and does not require additional modalities such as diffusion or functional MRI, which facilitates the potential translation of such automated techniques to clinical practice. The advantages of this approach for assessing children with CP are highlighted by the improved correlations compared to the more sophisticated approach used in FIRST. Future work will involve devising methods for robustly segmenting the subcortical anatomies for each patient, allowing more accurate measures of enlargement to be derived.

5.5 Conclusions

This chapter presented an automated method for robustly detecting and quantifying a subset of CP associated injuries, by quantifying ventricular enlargement and its impingement upon local anatomical structures. Using the SSM method, a model describing the variability in the shape of healthy ventricles was used to identify regions of enlargement related to developmental disturbances in ventricles segmented from structural MRIs. A ROC analysis showed that this SSM accurately classifies ventricles as enlarged or healthy (AUC 0.889 using a single SSM, 0.925 for three SSMs). Quantifications of the effect of ventricular enlargement on adjacent deep WM and GM structures were shown to have a strong correlation with multiple clinical scores, including: motor (R squared 0.62, $p < 0.008$), executive (0.55, $p < 0.008$) and communicative function (0.50, $p < 0.008$), especially in comparison to more standard atlas based segmentation approaches (R squared 0.25, 0.13 and 0.13 for the same clinical scores, $p < 0.008$ for the first value, $p > 0.008$ for the remaining values). These results illustrate the potential for quantification of MRIs for further elucidating the relationship between observable physical brain injury and clinically observed symptoms, with potential to better tailor treatments for patients. In the following chapters, automated strategies for the segmentation of other types of injury observed in children with CP are detailed, including cortical malformations and WM or GM lesions, and assess their impact on clinical outcomes.

6. Characterising cortical morphology in a cohort of children with unilateral cerebral palsy

6.1 Introduction

An important class of injury in children with CP are cortical malformations, as they crucially impact the cortical GM responsible for the generation of neural signals. Alterations of the cortical surface are the result of several types of lesions observed in children with CP [Bax et al., 2006], as it relates to either environmental or genetic insult [Barkovich et al., 2012; Leventer et al., 2008] to the neuronal architecture critical for brain function [Collin et al., 2014]. The injury appears as a heterogeneous group of congenital cerebral alterations, which results in several clinical types. In particular, in unilateral CP, the type of injury includes (by frequency): PWM lesions (45%), GM lesions (30%) and brain maldevelopments (14%) [Cioni et al., 1999]. All these abnormalities can result in abnormal cortical folding, altered gyri, abnormally thick folds (pachygyria) and abnormal fluid filled clefts arising from primary (for cortical GM involvement) or secondary (for WM involvement) origin, which contribute to functional impairments irrespective of aetiology. MRI is pivotal for defining alterations due to cerebral injury, however the current qualitative clinical assessments based on aetiology [Cioni et al., 1999; Krägeloh-Mann and Horber, 2007] are too broad, and not sufficient to describe the large variability in appearance or impact of these alterations [Feys et al., 2010]. Quantitative image analysis techniques are needed to develop models which can quantify the severity of abnormalities due to injury, and to link cortical structure to patient function.

An automated quantitative analysis of cortical shape has the potential to comprehensively characterise the shape of the cortex and relate this shape to a range of functional outcomes. In the CP setting, the heterogeneity of possible alterations due to lesions necessitates the use of several measures of shape to fully characterise cortical morphology. Cortical thickness is one important measure that increases during development [Shaw et al., 2006], which can be used to detect and quantify primary or secondary pachygyria. Cortical thickness has been used in many studies in order to characterise healthy development [Sowell et al., 2004], abnormal development [Moeskops et al., 2015], and to investigate cortical thinning due to schizophrenia [Rimol et al., 2012] and Alzheimer's disease [Haidar and Soul, 2006]. The curvature of the cortex [Rodriguez-

Carranza et al., 2008] and sulcal depth [van Essen, 2005] are alternative measures that reflect the changes in cortical surface area arising from gyrification during development [Dubois et al., 2008a]. Consequently, these measures are important for identifying changes in cortical folding related to several brain malformations such as lissencepahly, polymicrogyria or schizencephaly, with multiple studies highlighting the sensitivity of these measures in detecting cortical abnormalities [van Essen et al., 2006; Nordahl et al., 2007; White et al., 2003; Zhang et al., 2015].

Current cortical analyses typically use combinations of these shape measures within surface-based morphometry frameworks to identify statistically significant differences between diseased or injured brains and healthy controls [Dierker et al., 2015; Park et al., 2009; Schaer et al., 2008]. However, the severity of alterations observed in children with CP, such as those illustrated in Figure 6.1, introduces significant errors into the registration of cortical surfaces required by morphometric analyses. In the CP setting, FreeSurfer is frequently used to extract and parcellate the cortical surface [Kelly et al., 2015; Papadelis et al., 2014; Rose et al., 2011] and to compute multiple measures of cortical shape [Danti et al., 2015; Ma et al., 2015; Shollenbarger et al., 2015]. This method however relies on an accurate deformation of a surface mesh, necessitating manual intervention or the exclusion of severely injured data. VBM [Ashburner and Friston, 2000] is also a commonly used approach for assessing cortical GM changes between healthy and unhealthy groups [Giménez et al., 2006], correlating image features to outcome [Northam et al., 2011; Soria-Pastor et al., 2008], and investigating longitudinal changes in structure related to plasticity [Giuliani et al., 2011; Sterling et al., 2013; Thomas et al., 2009]. This approach has been found to be susceptible to false positives due to the complicated structure of the neocortex [Scarpazza et al., 2015], and is similarly hindered by severe injury, which affects the accuracy of the image registration. Additionally, although a combination of these cortical shape measures have been correlated with brain volume [Im et al., 2008], Intelligence Quotient (IQ) [Im et al., 2006] and cognitive scores [Dubois et al., 2008a; Jouvent et al., 2008], and have been tracked longitudinally over the development of pre-term infants [Chung et al., 2003; Dubois et al., 2008b], no such correlations have been made for CP specifically, primarily due to the difficulty in segmenting and labelling GM tissue on regions of severe injury.

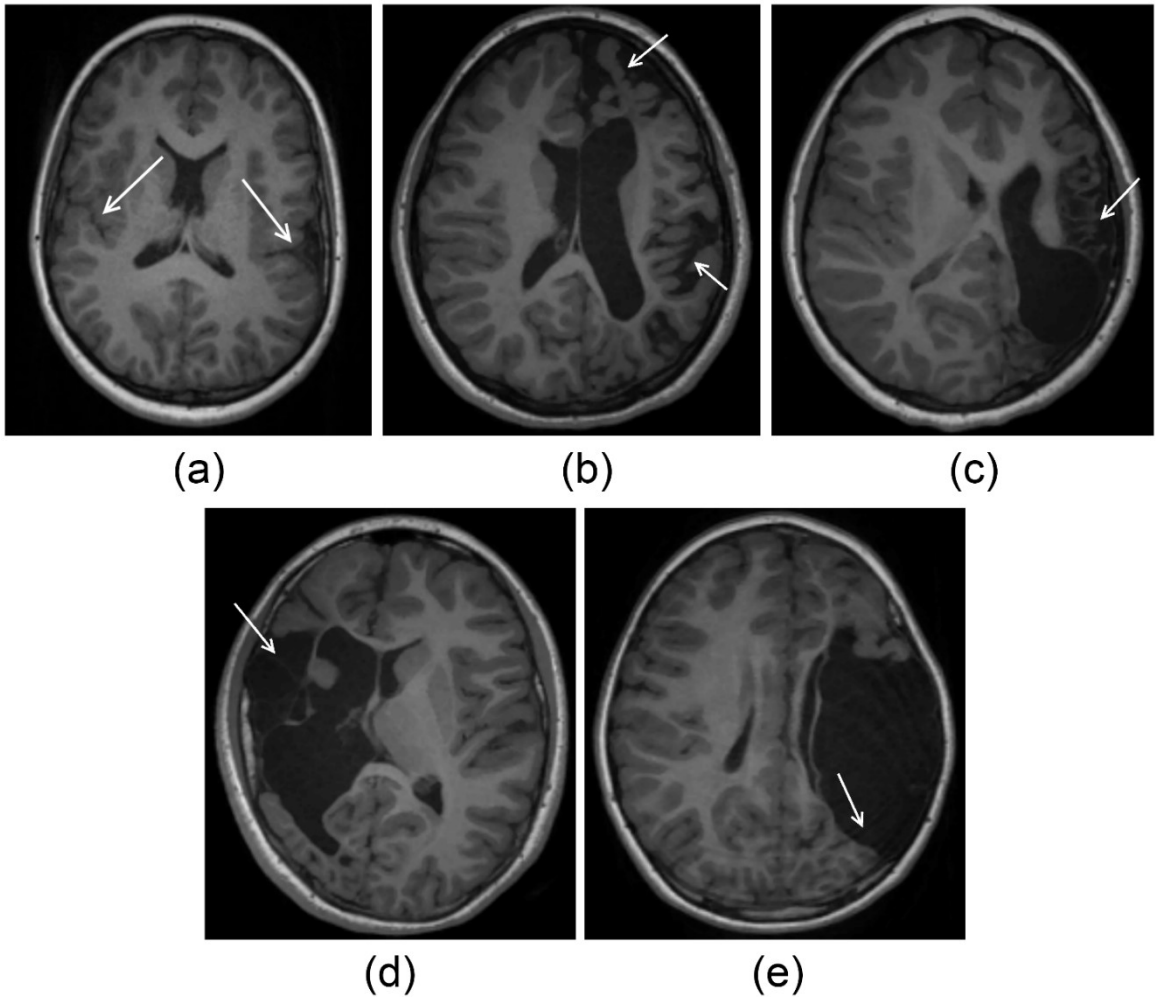

Fig. 6.1 An illustration of the extensive injury common in CP patients resulting in abnormal folding and abnormal fluid filled areas (bilateral perisylvian polymicrogyria (arrow, a), ventriculomegaly (b-d) and abnormal fluid filled clefts (arrow, b-c) or cysts (arrowhead, d-e). Secondary alterations of the cortical surface were caused by: (b-c) PWM lesions and (d-e) CDGM lesions.

Provided these technical difficulties can be overcome and a robust and sensitive characterisation of the cortical surface can be obtained, several hypotheses related to cortical injury and compensatory mechanisms in children with CP can be investigated. Firstly, since cortical shape is an important consideration of clinicians reviewing abnormalities that are visible in MRIs [Guerrini and Dobyns, 2014; Leventer et al., 2008], automated measures of cortical shape could readily be applied to identify and quantify the differences between children with cortical alterations and TDC. Secondly, in cases with unilateral injury, abnormalities in the uninjured hemisphere relative to the typical population

will occur as a result of either secondary microstructural damage due to altered influences of the injured hemisphere, or potential plasticity mechanisms which have been observed in animal models [Kolb and Gibb, 2007], stroke patients [Ward, 2005] and children with CP [Krägeloh-Mann, 2004]. It could also help establish whether subtle cortical alterations exist in children with other forms of injury such as PWM lesions (i.e. PVL or ventricular enlargement due to loss of PWM injury). Finally, measures of healthy (or unhealthy) cortical shape taken from multiple cortical regions with a known functional role could be correlated to patient function, revealing the structure-function models of the brain.

In this chapter, it is hypothesised that shape measures in the injured classes (alterations present within the ipsilateral hemisphere or bilateral alterations due to brain injury in clinically unilateral CP), are different from TDC. It is also hypothesised that cortical shape contralateral to the side of injury differs from TDC, potentially due to mechanisms of plasticity. Finally, it is hypothesised that children with clinically diagnosed unilateral CP but with other (non-cortical) forms of injury will nevertheless contain subtle changes in cortical measures relative to the TDC. To test these hypotheses, the differences in shape measures between healthy and altered brains of children with unilateral CP were investigated. The extent of the relationship between the severity of cortical alteration and multiple clinical scores of function in a cohort of patients diagnosed with unilateral CP are also established. To achieve this, the EM segmentation algorithm with a modified MRF implementation which removes the reliance on atlas based priors in order to obtain segmentations that are robust in the presence of injury [Pagnozzi et al., 2015] was used. Such robustness is necessary when alterations are as severe as those often observed in patients with CP. Using the segmented regions, measures of cortical thickness, curvature and sulcal depth are computed in order to capture the heterogeneous range of values observed in children with CP and TDC. Comparisons were performed between the TDC and children with unilateral alterations, bilateral alterations, and CP cases without visible cortical alterations. Subsequent correlation to clinical performance scores including motor function, cognitive function, visual acuity and communicative ability were performed using the cortical measures in units of z-score normalised by the variance of individuals within the healthy population. The derived models of structure and function are intended to facilitate future improvements to the selection of therapies tailored to individual patients, and addresses Aim 1 of this thesis, “develop several automated segmentation approaches

to delineate the three main classes of injury observed in children with CP; cortical malformations, WM injury and ventricular enlargement". This work has also been published, and is available at doi: 10.1002/hbm.23262.

6.2 Materials and Methods

6.2.1 Study Participants

All 139 children recruited as part of the studies detailed in Section 3.2.1 have been included in this chapter.

6.2.2 Shape analysis of cortical segmentations

Segmentation of the cerebral tissues on all 139 T1-weighted MRIs was performed using a modified EM-MRF, from which cortical GM segmentations were subsequently identified. Three measures of cortical shape; cortical thickness, sulcal depth and curvature were computed for all GM segmentations obtained using the proposed EM-weighted MRF method described in Chapter 4. An illustration of these three cortical measures, illustrated on the cortical mesh of a patient with an observed unilateral malformation, is shown in Figure 6.2. A description of how these shape measures were computed, and how cortical regions were segmented, is given below.

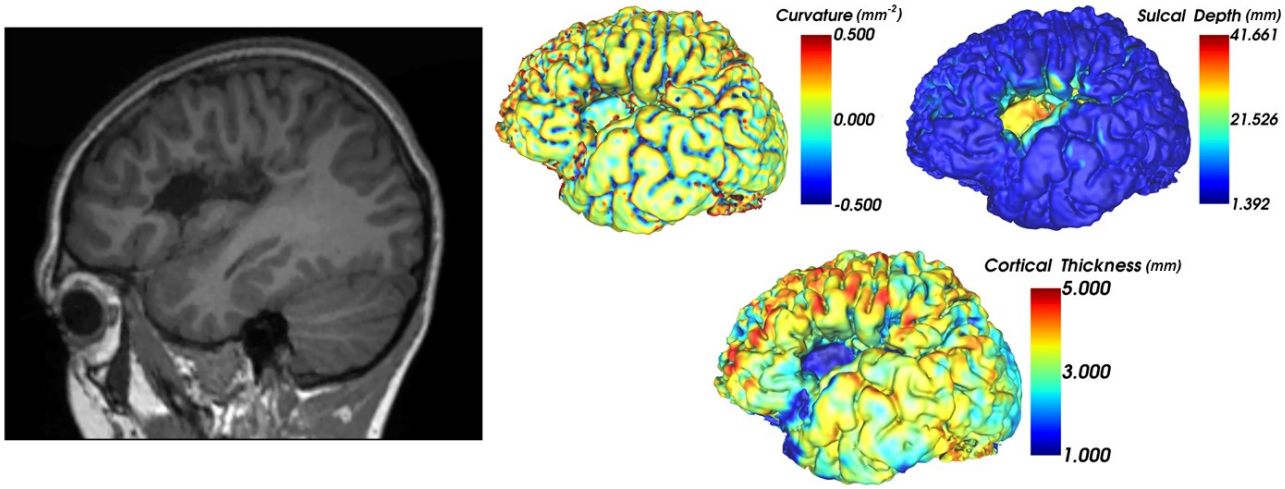

Fig. 6.2 The structural MRI of a patient with a unilateral malformation, and the measured cortical thickness, curvature and sulcal depth, displayed on the VTK mesh for the injured hemisphere.

As the methodology presented in this chapter is primarily focused on identifying primary cortical malformations and no other primary lesion types, including WM and GM lesions, as well as secondary ventricular enlargement, the effects of these other lesion types were removed from the shape analysis. Specifically, secondary ventricular enlargement was removed by masking out the segmented lateral ventricles from the brain mask, which otherwise could influence measures of sulcal depth if the ventricle extended to the skull. In cases where entire cortical regions are missing due to tissue loss, resulting in secondary enlargement of the ventricles, shape measures from these cortical regions would be subsequently be masked out in this process, and treated as a missing value in the statistical methodology. Additionally, the presence of lesions was not accounted for in the brain segmentation, as the presence of GM lesions could affect measures of cortical thickness and curvature.

6.2.2.1 Computing cortical thickness and sulcal depth

For all 139 MRIs, cortical thickness and sulcal depth measures were computed by solving Laplace's equation [Jones et al., 2000]. This voxel-based approach for measuring the distance between non-intersecting surfaces was used, primarily due to its robustness to severe injury as it does not rely on accurate mesh registration. Additionally, this approach is more computationally efficient compared to the relatively time-consuming surface based methods [Das et al., 2009]. To measure cortical thickness, the voxels adjacent to the WM/GM boundary were labelled as such, as were the voxels adjacent to the GM/CSF boundary. The remaining voxels from this segmentation were iteratively recomputed as the average of its six adjacent neighbouring voxels. After several iterations, a local gradient was computed for every voxel within the segmentation and normalised to have unit magnitude. Subsequently, each location of the outer surface was propagated along the gradient field until the inner surface was reached, forming one path per voxel. This approach yields a smooth topological one-to-one mapping between each surface of the cortex, allowing thickness measures to be computed as the cumulative distance from the interior of the cortex to its corresponding point on the exterior of the cortex. Similarly, both sides of the subdural CSF segmentation were identified from the EM-MRF segmentation, and Laplace's approach was used to compute a smooth mapping between the CSF adjacent to the skull and the CSF adjacent to the sulci and gyri of the cortical surface. The

distance between these two regions (i.e. surfaces) of CSF was called the sulcal depth. These two measures are illustrated in Figure 6.3.

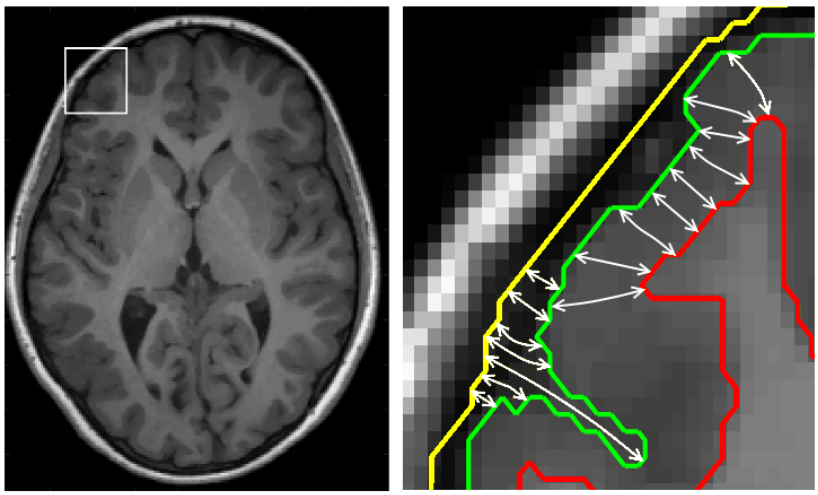

Fig. 6.3 An illustration of the cortical thickness and sulcal depth shape measures on a region from a healthy brain shown in (a). In (b), the outer (subdural) surface of the CSF is shown in yellow, the CSF/GM interface is shown in green, and the GM/WM interface is shown in red. Examples of measures of cortical thickness and sulcal depth are illustrated as white arrows between the yellow and green, and green and red contours, respectively.

Cortical thickness and sulcal depth measures computed from the 44 healthy MR scans were isolated, and the mean and standard deviation was identified for each cortical region labelled on the Colin 27 AAL atlas. This models the healthy variation of these shape measures in each cortical region as a Gaussian distribution. The computed shape cortical thickness and sulcal depth measures obtained from target MR scans, which may or may not have a malformed cortex, were converted to a z-score using the distribution of parameters obtained from the TDC, as shown in Eq 6.1. The signed value of the z-score was then used as independent variables in the subsequent linear regression models, .e.g. for cortical thickness:

$$z_{thick} = \frac{x_{thick,target} - \mu_{thick,healthy}}{\sigma_{thick,healthy}} \qquad Eq\ 6.1$$

6.2.2.2 Computing exterior surface mesh and cortical curvature

The 139 GM segmentations were also converted to meshes using VTK [Shroeder et al., 2006]. This mesh was decimated and smoothed, before measures of curvature are

computed using the Gauss curvature from VTK. The Gaussian curvature (K) at a vertex v is defined below:

$$K(v) = 2 * \pi - \sum_{facet\ f\ of\ v} angle_{f\ at\ v} \qquad Eq\ 6.2$$

where the contribution of each facet is weighted by $Area(facet)/3$, and is in units of mm^{-2}. Using this 3D mesh, absolute curvature measures computed from the 44 healthy MR scans were extracted, and the standard deviation was identified for each cortical region labelled on the AAL atlas. The mean and standard deviation of the measured curvature from MR scans of children with CP is computed in each cortical region. As alterations may appear as either excessively folded gyri or an excessively smooth cortex, a signed z-score was again used for curvature.

6.2.3 Anatomical labelling of cortical regions

Cortical regions, such as the precentral and postcentral gyri, were identified on all 139 MRIs by propagating the cortical labels from the AAL atlas to the cortical GM of each patient using level sets [Adalsteinsson and Sethian, 1995; Osher and Sethian, 1988]. Traditionally, this approach is used to compute the propagation of fronts by solving the Eikonal equation [Sethian, 1996], which inherently accounts for topological changes such as branching. In this application, the method yields a 4D level set function, which contains the topological mapping between the outer GM surface of the *subject* and the outer GM surface of the *atlas*. Additionally, unlike the Laplacian approach, the level set function can produce a topological mapping between intersecting surfaces, which occurs frequently in the comparison between atlas and subject. Furthermore this mapping can extend across large distances, allowing for correspondences between healthy and severely malformed cortical surfaces, as illustrated in Figure 6.4. Using a MATLAB implementation of level sets [Li et al., 2011], the AAL cortical labels were propagated down the gradient of the level set function to the outer GM surface of each subject.

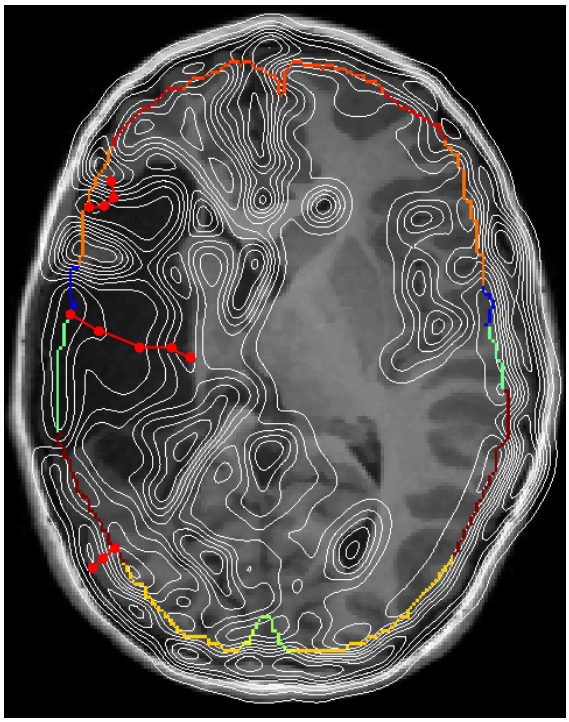

Fig. 6.4 The propagation of the AAL GM labels using the level set function for an image with severe alteration. The in-plane gradient of the level set is illustrated with the white contour lines, and the multi-coloured cortical surface represents the cortical labels from the AAL atlas. Propagation of three points from the atlas label to locations on the subject's cortex is shown, with two points being close to their target and the third being relatively distant from its target, yet still generating a successful labelling.

6.2.4 Selection of cortical grey matter regions

A succinct set of 12 cortical regions related to each of the six clinical scores were chosen from the AAL atlas for the subsequent statistical analyses. For the AHA test of bimanual hand function, areas critical to motor tasks such as the primary motor cortex, supplementary motor area and the primary somatosensory cortex [Shibasaki et al., 1993] were included, as well as the posterior parietal cortex which has a role in reaching tasks [Kertzman et al., 1997]. These regions have also been identified as important for hand motor function from several functional MRI studies examining cortical activation following hand tapping tasks [Jäncke et al., 2000; Lotze et al., 1999; Lutz et al., 2005].

For the BRIEF score of executive function, the insular and cingulate cortices were chosen based on their known role in both cognitive tasks [Sridharan et al., 2008] and emotional processes [Bush et al., 2000] respectively. Regions selected for the TVPS test for visual

perception include the primary visual cortex which is involved in visual processing [Lee et al., 1998], the inferior temporal gyrus which is involved in visual memory [Eskandar et al., 1992], and both the lingual and fusiform gyri which have a role in processing letters [Mechelli et al., 2000] and faces [Gorno-Tempini et al., 1998]. The inferior frontal gyrus was included for the VOC score as it contains Broca's area, which has a known role in speech production [Papoutsi et al., 2009], and the superior temporal gyrus which contains the primary auditory cortex and has a known role in speech perception and production [Buchsbaum et al., 2001]. An outline of the selected cortical regions for each clinical score is outlined in Table 6.1.

Table 6.1. The manually selected cortical regions from the AAL atlas used as predictor variables for the linear models.

Motor regions (AHA)	**Executive function regions (BRIEF)**	**Visual regions (TVPS)**	**Vocabulary regions (VOC)**
Primary motor cortex	Insular cortex	Primary visual cortex	Inferior frontal gyrus
Supplementary motor area	Cingulate cortex	Lingual gyrus	Superior temporal gyrus
Primary somatosensory cortex		Fusiform gyrus	
Posterior parietal cortex		Inferior temporal gyrus	

6.2.5 Statistical methodology

To investigate the differences in measured cortical shape between scanner sequences, a Hotelling's T-squared test was performed on the mean cortical thickness, mean curvature and mean sulcal depth of each patient with each of the three scanner sequences.

A linear mixed-effects model was fitted in order to examine differences in cortical shape measure based on the categorical class of injury, as detailed below, controlling for cortical region, scanner and sequence, patient age and gender. Twelve models were constructed, one for each of the three cortical shape measures, and stratified by the four functional groupings of cortical regions, as outlined in Table 6.1. Bonferroni correction (α = 0.05/12 tests, 0.004) was performed to account for multiple comparisons. In each model, a categorical predictor variable describing the aetiological class of injury was included, as well as three covariates, patient age, gender and cortical region defined in the previous section. Patient ID was included in the model as a mixed effect, to account for the fact that

shape measures of each cortical region are quantified for individual patients. The five defined categories for the class of injury include cortical measures obtained from the TDC (n = 44), cortical measures obtained from the ipsilateral hemisphere of children with unilateral alterations (n = 34), cortical measures obtained from the contralateral hemisphere of children with unilateral alterations (n = 34), cortical measures obtained from children with bilateral alterations (n = 7), and cortical measures obtained from children diagnosed with CP but with other (non-cortical) forms of injury (n = 54). This latter class included children with PWM injury and ventricular enlargement.

Multivariable regression analyses were constructed using the R statistical software environment, version 3.2.2 [The R Development Core Team, 2008], to identify the significant cortical shape predictors of multiple patient outcomes. Using the three measures of cortical shape in the cortical regions propagated from the AAL atlas, four models were constructed with the absolute z-scores of the shape measures (relative to the cortical regions of the TDC) being the independent (predictor) variable, and the four clinical scores of patient function being the dependent variable in each model. Patient age, gender and scanner sequence were also included as covariates in the models. To identify optimal sets of markers associated with outcome, data-driven variable selection using the 'stepAIC' package in R was utilised. This package aims to remove variables that do not explain sufficient variance in the clinical score based on their AIC [Sugiura, 2007]. Note that variable selection was performed on different sets of independent variables, based on the different groups of cortical regions shown in Table 6.1, and used different outcome variables also highlighted by this table, hence there was no overlap between the models. This process was completed using 75% of the data (training), with optimal sets of markers then used to validate the models performance using the remaining test data set (25%). Multiple comparisons on the trained regression models was accounted for using Bonferroni correction (α = 0.05/4 tests, 0.0125). Optimal training models yielded partial regression coefficients, indicating the relative influence of each shape measure and cortical region affecting the neurological outcome used in the model, and a multiple R-squared, which describes the amount of variance in the clinical score explained by the weighted measures of cortical shape.

As the data used in this and the two subsequent chapters include different numbers of subjects, albeit with patient overlap between the chapters, train-test partitions were performed separately in each chapter. This separation was performed using a random selection of the data available in each analysis, followed by a manual check to ensure both partitions were age-matched and showed no significant gender bias.

These model results are compared against the next best performing segmentation software, Atropos, as observed in Chapter 4. Cortical GM segmentations from this software underwent the same processes to measure cortical thickness, sulcal depth and curvature, and the same regression analyses.

6.3 Results

6.3.1 Investigating cortical shape differences between MR scanner sequence

Hotelling's T-squared statistics quantifying the differences in mean cortical shape measures between the 3T Siemen's scanner sequence and the first 1.5T GE scanner sequence was 1.425 (p = 0.258), between the 3T scanner sequences and the second 1.5T scanner sequence was 1.764 (p = 0.197), and between the two different 1.5T scanner sequences was 1.764 (p = 0.178). None of these differences was found to be significant, signifying that despite the differences in scanner sequence and image quality, these differences were resolved by the image alignment and resampling pre-processing steps of the proposed pipeline, hence the computed cortical shape measures were not significantly different.

6.3.2 Measured cortical shape changes due to alteration

The three measures of cortical shape compared between the five aetiological classes of injury are outlined in Table 6.2. Note that all comparisons between these groups have been performed taking into account cortical region, patient age and gender.

Table 6.2 shows that there were significant decreases in cortical thickness observed for children with ipsilateral alterations on the side of injury, compared to the TDC, for the motor and visual regions (p < 0.004). In contrast, there were significant increases in cortical thickness observed on the contralateral side for both motor regions compared to TDC (p < 0.004), with executive function and vocabulary regions also being thicker than the corresponding healthy measure, however this latter finding was not significant (p >

0.004). No significant differences were observed between children with CP but without cortical alterations, and the TDC.

Table 6.2 also shows that there were significant reductions in the curvature of the ipsilateral hemisphere of children with unilateral injury compared to the TDC for executive function regions ($p < 0.004$). In many of the remaining cases, the curvature of children with any type of observed radiological injury where also less curved than the TDC, albeit these did not reach significance ($p > 0.004$).

There were significant increases in sulcal depth observed for children with ipsilateral cortical alterations (on the side of injury) compared to the TDC for motor, executive function and visual cortical regions ($p < 0.004$). Sulcal depth on the contralateral side, however, was significantly decreased compared to the TDC, for vocabulary regions ($p < 0.004$).

Table 6.2. The measured differences in cortical shape measure between TDC ($n = 44$), the ipsilateral hemisphere of children with unilateral alterations ($n = 34$), the contralateral hemisphere of children with unilateral alterations ($n = 34$), both hemispheres from children with bilateral alterations ($n = 7$), and both hemispheres of children diagnosed with CP but with other (non-cortical) forms of injury ($n = 54$). The differences between injured and healthy cortices are also shown along with the significance of the difference and the corresponding SE. For these models, cortical region, age and gender are included as covariates, and patient ID was included as a mixed effect, taking into account that multiple observations per patient corresponding to different regions were used.

Motor regions									
	Cortical thickness (mm)			Curvature (mm^{-2})			Sulcal depth (mm)		
In Cortex:	*Mean*	*Difference*	*SE*	*Mean*	*Difference*	*SE*	*Mean*	*Difference*	*SE*
healthy	*2.947*			*0.490*			*8.627*		
with bilateral alterations	*3.210*	0.263	0.248	*0.424*	-0.066	0.064	*10.296*	1.669	0.549
ipsilateral to alterations	*2.442*	**-0.505***	0.132	*0.418*	-0.072	0.030	*10.421*	**1.794***	0.456
contralateral to alterations	*3.378*	**0.431***	0.153	*0.470*	-0.020	0.039	*7.583*	-1.044	0.408
with other (non-cortical) forms of injury	*3.325*	0.378	0.202	*0.455*	-0.035	0.034	*8.327*	-0.300	0.427
Executive function regions									

In Cortex:	Cortical thickness (mm)			Curvature (mm^{-2})			Sulcal depth (mm)		
	Mean	*Difference*	*SE*	*Mean*	*Difference*	*SE*	*Mean*	*Difference*	*SE*
healthy	*2.788*			*0.882*			*26.963*		
with bilateral alterations	*2.391*	-0.397	0.196	*0.668*	-0.214	0.198	*26.339*	-0.624	1.382
ipsilateral to alterations	*2.701*	-0.087	0.130	*0.219*	**-0.663****	0.135	*31.075*	**4.112****	0.834
contralateral to alterations	*2.872*	0.084	0.128	*0.609*	-0.273	0.252	*25.244*	-1.719	1.16
with other (non-cortical) forms of injury	*2.752*	-0.036	0.117	*0.812*	-0.070	0.123	*27.938*	0.975	0.754

Visual regions

In Cortex:	Cortical thickness (mm)			Curvature (mm^{-2})			Sulcal depth (mm)		
	Mean	*Difference*	*SE*	*Mean*	*Difference*	*SE*	*Mean*	*Difference*	*SE*
healthy	*1.960*			*0.442*			*6.633*		
with bilateral alterations	*1.286*	-0.537	0.201	*0.400*	-0.042	0.058	*5.493*	-1.140	0.976
ipsilateral to alterations	*1.380*	**-0.580****	0.144	*0.390*	-0.052	0.032	*8.388*	**1.755***	0.625
contralateral to alterations	*1.762*	-0.198	0.167	*0.461*	0.019	0.033	*5.834*	-0.799	0.599
with other (non-cortical) forms of injury	*1.664*	-0.296	0.154	*0.401*	-0.041	0.030	*6.497*	-0.136	0.553

Vocabulary regions

In Cortex:	Cortical thickness (mm)			Curvature (mm^{-2})			Sulcal depth (mm)		
	Mean	*Difference*	*SE*	*Mean*	*Difference*	*SE*	*Mean*	*Difference*	*SE*
healthy	*2.962*			*0.449*			*7.893*		
with bilateral alterations	*2.545*	-0.417	0.175	*0.391*	-0.058	0.046	*8.010*	0.117	0.641
ipsilateral to alterations	*2.836*	-0.126	0.104	*0.389*	-0.060	0.024	*8.694*	0.801	0.356
contralateral to alterations	*3.051*	0.089	0.004	*0.396*	-0.053	0.024	*6.601*	**-1.292***	0.348
with other (non-cortical) forms of injury	*2.977*	0.015	0.090	*0.404*	-0.045	0.021	*7.005*	-0.888	0.307

Asterisked correlations were found to be statistically significant: * $p < 0.004$; ** $p < 0.0008$, *** $p < 0.00008$. Correlations in bold have a statistical significance of $p < 0.004$.

6.3.3 Modelling cortical shape biomarkers to clinical outcomes

The shape features from the multivariable regression analyses that were retained following data-driven variable selection are as follows. For the AHA motor score, retained regions include thickness, curvature and sulcal depth of the primary motor cortex, thickness of the primary somatosensory cortex and thickness and sulcal depth of the posterior parietal cortex. Retained regions for the BRIEF score include all three shape measures for the cingulate cortex, and the thickness and sulcal depth of the insular cortex. For this model, the data-driven variable selection only removed one cortical shape feature, suggesting that all these predictor variables explain a unique portion of variance in the executive function score. For the TVPS model, retained predictors include the curvature and sulcal depth in the primary visual cortex, thickness of the inferior temporal gyrus, and thickness of the fusiform gyrus. For the VOC model, cortical thickness and curvature of the inferior frontal gyrus, and the cortical thickness of the superior temporal gyrus, were retained. All retained predictors following the data-driven variable selection in the training set were statistically significant ($p < 0.05$), except for the curvature and sulcal depth of the cingulate cortex, and the thickness and sulcal depth of the insular cortex in the BRIEF model. The regression coefficients and standard errors of the strongly significant cortical features ($p < 0.005$), as well as patient age, gender and scanner sequence, are provided in Table 6.3.

The R-squared of the linear models for each of the clinical scores, provided in Table 6.3, represents the proportion of variance in the clinical score explained by the model constructed on the training set, while the r^2 derived from the model validation represents how well the model performed on the test set.

Table 6.3. Summary of the four trained age-matched regression models, including the regression coefficients and standard errors of only the significant (p < 0.005) cortical regions retained from the data-driven variable selection, as well as patient age, gender and scanner sequence for all models. The multiple R-squared of the trained models, and the squared correlation between the predictions of the trained model on the test set and the test set outcomes are provided, with the significance of these values compared against a Bonferroni corrected alpha value (α = 0.05/4, 0.0125).

AHA			
Cortical region	Regression coefficient	SE	
Primary somatosensory cortex - cortical thickness	-26.612***	6.445	
Primary somatosensory cortex - curvature	-14.169 ***	3.181	
Primary somatosensory cortex - sulcal depth	8.426***	1.931	
Posterior parietal cortex - cortical thickness	12.962**	4.543	
Age	2.009***	0.262	
Gender (Reference: male)	5.548	3.809	
Scanner & sequence (Reference: UQCPRRC)	-0.625	3.323	
R-squared of trained model			**0.78*** **
Predicted r2 on the test set			**0.33** **
BRIEF			
Cortical region	Regression coefficient	SE	
Age	0.851***	0.092	
Gender (Reference: male)	4.246**	1.388	
Scanner & sequence (Reference: UQCPRRC)	-0.818	1.337	
R-squared of trained model			**0.89*** **
Predicted r2 on the test set			**0.03**
TVPS			
Cortical region	Regression coefficient	SE	
Primary visual cortex - curvature	-4.621 **	1.182	
Inferior temporal gyrus - curvature	5.065**	1.565	
Age	2.897***	0.512	
Gender (Reference: male)	1.311	3.999	
Scanner & sequence (Reference: UQCPRRC)	0.514	3.316	
R-squared of trained model			**0.82*** **
Predicted r2 on the test set			**0.44** **
VOC			
Cortical region	Regression coefficient	SE	
Inferior frontal gyrus - cortical thickness	-2.065**	0.565	

Age	2.017***	0.366	
Gender (Reference: male)	5.595	3.224	
Scanner & sequence (Reference: UQCPRRC)	0.890	2.784	
R-squared of trained model			**0.90*** **
Predicted r2 on the test set			**0.39** **

Asterisked regression coefficients were found to be statistically significant: ** $p < 0.01$, *** $p < 0.001$. Model correlations in bold have a statistical significance of $p < 0.0125$. Asterisked model and validation correlations were found to be statistically significant: ** $p < 0.003$, *** $p < 0.0003$.

Although all trained models were statistically significant ($p < 0.0125$), only three obtained significant correlations in the independent test set ($p < 0.0125$). Interestingly, reductions in curvature and increases in sulcal depth in the primary somatosensory cortex were strongly associated with poorer AHA outcomes, reflecting that reduced surface area, and hence cortical volume, of this cortical region is predictive of motor function. For communication outcomes, decreases in cortical thickness in the inferior frontal gyrus (the cortical region containing Broca's area) were also strongly significant ($p < 0.005$), suggesting that tissue loss, reflected in the cortical thickness measure, is an important cortical predictor of these outcomes. For vision, only curvature features were found to be strongly significant ($p < 0.005$), potentially a result of the thinner cortex and shallower sulci present in the posterior sections of the brain. Nevertheless, reductions in the curvature of the primary visual cortex, which again may be a reflection of reduced cortical volume in this area, was the most indicative predictor of patient vision.

Patient age was observed to be a significant predictor of all clinical outcomes ($p < 0.001$), indicating older children performed better at the different tasks. Patient gender was only significantly related to the BRIEF outcome, with girls performing better on the survey of executive functioning compared to boys. Despite age and gender being significant in this model, these findings did not generalise to the test set. MR scanner and sequence was not significant in any regression model, highlighting that differences in sources of data did not explain a significant portion of variance in the clinical outcomes.

6.3.4 Comparison to Atropos

The summary of the regression models using the Atropos segmentations is provided in Table 6.4 below. Although these models have a similar R-squared in the training set to the

models constructed using the proposed method, these models elucidate consistently fewer strongly significant cortical regions ($p < 0.005$), and only show significant correlations in the test set for the VOC model.

Table 6.4. R-squared of linear models constructed from the shape measures computed using ANT's Atropos for both training and test sets. For each model, the regression coefficients and standard errors of only the significant ($p < 0.005$) cortical regions retained from the data-driven variable selection, as well as patient age, gender, and scanner sequence for all models. The multiple R-squared of the trained models and the squared correlation between the predictions of the trained model on the test set and the test set outcomes are provided, with the significance of these values Bonferroni corrected alpha value.

AHA		
Cortical region	Regression coefficient	Standard error
Primary motor cortex - Sulcal depth	42.994***	6.512
Age	-1.191	0.559
Gender (Reference: male)	11.781	3.772
Scanner & sequence (Reference: UQCPRRC)	-0.591	2.834
R-squared of trained model		**0.75*** **
Predicted r2 on the test set		0.01
BRIEF		
Cortical region	Regression coefficient	Standard error
Cingulate cortex - Cortical thickness	12.067***	2.386
Age	-0.427	0.243
Gender (Reference: male)	3.221	1.897
Scanner & sequence (Reference: UQCPRRC)	-1.898	1.239
R-squared of trained model		**0.92*** **
Predicted r2 on the test set		0.06
TVPS		
Cortical region	Regression coefficient	Standard error
Inferior temporal gyrus - Cortical thickness	28.002**	8.863
Age	0.498	3.183
Gender (Reference: male)	-5.875	3.417
Scanner & sequence (Reference:	1.372	2.498

UQCPRRC)		
R-squared of trained model		**0.86*** **
Predicted r2 on the test set		0.10
VOC		
Cortical region	Regression coefficient	Standard error
Age	3.560***	0.248
Gender (Reference: male)	1.835	3.954
Scanner & sequence (Reference: UQCPRRC)	5.171	2.923
R-squared of trained model		**0.86*** **
Predicted r2 on the test set		**0.41** **

Asterisked regression coefficients were found to be statistically significant: * $p < 0.05$; ** $p < 0.01$, *** $p < 0.001$. Model correlations in bold have a statistical significance of $p < 0.05/4$. Asterisked model correlation were found to be statistically significant: * $p < 0.001$; ** $p < 0.0025$, *** $p < 0.00025$.

6.4 Discussion

Using the proposed cortical analysis pipeline, significant differences in cortical shape measures were identified between children with cortical alterations due to congenital brain injury that resulted in unilateral CP, and typically developing children, that were consistent with known developmental processes. It was observed that children with alterations within the hemisphere of injury had significantly reduced cortical thickness compared to the TDC. The reduced cortical thickness observed in motor and visual cortical regions may be the result of tissue loss due to injury, as well as the cortical alterations interrupting the regional increases in cortical density that occur during healthy development [Gogtay et al., 2004; Sowell et al., 2004]. This finding is consistent with the regional reduction in cortical thickness associated with schizophrenia [Goldman et al., 2009; Narr et al., 2005] and children with a very low birth weight (VLBW) [Martinussen et al., 2005], which are both conditions which bear some relationship to CP [Beaino et al., 2010; Wu et al., 2013]. The ipsilateral cortical surface of children with unilateral injury was also found to have a reduced curvature compared to the TDC in motor, executive function and vocabulary regions. This reduction in curvature may be the result of injury interrupting the gyrification of the cortex that results in significant cortical expansion during healthy development [Hill et al., 2010], and is also consistent with findings of reduced gyrification in patients with schizophrenia [Sallet et al., 2003; White et al., 2003]. There were also significant increases

in sulcal depth observed on the ipsilateral side of children with unilateral alterations compared to the TDC for motor, executive function and visual cortical regions. Although higher sulcal depth implies increased cortical surface area [Im et al., 2006], the larger sulcal depth observed in most cases arises from reduced cortical migration due to dysplasia, or the presence of schizencephalic clefts. Observed differences between children with bilateral injury and the TDC were largely not significant, most likely due to the reduced number of children in this cohort with bilateral injury (n = 7).

Children with lesions that do not involve the cortex, which in this cohort included mostly PWM injury, were found to have significantly reduced cortical thickness in visual regions, and significant decreases in curvature and sulcal depth compared to the TDC for vocabulary regions. These findings all reflect a decrease in cortical volume, which is consistent with previous findings for children with PWM injury [Inder et al., 1999]. Overall, the contralateral hemisphere of children with unilateral alterations was observed to be significantly thicker, smoother and have reduced sulcal depth compared to the TDC, for all functional cortical regions. The reduced curvature and sulcal depth also reflect a reduced cortical volume on the contralateral side. The increase in cortical thickness however may be the result of plasticity as a mechanism to compensate for injury [He et al., 2007] on the side contralateral to injury, which is in line with previous findings [Kolb and Gibb, 2007; Krägeloh-Mann, 2004; Ward, 2005]. Overall, the measurable change in impaired cortical regions highlight the utility of the three shape measures used in this analysis to quantify cortical injury. There is value in characterising shape using a number of different shape measures as opposed to a single cortical volume measure, as the combination of increased thickness and reduced cortical folding may counteract the measure of cortical volume, making it more difficult to discriminate between altered and preserved cortical volumes. Furthermore, these findings highlight the utility in the proposed method for characterising cortical shape, as subtle cortical alterations arising from WM injury, or subtle cortical alterations observed on the apparently non-injured hemisphere, which may not be clearly visible in the MRI, may still be quantified using this approach, and hence contribute to the clinical assessment of children with CP.

The constructed multivariable linear regression models show a moderate multiple R-squared, i.e. goodness of fit, to all four clinical scores, with ranges between 0.78 and 0.90 in the training set. These measures represent the variance explained by the succinct set of

shape descriptors from specific cortical regions, which included 5 or fewer regions for all models. As expected, the multiple R-squared was reduced in the test set for all clinical scores, yet was still statistically significant for three of the four scores. The significant correlation on the independent test set highlights the ability of these models to generalise to unseen data and hence the general patient population. The BRIEF model of executive function was observed to not retain any cortical measures, and additionally did not perform well upon test set validation. This may be a reflection of the typically wider cortical involvement and the important role of WM for cognitive function, and the consequent limitation of only using a sparse set of cortical regions to model this function. In addition, separate regression models, constructed on subsets of the cohort with clinically diagnosed left and right side hemiplegia, are provided in Supplementary Figures A.1 and A.2, to visually highlight which cortical regions were associated with clinical outcomes in each clinical phenotype. Specific cortical regions and shape measures retained by the data-driven variable selection were from within a set of cortical regions pre-selected based on the literature. However, the final subset of variables included by the model, as shown in Table 6.3, as well as the sign of the regression coefficients, is a reflection of the patterns of injury present in this data, and should ideally be verified independently using another cohort of data. What these models demonstrate, however, is the ability to extract a succinct set of morphological biomarkers of cortical shape that are strongly linked to clinical outcome and generalise to unseen data.

There are a number of technical challenges limiting the sensitivity of the cortical shape analyses, including subtle occipital sulci that may be incorrectly delineated by the segmentation approach, thus yielding inaccurate shape measures in this location, as well as the presence of dura mater not fully resolved from the brain surface. However, segmentation results were visually inspected and manually corrected where necessary. Similarly, Atropos segmentations were manually corrected in these cases, however was observed to provide fewer cortical regions that strongly correlate with outcome (Table 6.4), and consequently reduced test set correlations when compared to the proposed method. This may arise from Atropos slightly over-segmenting the cortical GM due to initialisation with Otsu thresholding, causing the shape analysis to overestimate cortical thickness and underestimate curvature and sulcal depth (as subtle sulci are lost). However the erroneous omission of sulci, particularly thin (i.e. 1-voxel wide) extensions of CSF, occurred using

both Atropos and the EM-weighted MRF method detailed in Chapter 4, particularly on the lower resolution 1.5T MR images. In future, further tailoring the weighted MRF may help to resolve these subtle sulci. Another limitation was that the level set approach for delineating the cortical regions has not been validated in the present study. This is partly due to the time intensive process of manually segmenting multiple cortical regions on a large number of patients. Future investigations into this method will validate the level set approach for segmenting the motor cortical regions (e.g. M1S1) on a smaller portion of the data (approximately 20 patients, including patients' severe cortical injury). A final limitation is that the predictive models did not include other non-cortical, primary and secondary injuries, which would contribute to reduced patient functional outcomes. Methods for characterising these forms of injury, which are detailed in the adjacent chapters, are combined to overcome this limitation in Chapter 9.

A limitation of the proposed approach is that not all malformations, particularly subtle alterations, can be observed from the MRIs. A detection rate between 40 and 60% was reported for focal cortical dysplasia [Tassi et al., 2002], with subtle migration disturbances such as neuronal heterotopia requiring histology to accurately reveal [Hannan et al., 1999]. As such, the proposed cortical shape measures would not reveal these developmental injuries. Another limitation of the proposed cortical analysis pipeline is that it does not account for potentially altered structure-function relationships caused by plasticity in order to compensate for the presence of injury [Carmichael, 2003; Thiel et al., 2001]. These mechanisms may cause shifts in where particular functions are performed, confounding the structure-function relationships of the brain which the linear models attempt to elucidate. This would consequently reduce the multiple R-squared of these models as it introduces variance in the clinical score potentially not explained by cortical shape in the chosen cortical regions. Furthermore, as the study data are cross-sectional, the obtained results cannot be causally linked to plasticity-related mechanisms. Instead, longitudinal data are required in future studies to validate that such changes are indeed related to plasticity. Although VBM has frequently been used to identify longitudinal changes in GM density in the investigation of plasticity [Giuliani et al., 2011; Sterling et al., 2013; Thomas et al., 2009], the characterisation of cortical shape analysis can complement such approaches by quantifying alternate cortical changes caused by plasticity, such as the thickening of cortical GM or alternate changes in neuronal architecture [Feldman, 2009].

Combined with diffusion MRI, such a cortical analysis could help identify both the underlying WM and GM mechanisms of plasticity.

6.5 Conclusions

In this chapter, a method for the robust cortical GM segmentation and label atlas propagation using level sets was proposed, which are important modifications critical to CP data. This proposed approach allowed a quantifiable and reliable relationship between regional brain structure and function to be identified. Significant decreases in cortical thickness, curvature, and significant increases in sulcal depth were observed within the injured hemisphere(s) of children with unilateral CP compared to children with healthy development, as well as significant increases in cortical thickness, and significant decreases in curvature and sulcal depth were observed on the uninjured hemisphere of children with unilateral CP, highlighting potential compensatory mechanisms in these children. Using a succinct set of shape measures chosen from specific cortical regions, significant correlations with outcome were observed for three clinical functions, including motor function (R squared 0.78, $p < 0.001$), visual function (0.82, $p < 0.001$) and communication (0.90, $p < 0.001$), and performed well upon test set validation (R squared 0.33, 0.44, 0.39, all $p < 0.01$). Care needs to be taken when segmenting the GM and labelling cortical substructures, specifically, atlas based priors need adapting to deal with the problem of severe alterations that frequently occur in cerebral palsy, which nullifies the efficacy of atlas priors. In the following chapter, methods to quantify WM and GM lesions are presented, and in the penultimate chapter, all injury segmentation methods are combined to identify the most predictive biomarkers of injury.

7. Segmenting white and grey matter lesions from children with unilateral cerebral palsy

7.1 Introduction

The third and final class of injury observed in children with CP are WM and GM lesions. Of these injuries, destructive lesions are the most common, with periventricular WM lesion observed in around 50% of children with CP and cortical/subcortical GM lesions in approximately 20% [Bax et al., 2006; Krägeloh-Mann and Horber, 2007; Reid et al., 2014] of cases. MRI is a useful imaging procedure that is commonly used in clinical assessment for identifying and qualitatively characterising brain lesions, as both WM and cortical/deep GM lesions appear as regions of abnormal intensity. Although GM lesions are less common, they impact particularly critical structures of the brain including the basal ganglia, thalami and cortical GM, and lead to more severe motor impairments [Martinez-Biarge et al., 2010].

Despite the known negative prognostic implications of tissue lesions, the extent of the relationship between regional lesion burden and clinical function has yet to be quantified. This is of particular interest, as these relationships can help provide estimates of patient function from MRIs early in life, guiding therapeutic strategies for these children. For instance, such information can confirm whether lesion burden in specific brain regions lead to greater impairments to motor function, hence recommending more intensive therapeutic interventions. Hence, this study aims to quantify the correlation between the lesion burden in individual regions and multiples clinical scores which quantify motor, cognitive, communicative and visual function. The study considers both GM and WM lesions solely based on tissue involvement, independent to the timing of the lesion [Krägeloh-Mann and Horber, 2007]. Further these WM and GM involvements are considered separately, as it has been previously shown their impact on function differs [Krägeloh-Mann and Horber, 2007; Martinez-Biarge et al., 2010].

For the correlation between structure and function to be calculated, all lesions within large sets of data need to be delineated in three dimensions. Such an approach can be made practical by utilising an automated segmentation algorithm. The field of lesion segmentation is well researched, particularly in the MS setting. Although multiple reviews have been published discussing various lesion segmentation approaches [García-Lorenzo

et al., 2013; Lladó et al., 2012], no studies as yet have performed automated lesion segmentation in the CP setting. This may be due to the comparatively large morphological changes observed in children with CP, which invalidate the anatomical assumptions existing algorithms typically make, resulting in poor segmentation performance.

Hence in this chapter, a modified lesion segmentation method was used to quantitatively assess the functional impact of brain lesion involvement. As the method incorporates multiple lesion classes in order to automatically segment both WM and GM lesions, this approach, presents the first published quantitative assessment of functional impairment caused by GM lesion involvement in children with CP. In this approach, atlases were used to subdivide the GM regions into individual cortical and subcortical regions, and WM regions into regions with particular WM tracts. Regional WM and GM lesion burdens were computed, and used to predict clinical function using multivariable linear regression. Such approaches could have clinical utility as they can support the radiological assessment of MRIs, and help to tailor treatment strategies for children with CP. A particular advantage of the method is that it only relies on standard structural MRIs and does not resort to more sophisticated sequences that may not be widely available. It addresses Aim 1 of this thesis, “develop several automated segmentation approaches to delineate the three main classes of injury observed in children with CP; cortical malformations, WM injury and ventricular enlargement”, as well as Aim 3, “[comparing] the automated results against a state of the art”. The work in this chapter has been published, and is available at doi:10.1016/j.nicl.2016.05.018.

7.2 Materials and methods

7.2.1 Study Participants

Of the total 139 children recruited as part of the studies detailed in Section 3.2.1, only the 125 patients who also underwent T2-weighted scanning were included in this study: 107 children diagnosed with unilateral CP (57 male, 50 female, mean age 10.9, age range 7-16), and 18 children with healthy development (CHD) with (8 male, 10 female, mean age 11.4, age range 7-16) were included.

7.2.5 Lesion segmentation algorithm

An automated lesion segmentation approach tailored specifically for WM and GM lesion involvement in children with CP is presented. Segmentation of the three cerebral tissues

(WM, GM and CSF) was initially performed using an EM approach interleaved with the modified MRF formulation detailed in Chapter 4.

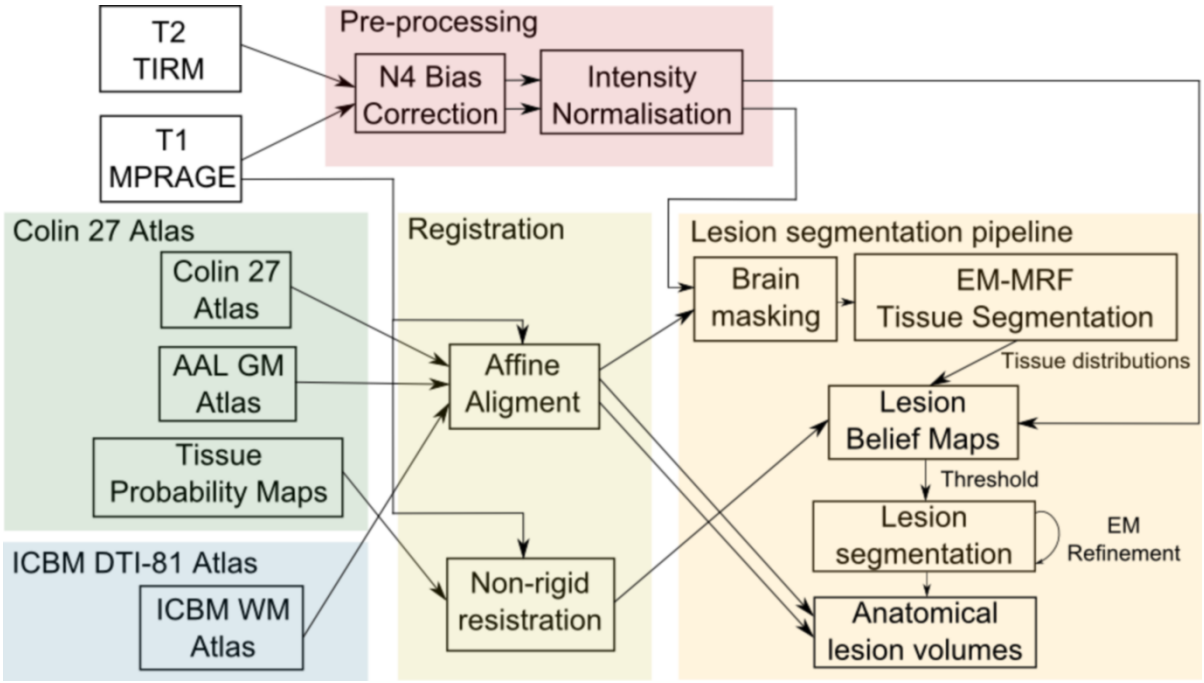

Fig. 7.1 An illustration of the lesion segmentation pipeline detailed in this chapter. Following pre-processing and an affine alignment to the Colin 27 atlas, the T1-MPRAGE undergoes brain masking and tissue segmentation steps. The tissue distributions obtained from this segmentation, along with the pre-processed T2-TIRM and non-rigidly registered Tissue Probability Maps (warped to the T1-MPRAGE), were used to construct lesion belief (probability) maps. Following thresholding, lesion segmentations were refined with the EM algorithm. Using the AAL GM and ICBM WM atlases, which were similarly aligned to the Colin 27 atlas (and by extension, the T1-MPRAGE), anatomical lesion volumes were extracted to use for the statistical analysis.

Initial lesion belief maps for each of the three types of lesions; WM lesions, GM lesions and internal capsule (IC) lesions were generated using the final estimates of tissue distributions obtained from the EM-MRF approach, the aligned T2-TIRM image and the registered WM and GM tissue probabilistic atlases. Denoting the T1-MPRAGE containing n voxels as $\boldsymbol{y} = \{y_i, i \in [1{:}n]\}$, the T2-TIRM as $\boldsymbol{x} = \{x, i \in [1{:}n]\}$, the registered TPMs of the WM, GM and CSF, and the parameterised Gaussian mean and standard deviation for each of the three tissue classes as $\Phi_{\mathrm{k}} = (\mu_k, \sigma_k)$, where $k \in \{WM, GM, CSF\}$, the formulae for the three lesion belief maps $lb = \{lb_i, i \in [1{:}n]\}$ is given in Equations 7.1-7.3.

$$lb_{WML,i} = abs\left(\frac{y_i - \mu_{WM}}{\sigma_{WM}}\right).x_i.TPM_{WM,i} \quad Eq\ 7.1$$

$$lb_{GML,i} = abs\left(\frac{y_i - \mu_{GM}}{\sigma_{GM}}\right).x_i.TPM_{GM,i} \quad Eq\ 7.2$$

$$lb_{ICL,i} = abs\left(\frac{y_i - (\mu_{WM} + \sigma_{WM})}{\sigma_{WM}}\right).x_i.TPM_{WM,i} \quad Eq\ 7.3$$

In each equation, abnormal tissue outliers were identified using an absolute z-score from the mean and standard deviation of the WM and GM distributions established in the EM-MRF segmentation. Note in Eq 7.3, IC lesions are segmented separately to WM lesions because the IC typically appears as a higher intensity in structural MRI, and was assumed to be 1 standard deviation above the mean WM intensity. This separate segmentation of IC lesions ensures the detection of this lesion type, which was necessary because they approach healthy WM intensity, and hence would not be detected in the lesion belief map for WM shown in Eq 7.1. Unlike the T1-MPRAGE, the T2-TIRM was normalised in intensity between 0 and 1, where the most hyperintense regions are characteristic of hemorrhagic injuries.

A threshold, t_{thresh}, is applied to each of the three lesion belief maps. Using the 75% training set, a ROC analysis was performed to establish which threshold for WM and GM lesions agreed best with the manual classification of lesions. Specifically, the Equal Error Rate (EER), which enforces equal importance to false positives and false negatives, was used to determine the optimal thresholds $t_{thresh,WM} = 0.85$ and $t_{thresh,GM} = 0.875$. These thresholds were used to test the performance of the lesion segmentation algorithm on the independent test set.

Provided more than one voxel exceeds the WM or GM thresholds, the initial lesion segmentation was refined using an EM approach. The mean and standard deviation of the lesion T1 intensity were obtained for the likely lesion voxels, and introduced as an additional lesion classes along with the three healthy tissue classes obtained from the EM-MRF segmentation. Tissue classes were then updated within the EM algorithm, with the lesion intensities modelled as a Gaussian distribution. The probability of the lesion class was weighted by the TIRM intensity, while the probability of the three healthy tissue classes was weighted by the inverse of the TIRM intensity (i.e. 1-TIRM). The tissue probability maps also weight the posterior probability of each segmented class. The

likelihood of each lesion class for the three lesion classes (WM, GM and IC) is given in Eq 7.4, e.g. for the WM lesion class:

$$p_{WML,i} = exp\left[-\left(\frac{y_i - \mu_{WML}}{\sigma_{WML}}\right)^2\right].x_i.TPM_{WM,i} \qquad Eq\ 7.4$$

The likelihood of the healthy tissue classes (WM, GM and CSF) are computed using Eq 7.5, e.g. for the WM:

$$p_{WM,i} = exp\left[-\left(\frac{y_i - \mu_{WM}}{\sigma_{WM}}\right)^2\right].(1 - x_i).TPM_{WM,i} \qquad Eq\ 7.5$$

This step is performed separately for WM lesions, GM lesions and IC lesions, yielding separate lesion segmentations in each instance. Post-processing of these lesion segmentations consists of a flood fill operation and morphological closing.

7.2.6 Anatomical lesion volume

Anatomical and regional involvement of the segmented lesions was computed using the AAL atlas, which contains CDGM labels, and the ICBM DTI-81 Atlas which contains WM tract labels. Both atlases were aligned to the same image space as the Colin 27 atlas [Rivest-Hénault et al., 2015]. Lesion involvement in each region was then computed as the sum of the lesion segmentation masked by the particular atlas label.

7.2.7 Statistical analysis

Participants were separated into four cohorts, the CHD children and children with WM (including IC lesions), GM lesions, or combined WM/GM lesions. Children with combined WM/GM lesions were grouped into either WM or GM cohorts for the regression analysis, based on which tissue lesion burden was greater in each participant. Both WM and GM lesion cohorts were randomly separated into 75%/25% training and test sets. In the training set, data-driven variable selection was performed using the Least Absolute Shrinkage and Selection operator (LASSO) method [Tibshirani, 1996] obtained from the 'glmnet' package in R statistical software Version 3.2.2, which implicitly performs variable selection with a sparsity term that minimises the sum of non-zero coefficients. Unlike 'stepAIC' used in the previous chapters, LASSO was chosen for the analysis in this chapter and for the rest of the thesis as it performs both feature selection and feature regularisation, and additionally allows the upper boundary on the regression coefficients to be manually set to zero. Enforcing negative coefficients was important, as this analysis

aims to identify biomarkers of lesion burden leading to *reductions* in patient function. LASSO was run with default alpha and lambda parameters.

Linear regression models were then constructed, using the regional volumes of the WM and GM lesions (in mL) identified from LASSO as independent variables, as well as patient age and gender, and the six clinical scores (AHA, BRIEF, SDQ, TVPS, WR and VOC) as the dependent variable. Multiple comparisons were corrected for using Bonferroni correction. Model residuals were normally distributed for each of the independent outcomes. To assess the generalisability of these models to unseen data, training model performance was validated via correlation between model predictions and the test set outcomes. Additionally, regression models including both WM and GM regional lesion volumes were constructed using the training set, with their performance again validated with the test set. Model comparisons between the WM and GM models, and the WM/GM combined model, were performed using Analysis of Variance (ANOVA), to determine if it is beneficial to consider both lesion types.

7.3 Results

7.3.1 Demographics information

The demographics of the four cohorts; the CHD children, those with WM (and/or IC) involvement, GM involvement, and those with combined WM/GM involvement, are presented in Table 7.1. The AHA score, and a measure of global brain injury severity provided from a manual template approach [Fiori et al., 2015], is provided for each cohort, split into those with unilateral and bilateral injury. Only children with WM lesions had observed bilateral injury, which was reflected in the reduced AHA score compared to children with unilateral WM injury. The five children with solely GM lesions had the greatest amount of observed injury from the MRI, with the highest injury severity score of all cohorts. These children, consequently, also had the poorest motor outcomes of all cohorts. Children with unilateral, combined WM/GM injury had similar measures of injury severity and similar AHA motor outcome to those children with bilateral WM lesions.

Table 7.1. Demographic characteristics for the CHD children, WM lesion cohort and the GM lesion cohort. For the CHD cohort, information of lesion laterality is not applicable, and their clinical scores were not obtained.

Cohort	CHD cohort	WM lesion	GM lesion	Combined WM/GM
Number of participants	18	80	5	22
Gender				
Male	8	40	4	13
Female	10	40	1	9
Age at scan (years)				
Mean ± standard deviation	11.42 ± 3.03	11.38 ± 2.92	11.80 ± 1.92	10.54 ± 2.65
Range (minimum - maximum)	7 - 16	5 - 17	9 - 14	6 - 15
Number with unilateral lesions	NA	55	5	22
Global brain injury severity score [Fiori et al., 2015]				
Mean ± standard deviation	0.00 ± 0.00	8.34 ± 5.12	14.00 ± 5.20	9.85 ± 5.64
Range (minimum - maximum)	0 - 0	2.5 - 20	9 - 21	2 - 20
Assisted Hand Assessment (AHA) Score				
Mean ± standard deviation	NA	75.58 ± 20.05	52.60 ± 31.30	64.61 ± 24.78
Range (minimum - maximum)	NA	41 - 98	26 - 95	24 - 98.8
Number with bilateral lesions	NA	25	0	0
Global brain injury severity score [Fiori et al., 2015]				
Mean ± standard deviation	0.00 ± 0.00	8.43 ± 4.79	NA	NA
Range (minimum - maximum)	0 - 0	1 - 18.5	NA	NA
Assisted Hand Assessment (AHA) Score				
Mean ± standard deviation	NA	64.21 ± 19.04	NA	NA
Range (minimum - maximum)	NA	8 - 97	NA	NA

CHD, children with healthy development; GM, grey matter; NA, not available; WM, white matter.

Lesion burden frequency was also investigated across the entire cohort of 107 children with unilateral CP, which are shown in Figure 7.2. Most prevalent patterns of WM injury include intraventricvular haemorrhage (IVH) and PVL, frequently impacting the superior longitudinal fasciculus, corona radiata and PLIC. Frequent GM patterns of injury include IVH impacting the deep GM, the lenticular and caudate nuclei and the thalamus. Unilateral malformations were the main pattern of injury impacting cortical GM regions, including the temporal and frontal lobes, and the precentral gyrus.

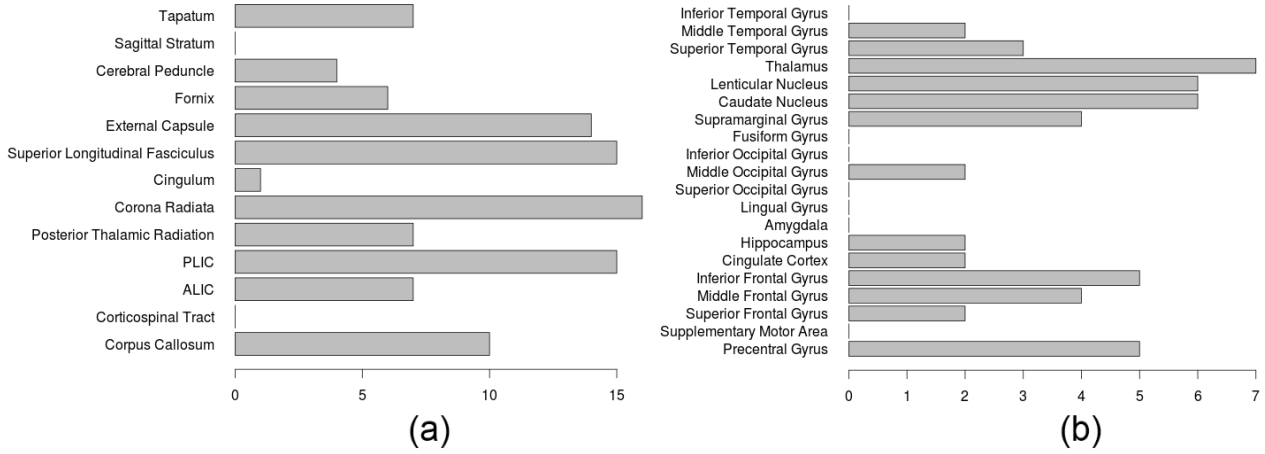

Fig. 7.2 The lesion frequency observed in (a) WM and (b) GM regions among the 107 children with unilateral CP. ALIC, anterior limb of the internal capsule; PLIC, posterior limb of the internal capsule

7.3.2 Validation of lesion segmentation algorithm

After training the lesion threshold values t_{thresh} in the training set, the performance of the lesion segmentation method was validated on the test set against a manual assessment of lesions using the semi-quantitative brain lesion severity scale [Fiori et al., 2015]. Table 7.2 shows the segmentation performance on the WM lesion cohort, the GM lesion cohort, and all cohorts combined.

Table 7.2. Lesion segmentation performance compared to the manual ground truth assessment of lesions on the independent test set.

Performance measures	WM lesions	GM lesions	Combined
Sensitivity	0.933	0.818	0.939
Specificity	0.765	0.972	0.929
Accuracy	0.872	0.936	0.936
False positive rate	0.235	0.028	0.071
False negative rate	0.067	0.182	0.061

Lesion segmentation performance in the GM had the highest false negative rate, reflecting the difficulty identifying GM lesions due to their more subtle changes in intensity. Conversely, WM lesions had the highest false positive rate, indicating that the false detection of lesions, either from WM intensity changes or moderate intensities in the T2-TIRM, was more common. For the TDC in the test set, none had lesions identified by the lesion segmentation approach. An illustration of lesion segmentation performance in cases of GM, WM and IC lesions are provided in Figure 7.3.

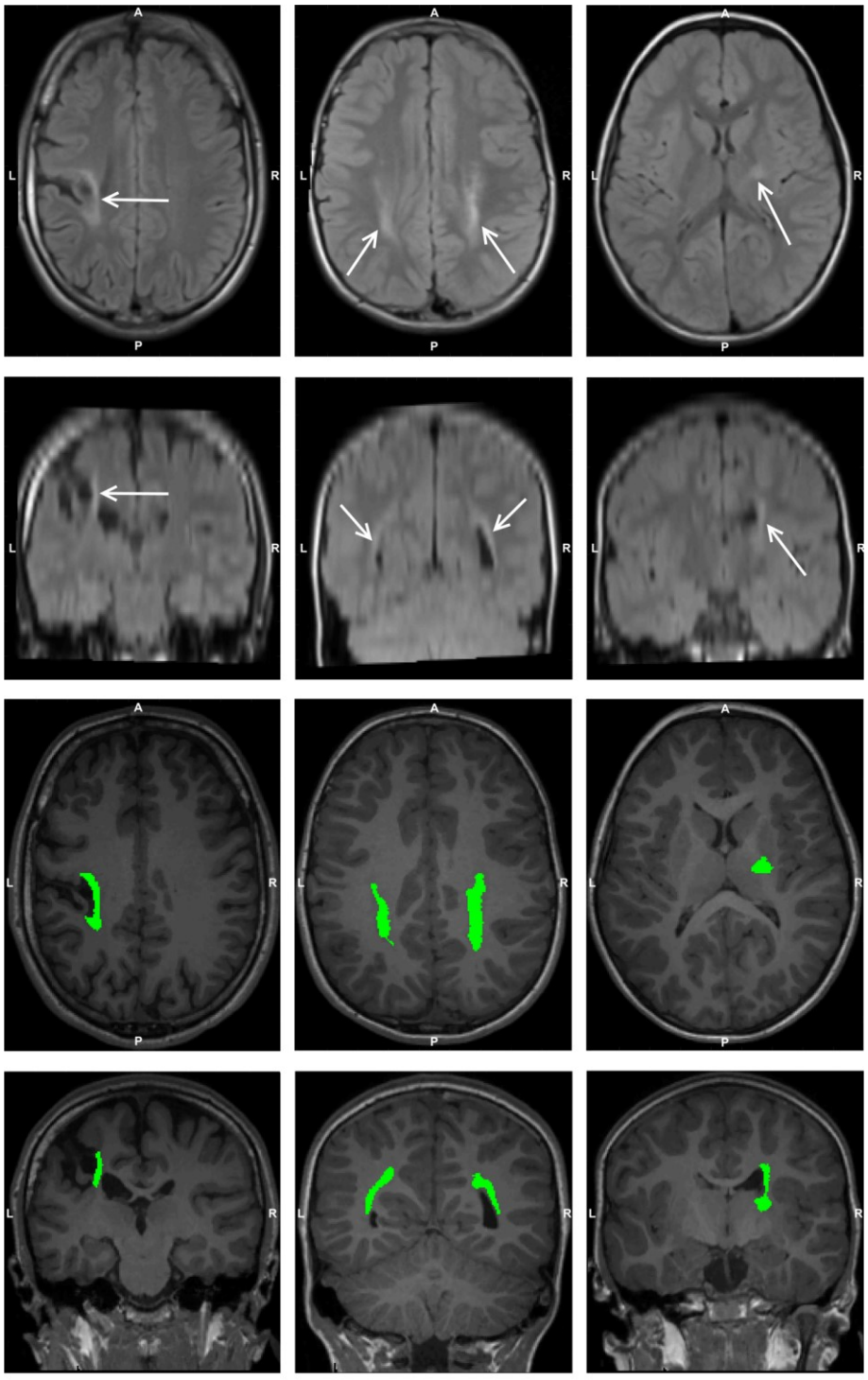

Fig. 7.3 Examples of a GM lesion (column (a)), WM lesions (column (b)) and IC lesions (column (c)). The top two rows show the axial and coronal slices of the same T2-TIRM image, where the hyperintense lesions are indicated with white arrows. The segmented lesions, highlighted in green, are presented on the corresponding axial and coronal slices of the T1-MPRAGE image in the bottom two rows. A, anterior; L, left; P, posterior; R, right.

7.3.3 Comparison to gold standard segmentation approach

To validate the lesion segmentation approach, its performance is compared to the current state of the art lesion segmentation software, the Lesion Segmentation Toolbox (LST) [Schmidt et al., 2012]. The sensitivity, specificity, and several other performance measures of each approached compared to the manual expert classification of lesions is performed and provided in Table 7.3.

Table 7.3. Lesion segmentation performance of the approach used in this paper, and SPM's LST on the 25% independent test set, compared to the manual ground truth assessment of lesions.

Performance measure	Sensitivity	Specificity	Accuracy	False positive rate	False negative rate
Proposed approach	0.939	0.929	0.936	0.071	0.061
SPM's LST	0.893	0.351	0.729	0.649	0.107

The proposed approach was found to have a greater lesion segmentation accuracy compared to LST on these data (0.936 versus 0.729). The approach used in LST was observed to more frequently produce false positive lesion segmentations, which potentially arises from an inaccurate threshold κ chosen by this method to produce an initial lesion belief map [Schmidt et al., 2012]. One example of this false positive segmentation occurring is provided in Figure 7.4.

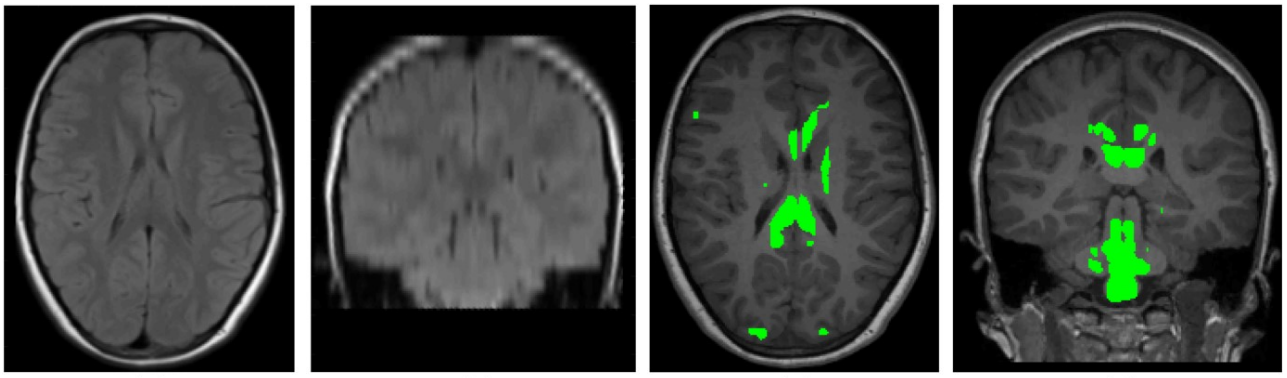

Fig. 7.4 An (a) axial and (b) coronal view of the T2 TIRM of a patient with no lesions observed by the manual expert, and the corresponding (c) axial and (d) coronal views of the T1 MPRAGE images with the false lesion segmentations obtained from the LST method shown in green.

7.3.4 Correlation with patient outcome

The regression models constructed on the training set are detailed in Table 7.4. In this table, the regression coefficients can be interpreted as the reduction in the clinical score for every 1mL of lesion present in that anatomy. The multiple R-squared of the models, which measure strength of the correlation between the outcome and the model predictions, were compared against a Bonferroni corrected alpha value (α = 0.05/6 tests, 0.008), however the *p*-values of each feature were not corrected, and simply reflects the strength of that feature within the chosen model.

Table 7.4. The retained anatomical regions, and corresponding standardised regression coefficients and standard errors, of the GM and WM lesion models, for the six clinical outcome scores, modelled on the 75% training set. For each model, the multiple R-squared is provided. Features that are significant ($p < 0.05$) in multiple models are bolded.

AHA					
	GM			**WM**	
Variable name	Regression coefficient	Standard error	Variable name	Regression coefficient	Standard error
Superior frontal gyrus	-0.265	0.154	Corpus callosum	-0.018	0.015
Lenticular nucleus	-0.128***	0.036	**Corona radiata**	-0.005***	0.001
Thalamus	-0.065***	0.015	**External capsule**	-0.016***	0.004
Middle frontal gyrus	-0.228**	0.083	**Cerebral peduncle**	-0.111**	0.034
			Cingulum	-0.266	0.264
Multiple R-squared		**0.433*** **	Multiple R-squared		**0.514*** **
BRIEF					
	GM			**WM**	
Variable name	Regression coefficient	Standard error	Variable name	Regression coefficient	Standard error
Caudate nucleus	-0.2119*	0.048	**PLIC**	-0.121***	0.020
Lenticular	-0.426***	0.119	ALIC	-0.050	0.050
Superior frontal gyrus	-0.122*	0.058	Cingulum	-2.012	2.080
Middle frontal gyrus	-0.549	0.294			
Multiple R-squared		**0.263*** **	Multiple R-squared		**0.386*** **
SDQ					

	GM			WM	
Variable name	Regression coefficient	Standard error	Variable name	Regression coefficient	Standard error
Middle frontal gyrus	-0.063	0.036	Corpus callosum	-0.007	0.008
Superior frontal gyrus	-0.101	0.072	**PLIC**	-0.009**	0.003
Cingulate cortex	-0.061	0.047	**Corona radiata**	-0.003***	0.001
Lenticular nucleus	-0.034	0.019	External capsule	-0.002	0.002
Multiple R-squared		**0.174***	Multiple R-squared		**0.529*****

TVPS

	GM			WM	
Variable name	Regression coefficient	Standard error	Variable name	Regression coefficient	Standard error
Middle occipital gyrus	-0.200	0.084	Posterior thalamic radiations	-0.004	0.130
Middle frontal gyrus	-0.131	0.236	**PLIC**	-0.068***	0.017
Superior frontal gyrus	-0.083	0.396	Fornix	-0.010	0.130
Inferior frontal gyrus	-0.119	0.065	**Superior longitudinal fasciculus**	-0.029**	0.009
Multiple R-squared		**0.202****	Multiple R-squared		**0.507*****

WR

	GM			WM	
Variable name	Regression coefficient	Standard error	Variable name	Regression coefficient	Standard error
Middle occipital gyrus	-0.036*	0.018	**Fornix**	-0.093**	0.033
Superior temporal gyrus	-0.022	0.024	**Superior longitudinal fasciculus**	-0.012*	0.002
Supramarginal gyrus	-0.053*	0.021	Posterior thalamic radiations	-0.003	0.005
Hippocampus	-0.742	0.703	Corpus callosum	-0.013	0.009
Multiple R-squared		**0.265*****	Multiple R-squared		**0.280*****

VOC

	GM			WM	
Variable name	Regression coefficient	Standard error	Variable name	Regression coefficient	Standard error
Precentral gyrus	-0.037*	0.017	**External capsule**	-0.015***	0.003

Middle temporal gyrus	-0.041	0.069	Tapatum	-0.019	0.011
Superior occipital gyrus	-0.266	0.879	**Superior longitudinal fasciculus**	-0.015***	0.003
Middle occipital gyrus	-0.049	0.086	Sagittal Stratum	-0.057	0.615
Multiple R-squared		**0.117***	Multiple R-squared		**0.491*****

Asterisked correlations were found to be statistically significant: * $p < 0.008$; ** $p < 0.0016$, *** $p < 0.00016$. Correlations in bold have a statistical significance of $p < 0.008$.

Significant ($p < 0.05$) regions that were retained by the training models include the superior longitudinal fasciculus and the PLIC (in 3 of the 6 models), and the lenticular nucleus, corona radiata and external capsule (all in 2 of the 6 models). All models were found significant ($p < 0.0008$). The performance of these trained WM and GM models, as well as the WM/GM combined models, on the independent test set are shown in Table 7.5. Two of the six GM and WM alone models were found to be significant ($p < 0.008$), while four of the six combined WM/GM models were found to be significant ($p < 0.008$).

Table 7.5. The Pearson's R correlation between the predicted outcomes in the test set using the trained linear regression models and the clinical scores of the test set.

	GM models		**WM models**		**WM/GM Combined**	
	Pearson's R correlation	95% Confidence Interval	Pearson's R correlation	95% Confidence Interval	Pearson's R correlation	95% Confidence Interval
AHA	**0.504***	(0.200, 0.719)	**0.641****	(0.387, 0.805)	**0.670*****	(0.429, 0.822)
BRIEF	-0.006	(-0.392, 0.382)	0.263	(-0.138, 0.590)	0.269	(-0.132, 0.594)
SDQ	0.182	(-0.327, 0.610)	**0.742****	(0.408, 0.901)	**0.751****	(0.424, 0.905)
TVPS	**0.533***	(0.184, 0.763)	0.304	(-0.094, 0.619)	**0.614****	(0.297, 0.809)
WR	0.435	(0.057, 0.704)	0.063	(-0.332, 0.440)	**0.493***	(0.130, 0.739)
VOC	0.077	(-0.319, 0.452)	-0.073	(-0.448, 0.323)	0.085	(-0.313, 0.457)

Asterisked correlations were found to be statistically significant: * $p < 0.008$; ** $p < 0.0016$, *** $p < 0.00016$. Correlations in bold have a statistical significance of $p < 0.008$.

7.3.5 Correlation with patient outcome using LST lesion segmentations

The lesion segmentations provided from the state-of-the-art SPM LST approach were masked using the GM and WM labelled atlases similar to the proposed method. The correlations between these regional lesion burdens and patient outcome were investigated using the same statistical methodology. The performance of the trained LASSO regression models in the independent test set using these lesion data are given in Table 7.6 below. The magnitude of these correlations were noticeably less than the corresponding values using the proposed lesion segmentation algorithm shown in Table 7.5, with no models achieving statistical significance ($p < 0.008$).

Table 7.6. The Pearson's R correlation between the predicted outcomes in the test set, using the regression models on the SPM LST lesion segmentation data, and the clinical scores of the test set.

	GM models		**WM models**		**WM/GM Combined**	
	Pearson's R correlation	95% Confidence Interval	Pearson's R correlation	95% Confidence Interval	Pearson's R correlation	95% Confidence Interval
AHA	0.076	(-0.246, 0.382)	-0.127	(-0.425, 0.196)	0.347	(0.035, 0.597)
BRIEF	0.150	(-0.215, 0.479)	0.412	(0.005, 0.448)	0.090	(-0.273, 0.431)
SDQ	-0.156	(-0.542, 0.284)	-0.206	(-0.578, 0.236)	-0.249	(-0.607, 0.193)
TVPS	0.274	(-0.095, 0.578)	0.235	(0.019, 0.301)	0.227	(-0.145, 0.543)
WR	0.380	(0.030, 0.647)	0.313	(-0.046, 0.601)	0.365	(0.012, 0.637)
VOC	-0.323	(-0.608, 0.035)	-0.304	(-0.594, 0.056)	-0.025	(-0.376, 0.332)

Asterisked correlations were found to be statistically significant: * $p < 0.008$; ** $p < 0.0016$, *** $p < 0.00016$. Correlations in bold have a statistical significance of $p < 0.008$.

7.3.6 Independence of WM and GM lesion burden

The table quantifying the amount of co-dependence between the WM only, GM only, and the combined WM/GM models, using the ANOVA is provided in Table 7.7. Briefly, the combined WM/GM models for the BRIEF and SDQ measures were not significantly different from the WM alone models, and the WM/GM models for the TVPS and WR

measures were not significantly different from the GM alone models for the respective measures ($p > 0.05$). The differences between the remaining models were significant ($p < 0.04$), suggesting that although there is limited co-dependence between WM and GM involvement in explaining functional outcomes, there is substantial independence between the impact of WM and GM injuries on five of the six functional outcomes.

Table 7.7. ANOVA comparisons between the GM and WM only models, and the models combining WM and GM lesion involvement.

AHA					
	Residual Sum of Squares	Degrees of Freedom	Mean Square	F	Significance
WM/GM combined	81617	-	-	-	-
WM only	93130	-6	-11514	2.563	0.023*
GM only	110550	-8	-28933	4.830	<0.001***
BRIEF					
	Residual Sum of Squares	Degrees of Freedom	Mean Square	F	Significance
WM/GM combined	735037	-	-	-	-
WM only	825191	-7	-90154	1.542	0.164
GM only	973689	-4	-238652	7.143	<0.001***
SDQ					
	Residual Sum of Squares	Degrees of Freedom	Mean Square	F	Significance
WM/GM combined	6013.7	-	-	-	-
WM only	6386.7	-7	-373.07	0.541	0.800
GM only	11366.0	-8	-5352.3	6.787	<0.001***
TVPS					
	Residual Sum of Squares	Degrees of Freedom	Mean Square	F	Significance
WM/GM combined	439456	-	-	-	-
WM only	414153	-2	-215837	21.365	<0.001***
GM only	655292	-6	-40342	1.331	0.252
WR					
	Residual	Degrees of	Mean Square	F	Significance

	Sum of Squares	Freedom			
WM/GM combined	27956	-	-	-	-
WM only	29640	-4	-3228.4	2.598	0.041*
GM only	31184	-4	-1684.1	1.355	0.256
			VOC		
	Residual Sum of Squares	Degrees of Freedom	Mean Square	F	Significance
WM/GM combined	81786	-	-	-	-
WM only	148175	-4	-66390	18.264	<0.001***
GM only	96119	-5	-14333	3.155	0.011*

Asterisked correlations were found to be statistically significant: * $p < 0.008$; ** $p < 0.0016$, *** $p < 0.00016$.

7.4 Discussion

An accurate, validated method for the automatic segmentation of WM and GM lesions has been applied to a cohort of children with unilateral CP. The correlation between regional lesion involvement and functional outcome was examined. Lesion involvements explained between 12-53% of the variance in the clinical score across all training models. Including information related to the timing and type of the insults, which cannot be automatically determined using the proposed approach, would further increase the amount of variance explained by these models. The anatomical regions with significant relationships to clinical function ($p < 0.05$) concurred with previous studies of the roles of individual regions ($p < 0.05$) including the thalamus [Haber and Calzavara, 2009], lenticular [Middleton and Strick, 2000] and caudate nuclei [Grahn et al., 2008], corona radiata [Kraus et al., 2007], cerebral peduncle [Cho et al., 2007], PLIC [Kinnunen et al., 2011], external capsule [Fazio et al., 2009] and superior-longitudinal fasciculus [Bernal and Altman, 2010]. Patient age and gender were not observed to be significant predictors of outcome in any trained model. Four of these twelve trained structure-function regression models remained significant after Bonferroni correction in the validation test set, suggesting that these models specifically have identified real, underling relationships in the brain. Overall, these findings demonstrate that these models could help predict functional outcomes arising from lesions in all children with clinically diagnosed unilateral CP.

It was observed that the models consisting of WM lesion involvement had a higher multiple R-squared compared to the corresponding GM models for all six clinical scores, which may be a result of the greater frequency of WM involvement observed in this cohort (Table 7.1). However, two of the six GM models were found to be significantly predictive of outcomes in the independent test set ($p < 0.008$), the same number as the number of significant WM models (Table 7.5). The important impact of GM involvement on outcome observed in this independent test set is consistent with previous findings that children with cortical or deep GM lesions showed noticeable motor and sensory deficits [Martinez-Biarge et al., 2010]. Furthermore combining both WM and GM information led to consistently higher correlations in this test set, reaching significance in three of the six combined models ($p < 0.008$). Finally, the substantial independence between the impact of WM and GM injuries on five of the six functional outcomes shown in Table 7.7 highlights the value in characterising both classes of lesions. Although GM lesions were found to be predictive of multiple functional impairments, they are comparatively more difficult to segment than WM lesions, as illustrated in the performance measures in Table 7.2. Despite this, future studies into CP as well as other cerebral injuries, including multiple sclerosis and stroke, are recommended to quantify the extent of GM injury to provide an assessment of functional impairment.

A technical limitation of the present study is the severe extent of injury present in approximately 25% of children with CP. Although the non-rigid registration techniques used to align the tissue probability maps and atlas labels provide the best possible alignment of the corresponding images, errors were still introduced in severely injured data with significant tissue loss or morphological changes. Additionally, the presence of other injuries such as brain malformations, cases of ventricular enlargement without any associated WM signal abnormalities, or cystic GM loss (which appears black in the TIRM, and potentially mislabelled as CSF in the segmentation) [Krägeloh-Mann and Horber, 2007], have not been identified with the proposed approach. The presence of these injuries introduces additional variance in the clinical motor outcome score not explained solely by the lesion predictor variables, reducing the multiple R-squared of the trained models, necessitating the use of additional injury detection methods. Alternatively for large-scale injuries, biomarkers of ventricular enlargement, cortical malformation or lesion volume may explain the same variance in clinical outcome, confounding the association of

each specific injury to function. Therefore the combination of these biomarkers is used to construct the comprehensive regression models of injury in Chapter 8, in order to distil these individual associations. Another limitation of this study is that the effects of potential plasticity, which may lead to the translocation of specific functions on the cortex. Plasticity has not been accounted for in the regression models and could lead to an unexplained variance in the clinical outcome in these participants. Although LASSO was used in the present analysis, which uses an L_1 penalty term, alternative feature selection and regularisation methods could be used, including ridge regression [Hoerl and Kennard, 1970] and elastic-nets [Zou and Hastie, 2005]. These approaches use an L_2 penalty term, and a mix of L_1 and L_2 penalty terms, respectively. However LASSO was chosen for this analysis as it enforces the greatest sparsity among the model coefficients, resulting in the most interpretable model.

A strength of the present study is that the proposed segmentation approach only requires structural MR images, which are well established sequences and are common in clinical practice. In future, a combination of automated methods for detecting all classes of injury from structural MRIs will be combined to provide a complete assessment of injury and estimation of impairment for children with CP. These estimates can help guide what therapeutic interventions for motor, cognitive, visual or communicative function may be required for individual children, and assisting these interventions to be performed earlier in life, where neuroplasticity may have a greater effect [Cioni et al., 2011]. Furthermore, as children with unilateral CP may not respond well to lateralised interventions such as Constraint-Induced Movement Therapy (CIMT), the severity and laterality of brain lesions may guide the potential clinical utility of unimanual CIMT versus bimanual training. Future investigations will also look to apply this approach to children with bilateral CP, when data becomes available.

7.5 Conclusions

This chapter presented a robust method for performing automated brain lesion segmentation from T1-weighted MRI sequences alone, and applied to the segmentation of both WM and GM lesions from children with unilateral CP. Its performance was validated against manual expert classifications of lesions with an accuracy of 0.936, and outperformed the current state-of-the-art lesion segmentation approach with an accuracy of 0.729. After computing regional WM and GM lesion burden, LASSO was used to identify regional burdens related to individual clinical functions separately for WM and GM lesions. The automatically selected regions conformed to established relationships between anatomical regions and function, with significant correlations observed between regional lesion burden and motor (0.670, $p < 0.008$), cognitive (0.751, $p < 0.008$), visual (0.614, $p < 0.008$) and communicative function (0.533, $p < 0.008$). GM lesions led to a significant and generalisable reduction in functional outcomes comparable in magnitude to WM lesions, demonstrating the importance of quantifying GM lesion involvement. In the following chapter, the measures of injury obtained from the methods described in the previous two chapters are combined, and are used to characterise the prevalence of injury in this cohort of children with CP. Additionally, the independence of these measures of injury was examined to determine the most predictive image biomarkers of patient function.

8. Combining injury detection methods to characterise injury and predict clinical outcomes in a cohort of children with unilateral CP

8.1 Introduction

In previous chapters, it was mentioned that MRI is strongly recommended to elucidate the timing and aetiology of brain insults that cause CP [Korzeniewski et al., 2008] to help facilitate therapeutic selection [Accardo et al., 2004], and is the current standard for assessing injury in clinical practice. Current characterisation of injuries related to CP are broadly grouped into three classes based on aetiological patterns [Krägeloh-Mann et al., 2007]: brain maldevelopments (of which cortical malformations are the main type) occurring from disturbances in the first and second trimesters; periventricular white matter injury (and potentially the secondary enlargement of the ventricles due to primary tissue loss) occurring from disturbances in the early third trimester; and cortical/deep grey matter injury occurring from disturbances in the late third trimester. The use of these characterisations are common, and many studies have investigated the prevalence of these aetiologies of injury within specific cohorts of children with CP [Bax et al., 2006; Krägeloh-Mann et al., 2007; Legault et al., 2011]. However, as a rule, these classifications have only been qualitatively assessed, disregarding the location and severity of lesions observed from the structural MRI (sMRI).

Quantitative measures of injury, accounting for injury severity and anatomical location, have the potential to better quantify the relationship (if any) between brain lesions and functional outcomes [Arnfield et al., 2013]. Furthermore, in future, such characterisations of injury may allow for valid and reliable predictions of patient impairment from MRIs acquired very early in life, which has implications for the selection of treatment strategies. However, this requires lesion volumes to be segmented in three dimensional images, which is too laborious to perform manually on large cohorts of data. Automated techniques are necessary to perform these segmentations in a repeatable and time-efficient manner. Such techniques need to be tailored to the specific challenges present in the sMRI of children with CP, including the potentially severe morphological alterations and the heterogeneous appearance of lesions, which are illustrated in Figure 1. However, no study has utilised the comprehensive quantifications of injury that automated approaches allow,

nor have they examined the utility of using these quantifications to predict clinical function. As a result, it remains unclear whether quantitative measures of brain injury can usefully augment the current classifications of brain injury in the clinical setting to produce finer estimates of patient function.

In this chapter, the three developed automated approaches from the previous chapters are used to characterise the prevalence of injury in this cohort of children with unilateral CP. These approaches identify the three main aetiologies of injury based on current classifications [Krägeloh-Mann and Horber, 2007]; including a tailored segmentation strategy and cortical shape analysis pipeline to detect cortical malformations [Pagnozzi et al., 2016b], a lesion-as-outlier segmentation strategy using T1- and T2-weighted MRIs for the detection of white and grey matter lesions [Pagnozzi et al., 2016a], and a statistical shape model (SSM) of healthy ventricular shape to detect the secondary enlargement of ventricles [Pagnozzi et al., 2016c]. These biomarkers were used to characterise the prevalence of injury in this cohort, and used to construct regression models with several scores of clinical function, including motor, cognitive, communicative and visual ability. Such models can improve our understanding of the relationship between the extent and topography of brain lesions and clinical function in children with CP. This work addresses Aim 2 of the thesis, combining all of the aforementioned approaches to “establish a statistical methodology that translates image-derived measures of injury severity to patient functional impairment, and thus determine the elucidated impact between brain injuries to patient outcomes”. In future, this understanding can help provide insights into neuroplasticity [Krägeloh-Mann and Horber, 2007]. However the immediate goal of these models is to provide valid and reliable estimates of patient function, which can help to tailor treatment strategies, potentially leading to improved gains in patient function for children with CP.

8.2 Materials and Methods

8.2.1 Study Participants

All 139 children recruited as part of the studies detailed in Section 3.2.1 have been included in this chapter.

8.2.2 Image Biomarkers

Image-processing techniques were used to identify and quantify three types of injury observed in the MRIs of children with CP [Krägeloh-Mann and Horber, 2007]. These methods and their performance are detailed in the following sections. An overview of the pipeline of these automated methods are illustrated in Figure 8.1.

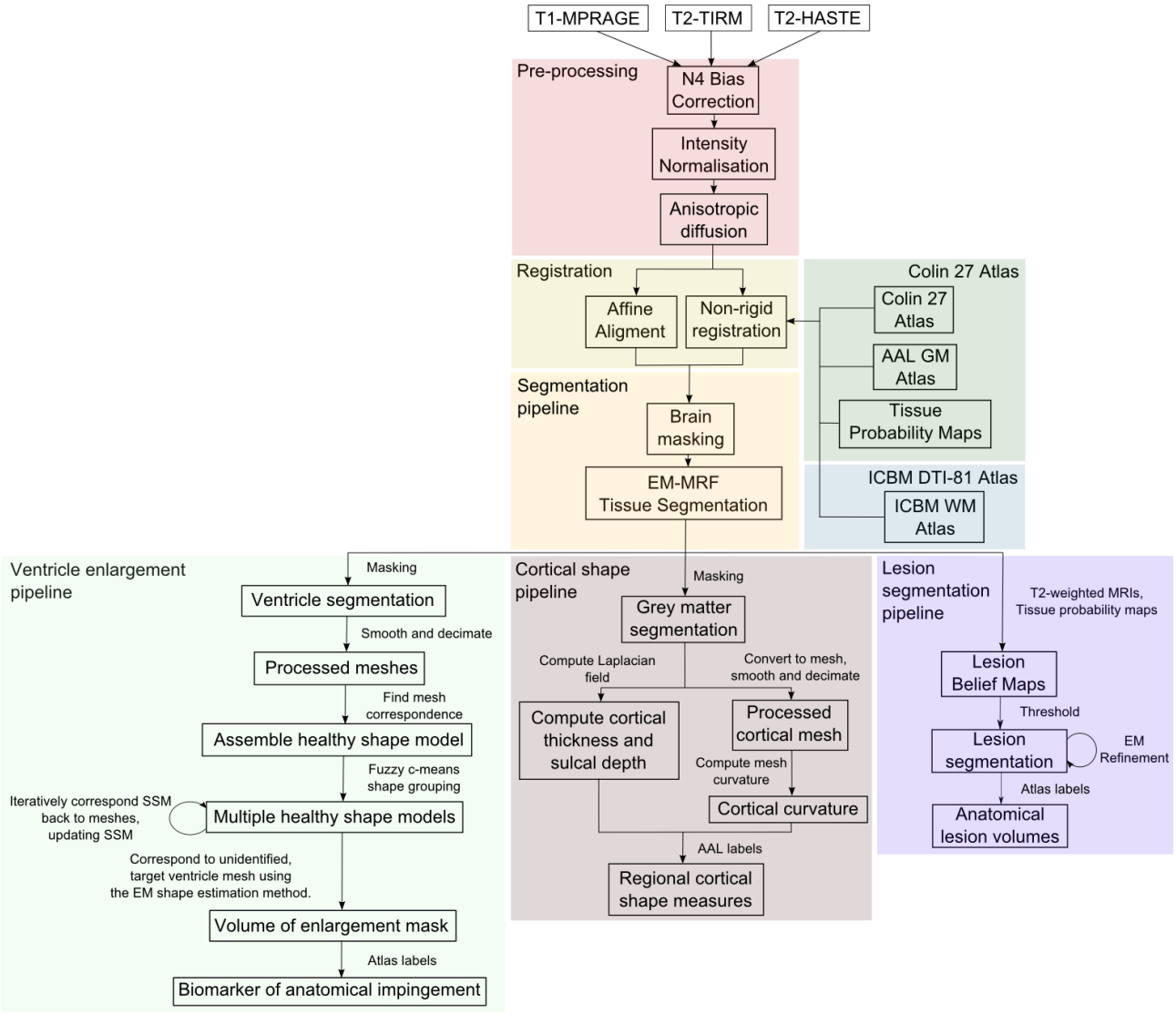

Fig. 8.1. The overall processing pipeline, including pre-processing steps (in red), registration (in yellow) of the utilised atlases (in green and blue), and the brain masking and tissue segmentation approaches described in Chapter 4 (in orange), which facilitate the detection of ventricular enlargement using the method from Chapter 5 (in light green), cortical shape measures using the approach from Chapter 6 (in brown), and lesion burden method using the method described in Chapter 7 (in purple).

8.2.2.1 Identifying cortical malformations

Cortical malformations, which appear as a heterogeneous range of abnormal cortical shapes, were identified in this study using a brain tissue segmentation algorithm that accommodates severe injury [Pagnozzi et al., 2015], and three shape measures computed from the cortical grey matter segmentation (cortical thickness, curvature, sulcal depth) in order to quantify shape abnormalities [Pagnozzi et al., 2016b] in each cortical region defined by the Automated Anatomical Labelling (AAL) atlas, as described in Chapter 6. An illustration of these cortical measures in three patients with observed cortical alterations are shown in Figure 8.2. Note for these figures, the cortical measures, which were obtained only on the cortical surface, were smoothed across the entire cortical grey matter segmentation. Biomarkers from this approach are an absolute z-score from healthy cortical shape measures measured from the corresponding cortical region among the 44 CHD children. Unlike an absolute measure of cortical shape (such as cortical thickness in millimetres), a z-score relative to healthy cortical shape aligns with the subsequent volumes of lesion burden and ventricular enlargement volume, where larger values represent greater injury severity. This facilitates the interpretation of the regression model coefficients.

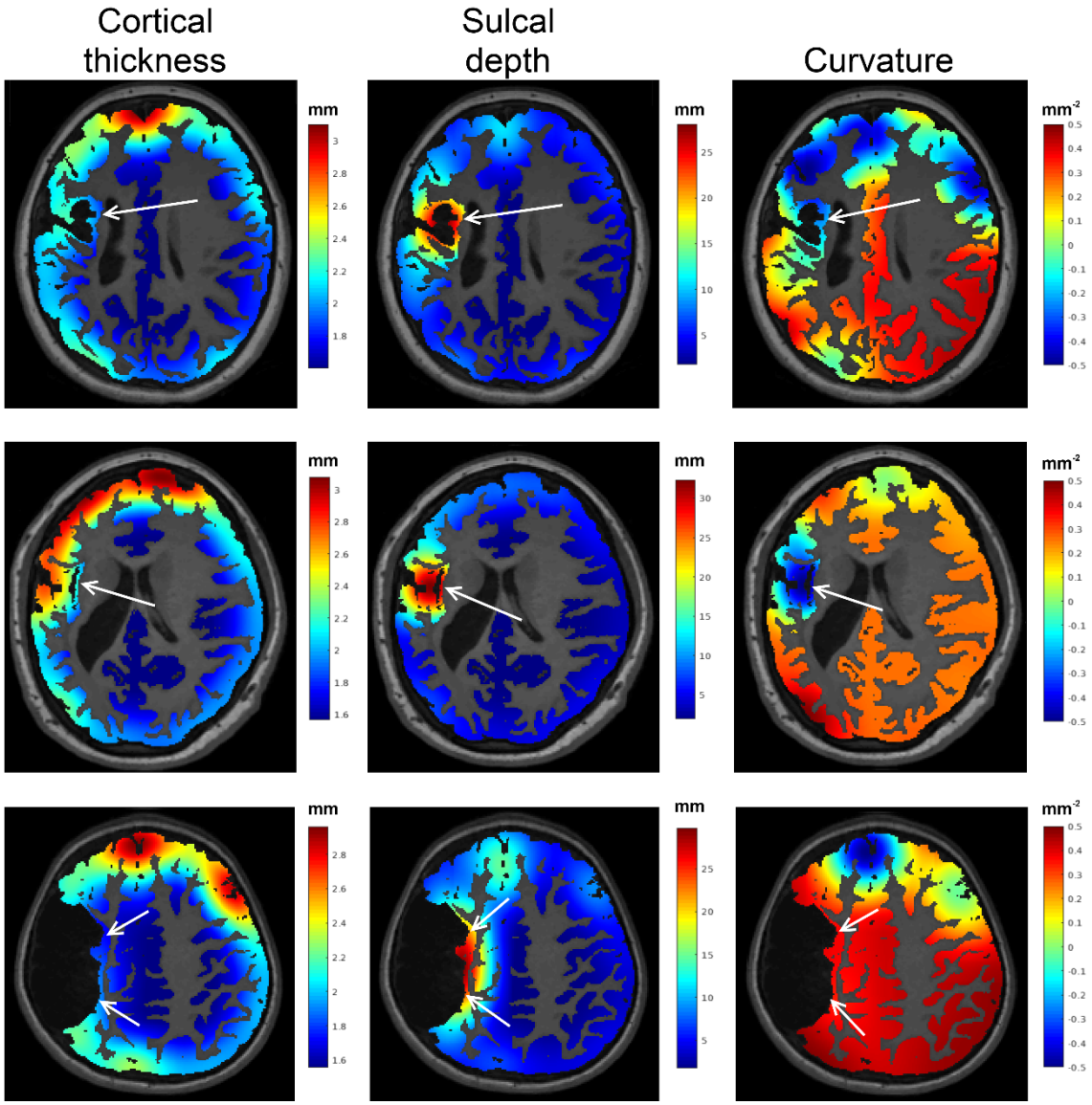

Fig. 8.2. An illustration of three cases with cortical malformations, and the measured cortical thickness (in mm), sulcal depth (in mm) and curvature (in mm^{-2}) of these cortices. Regions of injury were observed to have higher sulcal depths, and reduced cortical thickness and curvature.

8.2.2.2 Identifying white and grey matter lesions

White and grey matter lesions were identified using the lesion segmentation algorithm tailored to CP data described in Chapter 7, which contains multiple lesion classes to identify both types of lesions [Pagnozzi et al., 2016a]. Biomarkers from this approach are a lesion volume (in mL) in the different brain regions, identified using the AAL grey matter atlas and the ICBM DTI-81 white matter parcellation atlas (International Consortium for

Brain Mapping, CA) respectively. This approach achieved a sensitivity of 94% and a specificity of 93% for both white and grey matter lesions [Pagnozzi et al., 2016a]. Although it was observed that the specificity of WM lesion segmentations alone were comparatively lower due to more frequent variations in WM intensity, while the sensitivity of GM lesion segmentations alone were comparatively lower due to reduced contrast observed for GM lesions.

8.2.2.3 Identifying ventricular enlargement

Ventricular enlargement was identified using a SSM of healthy lateral ventricles to extract volumes of enlargement, and compute their impingement on nearby deep grey matter anatomies [Pagnozzi et al., 2016c], as detailed in Chapter 5. Biomarkers from this approach include a volume of ventricular enlargement (in mL) in the deep grey matter anatomies, as determined by the AAL grey matter atlas. Note that this is not the entire lateral ventricular volume, solely the volume of the region that is thought to be enlarged, compared to typically developing children. Three cases illustrating these segmented regions are shown in Figure 8.3.

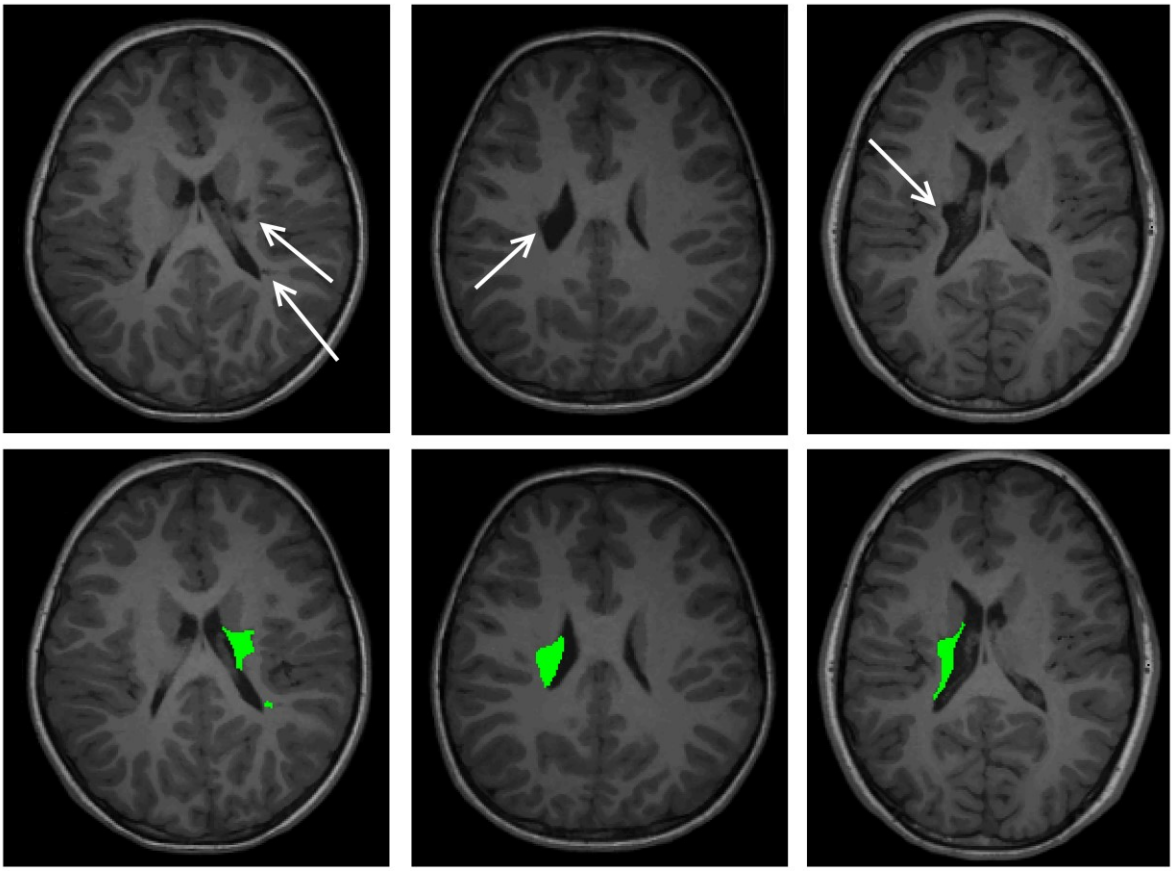

Fig. 8.3. Illustration of three cases of enlarged ventricles due to injury, and the segmentation of the enlarged volumes from the nearest healthy ventricle shape.

8.2.4 Statistical Methodology

The relationship between the brain injury and patient outcomes were investigated using regression models, where the image derived biomarkers of injury are the independent predictor variables, and the several clinical test scores are the dependent outcome variables. Initially, to obtain unbiased estimates, the data were partitioned, with regression models trained on 75% of the data and their performance validated on the independent 25% test set. These regression models were constructed with the LASSO method [Tibshirani, 1996], using the 'glmnet' package in R statistical software Version 3.2 [The R Development Core Team, 2008]. LASSO was chosen over other approaches, such as least squares, because of its inherent variable selection and regularisation properties. In the LASSO approach, predictor variables that are not strongly associated with the clinical outcomes are removed from the model. LASSO was run with default lambda and alpha

parameters that define the weight and type of the regularisation penalty respectively. Patient age and gender were included in all models and to account for the variance in different scanner sequences used in this study, scanner sequence was included as a categorical variable in each model. The regression coefficients of each model, which encode the relative weights of individual biomarkers impacting clinical outcome, were enforced to be negative. This was done in order to only extract correlations where observed injury led to reductions in patient outcome. Interaction effects were excluded to reduce the total number of model parameters and hence prevent model over-fitting. In total, six models were constructed, one for each of the six clinical scores (AHA, BRIEF, SDQ, TVPS, WR and VOC). Multiple comparisons of the models were corrected for using a Bonferroni correction, while model residuals were observed to be normally distributed for each of the dependent outcomes. An analysis of variance (ANOVA) was performed to compare the complete models from all biomarkers combined, and the biomarkers of each type of injury individually, to ascertain if it is beneficial to look at all kinds of injury observed in the MRIs concurrently.

8.3 Results

8.3.1 Characterisation of injury in the cohort

The prevalence of injury, as determined by our automated analyses, in our cohort is illustrated in Figure 8.4. Prevalence is shown as a Venn diagram, to illustrate that each individual patients may have a combination of the three classes of injury. Binary characterisation of injury was classified as the presence of any enlarged ventricles or white/grey matter lesions (greater than 0 mL anywhere in the brain), or a regional cortical shape with a computed z-score > 2.5 compared to corresponding healthy cortical shape (for any cortical shape and region). Of the 139 children in our cohort, 109 were classified as having some form of injury, with 15% of the cohort having all three types of injury identified. Ventricular enlargement was the most common form of injury (observed in 68% of children), followed by white/grey matter lesions (55%) and cortical malformations (30%). As expected from the known aetiology of injury, ventricular enlargement was observed in over 60% of patients with white/grey matter lesions. False positive characterisations of ventricular enlargement, caused by slight alignment errors of the ventricular meshes, explains why 14 children with typical brain development were incorrectly identified as possessing some form of brain injury.

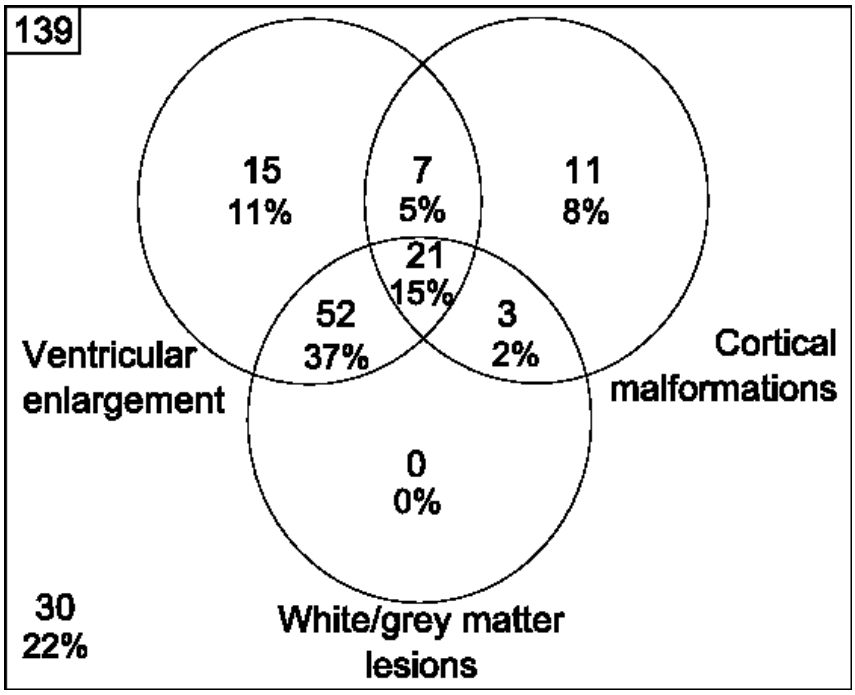

Fig. 8.4. A Venn diagram characterising the observed prevalence of ventricular enlargement, cortical malformations and WM/GM lesions observed in this cohort using the described automated techniques.

8.3.2 Observed structure-function relationships

The image biomarkers retained from LASSO, and their respective regression coefficients for each of the six models, are given in Table 8.1 below. In these models, the cortical shape biomarkers (labelled 'Cortical thickness', 'Curvature' or 'Sulcal depth') represent the reduction in clinical outcome for a 1 unit increase in z-score from healthy shape in that cortical region, while the lesion biomarkers (labelled 'Lesion') and ventricular enlargement biomarkers (labelled 'Ventricle enlargement') represent the decrease in clinical score from an increase in 1mL of lesion, or enlarged ventricle respectively, in that anatomy. In this table, we note that the p-values of each biomarker are uncorrected, and simply reflect the strength of that feature within the chosen model. However, the adjusted R-squared of the models, which measure strength of the correlation between the outcome and the model predictions, were compared against a Bonferroni corrected alpha value (0.05/6 tests, 0.008).

Table 8.1. The retained anatomical regions, and corresponding regression coefficients (including standard errors) of the six regression models modelled on the 75% training set. For each model, the multiple R-squared is provided. Features that are significant (p < 0.05) in multiple models are bolded.

AHA		
Independent variable	*Regression coefficient*	*Standard error*
(Intercept)	116.80***	4.741
Supplementary motor area - Curvature	-7.462*	2.828
Primary somatoensory cortex - Curvature	-15.157***	3.810
Cingulate - Cortical thickness	-14.063***	3.259
Lingual gyrus - Sulcal depth	-13.062**	4.306
Middle temporal gyrus - Sulcal depth	-14.887***	2.566
Lenticular nucleus - Lesion	-0.051**	0.017
External capsule - Lesion	-0.012***	0.003
Cerebral peduncle - Lesion	-0.044*	0.020
Age	0.302	0.599
Gender (Reference: Male)	1.733	3.547
MR Sequence (Reference: QCPRRC)	-4.850	4.820
Adjusted R-squared		**0.728*** **
BRIEF		
Independent variable	*Regression coefficient*	*Standard error*
(Intercept)	202.195***	19.884
Primary somatosensory cortex - Sulcal depth	-11.116	6.205
Insula - Curvature	-15.949	9.506
Occipital gyrus - Curvature	15.342	9.1775
Inferior temporal gyrus - Curvature	-21.469**	7.685
Premotor cortex - Cortical thickness	-12.619	9.222
Middle temporal gyrus - Cortical thickness	-16.595	9.875
Middle frontal gyrus - Lesion	-0.049	0.033
Caudate nucleus - Lesion	-0.053	0.038
Age	1.267	1.662
Gender (Reference: Male)	18.522*	8.958
MR Sequence (Reference: QCPRRC)	2.499	12.254
Adjusted R-squared		**0.310***
SDQ		
Independent variable	*Regression coefficient*	*Standard error*
(Intercept)	81.750***	5.252
Primary motor cortex - Cortical thickness	-2.392*	1.099
Primary motor cortex - Sulcal depth	-1.286	0.808
Insula - Curvature	-4.839***	1.239

Cingulate cortex - Cortical thickness	-2.656*	1.090
Cingulate cortex - Curvature	-1.631**	0.527
Fusiform gyrus - Curvature	-1.057	0.774
Lingual gyrus - Curvature	-2.268	1.161
Lingual gyrus - Sulcal depth	-1.238	5.313
Inferior temporal gyrus - Sulcal depth	-4.963***	0.973
Premotor cortex - Cortical thickness	-3.196*	1.368
Middle temporal gyrus - Curvature	-4.221**	1.207
Superior occipital gyrus - Lesion	-0.090	0.059
Superior temporal gyrus - Lesion	-0.005	0.003
Corona radiata - Lesion	-0.001***	<0.001
Age	0.222	0.242
Gender (Reference: Male)	1.835	1.615
MR Sequence (Reference: QCPRRC)	0.424	1.554
Adjusted R-squared		**0.707*** **

TVPS

Independent variable	*Regression coefficient*	*Standard error*
(Intercept)	135.004***	10.693
Primary motor cortex - Cortical thickness	-7.782	5.024
Rolandic operculum - Cortical thickness	-2.814	3.447
Supplementary motor area - Curvature	-4.382	3.599
Primary sensory cortex - Sulcal depth	-2.557	3.536
Insula - Sulcal depth	-2.248*	0.981
Cingulate cortex - Curvature	-2.234	1.915
Fusiform gyrus - Cortical thickness	-18.213	15.334
Superior temporal gyrus - Cortical thickness	-3.800	6.289
Primary visual cortex - Cortical thickness	-7.382	5.339
Lingual gyrus - Curvature	-1.570	4.327
Inferior temporal gyrus - Sulcal depth	-4.191	3.650
Inferior frontal gyrus - Cortical thickness	-4.720	4.499
Middle temporal gyrus - Cortical thickness	-2.192	5.176
Middle frontal gyrus - Lesion	-0.019	0.015
Hippocampus - Lesion	-0.264	0.395
Superior occipital gyrus - Lesion	-0.295	0.238
Supramarginal - Lesion	-0.019	0.019
Caudate nucleus - Lesion	-0.008	0.019
Posterior thalamic radiations - Lesion	-0.002	0.004
Age	0.487	1.102
Gender (Reference: Male)	3.421	5.340
MR Sequence (Reference: QCPRRC)	0.322	6.475
Adjusted R-squared		**0.577*** **

WR

Independent variable	*Regression coefficient*	*Standard error*

(Intercept)	96.247***	10.067
Cingulate cortex - Cortical thickness	-1.295	3.420
Cingulate cortex - Curvature	-0.734	1.395
Fusiform gyrus - Curvature	-0.930	2.292
Angular gyrus - Cortical thickness	-1.054	4.395
Primary visual cortex - Cortical thickness	-6.516	3.584
Primary visual cortex - Sulcal depth	-5.695	8.091
Cuneus - Curvature	-1.557	2.771
Lingual gyrus - Sulcal depth	-8.600	17.606
Occipital gyrus - Curvature	-11.531**	3.856
Inferior temporal gyrus - Curvature	-3.649	2.288
Inferior temporal gyrus - Sulcal depth	-2.910	2.340
Middle frontal gyrus - Cortical thickness	-3.372	2.852
Gyrus rectus - Curvature	-1.219	2.088
Precentral gyrus - Lesion	-0.003	0.005
External capsule - Lesion	-0.002	0.003
Cerebral peduncle - Lesion	-0.003	0.016
Age	-2.272***	0.532
Gender (Reference: Male)	-3.423	2.39
MR Sequence (Reference: QCPRRC)	-6.935*	3.115
Adjusted R-squared		**0.385***

VOC

Independent variable	*Regression coefficient*	*Standard error*
(Intercept)	8.980	22.027
Supplementary motor area - Curvature	-0.810	2.795
Primary somatosensory cortex - Cortical thickness	-7.609	3.801
Insula - Sulcal depth	-0.364	0.871
Cingulate cortex - Curvature	-0.674	1.341
Angular gyrus - Curvature	-0.713	4.449
Angular gyrus - Sulcal depth	-0.919	1.429
Primary visual cortex - Cortical thickness	-2.845	4.301
Lingual gyrus - Curvature	-3.136	3.246
Inferior temporal gyrus - Sulcal depth	-0.979	3.168
Posterior parietal gyrus - Sulcal depth	-5.267	2.609
Gyrus rectus - Cortical thickness	-5.610	3.997
Middle temporal gyrus - Cortical thickness	-1.371	3.507
Middle frontal gyrus - Lesion	-0.014	0.019
Inferior frontal gyrus - Lesion	-0.006	0.009
Cingulate cortex - Lesion	-0.011	0.062
Hippocampus - Lesion	-0.325	0.183
Middle occipital gyrus - Lesion	-0.017	0.016
Caudate nucleus - Lesion	-0.020	0.014

Posterior thalamic radiations - Lesion	-0.002	0.004	
Cingulum - Lesion	-0.034	0.249	
Age	4.090***	0.805	
Gender (Reference: Male)	0.608	3.013	
MR Sequence (Reference: QCPRRC)	-2.695	3..807	
Adjusted R-squared			**0.575*** **

Asterisked feature correlations were found to be statistically significant: * $p < 0.05$; ** $p < 0.01$, *** $p < 0.001$. Correlations in bold have a statistical significance of $p < 0.05$. Asterisked model correlations were found to be statistically significant: * $p < 0.008$; ** $p < 0.0016$, *** $p < 0.00016$.

8.3.3 Analysis of predictive biomarkers

The performance of the predictive regression models are shown in Table 8.2. Five of the six data-driven models were statistically significant ($p < 0.008$) in the 25% test set. Although the correlations for the manually chosen biomarkers were generally smaller than the corresponding data-driven models, four of these six models were statistically significant ($p < 0.008$).

Table 8.2. Pearson's R correlation between the predicted outcomes in the test set using the trained regression models and the clinical scores of the test set, for both the data-driven and manually chosen models.

	Pearson's R correlation	*95% Confidence Interval*
AHA	**0.706****	(0.488, 0.841)
BRIEF	0.482	(0.124, 0.729)
SDQ	**0.795****	(0.456, 0.932)
TVPS	**0.617***	(0.252, 0.827)
WR	**0.545***	(0.161, 0.786)
VOC	**0.682****	(0.354, 0.860)

8.3.4 Assessment of independence of biomarker-type

To assess the independence of the different categories of biomarkers, an ANOVA analysis was performed to compare the complete models obtained from the data-driven variable selection, and models constructed using only the biomarkers from this model of a specific injury class (i.e. cortical biomarkers and lesion biomarkers separately). The summary of these analyses is provided in Table 8.3. Model comparisons to the ventricle enlargement biomarkers alone were omitted as no ventricular enlargement biomarkers were retained by

LASSO in any model. All models containing only cortical shape or lesion burden biomarkers were found to be significantly different from the complete regression models ($p < 0.05$), except for the cortical biomarker only model for TVPS ($p = 0.109$). This suggests that the two different sets of biomarkers explain different portions of variance in the clinical score of children with CP.

Table 8.3. ANOVA model comparisons between the complete regression models, and the models constructed with the cortical shape and lesion burden biomarkers only.

AHA					
	Residual Sum of Squares	*Degrees of Freedom*	*Mean Square*	*F*	*Significance*
Complete model	7161.1	-	-	-	-
Cortical biomarkers only	12478.6	-3	-5317.5	12.623	<0.001***
Lesion biomarkers only	20031.5	-5	-12870	18.332	<0.001***
BRIEF					
	Residual Sum of Squares	*Degrees of Freedom*	*Mean Square*	*F*	*Significance*
Complete model	26360	-	-	-	-
Cortical biomarkers only	32537	-3	-6177.1	3.125	0.036*
Lesion biomarkers only	44323	-7	-17963	3.894	0.002**
SDQ					
	Residual Sum of Squares	*Degrees of Freedom*	*Mean Square*	*F*	*Significance*
Complete model	122.92	-	-	-	-
Cortical biomarkers only	276.38	-4	-153.46	6.554	0.001**
Lesion biomarkers only	627.53	-12	-504.61	7.184	<0.001***
TVPS					
	Residual Sum of Squares	*Degrees of Freedom*	*Mean Square*	*F*	*Significance*
Complete model	3704.2	-	-	-	-
Cortical biomarkers only	5131.4	-6	-1427.2	1.927	0.109

Lesion biomarkers only	7877.5	-13	-4173.3	2.600	0.015*
			WR		
	Residual Sum of Squares	*Degrees of Freedom*	*Mean Square*	*F*	*Significance*
Complete model	1883.6	-	-	-	-
Cortical biomarkers only	2963.5	-5	-1079.7	3.554	0.012*
Lesion biomarkers only	4754.9	-15	-2871.3	3.150	0.003**
			VOC		
	Residual Sum of Squares	*Degrees of Freedom*	*Mean Square*	*F*	*Significance*
Complete model	1348.5	-	-	-	-
Cortical biomarkers only	3318.4	-10	-1969.9	3.506	0.006**
Lesion biomarkers only	4263.5	-14	-2915	3.706	0.002**

8.4 Discussion

The findings from this chapter support the early characterisation of brain injury from the structural MRIs of children with CP, into the defined classes based on aetiologies [Krägeloh-Mann et al., 2007]. Using automated approaches for quantifying these respective injuries, a prevalence of injury in our cohort was found to be comparable to studies on other cohorts of children with CP [Bax et al., 2006; Krägeloh-Mann and Horber, 2007; Legault et al., 2011]. Leveraging the quantifications that these automated methods allow, models of brain injury to patient function were generated. Assessing the performance of these models on the unseen test set determined how well these observed relationships could predict functional outcomes in children with observed brain injury. Five of the six models were observed to obtain significant correlations in this test set, with only the Brief model not achieving significance. As Brief measures executive function, we hypothesise that reduced executive outcomes may primarily arise from the loss of white matter connectivity, which would require diffusion MRI and tractography to identify [Rose et al., 2011]. On its own, sMRI does not assess neural connectivity and the inclusion of diffusion data may result in greater association of these outcomes. However, unlike sMRI, there is not yet a routine and widely accepted method for diffusion MRI acquisition and processing of data [Jones et al., 2013]. The significant correlations observed for the other

clinical scores demonstrates the clinical utility of these predictive models in estimating patient function in order to provide early and effective therapeutic interventions.

Although the model features were retained from a data-driven process, the significant regions conform to known structure-function relationships of the brain. For instance, the supplementary motor area has known associations with intended voluntary action [Goldberg, 2010], the primary somatosensory cortex has been associated with the mental rehearsal of motor acts [Porro et al., 1996], the anterior cingulate has known motor regions regulating the interactions between cognitive and motor control [Paus, 2001], supporting the observed importance of these regions in the AHA model (Table 8.1). Additional significant regions in the AHA model include the lenticular nucleus, which is known to control a variety of movements [Middleton and Strick, 2000], and is connected to the external capsule [Henry et al., 2004], and the cerebral peduncle, which contains WM fibres of the corticospinal tract and has previously been shown to be predictive of motor deficits [Laundre et al., 2005]. For the Brief and SDQ models of cognitive function, several of the retained regions (inferior temporal gyrus, primary motor cortex, insular cortex, cingulate cortex, premotor cortex and corona radiata) have known associations with cognition and executive functioning. For instance, the inferior temporal gyrus, which was significantly retained in both models, has a known role in verbal fluency and cognition, and is commonly affected in AD [Scheff et al., 2011]. The observation in the Brief model that girls had higher reported executive functioning than boys may be due to females maturing earlier than males [Waber, 1976], or arising from the currently unexplained phenomenon that males with CP tend to exhibit more severe impairment [Jarvis et al., 2005]. Other significant features retained in the SDQ model include the primary motor and premotor cortices, which have both been shown to be responsible for motor learning and cognitive actions [Rizzolatti et al., 2002; Sanes and Donoghue, 2000], the cingulate cortex that has been associated with the regulation of varied mental and emotional activity [Bush et al., 2000], and the corona radiata which has been associated with mental calculation and information processing [Sasson et al., 2012]. The insular cortex, which was retained in both models for cognition (SDQ) and vision (TVPS) , has known associations with multiple sensory areas, influencing awareness of somatosensation and goal directed cognition [Chang et al., 2013], and the processing of visual information [Nagai et al., 2007]. We hypothesise that the presence of the occipital gyrus in the word reasoning model may

arise from the known roles in the auditory and spatial information and stimuli [Renier et al., 2010], including sound localisation, which are required to perform well in the WPPSI-III subtests for communication. Age was retained in both models for vocabulary (VOC) and word reasoning (WR), potentially reflecting the known improvements in articulation [Kilminster and Laird, 2014] and phonological skills [Snowling and Hulme, 1994] occurring during childhood development.

Ventricular enlargement biomarkers were observed to be removed by LASSO's variable selection for all models of clinical function. This may due to ventricular enlargement being a secondary injury caused by primary periventricular white matter tissue loss [Melhem et al., 2000; Palmer, 2004]. Consistent with this aetiology, most children with ventricular enlargement in this cohort had white or grey matter tissue lesions. As a result, both ventricular enlargement and lesion biomarkers explain similar portions of variance in these children's functional outcomes. Since the ventricular enlargement biomarkers were removed by LASSO, this indicates that they explain relatively less variance in the functional outcomes than the lesion biomarkers. However, it was observed that both cortical morphology and lesion burden variables were retained by LASSO for all six models. The independence of these biomarkers is further demonstrated in the ANOVA supplementary table, identifying that the two sets of factors explain independent portions of variance in five of the six models. These findings highlight the benefit of quantifying both biomarkers for the assessment of MRIs.

Although the developed automated approaches were designed to be robust to the presence of severe brain injury, there are a number of technical limitations with these methods. Firstly, despite most of these approaches requiring only an affine alignment of atlases, which is mostly driven by the alignment of the skull, there are registration errors introduced in the deformable registration of the tissue probability maps used in the lesion segmentation pipeline. The brain masking segmentation step occasionally incorporates dura into the brain mask and miss subtle cortical sulci. In these cases, manual editing of the segmentations is required, as instances of either error will affect the cortical shape measures computed in the cortical analysis pipeline. The presence of slight correspondence errors between the ventricular shape models led to a large number of false positive classifications of ventricular enlargement, contributing to the 14 false positive classification of brain injury in typically developing children. This misclassification could be

minimized by using Procrustes alignment prior to SSM fitting in order to reduce the misalignment of the ventricles, and to use maps to down weight regions of detected “enlargement” near the anterior horn of the lateral ventricles, where this misalignment typically occurs. Due to the risk of over-fitting on the limited available training data, no interaction terms were included for account for potential feature covariance, nor was WM connectivity information incorporated in the current study. The inclusion of diffusion data the model will be important in the future, because structural MRI alone cannot account for the variable influence of neuroplastic mechanisms that lead to altered structure-function relationships to compensate for the presence of injury [Carmichael, 2003; Thiel et al., 2001]. These altered relationships confound the relationships between injury and impairment that the regression models attempt to elucidate, introducing unexplained variance in the clinical scores and potentially reducing the multiple R-squared of these models.

The main strength of this study is that the developed injury segmentation approaches only requiring well established T1-weighted sequences. More sophisticated diffusion and functional sequences are not as widely available, and have longer scanning times which complicate the imaging of young children. The development of automated techniques that only require these rapid and established sequences help facilitate potential translation to clinical practice. Secondly, this study encapsulates the full range of primary and secondary injuries characterised previously [Krägeloh-Mann et al., 2007], as well as patient age and gender, allowing for comprehensive characterisation of brain injury from sMRI. In future, image analysis in the CP setting needs to move towards more automated quantification of injury, as it allows quantitative relationships between brain injury and outcome to be elucidated for children with both unilateral and bilateral CP. These associations have the potential to build upon the understanding of the brains structure-function relationships, which is an important prerequisite for understanding reorganisation and plasticity. Furthermore, there is potential in using these associations to produce estimates of patient function, which have important clinical implications for dictating the type and intensity of intervention that may be required, early in life in order to optimise functional outcomes.

Although the classification of preterm infants and infants born at term age was not recorded as part of this study, the characterisation of injury in this chapter can help investigate the development of children born preterm. Preterm infants have an increased

incidence of brain injuries [Volpe, 2009], including PVL and deep GM injury, and have been observed to have reduce long-term neurodevelopmental outcomes [Petrini et al., 2009]. Furthermore, there is the potential to use the described approaches to characterise longitudinal changes in brain structure as a result of neuroplastic mechanisms, occurring through early childhood development or in response to therapeutic rehabilitation. Using the segmentation approaches to detect changes in cortical volume arising from neuroplasticity in the GM, combined with diffusion MRI approaches to detect neuroplastic changes in the WM [Reid et al., 2016], the effects of plasticity can be comprehensively quantified. Such studies could be used to elucidate how brain structure changes in response to injury or therapy, and possibly also the mechanisms of plasticity underlying these changes, with associated implications for patient function. Such information could lead to tailored therapy for patients to best leverage these recuperative mechanisms.

8.5 Conclusion

In this chapter, several validated, automated approaches for identifying three different aetiologies of brain injury applied to a cohort of children diagnosed with unilateral CP. Similar prevalence's of cortical malformations (observed in 30% of children), white and grey matter lesions (55%) and secondary ventricular enlargement (68%) were observed to previous studies on populations of children with CP. Furthermore, significant correlations were observed between the biomarkers of injury and multiple scores of patient motor, cognitive, visual and communicative function. These structure-function relationships generalised to unseen data, with correlations between 0.482 and 0.795, and retained predictor variables that conformed to known roles of brain structures. There was significant independence between cortical morphology and tissue lesions in explaining functional outcomes, highlighting the benefit of quantifying both of these types of injury for clinical assessment. These findings supports the early elucidation and characterisation of brain injury from sMRI in the clinical assessment of children with CP. In future, automated methods are needed to build on our understanding of the brain's structure-function relationship, in order to better understand neuroplasticity, and produce estimates of patient function that has clinical utility in guiding rehabilitation strategies.

9. Discussion and Conclusion

9.1 Novel contributions

Several contributions have been made in this thesis towards the goal of accurately identifying and quantifying cerebral injury from the T1- and T2-weighted MRI of in children with CP.

These contributions include

1. the development of several automated segmentation approaches to delineate the three main classes of injury observed in children with CP, including:
    a. the development of a robust segmentation algorithm that minimises reliance on atlas priors and uses a modified spatial term
    b. the utilisation of an SSM procedure to model healthy ventricle shape, and use this to delineate regions of involvement into nearby anatomies
    c. the development of a shape analysis and label propagation pipeline for the characterisation of cortical shape and the development of cortical biomarkers of injury
    d. the development of a WM and GM lesion segmentation pipeline for the quantification of regional tissue loss due to injury
2. a statistical methodology that translates image-derived measures of injury severity to patient functional impairment, and thus determined the impact of brain injury on patient outcomes
    a. identified that the several biomarkers of injury are all predictive of functional impairments, and have independent effects of clinical outcomes
3. comparisons of the automated results against a manual gold standard, confirming the automated results strongly agree with the manual expert, and improve upon the current state of the art techniques, highlighting their inapplicability to the CP setting due to inaccurate assumptions

The contributions address the three aims of this thesis. The main findings of these papers are summarised below.

9.1.1 Current role of structural MRI

The current role of structural MRI is as the standard imaging modality used in the clinical assessment of brain injury, and will only increase in the future based on the American Academy of Neurology's recommendation that all children with CP have a structural MRI at 2 years of age. Although diffusion and functional MRI's are prevalent in the literature [Faria et al., 2010; Faria et al., 2011; Oishi et al., 2011; Oishi et al., 2013; Yoshida et al., 2013], the long scanning times for diffusion MRI complicate the imaging of young children, and are currently not the standard for clinical assessment [Saunders et al., 2007]. It is advantageous to assess individual focal lesions from structural MRI.

State of the art image processing techniques were identified from the literature, and summarised in the systematic review (Chapter 2), with specific focus to the technical challenges of the CP setting. Since the completion of the systematic review, an additional 12 original articles have been published that met the inclusion criteria of the review. One study assessing ventricular shape using SSMs proposed for neonatal MRIs has been published [Qiu et al., 2015]. This method, however, utilises deformable registration to obtain point-wise correspondences to injury, which introduces significant errors in the CP setting. A number of cortical analysis methods have been published, measuring cortical thickness and surface area to analyse changes related to schizophrenia [Kong et al., 2015] and epilepsy [Ahmed et al., 2015; Ristić et al., 2015] using FreeSurfer, while sulcal depth computed using BrainVISA was utilised as a biomarker to classify AD [Andersen et al., 2015]. Additionally, the temporal alignment of cortical surfaces has been proposed using surface inflation [Li et al., 2015a], but this is not suited to brains with severe injury. A potentially viable method, called the multi-contrast multi-scale surface registration (MMSR), leverages the topological properties of the level set framework to assist cortical alignment [Tardif et al., 2015].

Many lesion segmentation methods have been published, particularly in the MS [Guizard et al., 2015; Mechrez et al., 2015; Roura et al., 2015] and stroke [Ozenne et al., 2015] setting. Although similar, these approaches require non-rigid registration of the patient MRIs, which is difficult for MRIs containing severe brain injury. The EM method with a modified mixture model, which is similar to an MRF, was used to identify both WM and GM lesions in the case of ischemic stroke [Ozenne et al., 2015]. To date, none of these

methods have been applied to CP. The automated image processing pipeline developed as part of this thesis aimed to address this issue.

9.1.2 Tissue segmentation in the presence of severe injury

As mentioned throughout this thesis, the severity of injury in the CP setting can mean that brain structure deviates significantly from healthy atlases. Consequently, tissue segmentation, which is necessary to perform for subsequent analyses of injury, remains a fundament challenge. Image pre-processing was implemented to alleviate as much of the image bias, noise and artefacts as possible. To tackle to problem of accommodating injury variability, the adaptive EM algorithm, which can estimate tissue classes using one or more MR modalities that is robust to scanning parameters, initialised with a data-driven peak-finding approach rather than atlas priors, was used. This method, interleaved with a weighted MRF formulation that enforces spatial homogeneity of labels corresponding to intensity homogeneity, was developed as part of this thesis, and is detailed in Chapter 4. Although the use of sophisticated multi-atlas techniques are the state-of-the-art approaches commonly used for current studies, these methods fail in the presence of extreme deformation. The proposed approach highlights the potential of adapting simple, existing approaches for this unique clinical problem. Such approaches benefit from their simplicity by providing greater computational efficiency and are robust to cases that significantly differ from healthy priors. It was shown that a reduced reliance on atlas priors yielded improved segmentation accuracy of the cortical GM, particularly for injured data sets [Pagnozzi et al., 2015].

9.1.3 Assessment of ventricular enlargement

Modelling ventricular shape using SSMs has been frequently performed in the detection of ventricular enlargement corresponding to AD. However the accuracy of these methods critically rely on an accurate point-wise correspondence between ventricular shapes, which in the case of irregular and highly variable enlargement observed in children with CP, is a technical challenge. The approach developed in this thesis was to tailor the SSM method for use in the CP setting, by avoiding the construction of a model of injury and solely construct a healthy SSM. As this model contains all observed healthy variability in ventricle shape, injury is represented as the residual volume between a target shape and the closest healthy ventricle shape provided by the transformed SSM (Chapter 5). This representation of injury is unique to this approach, allows identification of subtle injury on

ventricles with a small volume, and avoids false positive detection of enlargement in healthy ventricles with a large volume, compared to a distance from the mean representation of injury used in other SSM studies [Apostolova et al., 2012; Chou et al., 2007; Ferrarini et al., 2008a; Thompson et al., 2004]. This was demonstrated by the improved ROC performance of the residual volume over the magnitude of SSM deformation compared to the manual classification of injury [Pagnozzi et al., 2016c]. The second development was the utilisation of this volume to extract a surrogate marker of injury to surrounding subcortical GM structures, including the caudate nucleus, thalamus and lenticular nucleus, as well as the internal capsule. Although this is an indirect approach, the segmentation of these structures directly is challenging due to the reduced tissue contrast of these structures and the requirement of deformable atlas registration, whereas the ventricle segmentation is robust even in cases of injury due to the high contrast of the ventricular boundary. As shown in Chapter 5, these surrogate markers were strongly correlated with multiple clinical scores of patient function, highlighting the value to be gained from this biomarker.

9.1.5 Assessment of cortical malformations

Quantifying cortical shape has been performed frequently in studies observing cortical development, and shape changes due to WS, autism and injury associated with CP. These studies, however, utilise deformable registration both for segmenting the cortical GM, and for estimating cortical thickness or sulcal depth measures, which critically fail on patients with extensive tissue loss. In the approach developed in this thesis, tissue segmentations were obtained using an automated EM-weighted MRF segmentation initialised with robust data-driven techniques, and improved with a modified spatial kernel, which yielded improved cortical segmentations [Pagnozzi et al., 2015]. From this cortical GM segmentation, multiple shape measures were computed in order to detect the spectrum of possible malformations; cortical thickness to detect pachygyria, curvature to detect polymicrogryia and schizencephaly, and sulcal depth to detect lissencephaly (Chapter 6). Instead of using deformable surface registration, the voxel-based Laplacian approach was used to compute cortical thickness and sulcal depth, which provides computational efficiency over mesh-based methods and robustness to injury. Curvature was computed using the VTK toolkit. Another technical novelty that was implemented in this pipeline was the implementation of level sets to map these shape measures from

cortical regions to the standard AAL atlas, by allowing labels to be propagated down the 4D level set function in a smooth topological manner that allows for intersection between the subject and atlas cortices. Converting shape measures to an absolute z-score relative to the healthy shape measures from the corresponding cortical regions allows for a quantification of cortical malformation. Moderate correlations between the constructed models and patient function, and a succinct set of biomarkers for each score that were consistent with the known structure-function relationship of the brain, were identified, and were observed to generalise to an unseen data set [Pagnozzi et al., 2016b].

9.1.6 Assessment of focal lesions

Due to the prevalence of WM and GM injury observed in children with CP [Bax et al., 2006], a lesion segmentation approach was developed as part of the framework of automated methods (Chapter 7). Although existing lesion segmentation software is available, the use of a variable lesion likelihood threshold and the lack of a GM lesion class limits its performance on CP data. In Chapter 7, a modified version of the fully automated EM-weighted MRF segmentation from Chapter 4 was proposed which incorporated T2-weighted MRI and registered TPMs to weight lesion and healthy tissue class likelihoods. This approach incorporates three separate lesion classes; WM lesion, GM lesion and internal capsule lesion, which is a unique approach tailored to identifying the full spectrum of lesions observed in children with CP. Furthermore, this approach is robust to injury severity, only requiring an affine alignment of atlas tissue priors. The improved performance of this approach compared to the available state-of-the-art LST toolbox in SPM, and maintains higher performance with increasing injury severity [Pagnozzi et al., 2016a]. This lesion volume was utilised to compute regional WM and GM involvement, which were found to be significantly correlated with multiple outcomes, and performed well upon test set validation. This analysis also identified the relative greater importance of GM lesions when predicting patient outcome, which is supported in the literature [Krägeloh-Mann et al., 2007; Martinez-Biarge et al., 2010].

9.2 Implications

The work presented in this thesis lays the foundation for the development of a clinical tool that can assist clinicians with the assessment of the MRIs of children with CP. The automated approaches developed as part of this thesis can provide an accurate segmentation of healthy brain structures and identified injury, allowing it to be a clinically useful tool. Additional information quantifying the extent of injury, and using statistical models to provide predictions of impairment, are also provided by these methods, which could greatly enhance the tailoring of treatment strategies for individual patients. Overall, this thesis paves the way for automated image analysis methods in CP and automates the current semi-quantitative radiological scoring methods proposed in the CP setting [Fiori et al., 2014; Inder et al., 2003; Kidokoro et al., 2013; Miller et al., 2005; Shiran et al., 2014; Sie et al., 2005; Skiöld et al., 2013].

The ability of the proposed approaches to be robust to injury severity is important for the clinical utility of the proposed tool. Methods must be able to provide automated analyses for severely injured brains, but conversely be sensitive enough to detect subtly injury that clinicians may oversee. In this cohort, it was observed that only 2 children diagnosed with CP with mild to moderate functional impairments had no observed injury in the MRI, which equates to approximately 2% false negative rate overall. However, care must be taken in the detection of extremely slight injury in this context, as injury identified by clinicians should be considered as the ground truth. Nevertheless, as all of the developed approaches continuously and quantitatively assess injury, this allows even subtle injury to be measured using these methods, which were found to agree with the experts' manual classification of injury in a majority of cases. Additionally, the simplicity of the proposed methods in this thesis makes them robust in the presence of severe injury. Although severely injured cases would be easily detected by trained experts, an automated quantification of injury is still beneficial, for both comprehending injury severity, and for providing an estimate of function.

Although the automated approaches developed in this thesis have been tailored for children with CP, these methods can be applied to any cerebral pathology with similar appearing lesions, highlighting potential value for the elderly and neonatal populations. The proposed EM-weighted MRF method can be applied to the task of brain tissue segmentation for many different populations. The shape models of ventricular enlargement

could be applied to investigations into AD, where the distance-from-the-mean definition of injury may be more suitable. The cortical shape analysis could be extended to any shape affecting pathology, including autism, WS and schizophrenia, or could track these shape measures longitudinally through development. Finally, the lesion segmentation approach can be applied to the detection of WM lesions in MS with any T2-weighted modality applicable with the proposed approach. The application of these approaches to brain tumours is also possible, with the developed EM-MRF segmentation potentially discriminating between necrotic, hypoxic and active parts of the tumour, which demonstrates the wide applicability of the tools developed in this thesis.

These investigations into CP related injury highlight (1) the reliance on atlas priors should be minimised and instead rely on adaptive approaches and data-driven modifications to enhance segmentations in regions of severe injury, which deviate significantly from healthy atlases, (2) utilise unsupervised approaches for lesion segmentation with dedicated WM and GM lesion classes, (3) the use of multiple shape measures to fully parameterise cortical topology, and (4) the construction of shape models of injury should be avoided, and instead measure residual volumes from the closest healthy shape from the model manifold.

9.3 Limitations

A limitation of the work contained in this thesis is the variable influence of plasticity, which is dependent on a number of genetic and environmental factors [Belsky and Pluess, 2009; Chapman et al., 2003]. The approaches presented in this thesis assume normal structure-function relationships, and build models relating biomarkers of injury to patient outcome accordingly. However plasticity alters this relationship and consequently reduces the accuracy of the trained models. The detection of plasticity mechanisms is required to account for changes in the structure-function relationships when using the proposed techniques. Mechanisms of GM plasticity include neurogenesis and alterations in dendritic arbour [Feldman, 2009], often appearing as changes in cortical thickness and volume [Zatorre et al., 2012] which could be quantified using the cortical analysis proposed in Chapter 6. Changes in WM, however, include altered WM connections and tract structure, require additional modalities such as diffusion MRI quantify the microstructural properties of the WM tracts. Combining structural and diffusion MRI, both the underlying WM and GM neuroplastic mechanisms could be identified, facilitating investigations into plasticity. For

instance, functional MRI driven diffusion tractography [Reid et al., 2016] can help to identify patient-specific cortical networks associated with particular functions, potentially allowing these approaches to avoid assumptions of normal structure-function relationships. Furthermore both structural and diffusion MRI were used in conjunction with the semi-quantitative brain lesion severity scale to explore the relationship between brain injury and motor and sensory function with insights into the mechanisms of plasticity [Fiori et al., 2015]. A related limitation is that the data used in these studies is cross-sectional, preventing any findings to be associated with plasticity. To address this limitation in future studies, longitudinal data sets are required so that changes in brain structure within individual patients can be causally linked to neuroplasticity mechanisms.

Another limitation is the lack of quantitative validation of the developed methods in the CP setting. Quantitative comparisons to alternate state of the art approaches have been performed, which in certain cases have been tailored to enhance prior relaxation and the initialisation method. However, these state of the art approaches have not been developed specifically for the CP setting, and the severe injury that may be observed. Ideally validation of the proposed approaches developed in this thesis should be performed against manual segmentations of injury, for instance 3D segmentations of lesions or quantitative characterisations of cortical shape. However the time intensive nature of segmenting voxels of injury for the 100+ data sets involved in this study is infeasible, and has thus not been available for validation studies. Instead, validation against only the qualitative classifications of injury, provided by a manual expert experienced at assessing the MRIs of children with CP, was performed throughout this thesis. Furthermore, these manual classifications of injury came from one expert child neurologist, and as such does not provide any information on inter- and intra-rater reliability metrics, which have shown to be as high as 7% and 23% in Multiple sclerosis lesion segmentation [Zijdenbos et al., 2002]. In future, provided manually segmented data sets from multiple experts are available, further validation studies should be performed on this new data.

A final limitation of the work in this thesis was the use of non-standard measures of patient outcome. Although all the clinical measures used in this thesis have been shown to be valid and reliable [Bourdon et al., 2005; Frostig et al., 1961; Gioia et al., 2002; Krumlinde-Sundholm et al., 2007; Wechsler, 1967], future work should look to validate the observed structure-function relationships on more thorough or widely used clinical scores, such as

the GMFCS for gross motor function, the MACS for hand function, the CFCS for communicative ability or the IQ for intelligence and cognition.

9.4 Future work

The future work for the automated framework presented in this thesis will be to develop the investigated approaches into a tool useful in the clinical setting. This will involve translating these methods from MATLAB to C++ or C#, and including software developed in-house code at The Australian e-Health Research Centre group as well as the freely available ITK and VTK packages, to generate a standalone application that clinicians can run on their computer. Unlike MATLAB, the C-based languages are applicable with the established ITK and VTK imaging libraries, allows for a fast implementation of the procedures, and can be run on any computer.

Broader recommendations for future work in the automated image analysis of brain MRIs are to use methods that can accommodate patients with potentially severe injuries, either by employing relatively simple yet robust approaches as in this thesis, or alternatively developing methods which selectively relax atlas priors in regions that differ significantly from healthy anatomy. The clinical recommendations based on this research are to push towards performing neuroimaging on children early in life, and using the quantifications of injury severity provided by automated techniques such as those presented in the thesis to provide predictions of multiple patient outcomes. It is also recommended to use such approaches for longitudinal studies, allowing injury observed early in life at the time of scanning to be causally linked to long term functional outcomes, allowing differing trajectories of improvement based on different rehabilitation and therapies to be examined. As adults with CP have been observed to consume a large amount of healthcare resources [Pons et al., 2016], characterising these trajectories and optimising treatment strategies will lead to improved outcomes and reduced reliance on healthcare services for patients with CP.

The automated measures of injury presented throughout this thesis are biomarkers based on the defined aetiologies of injury observed in children with CP. However, as yet, they are not clinically established biomarkers. In order to have these measures accepted in clinical practice, future efforts will involve collaboration with paediatricians, providing them with the developed methods and the information that these methods provide. Long term usage and

refinement of these methods can lead to a consensus on the biomarkers that have most diagnostic value, best classify the extent of injury or best predict prognoses of patient function. Additionally, the use of these characterisations of injury as part of clinical trials investigating rehabilitation could help reveal biomarkers predictive of response to an intervention, which is critical in the development of effective therapies.

A critical intention of the developed framework is its application to the clinical assessment of neonates. As the American Academy of Neurology has recommended all children with CP have an MRI at 2 years of age, this tool has the potential to provide additional clinical value at this crucial developmental period. As mentioned previously, there is currently no medical tool in place to assist the clinical assessment of the MRIs of children with developmental disorders, leaving room for FDA-approved devices to solve this unique clinical problem. The integration of such a medical imaging solution still requires substantial development, including collaborations with medical professionals in order to implement and develop the necessary training resources, however the development of a cloud-based tool allowing users to upload an image and receive a volumetric report of brain structure is being planned. An example clinical report, providing details of lesion burden and cortical morphology relative to healthy development for a selected patient, is provided in Supplementary Figure A.3 as a demonstration of the information this tool can provide. The automated delineation of injury can help clinicians better establish the timing and aetiology of injury, while the predictive models of patient function have substantial implications for the development of treatment strategies. This has significant value for tailoring patient specific treatment strategies to be implemented at an earlier age, which if effective, can lead to greater long-term gains in functionality for children with CP.

Bibliography

Accardo J, Kammann H, Hoon Jr AH (2004): Neuroimaging in cerebral palsy. J Pediatr 145:S19–S27. http://www.sciencedirect.com/science/article/pii/S0022347604004147.

Ad-Dab'bagh Y, Einarson D, Lyttelton O, Muehlboeck JS, Mok K, Ivanov O, Vincent RD, Lepage C, Lerch J, Fombonne E, Evans AC (2006): CIVET image-processing environment: A fully automated comprehensive pipeline for anatomical neuroimaging research. In: . Proceedings from OHBM: The 12th Annual Meeting of the Organization for Human Brain Mapping. Florence, Italy.

Adalsteinsson D, Sethian JA (1995): A Fast Level Set Method for Propagating Interfaces. J Comput Phys 118:269–277. http://www.sciencedirect.com/science/article/pii/S0021999185710984.

Adaszewski S, Dukart J, Kherif F, Frackowiak R, Draganski B (2013): How early can we predict Alzheimer's disease using computational anatomy? Neurobiol Aging 34:2815–26. http://www.ncbi.nlm.nih.gov/pubmed/23890839.

Ahmed B, Brodley CE, Blackmon KE, Kuzniecky R, Barash G, Carlson C, Quinn BT, Doyle W, French J, Devinsky O, Thesen T (2015): Cortical feature analysis and machine learning improves detection of "MRI-negative" focal cortical dysplasia. Epilepsy Behav 48:21–8. http://www.sciencedirect.com/science/article/pii/S1525505015002322.

Aisen ML, Kerkovich D, Mast J, Mulroy S, Wren TAL, Kay RM, Rethlefsen SA (2011): Cerebral palsy: clinical care and neurological rehabilitation. Lancet Neurol 10:844–852. http://www.sciencedirect.com/science/article/pii/S1474442211701764.

Alhazmi F, Alghamdi J, Mackenzie I, Kemp G, Sluming V (2015): Cortical Thickness and Sulcal Depth in Mild-to-Moderate Hearing Loss. In: . European Congress of Radiology. Vienna, Austria.

Aljabar P, Heckemann R a, Hammers A, Hajnal J V, Rueckert D (2009): Multi-atlas based segmentation of brain images: atlas selection and its effect on accuracy. Neuroimage 46:726–38. http://www.sciencedirect.com/science/article/pii/S1053811909001554.

Anbeek P, Vincken KL, Vanosch M, Bisschops RHC, Vandergrond J, van Osch MJP, Bisschops RHC, van der Grond J (2004): Automatic segmentation of different-sized white matter lesions by voxel probability estimation. Med Image Anal 8:205–215. http://www.ncbi.nlm.nih.gov/pubmed/15450216.

Andersen SK, Jakobsen CE, Pedersen CH, Rasmussen AM, Plocharski M, Østergaard LR (2015):

Classification of Alzheimer's Disease from MRI Using Sulcal Morphology. Image Anal 9127:103–113. http://link.springer.com/chapter/10.1007/978-3-319-19665-7_9.

Biomarkers and surrogate endpoints: Preferred definitions and conceptual framework (2001): . Clin Pharmacol Ther 69:89–95. http://doi.wiley.com/10.1067/mcp.2001.113989.

Apostolova LG, Green AE, Babakchanian S, Hwang KS, Chou Y-Y, Toga AW, Thompson PM (2012): Hippocampal atrophy and ventricular enlargement in normal aging, mild cognitive impairment (MCI), and Alzheimer Disease. Alzheimer Dis Assoc Disord 26:17–27. http://www.pubmedcentral.nih.gov/articlerender.fcgi?artid=3286134&tool=pmcentrez&rendertype=abstract.

Argyropoulou MI (2010): Brain lesions in preterm infants: initial diagnosis and follow-up. Pediatr Radiol 40:811–818. http://link.springer.com/content/pdf/10.1007/s00247-010-1585-y.pdf.

Arnfield E, Guzzetta A, Boyd R (2013): Relationship between brain structure on magnetic resonance imaging and motor outcomes in children with cerebral palsy: A systematic review. Res Dev Disabil 34:2234–2250. http://www.sciencedirect.com/science/article/pii/S0891422213001352.

Artaechevarria X, Munoz-Barrutia A, Ortiz-de-Solorzano C (2009): Combination strategies in multi-atlas image segmentation: application to brain MR data. IEEE Trans Med Imaging 28:1266–77. http://www.ncbi.nlm.nih.gov/pubmed/19228554.

Ashburner J, Friston KJ (2000): Voxel-Based Morphometry — The Methods. Neuroimage 821:805–821.

Ashburner J, Friston KJ (2005): Unified segmentation. Neuroimage 26:839–51. http://www.sciencedirect.com/science/article/pii/S1053811905001102.

Ashwal S, Russman BS, Blasco P a., Miller G, Sandler A, Shevell M, Stevenson R (2004): Practice Parameter: Diagnostic assessment of the child with cerebral palsy: Report of the Quality Standards Subcommittee of the American Academy of Neurology and the Practice Committee of the Child Neurology Society. Neurology 62:851–863. http://www.neurology.org/content/62/6/851.short.

Avants BB, Tustison NJ, Wu J, Cook PA, Gee JC (2011): An open source multivariate framework for n-tissue segmentation with evaluation on public data. Neuroinformatics 9:381–400. http://www.pubmedcentral.nih.gov/articlerender.fcgi?artid=3297199&tool=pmcentrez&rendertype=abstract.

Awate SP, Tasdizen T, Foster N, Whitaker RT (2006): Adaptive Markov modeling for mutual-information-based, unsupervised MRI brain-tissue classification. Med Image Anal 10:726–39.

http://www.sciencedirect.com/science/article/pii/S1361841506000569.

Babalola KO, Cootes TF, Twining CJ, Petrovic V, Taylor CJ (2008): 3D brain segmentation using active appearance models and local regressors. Med Image Comput Comput Assist Interv 11:401–8. http://www.ncbi.nlm.nih.gov/pubmed/18979772.

Bach Cuadra M, De Craene M, Duay V, Macq B, Pollo C, Thiran J-P (2006): Dense deformation field estimation for atlas-based segmentation of pathological MR brain images. Comput Methods Programs Biomed 84:66–75. http://www.sciencedirect.com/science/article/pii/S0169260706001775.

Balafar MA, Ramli AR, Saripan MI, Mashohor S (2010): Review of brain MRI image segmentation methods. Artif Intell Rev 33:261–274. http://link.springer.com/10.1007/s10462-010-9155-0.

Barkovich AJ, Kjos BO (1992a): Nonlissencephalic cortical dysplasias: correlation of imaging findings with clinical deficits. AJNR Am J Neuroradiol 13:95–103. http://www.ajnr.org/content/13/1/95.short.

Barkovich AJ, Kjos BO (1992b): Schizencephaly: correlation of clinical findings with MR characteristics. AJNR Am J Neuroradiol 13:85–94. http://www.ajnr.org/content/13/1/85.short.

Barkovich AJ, Guerrini R, Kuzniecky RI, Jackson GD, Dobyns WB (2012): A developmental and genetic classification for malformations of cortical development : update 2012. Brain 135:1348–1369.

Barra V, Frenoux E, Boire J (2002): Automatic volumetric measurement of lateral ventricles on magnetic resonance images with correction of partial volume effects. … Magn Reson Imaging 22:16–22. http://onlinelibrary.wiley.com/doi/10.1002/jmri.10032/full.

Bartlett DJ, Palisano RJ (2002): Physical Therapists' Perceptions of Factors Influencing the Acquisition of Motor Abilities of Children With Cerebral Palsy: Implications for Clinical Reasoning. Phys Ther 82:237–248. http://ptjournal.apta.org/content/82/3/237.short.

Baum LE, Petrie T (1966): Statistical Inference for Probabilistic Functions of Finite State Markov Chains. Ann Math Stat 37:1554–1563.

Bax M, Goldstein M, Rosenbaum P, Leviton A, Paneth N, Dan B, Jacobsson B, Damiano D (2005): Proposed definition and classification of cerebral palsy, April 2005. Dev Med Child Neurol 47:571–576. http://www.journals.cambridge.org/abstract_S001216220500112X.

Bax M, Tydeman C, Flodmark O (2006): Clinical and MRI correlates of cerebral palsy: the European Cerebral Palsy Study. JAMA 296:1602–8. http://www.ncbi.nlm.nih.gov/pubmed/17018805.

Beaino G, Khoshnood B, Kaminski M, Pierrat V, Marret S, Matis J, Ledésert B, Thiriez G, Fresson J, Rozé J-C, Zupan-Simunek V, Arnaud C, Burguet A, Larroque B, Bréart G, Ancel P-Y (2010): Predictors of cerebral palsy in very preterm infants: the EPIPAGE prospective population-based cohort study. Dev Med Child Neurol 52:e119-25. http://www.ncbi.nlm.nih.gov/pubmed/20163431.

Belsky J, Pluess M (2009): The Nature (and Nurture ?) of Plasticity in Early Human Development. Perspect Psychol Sci 4:345–351.

Bernal B, Altman N (2010): The connectivity of the superior longitudinal fasciculus: a tractography DTI study. Magn Reson Imaging 28:217–25. http://www.sciencedirect.com/science/article/pii/S0730725X09001672.

Bezdek JC (1993): Review of MR image segmentation techniques using pattern recognition. Med Phys 20:1033. http://europepmc.org/abstract/med/8413011.

Bezdek JC, Ehrlich R, Full W (1984): FCM : The fuzzy c-means clustering algorithm. Comput Geosci 10:191–203.

de Boer R, Vrooman HA, van der Lijn F, Vernooij MW, Ikram MA, van der Lugt A, Breteler MMB, Niessen WJ (2009): White matter lesion extension to automatic brain tissue segmentation on MRI. Neuroimage 45:1151–1161. http://www.sciencedirect.com/science/article/pii/S1053811909000561.

Bosanquet M, Copeland L, Ware R, Royd R (2013): A systematic review of tests to predict cerebral palsy in young children. Dev Med Child Neurol 55:418–426.

Boudraa AO, Dehak SM, Zhu YM, Pachai C, Bao YG, Grimaud J (2000): Automated segmentation of multiple sclerosis lesions in multispectral MR imaging using fuzzy clustering. Comput Biol Med 30:23–40. http://www.ncbi.nlm.nih.gov/pubmed/10695813.

Bourdon KH, Goodman R, Rae DS, Simpson G, Koretz DS (2005): The Strengths and Difficulties Questionnaire: U.S. normative data and psychometric properties. J Am Acad Child Adolesc Psychiatry 44:557–64. http://www.sciencedirect.com/science/article/pii/S0890856709616312.

Boyd RN, Mitchell LE, James ST, Ziviani J, Sakzewski L, Smith A, Rose S, Cunnington R, Whittingham K, Ware RS, Comans TA, Scuffham PA (2013a): Move it to improve it (Mitii): study protocol of a randomised controlled trial of a novel web-based multimodal training program for children and adolescents with cerebral palsy. BMJ Open 3:e002853.

Boyd RN, Ziviani J, Sakzewski L, Miller L, Bowden J, Cunnington R, Ware R, Guzzetta A, Al Macdonell R, Jackson GD, Abbott DF, Rose S (2013b): COMBIT: protocol of a randomised comparison trial of COMbined modified constraint induced movement therapy and bimanual

intensive training with distributed model of standard upper limb rehabilitation in children with congenital hemiplegia. BMC Neurol 13:68.

Bradley AP (1997): The use of the area under the ROC curve in the evaluation of machine learning algorithms. Pattern Recognit 30:1145–1159. http://www.sciencedirect.com/science/article/pii/S0031320396001422.

Brandt ME, Kharas YF (1993): Simulation studies of fuzzy clustering in the context of brain magnetic resonance imaging. In: pp 197–203. http://ieeexplore.ieee.org/ielx2/1092/7721/00324188.pdf?tp=&arnumber=324188&isnumber=7721.

Bricq S, Collet C, Armspach J-P (2008a): Markovian segmentation of 3D brain MRI to detect Multiple Sclerosis lesions. In: . 2008 15th IEEE International Conference on Image Processing. IEEE. pp 733–736. http://ieeexplore.ieee.org/lpdocs/epic03/wrapper.htm?arnumber=4711859.

Bricq S, Collet C, Armspach JP (2008b): Unifying framework for multimodal brain MRI segmentation based on Hidden Markov Chains. Med Image Anal 12:639–52. http://www.ncbi.nlm.nih.gov/pubmed/18440268.

Buchsbaum BR, Hickock G, Humphries C (2001): Role of left posterior superior temporal gyrus in phonological processing for speech perception and production. Cogn Sci 25:663–678.

Bush G, Luu P, Posner MI (2000): Cognitive and emotional influences in anterior cingulate cortex. Trends Cogn Sci 4:215–222. http://www.sciencedirect.com/science/article/pii/S1364661300014832.

Cárdenes R, Warfield SK, Macías EM, Santana JA, Ruiz-Alzola J (2003): An Efficient Algorithm for Multiple Sclerosis Lesion Segmentation from Brain MRI. Lect Notes Comput Sci 2809:542–551.

Cardoso MJ, Melbourne A, Kendall GS, Modat M, Hagmann CF, Robertson NJ, Marlow N, Ourselin S (2011): Adaptive Neonate Brain Segmentation. In: . Medical Image Computing and Computer-Assisted Intervention–MICCAI 2011. Springer Berlin Heidelberg. p pp 378-386.

Cardoso MJ, Clarkson MJ, Ridgway GR, Modat M, Fox NC, Ourselin S (2009): Improved Maximum a Posteriori Cortical Segmentation by Iterative Relaxation of Priors. In: . Medical Image Computing and Computer-Assisted Intervention–MICCAI 2009. Springer Berlin Heidelberg. pp 441–449.

Carmichael ST (2003): Plasticity of Cortical Projections after Stroke. Neurosci 9:64–75. http://nro.sagepub.com/content/9/1/64.short.

Caunce A, Taylor CJ (2001): Building 3D sulcal models using local geometry. Med Image Anal 5:69–80. http://www.ncbi.nlm.nih.gov/pubmed/11231178.

Chai J-W, Chen CC, Wu Y-Y, Chen H-C, Tsai Y-H, Chen H-M, Lan T-H, Ouyang Y-C, Lee S-K (2015): Robust volume assessment of brain tissues for 3-dimensional fourier transformation MRI via a novel multispectral technique. PLoS One 10:e0115527. http://journals.plos.org/plosone/article?id=10.1371/journal.pone.0115527.

Chang LJ, Yarkoni T, Khaw MW, Sanfey AG (2013): Decoding the role of the insula in human cognition: functional parcellation and large-scale reverse inference. Cereb Cortex 23:739–49. http://cercor.oxfordjournals.org/content/23/3/739.full.

Chapman SB, Max JE, Gamino JF, Mcglothlin JH, Cliff SN (2003): Discourse Plasticity in Children After Stroke : Age at Injury and Lesion Effects. Pediatr Neurol 29:34–41.

Chen ZJ, He Y, Rosa-Neto P, Germann J, Evans AC (2008): Revealing modular architecture of human brain structural networks by using cortical thickness from MRI. Cereb Cortex 18:2374–81. http://cercor.oxfordjournals.org/content/18/10/2374.short.

Cheng I, Miller SP, Duerden EG, Sun K, Chau V, Adams E, Poskitt KJ, Branson HM, Basu A (2015): Stochastic process for white matter injury detection in preterm neonates. NeuroImage Clin 7:622–30. http://www.sciencedirect.com/science/article/pii/S2213158215000339.

Cho SH, Kim DG, Kim DS, Kim YH, Lee CH, Jang SH (2007): Motor outcome according to the integrity of the corticospinal tract determined by diffusion tensor tractography in the early stage of corona radiata infarct. Neurosci Lett 426:123–7. http://www.sciencedirect.com/science/article/pii/S0304394007009317.

Chou H-F, Lin M-F, Chen C-Y, Shen E-Y (2012): Three-Dimensional Brain Images in Preterm Children With Periventricular Leukomalacia. Pediatr Neonatol 53:45–48. http://www.sciencedirect.com/science/article/pii/S1875957211001732.

Chou Y, Leporé N, Zubicaray GI De, Rose SE, Carmichael OT, Becker JT, Toga AW, Thompson PM, Imaging N, Angeles L (2007): Automated 3D mapping & shape analysis of the lateral ventricles via fluid registration of multiple surface-based atlases. Biomed Imaging From Nano to Macro, 2007 ISBI 2007 4th IEEE Int Symp:1288–1291.

Chung MK, Worsley KJ, Robbins S, Paus TT, Taylor J, Giedd JN, Rapoport JL, Evans AC (2003): Deformation-based surface morphometry applied to gray matter deformation. Neuroimage 18:198–213. http://www.ncbi.nlm.nih.gov/pubmed/12595176.

Ciofolo C, Barillot C (2009): Atlas-based segmentation of 3D cerebral structures with competitive level sets and fuzzy control. Med Image Anal 13:456–70.

http://www.sciencedirect.com/science/article/pii/S1361841509000073.

Cioni G (2000): Correlation between visual function, neurodevelopmental outcome, and magnetic resonance imaging findings in infants with periventricular leucomalacia. Arch Dis Child - Fetal Neonatal Ed 82:134F–140. http://fn.bmj.com/content/82/2/F134.full.

Cioni G, Sales B, Paolicelli P, Petacchi E, Scusa M, Canapicchi R (1999): MRI and Clinical Characteristics of Children with Hemiplegic Cerebral Palsy. Neuropediatrics 30:249–255. http://europepmc.org/abstract/med/10598836.

Cioni G, D'Acunto G, Guzzetta A (2011): Perinatal brain damage in children: neuroplasticity, early intervention, and molecular mechanisms of recovery. Prog Brain Res 189:139–54. http://www.sciencedirect.com/science/article/pii/B9780444538840000221.

Cioni G, Di Paoo MC, Bertuccelli B, Paolicelli PB, Canapicchi R (1997): MRI findings and sensorimotor development in infants with bilateral spastic cerebral palsy. Brain Dev 19:245–253. http://www.sciencedirect.com/science/article/pii/S038776049700569X.

Cocosco CA, Zijdenbos AP, Evans AC (2003): A fully automatic and robust brain MRI tissue classification method. Med Image Anal 7:513–527. http://www.sciencedirect.com/science/article/pii/S1361841503000379.

Cohen J (1988): Statistical power analysis for the behavioral sciences 2nd ed. Hillsdale, NJ: Lawrence Erlbaum Associates.

Collin G, Sporns O, Mandl RCW, van den Heuvel MP (2014): Structural and functional aspects relating to cost and benefit of rich club organization in the human cerebral cortex. Cereb Cortex 24:2258–67. http://cercor.oxfordjournals.org/content/24/9/2258.abstract.

Combès B, Prima S (2010): An efficient EM-ICP algorithm for symmetric consistent non-linear registration of point sets. Med Image Comput Comput Assist Interv 13:594–601. http://www.pubmedcentral.nih.gov/articlerender.fcgi?artid=3077756&tool=pmcentrez&rendertype=abstract.

Cootes TF, Edwards GJ, Taylor CJ (2001): Active Appearance Models. IEEE Trans Pattern Anal Mach Intell 23:681–685.

Cortes C, Vapnik V (1995): Support-Vector Networks. Mach Learn 20:273–297.

Counsell SJ, Rutherford MA, Cowan FM, Edwards AD (2003): Magnetic resonance imaging of preterm brain injury. Arch Dis Child - Fetal Neonatal Ed 88:F269–F274. http://fn.bmj.com/content/88/4/F269.short.

Dale AM, Fischl B, Sereno MI (1999): Cortical surface-based analysis. I. Segmentation and surface

reconstruction. Neuroimage 9:179–94. http://www.sciencedirect.com/science/article/pii/S1053811998903950.

Danti S, Toschi N, Diciotti S, Tessa C, Poletti M, Del Dotto P, Lucetti C (2015): Cortical thickness in de novo patients with Parkinson disease and mild cognitive impairment with consideration of clinical phenotype and motor laterality. Eur J Neurol 22:1564–1572. http://www.ncbi.nlm.nih.gov/pubmed/26212370.

Das SR, Avants BB, Grossman M, Gee JC (2009): Registration based cortical thickness measurement. Neuroimage 45:867–79. http://www.sciencedirect.com/science/article/pii/S1053811908012780.

Dempster AP, Laird NM, Rubin DB (1977): Maximum likelihood from incomplete data via the EM algorithm. J R Stat Soc Ser B 39:1–38. http://citeseer.ist.psu.edu/viewdoc/summary?doi=10.1.1.133.4884.

Dice LR (1945): Measures of the Amount of Ecologic Association Between Species. Ecology, Vol. 26, No. 3. http://www.jstor.org/stable/1932409.

Dickerson BC, Feczko E, Augustinack JC, Pacheco J, Morris JC, Fischl B, Buckner RL (2009): Differential effects of aging and Alzheimer's disease on medial temporal lobe cortical thickness and surface area. Neurobiol Aging 30:432–40. http://www.pubmedcentral.nih.gov/articlerender.fcgi?artid=3703585&tool=pmcentrez&rendertype=abstract.

Dierker DL, Feczko E, Pruett JR, Petersen SE, Schlaggar BL, Constantino JN, Harwell JW, Coalson TS, Van Essen DC (2015): Analysis of Cortical Shape in Children with Simplex Autism. Cereb Cortex 25:1042–51. http://cercor.oxfordjournals.org/content/early/2013/10/27/cercor.bht294.abstract.

Djamanakova A, Faria A V, Hsu J, Ceritoglu C, Oishi K, Miller MI, Hillis AE, Mori S (2013): Diffeomorphic brain mapping based on T1-weighted images: improvement of registration accuracy by multichannel mapping. J Magn Reson Imaging 37:76–84. http://www.pubmedcentral.nih.gov/articlerender.fcgi?artid=3525783&tool=pmcentrez&rendertype=abstract.

Doya K (2000): Complementary roles of basal ganglia and cerebellum in learning and motor control. Curr Opin Neurobiol 10:732–739. http://www.sciencedirect.com/science/article/pii/S0959438800001537.

Dubois J, Benders M, Borradori-Tolsa C, Cachia A, Lazeyras F, Leuchter RH-V, Sizonenko S V., Warfield SK, Mangin JF, Hüppi PS (2008a): Primary cortical folding in the human newborn: an

early marker of later functional development. Brain 131:2028–2041. http://brain.oxfordjournals.org/content/131/8/2028.

Dubois J, Benders M, Cachia A, Lazeyras F, Leuchter RH-V, Sizonenko S V., Borradori-Tolsa C, Mangin JF, Hüppi PS (2008b): Mapping the Early Cortical Folding Process in the Preterm Newborn Brain. Cereb Cortex 18:1444–1454. http://cercor.oxfordjournals.org/content/18/6/1444.

Duda RO, Hart PE (1973): Pattern classification and scene analysis. Vol. 3. Wiley New York.

Dugas-Phocion G, Gonzalez MA, Lebrun C, Chanalet S, Bensa C, Malandain G, Ayache N (2004): Hierarchical segmentation of multiple sclerosis lesions in multi-sequence MRI. In: . 2004 2nd IEEE International Symposium on Biomedical Imaging: Macro to Nano (IEEE Cat No. 04EX821). IEEE. Vol. 2, pp 157–160. http://ieeexplore.ieee.org/lpdocs/epic03/wrapper.htm?arnumber=1398498.

Edgin JO, Inder TE, Anderson PJ, Hood KM, Clark CAC, Woodward LJ (2008): Executive functioning in preschool children born very preterm: relationship with early white matter pathology. J Int Neuropsychol Soc 14:90–101. http://journals.cambridge.org/abstract_S1355617708080053.

Eichenbaum H, Yonelinas AP, Ranganath C (2007): The medial temporal lobe and recognition memory. Annu Rev Neurosci 30:123–52. http://www.pubmedcentral.nih.gov/articlerender.fcgi?artid=2064941&tool=pmcentrez&rendertype=abstract.

Eskandar EN, Richmond BJ, Optican LM (1992): Role of inferior temporal neurons in visual memory. I. Temporal encoding of information about visual images, recalled images, and behavioral context. J Neurophysiol 68:1277–1295. http://www.ncbi.nlm.nih.gov/pubmed/1432084.

van Essen DC, Dierker D, Snyder AZ, Raichle ME, Reiss AL, Korenberg J (2006): Symmetry of Cortical Folding Abnormalities in Williams Syndrome Revealed by Surface-Based Analyses. J Neurosci 26:5470–5483. http://www.jneurosci.org/content/26/20/5470.

van Essen DC (2005): A Population-Average, Landmark- and Surface-based (PALS) atlas of human cerebral cortex. Neuroimage 28:635–62. http://www.ncbi.nlm.nih.gov/pubmed/16172003.

Faria A V., Hoon A, Stashinko E, Li X, Jiang H, Mashayekh A, Akhter K, Hsu J, Oishi K, Zhang J, Miller MI, van Zijl PCM, Mori S (2011): Quantitative analysis of brain pathology based on MRI and brain atlases—Applications for cerebral palsy. Neuroimage 54:1854–1861.

http://www.sciencedirect.com/science/article/pii/S1053811910012632.

Faria A V., Zhang J, Oishi K, Li X, Jiang H, Akhter K, Hermoye L, Lee S-K, Hoon A, Stachinko E, Miller MI, van Zijl PCM, Mori S (2010): Atlas-Based Analysis of Neurodevelopment from Infancy to Adulthood Using Diffusion Tensor Imaging and Applications for Automated Abnormality Detection. Neuroimage 52:415–428. http://www.ncbi.nlm.nih.gov/pmc/articles/PMC2886186/.

Fazio P, Cantagallo A, Craighero L, D'Ausilio A, Roy AC, Pozzo T, Calzolari F, Granieri E, Fadiga L (2009): Encoding of human action in Broca's area. Brain 132:1980–8. http://brain.oxfordjournals.org/content/early/2009/05/14/brain.awp118.full.

Feldman DE (2009): Synaptic mechanisms for plasticity in neocortex. Annu Rev Neurosci 32:33–55. http://www.pubmedcentral.nih.gov/articlerender.fcgi?artid=3071739&tool=pmcentrez&rendertype=abstract.

Ferrarini L, Palm WM, Olofsen H, van Buchem MA, Reiber JHC, Admiraal-Behloul F (2006): Shape differences of the brain ventricles in Alzheimer's disease. Neuroimage 32:1060–1069. http://www.sciencedirect.com/science/article/pii/S1053811906006331.

Ferrarini L, Palm WM, Olofsen H, van der Landen R, van Buchem MA, Reiber JHC, Admiraal-Behloul F (2008a): Ventricular shape biomarkers for Alzheimer's disease in clinical MR images. Magn Reson Med 59:260–267. http://onlinelibrary.wiley.com/doi/10.1002/mrm.21471/abstract.

Ferrarini L, Palm WM, Olofsen H, van der Landen R, Jan Blauw G, Westendorp RGJ, Bollen ELEM, Middelkoop H a M, Reiber JHC, van Buchem M a, Admiraal-Behloul F (2008b): MMSE scores correlate with local ventricular enlargement in the spectrum from cognitively normal to Alzheimer disease. Neuroimage 39:1832–8. http://www.ncbi.nlm.nih.gov/pubmed/18160312.

Feys H, Eyssen M, Jaspers E, Klingels K, Desloovere K, Molenaers G, De Cock P (2010): Relation between neuroradiological findings and upper limb function in hemiplegic cerebral palsy. Eur J Paediatr Neurol 14:169–77.

Fiori S, Cioni G, Klingels K, Ortibus E, Van Gestel L, Rose S, Boyd RN, Feys H, Guzzetta A (2014): Reliability of a novel, semi-quantitative scale for classification of structural brain magnetic resonance imaging in children with cerebral palsy. Dev Med Child Neurol 56:839–845.

Fiori S, Guzzetta A, Pannek K, Ware RS, Rossi G, Klingels K, Feys H, Coulthard A, Cioni G, Rose S, Boyd RN (2015): Validity of semi-quantitative scale for brain MRI in unilateral cerebral

palsy due to periventricular white matter lesions: Relationship with hand sensorimotor function and structural connectivity. NeuroImage Clin 8:104–109. http://www.sciencedirect.com/science/article/pii/S2213158215000728.

Fischl B, Dale AM (2000): Measuring the thickness of the human cerebral cortex from magnetic resonance images. Proc Natl Acad Sci U S A 97:11050–5. http://www.pnas.org/content/97/20/11050.abstract.

Fischl B, Sereno MI, Dale AM (1999): Cortical surface-based analysis. II: Inflation, flattening, and a surface-based coordinate system. Neuroimage 9:195–207. http://www.sciencedirect.com/science/article/pii/S1053811998903962.

Fischl B (2012): FreeSurfer. Neuroimage 62:774–81. http://www.sciencedirect.com/science/article/pii/S1053811912000389.

Fischl B, Salat DH, Busa E, Albert M, Dieterich M, Haselgrove C, van der Kouwe A, Killiany R, Kennedy D, Klaveness S, Montillo A, Makris N, Rosen B, Dale AM (2002): Whole brain segmentation: automated labeling of neuroanatomical structures in the human brain. Neuron 33:341–55. http://www.ncbi.nlm.nih.gov/pubmed/11832223.

Frostig M, Lefever DW, Whittlesey JRB (1961): A developmental test of visual perception for evaluating normal and neurologically handicapped children. Percept Mot Skills 12:383–394. http://www.amsciepub.com/doi/abs/10.2466/pms.1961.12.3.383.

Gabriel T, Tong Z, Gene G (1996): Optimal surface smoothing as filter design. Ed. Bernard Buxton, Roberto Cipolla Computer V. Berlin, Heidelberg: Springer Berlin Heidelberg. Vol. 1064. Lecture Notes in Computer Science. http://link.springer.com/10.1007/BFb0015518.

Gado M, Hughes CP, Danziger W, Chi D (1983): Aging, dementia, and brain atrophy: a longitudinal computed tomographic study. AJNR Am J Neuroradiol 4:699–702. http://www.ajnr.org/content/4/3/699.short.

García-Lorenzo D, Francis S, Narayanan S, Arnold DL, Collins DL (2013): Review of automatic segmentation methods of multiple sclerosis white matter lesions on conventional magnetic resonance imaging. Med Image Anal 17:1–18. http://www.sciencedirect.com/science/article/pii/S1361841512001338.

García-Lorenzo D, Lecoeur J, Arnold DL, Collins DL, Barillot C, Garc D (2009): Multiple Sclerosis Lesion Segmentation Using an Automatic Multimodal Graph Cuts. In: Yang, G-Z, Hawkes, D, Rueckert, D, Noble, A, Taylor, C, editors. Springer Berlin Heidelberg. Lecture Notes in Computer Science pp 584–591. http://link.springer.com/chapter/10.1007/978-3-642-04271-3_71.

García-Lorenzo D, Prima S, Arnold DL, Collins DL, Barillot C (2011): Trimmed-likelihood estimation for focal lesions and tissue segmentation in multisequence MRI for multiple sclerosis. IEEE Trans Med Imaging 30:1455–67. http://www.pubmedcentral.nih.gov/articlerender.fcgi?artid=3326634&tool=pmcentrez&rendertype=abstract.

Geman S, Geman D (1984): Stochastic Relaxation, Gibbs Distributions, and the Bayesian Restoration of Images. IEEE Trans Pattern Anal Mach Intell PAMI-6:721–741. http://ieeexplore.ieee.org/lpdocs/epic03/wrapper.htm?arnumber=4767596.

Gerig G, Styner M, Jones D, Weinberger D, Lieberman J (2001): Shape analysis of brain ventricles using SPHARM. … Image Anal …:171–178. http://ieeexplore.ieee.org/xpls/abs_all.jsp?arnumber=991731.

Giménez M, Junqué C, Narberhaus A, Bargalló N, Botet F, Mercader JM (2006): White matter volume and concentration reductions in adolescents with history of very preterm birth: A voxel-based morphometry study. Neuroimage 32:1485–1498.

Gioia GA, Isquith PK, Retzlaff PD, Espy KA (2002): Confirmatory factor analysis of the Behavior Rating Inventory of Executive Function (BRIEF) in a clinical sample. Child Neuropsychol 8:249–57. http://www.tandfonline.com/doi/abs/10.1076/chin.8.4.249.13513.

Giroud M, Lemesle M, Madinier G, Billiar T, Dumas R (1997): Unilateral lenticular infarcts: radiological and clinical syndromes, aetiology, and prognosis. J Neurol Neurosurg Psychiatry 63:611–615. http://jnnp.bmj.com/content/63/5/611.short.

Giuliani NR, Drabant EM, Bhatnagar R, Gross JJ (2011): Emotion regulation and brain plasticity: expressive suppression use predicts anterior insula volume. Neuroimage 58:10–5. http://www.pubmedcentral.nih.gov/articlerender.fcgi?artid=3161031&tool=pmcentrez&rendertype=abstract.

Glenn OA (2009): MR imaging of the fetal brain. Pediatr Radiol 40:68–81. http://link.springer.com/content/pdf/10.1007/s00247-009-1459-3.pdf.

Goebel R (2012): BrainVoyager--past, present, future. Neuroimage 62:748–56. http://www.sciencedirect.com/science/article/pii/S1053811912001000.

Gogtay N, Giedd JN, Lusk L, Hayashi KM, Greenstein D, Vaituzis AC, Nugent TF, Herman DH, Clasen LS, Toga AW, Rapoport JL, Thompson PM (2004): Dynamic mapping of human cortical development during childhood through early adulthood. Proc Natl Acad Sci U S A 101:8174–9. http://www.pnas.org/content/101/21/8174.abstract.

Goldberg G (2010): Supplementary motor area structure and function: Review and hypotheses.

Behav Brain Sci 8:567. http://journals.cambridge.org/abstract_S0140525X00045167.

Goldman AL, Pezawas L, Mattay VS, Fischl B, Verchinski BA, Chen Q, Weinberger DR, Meyer-Lindenberg A (2009): Widespread reductions of cortical thickness in schizophrenia and spectrum disorders and evidence of heritability. Arch Gen Psychiatry 66:467–77. http://archpsyc.jamanetwork.com/article.aspx?articleid=483072#ref-yoa80119-4.

Gorno-Tempini ML, Price CJ, Josephs O, Vandenberghe R, Cappa SF, Kapur N, Trackowiak RS (1998): The neural systems sustaining face and proper-name processing. Brain 121:2103–2118. http://brain.oxfordjournals.org/content/121/11/2103.

Gower JC (1975): Generalized procrustes analysis. Psychometrika 40:33–51. http://link.springer.com/10.1007/BF02291478.

Graham J, Babalola KO, Honer WG, Lang D, Kopala L, Vandorpe R (2006): Lateral asymmetry in the shape of brain ventricles in control and schizophrenia groups. Biomed Imaging Nano to Macro, 2006 3rd IEEE Int Symp:414–417.

Grahn JA, Parkinson JA, Owen AM (2008): The cognitive functions of the caudate nucleus. Prog Neurobiol 86:141–55. http://www.sciencedirect.com/science/article/pii/S0301008208001019.

Grant PE, Barkovich AJ (1997): Neuroimaging in CP: Issues in pathogenesis and diagnosis. Ment Retard Dev Disabil Res Rev 3:118–128. http://onlinelibrary.wiley.com/doi/10.1002/(SICI)1098-2779(1997)3:2%3C118::AID-MRDD3%3E3.0.CO;2-N/abstract.

Greenspan H, Ruf A, Goldberger J (2006): Constrained Gaussian mixture model framework for automatic segmentation of MR brain images. IEEE Trans Med Imaging 25:1233–1245. http://ieeexplore.ieee.org/lpdocs/epic03/wrapper.htm?arnumber=1677729.

Guerrini R, Dobyns WB (2014): Malformations of cortical development: clinical features and genetic causes. Lancet Neurol 13:710–26. http://www.sciencedirect.com/science/article/pii/S1474442214700407.

Guizard N, Coupé P, Fonov VS, Manjón J V, Arnold DL, Collins DL (2015): Rotation-invariant multi-contrast non-local means for MS lesion segmentation. NeuroImage Clin 8:376–89. http://www.sciencedirect.com/science/article/pii/S2213158215000935.

Habas PA, Kim K, Rousseau F, Glenn OA, Barkovich AJ, Studholme C (2010): Atlas-based segmentation of developing tissues in the human brain with quantitative validation in young fetuses. Hum Brain Mapp 31:1348–58. http://www.pubmedcentral.nih.gov/articlerender.fcgi?artid=3306251&tool=pmcentrez&rendertype=abstract.

Haber SN, Calzavara R (2009): The cortico-basal ganglia integrative network: the role of the

thalamus. Brain Res Bull 78:69–74. http://www.sciencedirect.com/science/article/pii/S0361923008003420.

Haidar H, Soul JS (2006): Measurement of Cortical Thickness in 3D Brain MRI Data: Validation of the Laplacian Method. J Neuroimaging 16:146–153. http://onlinelibrary.wiley.com/doi/10.1111/j.1552-6569.2006.00036.x/abstract.

Han X, Jovicich J, Salat D, van der Kouwe A, Quinn B, Czanner S, Busa E, Pacheco J, Albert M, Killiany R, Maguire P, Rosas D, Makris N, Dale A, Dickerson B, Fischl B (2006): Reliability of MRI-derived measurements of human cerebral cortical thickness: the effects of field strength, scanner upgrade and manufacturer. Neuroimage 32:180–94. http://www.ncbi.nlm.nih.gov/pubmed/16651008.

Han X, Pham DL, Tosun D, Rettmann ME, Xu C, Prince JL (2004): CRUISE: cortical reconstruction using implicit surface evolution. Neuroimage 23:997–1012. http://www.ncbi.nlm.nih.gov/pubmed/15528100.

Hannan AJ, Servotte S, Katsnelson A, Sisodiya S, Blakemore C, Squier M, Molnár Z (1999): Characterization of nodular neuronal heterotopia in children. Brain:219–38. http://www.ncbi.nlm.nih.gov/pubmed/10071051.

Hatfield T, Wing DA, Buss C, Head K, Muftuler LT, Davis EP (2011): Magnetic resonance imaging demonstrates long-term changes in brain structure in children born preterm and exposed to chorioamnionitis. Am J Obstet Gynecol 205:384.e1-384.e8. http://www.ncbi.nlm.nih.gov/pmc/articles/PMC3188953/.

He R, Narayana P a (2002): Global optimization of mutual information: application to three-dimensional retrospective registration of magnetic resonance images. Comput Med Imaging Graph 26:277–92. http://www.ncbi.nlm.nih.gov/pubmed/12074923.

He Y, Chen ZJ, Evans AC (2007): Small-world anatomical networks in the human brain revealed by cortical thickness from MRI. Cereb Cortex 17:2407–19. http://cercor.oxfordjournals.org/content/17/10/2407.abstract.

Heckemann RA, Hajnal J V., Aljabar P, Rueckert D, Hammers A (2006): Automatic anatomical brain MRI segmentation combining label propagation and decision fusion. Neuroimage 33:115–26. http://www.ncbi.nlm.nih.gov/pubmed/16860573.

Heeger DJ, Ress D (2002): What does fMRI tell us about neuronal activity? Nat Rev Neurosci 3:142–51. http://www.ncbi.nlm.nih.gov/pubmed/11836522.

Heimann T, Meinzer H-P (2009): Statistical shape models for 3D medical image segmentation: A review. Med Image Anal 13:543–563.

http://www.sciencedirect.com/science/article/pii/S1361841509000425.

Henry LA, Millar S (1991): Memory span increase with age: A test of two hypotheses. J Exp Child Psychol 51:459–484. http://www.sciencedirect.com/science/article/pii/002209659190088A.

Henry RG, Berman JI, Nagarajan SS, Mukherjee P, Berger MS (2004): Subcortical pathways serving cortical language sites: initial experience with diffusion tensor imaging fiber tracking combined with intraoperative language mapping. Neuroimage 21:616–22. http://www.sciencedirect.com/science/article/pii/S1053811903005974.

Herrero M-T, Barcia C, Navarro JM (2002): Functional anatomy of thalamus and basal ganglia. Childs Nerv Syst 18:386–404. http://www.ncbi.nlm.nih.gov/pubmed/12192499.

Herskovits EH, Itoh R, Melhem ER (2001): Accuracy for Detection of Simulated Lesions : Comparison of Fluid-Attenuated Inversion-Recovery, Proton Density-Weighted, and T2-Weighted Synthetic Brain MR Imaging. Neuroradiology 176:1313–1318.

Hetts SW, Sherr EH, Chao S, Gobuty S, Barkovich AJ (2006): Anomalies of the corpus callosum: an MR analysis of the phenotypic spectrum of associated malformations. AJR Am J Roentgenol 187:1343–8. http://www.ajronline.org/doi/abs/10.2214/AJR.05.0146.

Hikosaka O, Sakamoto M, Usui S (1989): Functional properties of monkey caudate neurons. I. Activities related to saccadic eye movements. J Neurophysiol 61:780–98. http://jn.physiology.org/content/61/4/780.abstract.

Hill J, Inder T, Neil J, Dierker D, Harwell J, Van Essen D (2010): Similar patterns of cortical expansion during human development and evolution. Proc Natl Acad Sci U S A 107:13135–40. http://www.pnas.org/content/107/29/13135.short.

Himmelmann K, Uvebrant P (2011): Function and neuroimaging in cerebral palsy: a population-based study. Dev Med Child Neurol 53:516–521.

Hoerl AE, Kennard RW (1970): Ridge Regression: Biased Estimation for Nonorthogonal Problems. Technometrics 12:55–67. http://www.tandfonline.com/doi/abs/10.1080/00401706.1970.10488634.

Holmström L, Vollmer B, Tedroff K, Islam M, Persson JKE, Kits A, Forssberg H, Eliasson A-C (2010): Hand function in relation to brain lesions and corticomotor-projection pattern in children with unilateral cerebral palsy. Dev Med Child Neurol 52:145–52. http://www.ncbi.nlm.nih.gov/pubmed/19807768.

Hong Y, Gao Y, Niethammer M, Bouix S (2015): Shape analysis based on depth-ordering. Med Image Anal 25:2–10. http://www.medicalimageanalysisjournal.com/article/S1361841515000547/fulltext.

Hoon AH, Vasconcellos Faria A (2010): Pathogenesis, neuroimaging and management in children with cerebral palsy born preterm. Dev Disabil Res Rev 16:302–312.

Hoon Jr AH, Stashinko EE, Nagae LM, Lin DDM, Keller J, Bastian A, Campbell ML, Levey E, Mori S, Johnston M V, Hoon AH, Stashinko EE, Nagae LM, Lin DDM, Keller J, Bastian A, Campbell ML, Levey E, Mori S, Johnston M V (2009): Sensory and motor deficits in children with cerebral palsy born preterm correlate with diffusion tensor imaging abnormalities in thalamocortical pathways. Dev Med Child Neurol 51:697–704. http://www.pubmedcentral.nih.gov/articlerender.fcgi?artid=2908264&tool=pmcentrez&rendertype=abstract.

Horga G, Bernacer J, Dusi N, Entis J, Chu K, Hazlett EA, Haznedar MM, Kemether E, Byne W, Buchsbaum MS (2011): Correlations between ventricular enlargement and gray and white matter volumes of cortex, thalamus, striatum, and internal capsule in schizophrenia. Eur Arch Psychiatry Clin Neurosci 261:467–76. http://link.springer.com/article/10.1007/s00406-011-0202-x/fulltext.html.

Hufnagel H, Pennec X, Ehrhardt J, Ayache N, Handels H (2009): Computation of a probabilistic statistical shape model in a maximum-a-posteriori framework. Methods Inf Med 48:314–9. http://www.ncbi.nlm.nih.gov/pubmed/19562228.

Hüppi PS, Warfield S, Kikinis R, Barnes PD, Zientara GP, Jolesz FA, Tsuji MK, Volpe JJ (1998): Quantitative magnetic resonance imaging of brain development in premature and mature newborns. Ann Neurol 43:224–235. http://onlinelibrary.wiley.com/doi/10.1002/ana.410430213/abstract.

Hutton C, Vita E De, Ashburner J, Deichmann R, Turner R (2008): Voxel-based cortical thickness measurements in MRI. Neuroimage 40:1701–1710.

Im K, Lee JM, Lyttelton O, Kim SH, Evans AC, Kim SI (2008): Brain size and cortical structure in the adult human brain. Cereb Cortex 18:2181–91. http://cercor.oxfordjournals.org/content/18/9/2181.abstract.

Im K, Lee JM, Yoon U, Shin YW, Hong SB, Kim IY, Kwon JS, Kim SI (2006): Fractal dimension in human cortical surface: multiple regression analysis with cortical thickness, sulcal depth, and folding area. Hum Brain Mapp 27:994–1003. http://www.ncbi.nlm.nih.gov/pubmed/16671080.

Inder TE, Huppi PS, Warfield S, Kikinis R, Zientara GP, Barnes PD, Jolesz F, Volpe JJ (1999): Periventricular white matter injury in the premature infant is followed by reduced cerebral cortical gray matter volume at term. Ann Neurol 46:755–760. http://mw6fc7xe6k.scholar.serialssolutions.com/?sid=google&auinit=TE&aulast=Inder&atitle=Periventricular+white+matter+injury+in+the+premature+infant+is+followed+by+reduced+cere

bral+cortical+gray+matter+volume+at+term&id=doi:10.1002/1531-8249(199911)46:5%3C7.

Inder TE, Wells SJ, Mogridge NB, Spencer C, Volpe JJ (2003): Defining the nature of the cerebral abnormalities in the premature infant: a qualitative magnetic resonance imaging study. J Pediatr 143:171–9. http://www.sciencedirect.com/science/article/pii/S0022347603003573.

Iscan Z, Jin TB, Kendrick A, Szeglin B, Lu H, Trivedi M, Fava M, McGrath PJ, Weissman M, Kurian BT, Adams P, Weyandt S, Toups M, Carmody T, McInnis M, Cusin C, Cooper C, Oquendo MA, Parsey R V., DeLorenzo C (2015): Test-retest reliability of freesurfer measurements within and between sites: Effects of visual approval process. Hum Brain Mapp 36:3472–3485. http://doi.wiley.com/10.1002/hbm.22856.

Jain S, Sima DM, Ribbens A, Cambron M, Maertens A, Van Hecke W, De Mey J, Barkhof F, Steenwijk MD, Daams M, Maes F, Van Huffel S, Vrenken H, Smeets D (2015): Automatic segmentation and volumetry of multiple sclerosis brain lesions from MR images. NeuroImage Clin 8:367–375. http://www.sciencedirect.com/science/article/pii/S2213158215000959.

Jäncke L, Peters M, Himmelbach M, Nösselt T, Shah J, Steinmetz H (2000): fMRI study of bimanual coordination. Neuropsychologia 38:164–174. http://www.sciencedirect.com/science/article/pii/S0028393299000627.

Jarvis S, Glinianaia S V, Arnaud C, Fauconnier J, Johnson A, McManus V, Topp M, Uvebrant P, Cans C, Krägeloh-Mann I (2005): Case gender and severity in cerebral palsy varies with intrauterine growth. Arch Dis Child 90:474–9. http://adc.bmj.com/content/90/5/474.abstract.

Joliffe I (University of A (2005): Encyclopedia of Statistics in Behavioral Science. In: . Encyclopedia of Statistics in Behavioral Science. John Wiley & Sons, Ltd.

Jones DK, Knösche TR, Turner R (2013): White matter integrity, fiber count, and other fallacies: The do’s and don’ts of diffusion MRI. Neuroimage 73:239–254.

Jones SE, Buchbinder BR, Aharon I (2000): Three-dimensional mapping of cortical thickness using Laplace’s Equation. Hum Brain Mapp 11:12–32. http://onlinelibrary.wiley.com/doi/10.1002/1097-0193(200009)11:1%3C12::AID-HBM20%3E3.0.CO;2-K/abstract.

Joshi M, Cui J, Doolittle K, Joshi S, Van Essen D, Wang L, Miller MI (1999a): Brain segmentation and the generation of cortical surfaces. Neuroimage 9:461–76.

Joshi M, Cui J, Doolittle K, Joshi S, Van Essen D, Wang L, Miller MI (1999b): Brain segmentation and the generation of cortical surfaces. Neuroimage 9:461–76. http://www.ncbi.nlm.nih.gov/pubmed/10329286.

Joshi SC, Miller MI, Grenander U (1997): On the Geometry and Shape of Brain Sub-Manifolds. Int

J Pattern Recognit Artif Intell 11:1317–1343. http://www.worldscientific.com/doi/abs/10.1142/S0218001497000615.

Jouvent E, Mangin J-F, Porcher R, Viswanathan A, O'Sullivan M, Guichard J-P, Dichgans M, Bousser M-G, Chabriat H (2008): Cortical changes in cerebral small vessel diseases: a 3D MRI study of cortical morphology in CADASIL. Brain 131:2201–8. http://brain.oxfordjournals.org/content/131/8/2201.abstract.

Karimaghaloo Z, Shah M, Francis SJ, Arnold DL, Collins DL, Arbel T (2012): Automatic Detection of Gadolinium-Enhancing Multiple Sclerosis Lesions in Brain MRI Using Conditional Random Fields. IEEE Trans Med Imaging 31:1181–1194.

Kass M, Witkin A, Terzopoulos D, Palo S, Alto P (1988): Snakes: Active contour models. Int J Comput Vis 1:321–331. http://link.springer.com/10.1007/BF00133570.

Kelemen A, Szekely G, Gerig G (1998): Three-dimensional model-based segmentation of brain MRI. Proceedings Work Biomed Image Anal (Cat No98EX162):4–13. http://ieeexplore.ieee.org/lpdocs/epic03/wrapper.htm?arnumber=692374.

Kelly CE, Chan L, Burnett AC, Lee KJ, Connelly A, Anderson PJ, Doyle LW, Cheong JLY, Thompson DK (2015): Brain structural and microstructural alterations associated with cerebral palsy and motor impairments in adolescents born extremely preterm and/or extremely low birthweight. Dev Med Child Neurol 57:1168–1175. http://www.ncbi.nlm.nih.gov/pubmed/26195287.

Kempton MJ, Stahl D, Williams SCR, DeLisi LE (2010): Progressive lateral ventricular enlargement in schizophrenia: a meta-analysis of longitudinal MRI studies. Schizophr Res 120:54–62. http://www.sciencedirect.com/science/article/pii/S0920996410012077.

Kertzman C, Schwarz U, Zeffiro TA, Hallett M (1997): The role of posterior parietal cortex in visually guided reaching movements in humans. Exp Brain Res 114:170–183. http://link.springer.com/10.1007/PL00005617.

Kidokoro H, Neil JJ, Inder TE (2013): New MR imaging assessment tool to define brain abnormalities in very preterm infants at term. AJNR Am J Neuroradiol 34:2208–14. http://www.ajnr.org/content/34/11/2208.short.

Kilminster MGE, Laird EM (2014): Articulation Development in Children Aged Three to Nine Years. Aust J Hum Commun Disord 6:23–30. http://www.tandfonline.com/doi/abs/10.3109/asl2.1978.6.issue-1.04.

Kindermann R, Snell JL (1980): Markov random fields and their applications. American Mathematical Society Providence, RI.

Kinnunen KM, Greenwood R, Powell JH, Leech R, Hawkins PC, Bonnelle V, Patel MC, Counsell SJ, Sharp DJ (2011): White matter damage and cognitive impairment after traumatic brain injury. Brain 134:449–63. http://brain.oxfordjournals.org/content/early/2010/12/29/brain.awq347.long#ref-56.

Klein A, Hirsch J (2005): Mindboggle: a scatterbrained approach to automate brain labeling. Neuroimage 24:261–80. http://www.sciencedirect.com/science/article/pii/S1053811904005415.

Klein D, Mok K, Chen J-K, Watkins KE (2014): Age of language learning shapes brain structure: A cortical thickness study of bilingual and monolingual individuals. Brain Lang 131:20–24.

Knapp M (2002): Mesh decimation using VTK. Institute of Computer Graphics and Algorithms, Vienna University of Technology. https://www.cg.tuwien.ac.at/courses/Seminar/SS2002/Knapp_paper.pdf.

Kohonen T (1990): The self-organizing map. Proc IEEE 78:1464–1480. http://ieeexplore.ieee.org/lpdocs/epic03/wrapper.htm?arnumber=58325.

Kolb B, Gibb R (2007): Brain plasticity and recovery from early cortical injury. Dev Psychobiol 49:107–18. http://www.ncbi.nlm.nih.gov/pubmed/17299783.

Kong L, Herold CJ, Zöllner F, Salat DH, Lässer MM, Schmid LA, Fellhauer I, Thomann PA, Essig M, Schad LR, Erickson KI, Schröder J (2015): Comparison of grey matter volume and thickness for analysing cortical changes in chronic schizophrenia: a matter of surface area, grey/white matter intensity contrast, and curvature. Psychiatry Res 231:176–83. http://www.sciencedirect.com/science/article/pii/S092549271400331X.

Korzeniewski SJ, Birbeck G, DeLano MC, Potchen MJ, Paneth N (2008): A Systematic Review of Neuroimaging for Cerebral Palsy. J Child Neurol 23:216–227. http://jcn.sagepub.com/content/23/2/216.

Krägeloh-Mann I (2004): Imaging of early brain injury and cortical plasticity. Exp Neurol 190 Suppl:S84-90. http://www.sciencedirect.com/science/article/pii/S0014488604002274.

Krägeloh-Mann I, Helber A, Mader I, Staudt M, Wolff M, Groenendaal F, DeVries L (2002): Bilateral lesions of thalamus and basal ganglia: origin and outcome. Dev Med Child Neurol 44:477–84. http://www.ncbi.nlm.nih.gov/pubmed/12162385.

Krägeloh-Mann I, Horber V (2007): The role of magnetic resonance imaging in elucidating the pathogenesis of cerebral palsy: a systematic review. Dev Med Child Neurol 49:144–151. http://onlinelibrary.wiley.com/doi/10.1111/j.1469-8749.2007.00144.x/abstract.

Krägeloh-Mann I, Horber V, KrÃ¤geloh-Mann I, Horber V (2007): The role of magnetic resonance

imaging in elucidating the pathogenesis of cerebral palsy: a systematic review. Dev Med Child Neurol 49:144–151. http://onlinelibrary.wiley.com/doi/10.1111/j.1469-8749.2007.00144.x/abstract.

Kraus MF, Susmaras T, Caughlin BP, Walker CJ, Sweeney JA, Little DM (2007): White matter integrity and cognition in chronic traumatic brain injury: a diffusion tensor imaging study. Brain 130:2508–19. http://brain.oxfordjournals.org/content/130/10/2508.full.

Krigger KW (2006): Cerebral Palsy : An Overview. Am Fam Physician 73.

Krumlinde-Sundholm L, Holmefur M, Kottorp A, Eliasson AC (2007): The Assisting Hand Assessment: current evidence of validity, reliability, and responsiveness to change. Dev Med Child Neurol 49:259–64.

Kuban KCK, Leviton A (1994): Cerebral Palsy. N Engl J Med 330:188–195.

Kulak W, Sobaniec W, Kubas B, Walecki J, Smigielska-Kuzia J, Bockowski L, Artemowicz B, Sendrowski K (2007): Spastic Cerebral Palsy: Clinical Magnetic Resonance Imaging Correlation of 129 Children. J Child Neurol 22:8–14. http://jcn.sagepub.com/cgi/doi/10.1177/0883073807299953.

Kulakowski S, Larroche JC (1980): Cranial computerized tomography in cerebral palsy. An attempt at anatomo-clinical and radiological correlations. Neuropediatrics 11:339–353.

Kurowski B, Wade SL, Cecil KM, Walz NC, Yuan W, Rajagopal A, Holland SK (2009): Correlation of diffusion tensor imaging with executive function measures after early childhood traumatic brain injury. J Pediatr Rehabil Med 2:273–83. http://www.pubmedcentral.nih.gov/articlerender.fcgi?artid=3018823&tool=pmcentrez&rendertype=abstract.

Laundre BJ, Jellison BJ, Badie B, Alexander AL, Field AS (2005): Diffusion Tensor Imaging of the Corticospinal Tract before and after Mass Resection as Correlated with Clinical Motor Findings: Preliminary Data. AJNR Am J Neuroradiol 26:791–796. http://www.ajnr.org/content/26/4/791.short.

Ledig C, Heckemann RA, Hammers A, Lopez JC, Newcombe VFJ, Makropoulos A, Lötjönen J, Menon DK, Rueckert D (2015): Robust whole-brain segmentation: application to traumatic brain injury. Med Image Anal 21:40–58. http://www.sciencedirect.com/science/article/pii/S136184151400187X.

Ledig C, Wolz R, Aljabar P, Lotjonen J, Heckemann RA, Hammers A, Rueckert D (2012): Multi-class brain segmentation using atlas propagation and EM-based refinement. In: . 2012 9th IEEE International Symposium on Biomedical Imaging (ISBI). IEEE. pp 896–899.

http://ieeexplore.ieee.org/lpdocs/epic03/wrapper.htm?arnumber=6235693.

Lee TS, Mumford D, Romero R, Lamme VAF (1998): The role of the primary visual cortex in higher level vision. Vision Res 38:2429–2454. http://www.sciencedirect.com/science/article/pii/S0042698997004641.

Van Leemput K, Maes F, Vandermeulen D, Colchester A, Suetens P (2001): Automated segmentation of multiple sclerosis lesions by model outlier detection. IEEE Trans Med Imaging 20:677–688. http://ieeexplore.ieee.org/ielx5/42/20309/00938237.pdf?tp=&arnumber=938237&isnumber=20309.

Van Leemput K, Maes F, Vandermeulen D, Suetens P (1999): Automated model-based tissue classification of MR images of the brain. IEEE Trans Med Imaging 18:897–908. http://www.ncbi.nlm.nih.gov/pubmed/10628949.

Legault G, Shevell MI, Dagenais L (2011): Predicting Comorbidities With Neuroimaging in Children With Cerebral Palsy. Pediatr Neurol 45:229–232. http://www.sciencedirect.com/science/article/pii/S0887899411002748.

Leong S (1997): Is There a Zone of Vascular Vulnerability in the Fetal Brain Stem? Neurotoxicol Teratol 19:265–275. http://www.sciencedirect.com/science/article/pii/S0892036297000202.

Lerch JP, Pruessner JC, Zijdenbos A, Hampel H, Teipel SJ, Evans AC (2005): Focal decline of cortical thickness in Alzheimer's disease identified by computational neuroanatomy. Cereb Cortex 15:995–1001. http://cercor.oxfordjournals.org/content/15/7/995.short.

Lerch JP, Pruessner J, Zijdenbos AP, Collins DL, Teipel SJ, Hampel H, Evans AC (2008): Automated cortical thickness measurements from MRI can accurately separate Alzheimer's patients from normal elderly controls. Neurobiol Aging 29:23–30. http://www.ncbi.nlm.nih.gov/pubmed/17097767.

Leventer RJ, Guerrini R, Dobyns WB (2008): Malformations of cortical development and epilepsy. Dialogues Clin Neurosci 10:47–62. http://www.pubmedcentral.nih.gov/articlerender.fcgi?artid=3181860&tool=pmcentrez&rendertype=abstract.

Li C, Huang R, Ding Z, Gatenby JC, Metaxas DN, Gore JC (2011): A level set method for image segmentation in the presence of intensity inhomogeneities with application to MRI. IEEE Trans Image Process 20:2007–16. http://www.ncbi.nlm.nih.gov/pubmed/21518662.

Li G, Wang L, Shi F, Gilmore JH, Lin W, Shen D (2015a): Construction of 4D high-definition cortical surface atlases of infants: Methods and applications. Med Image Anal 25:22–36.

http://www.sciencedirect.com/science/article/pii/S1361841515000559.

Li XW, Li QL, Li SY, Li DY (2015b): Local manifold learning for multiatlas segmentation: application to hippocampal segmentation in healthy population and Alzheimer's disease. CNS Neurosci Ther 21:826–836. http://www.ncbi.nlm.nih.gov/pubmed/26122409.

van der Lijn F, den Heijer T, Breteler MMB, Niessen WJ (2008): Hippocampus segmentation in MR images using atlas registration, voxel classification, and graph cuts. Neuroimage 43:708–20. http://www.sciencedirect.com/science/article/pii/S1053811908008860.

Lindemer ER, Salat DH, Smith EE, Nguyen K, Fischl B, Greve DN (2015): White Matter Signal Abnormality Quality Differentiates MCI that Converts to Alzheimer's Disease from Non-converters. Neurobiol Aging 36:2447–2457. http://www.sciencedirect.com/science/article/pii/S0197458015002754.

Lladó X, Oliver A, Cabezas M, Freixenet J, Vilanova JC, Quiles A, Valls L, Ramió-Torrentà L, Rovira À (2012): Segmentation of multiple sclerosis lesions in brain MRI: A review of automated approaches. Inf Sci (Ny) 186:164–185. http://www.sciencedirect.com/science/article/pii/S0020025511005548.

Lohmann G, von Cramon DY (2000): Automatic labelling of the human cortical surface using sulcal basins. Med Image Anal 4:179–88. http://www.ncbi.nlm.nih.gov/pubmed/11145307.

Lorensen W, Cline H (1987): Marching cubes: a high resolution 3D surface construction algorithm. ACM SIGGRAPH Comput Graph 21:163–169.

Lötjönen JM, Wolz R, Koikkalainen JR, Thurfjell L, Waldemar G, Soininen H, Rueckert D (2010): Fast and robust multi-atlas segmentation of brain magnetic resonance images. Neuroimage 49:2352–65. http://www.sciencedirect.com/science/article/pii/S1053811909010970.

Lotze M, Montoya P, Erb M, Hülsmann E, Flor H, Klose U, Birbaumer N, Grodd W (1999): Activation of Cortical and Cerebellar Motor Areas during Executed and Imagined Hand Movements: An fMRI Study. J Cogn Neurosci 11:491–501. http://www.mitpressjournals.org/doi/abs/10.1162/089892999563553#.Vfuh0GxSsSs.

Lutz K, Koeneke S, Wüstenberg T, Jäncke L (2005): Asymmetry of cortical activation during maximum and convenient tapping speed. Neurosci Lett 373:61–6. http://www.sciencedirect.com/science/article/pii/S0304394004012200.

Ma Y, Koyama MS, Milham MP, Castellanos FX, Quinn BT, Pardoe H, Wang X, Kuzniecky R, Devinsky O, Thesen T, Blackmon K (2015): Cortical thickness abnormalities associated with dyslexia, independent of remediation status. NeuroImage Clin 7:177–86. http://www.sciencedirect.com/science/article/pii/S2213158214001697.

van der Maaten L, Postma EO, van den Herik HJ (2009): Dimensionality reduction: A comparative review. J Mach Learn Res 10:66–71.

MacDonald D, Kabani N, Avis D, Evans a C (2000): Automated 3-D extraction of inner and outer surfaces of cerebral cortex from MRI. Neuroimage 12:340–56. http://www.ncbi.nlm.nih.gov/pubmed/10944416.

Madden DJ, Bennett IJ, Song AW (2009): Cerebral white matter integrity and cognitive aging: contributions from diffusion tensor imaging. Neuropsychol Rev 19:415–35. http://www.pubmedcentral.nih.gov/articlerender.fcgi?artid=2787975&tool=pmcentrez&rendertype=abstract.

Makropoulos A, Ledig C, Aljabar P, Serag A, Hajnal J V., Edwards AD, Serena J. Counsell A, Rueckert D (2012): Automatic tissue and structural segmentation of neonatal brain MRI using Expectation-Maximization. In: . MICCAI Grand Challenge: Neonatal Brain Segmentation 2012 (NeoBrainS12).

Malladi R, Sethian J a., Vemuri BC (1995): Shape modeling with front propagation: a level set approach. IEEE Trans Pattern Anal Mach Intell 17:158–175. http://ieeexplore.ieee.org/lpdocs/epic03/wrapper.htm?arnumber=368173.

Marroquin JL, Vemuri BC, Botello S, Calderon F, Fernandez-Bouzas A (2002): An accurate and efficient bayesian method for automatic segmentation of brain MRI. IEEE Trans Med Imaging 21:934–45. http://www.ncbi.nlm.nih.gov/pubmed/12472266.

Martinez-Biarge M, Diez-Sebastian J, Rutherford MA, Cowan FM (2010): Outcomes after central grey matter injury in term perinatal hypoxic-ischaemic encephalopathy. Early Hum Dev 86:675–82. http://www.ncbi.nlm.nih.gov/pubmed/20864278.

Martinussen M, Fischl B, Larsson HB, Skranes J, Kulseng S, Vangberg TR, Vik T, Brubakk a-M, Haraldseth O, Dale a M (2005): Cerebral cortex thickness in 15-year-old adolescents with low birth weight measured by an automated MRI-based method. Brain 128:2588–96. http://www.ncbi.nlm.nih.gov/pubmed/16123146.

Mathur A, Inder T (2009): Magnetic resonance imaging—Insights into brain injury and outcomes in premature infants. J Commun Disord 42:248–255. http://www.sciencedirect.com/science/article/pii/S0021992409000367.

Maunu J, Lehtonen L, Lapinleimu H, Matomäki J, Munck P, Rikalainen H, Parkkola R, Haataja L (2011): Ventricular dilatation in relation to outcome at 2 years of age in very preterm infants: a prospective Finnish cohort study. Dev Med Child Neurol 53:48–54. http://www.ncbi.nlm.nih.gov/pubmed/21039438.

Mechelli A, Humphreys GW, Mayall K, Olson A, Price CJ (2000): Differential effects of word length and visual contrast in the fusiform and lingual gyri during reading. Proc Biol Sci 267:1909–13. http://rspb.royalsocietypublishing.org/content/267/1455/1909.short.

Mechrez R, Goldberger J, Greenspan H (2015): MS lesion segmentation using a multi-channel patch-based approach with spatial consistency. In: Ourselin, S, Styner, MA, editors. SPIE Medical Imaging. International Society for Optics and Photonics. p 94130O. http://proceedings.spiedigitallibrary.org/proceeding.aspx?articleid=2211401.

Melbourne A, Cardoso MJ, Kendall GS, J.Robertson N, Marlow N, Ourselin S (2012): NeoBrainS12 Challenge: Adaptive neonatal MRIbrain segmentation with myelinated whitematter class and automated extraction ofventricles I-IV. In: . MICCAI Grand Challenge: Neonatal Brain Segmentation 2012 (NeoBrainS12) p 16.

Melhem ER, Hoon AH, Ferrucci JT, Quinn CB, Reinhardt EM, Demetrides SW, Freeman BM, Johnston M V. (2000): Periventricular Leukomalacia: Relationship between Lateral Ventricular Volume on Brain MR Images and Severity of Cognitive and Motor Impairment1. Radiology 214:199–204. http://radiology.rsna.org/content/214/1/199.

Ment LR, Hirtz D, Hüppi PS (2009): Imaging biomarkers of outcome in the developing preterm brain. Lancet Neurol 8:1042–1055. http://www.sciencedirect.com/science/article/pii/S1474442209702571.

Mercuri E, Jongmans M, Bouza H, Haataja L, Rutherford M, Henderson S, Dubowitz L (1999): Congenital hemiplegia in children at school age: assessment of hand function in the non-hemiplegic hand and correlation with MRI. Neuropediatrics 30:8–13. http://europepmc.org/abstract/med/10222454.

Mewes AUJ, Hüppi PS, Als H, Rybicki FJ, Inder TE, McAnulty GB, Mulkern R V, Robertson RL, Rivkin MJ, Warfield SK (2006): Regional brain development in serial magnetic resonance imaging of low-risk preterm infants. Pediatrics 118:23–33. http://www.ncbi.nlm.nih.gov/pubmed/16818545.

Middleton FA, Strick PL (2000): Basal ganglia and cerebellar loops: motor and cognitive circuits. Brain Res Rev 31:236–250. http://www.sciencedirect.com/science/article/pii/S0165017399000405.

Miller SP, Ferriero DM, Leonard C, Piecuch R, Glidden D V, Partridge JC, Perez M, Mukherjee P, Vigneron DB, Barkovich AJ (2005): Early brain injury in premature newborns detected with magnetic resonance imaging is associated with adverse early neurodevelopmental outcome. J Pediatr 147:609–16. http://www.sciencedirect.com/science/article/pii/S0022347605005895.

Modat M, Ridgway GR, Taylor ZA, Lehmann M, Barnes J, Hawkes DJ, Fox NC, Ourselin S (2010): Fast free-form deformation using graphics processing units. Comput Methods Programs Biomed 98:278–84. http://www.sciencedirect.com/science/article/pii/S0169260709002533.

Moeskops P, Benders MJNL, Kersbergen KJ, Groenendaal F, de Vries LS, Viergever MA, Išgum I (2015): Development of Cortical Morphology Evaluated with Longitudinal MR Brain Images of Preterm Infants. PLoS One 10:e0131552. http://journals.plos.org/plosone/article?id=10.1371/journal.pone.0131552.

Morris AM, Williams JM, Atwater AE, Wilmore JH (1982): Age and Sex Differences in Motor Performance of 3 through 6 Year Old Children. Res Q Exerc Sport 53:214–221. http://www.tandfonline.com/doi/abs/10.1080/02701367.1982.10609342.

Mortamet B, Zeng D, Gerig G, Prastawa M, Bullitt E (2005): Effects of healthy aging measured by intracranial compartment volumes using a designed MR brain database. Med Image Comput Comput Assist Interv 8:383–91. http://www.pubmedcentral.nih.gov/articlerender.fcgi?artid=2430269&tool=pmcentrez&rendertype=abstract.

Mumford D, Shah J (1989): Optimal approximations by piecewise smooth functions and associated variational problems. Commun Pure Appl Math 42:577–685. http://doi.wiley.com/10.1002/cpa.3160420503.

Murgasova M, Dyet L, Edwards D, Rutherford M, Hajnal J V., Rueckert D (2006): Segmentation of Brain MRI in Young Children. In: . Medical Image Computing and Computer-Assisted Intervention–MICCAI 2006. Springer Berlin Heidelberg. p pp 687-694.

Nagai M, Kishi K, Kato S (2007): Insular cortex and neuropsychiatric disorders: a review of recent literature. Eur Psychiatry 22:387–94. http://www.sciencedirect.com/science/article/pii/S0924933807012825.

Narr KL, Bilder RM, Toga AW, Woods RP, Rex DE, Szeszko PR, Robinson D, Sevy S, Gunduz-Bruce H, Wang Y-P, DeLuca H, Thompson PM (2005): Mapping cortical thickness and gray matter concentration in first episode schizophrenia. Cereb Cortex 15:708–19. http://cercor.oxfordjournals.org/content/15/6/708.abstract.

Narr KL, Thompson PM, Sharma T, Moussai J, Blanton R, Anvar B, Edris A, Krupp R, Rayman J, Khaledy M, Toga AW (2001): Three-dimensional mapping of temporo-limbic regions and the lateral ventricles in schizophrenia: gender effects. Biol Psychiatry 50:84–97. http://www.sciencedirect.com/science/article/pii/S0006322300011203.

Nelson F, Poonawalla AH, Hou P, Huang F, Wolinsky JS, Narayana P a (2007): Improved

identification of intracortical lesions in multiple sclerosis with phase-sensitive inversion recovery in combination with fast double inversion recovery MR imaging. AJNR Am J Neuroradiol 28:1645–9. http://www.ncbi.nlm.nih.gov/pubmed/17885241.

Nestor SM, Rupsingh R, Borrie M, Smith M, Accomazzi V, Wells JL, Fogarty J, Bartha R (2008): Ventricular enlargement as a possible measure of Alzheimer's disease progression validated using the Alzheimer's disease neuroimaging initiative database. Brain 131:2443–54. http://brain.oxfordjournals.org/content/131/9/2443.full.

Njeh I, Sallemi L, Ayed I Ben, Chtourou K, Lehericy S, Galanaud D, Hamida A Ben (2015): 3D multimodal MRI brain glioma tumor and edema segmentation: a graph cut distribution matching approach. Comput Med Imaging Graph 40:108–19. http://www.sciencedirect.com/science/article/pii/S0895611114001608.

Nordahl CW, Dierker D, Mostafavi I, Schumann CM, Rivera SM, Amaral DG, Van Essen DC (2007): Cortical folding abnormalities in autism revealed by surface-based morphometry. J Neurosci 27:11725–35. http://www.ncbi.nlm.nih.gov/pubmed/17959814.

Northam GB, Liégeois F, Chong WK, Wyatt JS, Baldeweg T, S. Wyatt J, Baldeweg T (2011): Total brain white matter is a major determinant of IQ in adolescents born preterm. Ann Neurol 69:702–11. http://onlinelibrary.wiley.com/doi/10.1002/ana.22263/abstract.

Oishi K, Faria A V, Yoshida S, Chang L, Mori S (2013): Quantitative evaluation of brain development using anatomical MRI and diffusion tensor imaging. Int J Dev Neurosci 31:512–24. http://www.sciencedirect.com/science/article/pii/S0736574813001019.

Oishi K, Mori S, Donohue PK, Ernst T, Anderson L, Buchthal S, Faria A, Jiang H, Li X, Miller MI, van Zijl PCM, Chang L (2011): Multi-contrast human neonatal brain atlas: Application to normal neonate development analysis. Neuroimage 56:8–20. http://www.sciencedirect.com/science/article/pii/S1053811911000875.

Osher S, Sethian JA (1988): Fronts propagating with curvature-dependent speed: Algorithms based on Hamilton-Jacobi formulations. J Comput Phys 79:12–49. http://linkinghub.elsevier.com/retrieve/pii/0021999188900022.

Otsu N (1975): A threshold selection method from gray-level histograms. Automatica 11:23–27.

Owen AM, Downes JJ, Sahakian BJ, Polkey CE, Robbins TW (1990): Planning and spatial working memory following frontal lobe lesions in man. Neuropsychologia 28:1021–1034. http://www.sciencedirect.com/science/article/pii/002839329090137D.

Ozenne B, Subtil F, Østergaard L, Maucort-Boulch D (2015): Spatially regularized mixture model for lesion segmentation with application to stroke patients. Biostatistics 16:580–95.

http://biostatistics.oxfordjournals.org/content/early/2015/03/06/biostatistics.kxv004.short.

Pagnozzi AM, Dowson N, Bourgeat P, Bradley AP, Boyd RN, Rose S (2015): Expectation-maximization with image-weighted Markov Random Fields to handle severe pathology. In: . Digital Image Computing: Techniques and Applications (DICTA). Adelaide, SA. pp 1–6.

Pagnozzi AM, Dowson N, Doecke J, Fiori S, Bradley AP, Boyd RN, Rose S (2016a): Automated, quantitative measures of grey and white matter lesion burden correlates with motor and cognitive function in children with unilateral cerebral palsy. NeuroImage Clin 11:751–759.

Pagnozzi AM, Dowson N, Fiori S, Doecke J, Bradley AP, Boyd RN, Rose S (2016b): Alterations in regional shape on ipsilateral and contralateral cortex contrast in children with unilateral cerebral palsy and are predictive of multiple outcomes. Hum Brain Mapp 37:3588–3603. http://doi.wiley.com/10.1002/hbm.23262.

Pagnozzi AM, Shen K, Doecke JD, Boyd RN, Bradley AP, Rose S, Dowson N (2016c): Using ventricular modeling to robustly probe significant deep gray matter pathologies: Application to cerebral palsy. Hum Brain Mapp 37:3795–3809. http://doi.wiley.com/10.1002/hbm.23276.

Palmer FB (2004): Strategies for the early diagnosis of cerebral palsy. J Pediatr 145:S8–S11.

Paneth N, Hong T, Korzeniewski S (2006): The descriptive epidemiology of cerebral palsy. Clin Perinatol 33:251–67. http://www.sciencedirect.com/science/article/pii/S009551080600025X.

Panizzon MS, Fennema-Notestine C, Eyler LT, Jernigan TL, Prom-Wormley E, Neale M, Jacobson K, Lyons MJ, Grant MD, Franz CE, Xian H, Tsuang M, Fischl B, Seidman L, Dale A, Kremen WS (2009): Distinct genetic influences on cortical surface area and cortical thickness. Cereb Cortex 19:2728–35. http://cercor.oxfordjournals.org/content/early/2009/03/18/cercor.bhp026.full.

Pannek K, Boyd RN, Fiori S, Guzzetta A, Rose SE (2014): Assessment of the structural brain network reveals altered connectivity in children with unilateral cerebral palsy due to periventricular white matter lesions. NeuroImage Clin 5:84–92. http://www.sciencedirect.com/science/article/pii/S2213158214000746.

Papadelis C, Ahtam B, Nazarova M, Nimec D, Snyder B, Grant PE, Okada Y (2014): Cortical somatosensory reorganization in children with spastic cerebral palsy: a multimodal neuroimaging study. Front Hum Neurosci 8:725. http://www.pubmedcentral.nih.gov/articlerender.fcgi?artid=4162364&tool=pmcentrez&rendertype=abstract.

Papoutsi M, de Zwart JA, Jansma JM, Pickering MJ, Bednar JA, Horwitz B (2009): From phonemes to articulatory codes: an fMRI study of the role of Broca's area in speech

production. Cereb Cortex 19:2156–65. http://cercor.oxfordjournals.org/content/19/9/2156.short.

Parisot S, Duffau H, Chemouny S, Paragios N (2012): Joint Tumor Segmentation and Dense Deformable Registration of Brain MR Images. In: Ayache, N, Delingette, H, Golland, P, Mori, K, editors. Medical Image Computing …. Springer Berlin Heidelberg. Lecture Notes in Computer Science pp 651–658. http://link.springer.com/chapter/10.1007/978-3-642-33418-4_80.

Parisot S, Wells W, Chemouny S, Duffau H, Paragios N (2014): Concurrent tumor segmentation and registration with uncertainty-based sparse non-uniform graphs. Med Image Anal 18:647–59. http://www.medicalimageanalysisjournal.com/article/S1361841514000292/fulltext.

Park HJ, Lee JD, Kim EY, Park B, Oh MK, Lee SC, Kim JJ (2009): Morphological alterations in the congenital blind based on the analysis of cortical thickness and surface area. Neuroimage 47:98–106. http://www.sciencedirect.com/science/article/pii/S1053811909003358.

Patenaude B, Smith SM, Kennedy DN, Jenkinson M (2011): A Bayesian model of shape and appearance for subcortical brain segmentation. Neuroimage 56:907–22. http://www.sciencedirect.com/science/article/pii/S1053811911002023.

Paus T (2001): Primate Anterior Cingulate Cortex: Where Motor Control, Drive and Cognition Interface. Nat Rev Neurosci 2:417–24. http://www.ncbi.nlm.nih.gov/pubmed/11389475.

Perona P, Malik J (1990): Scale-space and edge detection using anisotropic diffusion. IEEE Trans Pattern Anal Mach Intell 12:629–639. http://ieeexplore.ieee.org/lpdocs/epic03/wrapper.htm?arnumber=56205.

Petrini JR, Dias T, McCormick MC, Massolo ML, Green NS, Escobar GJ (2009): Increased Risk of Adverse Neurological Development for Late Preterm Infants. J Pediatr 154:169–176.e3.

Pham DL, Prince JL (1999): Adaptive fuzzy segmentation of magnetic resonance images. IEEE Trans Med Imaging 18:737–52. http://www.ncbi.nlm.nih.gov/pubmed/10571379.

Pohl KM, Wells WM, Guimond A, Kasai K, Shenton ME, Kikinis R, Grimson WEL, Warfield SK (2002): Incorporating Non-rigid Registration into Expectation Maximization Algorithm to Segment MR Images. In: . Medical Image Computing and Computer-Assisted Intervention — MICCAI 2002. Springer Berlin Heidelberg. p pp 564-571.

Pollo C, Cuadra MB, Cuisenaire O, Villemure J-G, Thiran J-P (2005): Segmentation of brain structures in presence of a space-occupying lesion. Neuroimage 24:990–6. http://www.sciencedirect.com/science/article/pii/S1053811904005956.

Pons C, Brochard S, Gallien P, Nicolas B, Durufle A, Roquet M, Remy-Neris O, Garlantezec R

(2016): Medication, rehabilitation and health care consumption in adults with cerebral palsy: A population based study. Clin Rehabil:269215516663286. http://cre.sagepub.com/cgi/doi/10.1177/0269215516663286.

Porro CA, Francescato MP, Cettolo V, Diamond ME, Baraldi P, Zuiani C, Bazzocchi M, di Prampero PE (1996): Primary motor and sensory cortex activation during motor performance and motor imagery: a functional magnetic resonance imaging study. J Neurosci 16:7688–98. http://www.ncbi.nlm.nih.gov/pubmed/8922425.

Prastawa M, Gilmore JH, Lin W, Gerig G (2005): Automatic segmentation of MR images of the developing newborn brain. Med Image Anal 9:457–66. http://www.ncbi.nlm.nih.gov/pubmed/16019252.

Prastawa M, Guido G (2008): Automatic MS lesion segmentation by outlier detection and information theoretic region partitioning. In: . Grand Challenge Work.: Mult. Scler. Lesion Segm. Challenge pp 1–8.

Pueyo R, Junqué C, Vendrell P, Narberhaus A, Segarra D (2009): Neuropsychologic impairment in bilateral cerebral palsy. Pediatr Neurol 40:19–26. http://www.sciencedirect.com/science/article/pii/S0887899408003913.

Qiu W, Yuan J, Rajchl M, Kishimoto J, Chen Y, de Ribaupierre S, Chiu B, Fenster A (2015): 3D MR ventricle segmentation in pre-term infants with post-hemorrhagic ventricle dilatation (PHVD) using multi-phase geodesic level-sets. Neuroimage 118:13–25. http://www.sciencedirect.com/science/article/pii/S1053811915005248.

Rajchl M, Baxter JSH, McLeod AJ, Yuan J, Qiu W, Peters TM, Khan AR (2015): Hierarchical Max-Flow Segmentation Framework For Multi-Atlas Segmentation with Kohonen Self-Organizing Map Based Gaussian Mixture Modeling. Med Image Anal 27:45–56. http://www.sciencedirect.com/science/article/pii/S1361841515000729.

Ravikumar N, Castro-Mateos I, Pozo JM, Frangi AF, Taylor ZA (2015): 3D active shape models of human brain structures: application to patient-specific mesh generation. In: Hadjiiski, LM, Tourassi, GD, editors. SPIE Medical Imaging. International Society for Optics and Photonics. p 94142D. http://proceedings.spiedigitallibrary.org/proceeding.aspx?articleid=2211270.

Reid LB, Cunnington R, Boyd RN, Rose SE (2016): Surface-Based fMRI-Driven Diffusion Tractography in the Presence of Significant Brain Pathology: A Study Linking Structure and Function in Cerebral Palsy. Ed. Pew-Thian Yap. PLoS One 11:e0159540. http://dx.plos.org/10.1371/journal.pone.0159540.

Reid SM, Dagia CD, Ditchfield MR, Carlin JB, Meehan EM, Reddihough DS (2014): An Australian

population study of factors associated with MRI patterns in cerebral palsy. Dev Med Child Neurol 56:178–84. http://www.ncbi.nlm.nih.gov/pubmed/24428267.

Rekik I, Li G, Lin W, Shen D (2015): Prediction of Longitudinal Development of Infant Cortical Surface Shape Using a 4D Current-Based Learning Framework. Lect Notes Comput Sci Vol 9123:576–587.

Renier LA, Anurova I, De Volder AG, Carlson S, VanMeter J, Rauschecker JP (2010): Preserved functional specialization for spatial processing in the middle occipital gyrus of the early blind. Neuron 68:138–48. http://www.sciencedirect.com/science/article/pii/S0896627310007634.

Rettmann ME, Han X, Xu C, Prince JL (2002): Automated sulcal segmentation using watersheds on the cortical surface. Neuroimage 15:329–44. http://www.ncbi.nlm.nih.gov/pubmed/11798269.

Rickard T., Romero S., Basso G, Wharton C, Flitman S, Grafman J (2000): The calculating brain: an fMRI study. Neuropsychologia 38:325–335. http://www.sciencedirect.com/science/article/pii/S0028393299000688.

Rimol LM, Nesvåg R, Hagler DJ, Bergmann O, Fennema-Notestine C, Hartberg CB, Haukvik UK, Lange E, Pung CJ, Server A, Melle I, Andreassen OA, Agartz I, Dale AM (2012): Cortical volume, surface area, and thickness in schizophrenia and bipolar disorder. Biol Psychiatry 71:552–60. http://www.biologicalpsychiatryjournal.com/article/S0006322311011991/fulltext.

Ristić AJ, Daković M, Kerr M, Kovačević M, Parojčić A, Sokić D (2015): Cortical thickness, surface area and folding in patients with psychogenic nonepileptic seizures. Epilepsy Res 112:84–91. http://www.sciencedirect.com/science/article/pii/S0920121115000418.

Rivest-Hénault D, Dowson N, Greer PB, Fripp J, Dowling J (2015): Robust inverse-consistent affine CT–MR registration in MRI-assisted and MRI-alone prostate radiation therapy. Med Image Anal 23:56–69. http://www.sciencedirect.com/science/article/pii/S136184151500064X.

Rizzolatti G, Fogassi L, Gallese V (2002): Motor and cognitive functions of the ventral premotor cortex. Curr Opin Neurobiol 12:149–154. http://www.sciencedirect.com/science/article/pii/S0959438802003082.

Rodriguez-Carranza CE, Mukherjee P, Vigneron D, Barkovich J, Studholme C (2008): A framework for in-vivo quantification of regional brain folding in premature neonates. Neuroimage 41:462–478. http://www.ncbi.nlm.nih.gov/pmc/articles/PMC2741002/.

Ronan L, Scanlon C, Murphy K, Maguire S, Delanty N, Doherty CP, Fitzsimons M (2011): Cortical curvature analysis in MRI-negative temporal lobe epilepsy: a surrogate marker for malformations of cortical development. Epilepsia 52:28–34.

http://www.ncbi.nlm.nih.gov/pubmed/21198558.

Ronchetti E (1985): Robust model selection in regression. Stat Probab Lett 3:21–23. http://linkinghub.elsevier.com/retrieve/pii/0167715285900069.

Rose S, Guzzetta A, Pannek K, Boyd R (2011): MRI Structural Connectivity, Disruption of Primary Sensorimotor Pathways, and Hand Function in Cerebral Palsy. Brain Connect 1:309–316. http://online.liebertpub.com/doi/abs/10.1089/brain.2011.0034.

Rosenbaum P (2003): Cerebral palsy: what parents and doctors want to know. BMJ 326:970–974. http://www.pubmedcentral.nih.gov/articlerender.fcgi?artid=1125882&tool=pmcentrez&rendertype=abstract.

Rosenbaum P, Nigel P, Leviton A, Goldstein M, Bax M (2007): A report: the definition and classification of cerebral palsy April 2006. Dev Med Child Neurol 49:8–14. http://onlinelibrary.wiley.com/doi/10.1111/j.1469-8749.2007.tb12610.x/abstract.

Roura E, Oliver A, Cabezas M, Valverde S, Pareto D, Vilanova JC, Ramió-Torrentà L, Rovira À, Lladó X (2015): A toolbox for multiple sclerosis lesion segmentation. Neuroradiology 57:1031–43. http://www.ncbi.nlm.nih.gov/pubmed/26227167.

Rutherford M, Pennock J, Schwieso J, Cowan F, Dubowitz L (1996): Hypoxic-ischaemic encephalopathy: early and late magnetic resonance imaging findings in relation to outcome. Arch Dis Child - Fetal Neonatal Ed 75:F145–F151. http://fn.bmj.com/content/75/3/F145.abstract.

Rutherford MA, Supramaniam V, Ederies A, Chew A, Bassi L, Groppo M, Anjari M, Counsell S, Ramenghi LA (2010): Magnetic resonance imaging of white matter diseases of prematurity. Neuroradiology 52:505–21. http://search.proquest.com/docview/221140882/abstract?accountid=26957.

Sabuncu MR, Yeo BTT, Van Leemput K, Fischl B, Golland P (2010): A generative model for image segmentation based on label fusion. IEEE Trans Med Imaging 29:1714–29. http://www.pubmedcentral.nih.gov/articlerender.fcgi?artid=3268159&tool=pmcentrez&rendertype=abstract.

Sajja BR, Datta S, He R, Mehta M, Gupta RK, Wolinsky JS, Narayana P a (2006): Unified approach for multiple sclerosis lesion segmentation on brain MRI. Ann Biomed Eng 34:142–51. http://www.pubmedcentral.nih.gov/articlerender.fcgi?artid=1463248&tool=pmcentrez&rendertype=abstract.

Sajja BR, Datta S, He R, Narayana PA (2004): A Unified Approach for Lesion Segmentation on

MRI of Multiple Sclerosis. Conf Proc IEEE Eng Med Biol Soc 3:1778–1781.

Sallet PC, Elkis H, Alves TM, Oliveira JR, Sassi E, de Castro CC, Busatto GF, Gattaz WF (2003): Reduced Cortical Folding in Schizophrenia: An MRI Morphometric Study. Am J Psychiatry 160:1606–1613. http://ajp.psychiatryonline.org/doi/10.1176/appi.ajp.160.9.1606.

Sanes JN, Donoghue JP (2000): Plasticity and primary motor cortex. Annu Rev Neurosci 23:393–415. http://www.ncbi.nlm.nih.gov/pubmed/10845069.

Sanroma G, Wu G, Gao Y, Thung K-H, Guo Y, Shen D (2015): A transversal approach for patch-based label fusion via matrix completion. Med Image Anal 24:135–148. http://www.medicalimageanalysisjournal.com/article/S1361841515000894/fulltext.

Sasson E, Doniger GM, Pasternak O, Tarrasch R, Assaf Y (2012): Structural correlates of cognitive domains in normal aging with diffusion tensor imaging. Brain Struct Funct 217:503–15. http://www.ncbi.nlm.nih.gov/pubmed/21909706.

Saunders DE, Thompson C, Gunny R, Jones R, Cox T, Chong WK (2007): Magnetic resonance imaging protocols for paediatric neuroradiology. Pediatr Radiol 37:789–97. http://www.pubmedcentral.nih.gov/articlerender.fcgi?artid=1950216&tool=pmcentrez&rendertype=abstract.

Scarpazza C, Tognin S, Frisciata S, Sartori G, Mechelli A (2015): False positive rates in Voxel-based Morphometry studies of the human brain: should we be worried? Neurosci Biobehav Rev 52:49–55. http://www.sciencedirect.com/science/article/pii/S0149763415000536.

Schaer M, Cuadra MB, Tamarit L, Lazeyras F, Eliez S, Thiran J-P (2008): A surface-based approach to quantify local cortical gyrification. IEEE Trans Med Imaging 27:161–70. http://www.ncbi.nlm.nih.gov/pubmed/18334438.

Scheff SW, Price DA, Schmitt FA, Scheff MA, Mufson EJ (2011): Synaptic loss in the inferior temporal gyrus in mild cognitive impairment and Alzheimer's disease. J Alzheimers Dis 24:547–57. http://content.iospress.com/articles/journal-of-alzheimers-disease/jad101782.

Schmidt P, Gaser C, Arsic M, Buck D, Förschler A, Berthele A, Hoshi M, Ilg R, Schmid VJ, Zimmer C, Hemmer B, Mühlau M (2012): An automated tool for detection of FLAIR-hyperintense white-matter lesions in Multiple Sclerosis. Neuroimage 59:3774–3783. http://www.sciencedirect.com/science/article/pii/S1053811911013139.

Sethian JA (1996): A fast marching level set method for monotonically advancing fronts. Proc Natl Acad Sci 93:1591–1595. http://www.pnas.org/content/93/4/1591.short.

Shapiro SS, Wilk MB (1965): An analysis of variance test for normality (complete samples). Biometrika 52:591–611.

Shaw P, Greenstein D, Lerch J, Clasen L, Lenroot R, Gogtay N, Evans A, Rapoport J, Giedd J (2006): Intellectual ability and cortical development in children and adolescents. Nature 440:676–9. http://dx.doi.org/10.1038/nature04513.

Shen K, Fripp J, Mériaudeau F, Chételat G, Salvado O, Bourgeat P (2012a): Detecting global and local hippocampal shape changes in Alzheimer's disease using statistical shape models. Neuroimage 59:2155–2166. http://www.sciencedirect.com/science/article/pii/S105381191101175X.

Shen K, Bourgeat P, Fripp J, Meriaudeau F, Salvado O (2012b): Consistent estimation of shape parameters in statistical shape model by symmetric EM algorithm. In: Haynor, DR, Ourselin, S, editors. Proc. SPIE 8314, Medical Imaging 2012: Image Processing p 83140R. http://proceedings.spiedigitallibrary.org/proceeding.aspx?doi=10.1117/12.911746.

Shen K, Fripp J, Meriaudeau F, Chetelat G, Salvado O, Bourgeat P (2011): Localization of hippocampal atrophy in Alzheimer's disease. Alzheimer's Dement 7:S17–S18. http://www.alzheimersanddementia.com/article/S1552526011001798/fulltext.

Shen S, Szameitat AJ, Sterr A (2010): An improved lesion detection approach based on similarity measurement between fuzzy intensity segmentation and spatial probability maps. Magn Reson Imaging 28:245–54. http://www.ncbi.nlm.nih.gov/pubmed/19695812.

Shenton ME, Kikinis R, McCarley RW, Metcalf D, Tieman J, Jolesz F a (1991): Application of automated MRI volumetric measurement techniques to the ventricular system in schizophrenics and normal controls. Schizophr Res 5:103–13. http://www.ncbi.nlm.nih.gov/pubmed/1931803.

Shibasaki H, Sadato N, Lyshkow H, Yonekura Y, Honda M, Nagamine T, Suwazono S, Magata Y, Ikeda A, Miyazaki M, Fukuyama H, Asato R, Konishi J (1993): Both primary motor cortex and supplementarymotor area play an important role in complexfinger movement. Brain 116:1387–1398.

Shiee N, Bazin P, Pham D (2008): Multiple sclerosis lesion segmentation using statistical and topological atlases. In: . Grand Challenge Work.: Mult. Scler. Lesion Segm. Challenge pp 1–10.

Shiee N, Bazin P-L, Ozturk A, Reich DS, Calabresi PA, Pham DL (2010): A topology-preserving approach to the segmentation of brain images with multiple sclerosis lesions. Neuroimage 49:1524–35. http://www.sciencedirect.com/science/article/pii/S1053811909009823.

Shiran SI, Weinstein M, Sirota-Cohen C, Myers V, Ben Bashat D, Fattal-Valevski A, Green D, Schertz M (2014): MRI-Based Radiologic Scoring System for Extent of Brain Injury in Children

with Hemiplegia. AJNR Am J Neuroradiol 35:2388–96. http://www.ajnr.org/content/early/2014/05/22/ajnr.A3950.abstract.

Shollenbarger SG, Price J, Wieser J, Lisdahl K (2015): Impact of Cannabis Use on Prefrontal and Parietal Cortex Gyrification and Surface Area in Adolescents and Emerging Adults. Dev Cogn Neurosci 16:46–53. http://www.sciencedirect.com/science/article/pii/S1878929315000699.

Shroeder W, Martin K, Lorensen B (2006): The Visualization Toolkit. The Visualization Toolkit, 4th ed. Kitware. Kitware. http://vtk.org.

Sie LTL, Hart AAM, van Hof J, de Groot L, Lems W, Lafeber HN, Valk J, van der Knaap MS (2005): Predictive value of neonatal MRI with respect to late MRI findings and clinical outcome. A study in infants with periventricular densities on neonatal ultrasound. Neuropediatrics 36:78–89. https://www.thieme-connect.com/products/ejournals/abstract/10.1055/s-2005-837574.

Skiöld B, Eriksson C, Eliasson A-C, Adén U, Vollmer B (2013): General movements and magnetic resonance imaging in the prediction of neuromotor outcome in children born extremely preterm. Early Hum Dev 89:467–72. http://www.sciencedirect.com/science/article/pii/S0378378213000698.

Smith CD, Chebrolu H, Wekstein DR, Schmitt FA, Markesbery WR (2007): Age and gender effects on human brain anatomy: a voxel-based morphometric study in healthy elderly. Neurobiol Aging 28:1075–87. http://www.sciencedirect.com/science/article/pii/S0197458006001539.

Snowling M, Hulme C (1994): The development of phonological skills. Philos Trans R Soc Lond B Biol Sci 346:21–7. http://rstb.royalsocietypublishing.org/content/346/1315/21.short.

Sööt A, Tomberg T, Kool P, Rein R, Talvik T (2008): Magnetic Resonance Imaging in Children With Bilateral Spastic Forms of Cerebral Palsy. Pediatr Neurol 38:321–328. http://www.sciencedirect.com/science/article/pii/S0887899408000155.

Soria-Pastor S, Gimenez M, Narberhaus A, Falcon C, Botet F, Bargallo N, Mercader JM, Junque C (2008): Patterns of cerebral white matter damage and cognitive impairment in adolescents born very preterm. Int J Dev Neurosci 26:647–654. http://www.sciencedirect.com/science/article/pii/S0736574808001251.

Souplet J-C (2009): Évaluation de l’atrophie et de la charge lésionnelle sur des séquences IRM de patients atteints de sclérose en plaques. Université Nice Sophia Antipolis. https://tel.archives-ouvertes.fr/tel-00635295/.

Sowell ER, Thompson PM, Leonard CM, Welcome SE, Kan E, Toga AW (2004): Longitudinal mapping of cortical thickness and brain growth in normal children. J Neurosci 24:8223–31.

http://www.jneurosci.org/content/24/38/8223.long.

Sridharan D, Levitin DJ, Menon V (2008): A critical role for the right fronto-insular cortex in switching between central-executive and default-mode networks. Proc Natl Acad Sci U S A 105:12569–74. http://www.pnas.org/content/105/34/12569.short.

Sterling C, Taub E, Davis D, Rickards T, Gauthier L V., Griffin A, Uswatte G (2013): Structural neuroplastic change after constraint-induced movement therapy in children with cerebral palsy. Pediatrics 131:e1664-9. http://pediatrics.aappublications.org/content/131/5/e1664.full.

Stoerig P (2006): Blindsight, conscious vision, and the role of primary visual cortex. Prog Brain Res 155:217–34. http://www.sciencedirect.com/science/article/pii/S0079612306550125.

Styner M, Gerig G, Lieberman J, Jones D, Weinberger D (2003): Statistical shape analysis of neuroanatomical structures based on medial models. Med Image Anal 7:207–220.

Styner M, Lieberman J a, Pantazis D, Gerig G (2004): Boundary and medial shape analysis of the hippocampus in schizophrenia. Med Image Anal 8:197–203. http://www.ncbi.nlm.nih.gov/pubmed/15450215.

Styner M, Oguz I, Xu S, Pantazis D, Gerig G (2007): Statistical group differences in anatomical shape analysis using Hotelling T2 metric. In: Pluim, JPW, Reinhardt, JM, editors. Medical Imaging. International Society for Optics and Photonics. p 65123Z–65123Z–11. http://proceedings.spiedigitallibrary.org/proceeding.aspx?articleid=1299663.

Sugiura N (2007): Further analysts of the data by akaike' s information criterion and the finite corrections. Commun Stat - Theory Methods 7:13–26. http://www.tandfonline.com/doi/abs/10.1080/03610927808827599#.VMcImIqUekA.

Takakusaki K, Saitoh K, Harada H, Kashiwayanagi M (2004): Role of basal ganglia-brainstem pathways in the control of motor behaviors. Neurosci Res 50:137–51. http://www.sciencedirect.com/science/article/pii/S0168010204001737.

Talairach J, Tournoux P (1988): Co-planar stereotaxic atlas of the human brain. 3-Dimensional proportional system: an approach to cerebral imaging. Thieme.

Tan IL, van Schijndel RA, Pouwels PJW, Adèr HJ, Barkhof F (2002): Serial isotropic three-dimensional fast FLAIR imaging: using image registration and subtraction to reveal active multiple sclerosis lesions. AJR Am J Roentgenol 179:777–782.

Tardif CL, Schäfer A, Waehnert M, Dinse J, Turner R, Bazin P-L (2015): Multi-contrast multi-scale surface registration for improved alignment of cortical areas. Neuroimage 111:107–22. http://www.sciencedirect.com/science/article/pii/S105381191500097X.

Tassi L, Colombo N, Garbelli R, Francione S, Lo Russo G, Mai R, Cardinale F, Cossu M, Ferrario A, Galli C, Bramerio M, Citterio A, Spreafico R (2002): Focal cortical dysplasia: neuropathological subtypes, EEG, neuroimaging and surgical outcome. Brain 125:1719–32. http://www.ncbi.nlm.nih.gov/pubmed/12135964.

The McConnell Brain Imaging Centre (2012): Colin 27 Average Brain, Stereotaxic Registration Model, original 1998 version. http://www.bic.mni.mcgill.ca/ServicesAtlases/Colin27.

The R Development Core Team (2008): R: A language and environment for statistical computing. R Foundation for Statistical Computing. Vienna, Austria. http://www.r-project.org.

Thiel A, Herholz K, Koyuncu A, Ghaemi M, Kracht LW, Habedank B, Heiss WD (2001): Plasticity of language networks in patients with brain tumors: a positron emission tomography activation study. Ann Neurol 50:620–9. http://www.ncbi.nlm.nih.gov/pubmed/11706968.

Thomas AG, Marrett S, Saad ZS, Ruff DA, Martin A, Bandettini PA (2009): Functional but not structural changes associated with learning: an exploration of longitudinal voxel-based morphometry (VBM). Neuroimage 48:117–25. http://www.pubmedcentral.nih.gov/articlerender.fcgi?artid=2981435&tool=pmcentrez&rendertype=abstract.

Thompson PM, Toga AW (1997): Detection, visualization and animation of abnormal anatomic structure with a deformable probabilistic brain atlas based on random vector field transformations. Med Image Anal 1:271–294. http://www.medicalimageanalysisjournal.com/article/S1361-8415(97)85002-5/abstract.

Thompson PM, Hayashi KM, de Zubicaray GI, Janke AL, Rose SE, Semple J, Hong MS, Herman DH, Gravano D, Doddrell DM, Toga AW (2004): Mapping hippocampal and ventricular change in Alzheimer disease. Neuroimage 22:1754–1766. http://www.sciencedirect.com/science/article/pii/S105381190400196X.

Tibshirani R (1996): Regression Shrinkage and Selection via the Lasso. J R Stat Soc Ser B 58:267–288.

Tosun D, Reiss AL, Lee AD, Dutton RA, Hayashi KM, Bellugi U, Galaburda AM, Korenberg JR, Mills DL, Toga AW, Thompson PM (2006): Use of 3-D Cortical Morphometry for Mapping Increased Cortical Gyrification and Complexity in Williams Syndrome. In: . 3rd IEEE International Symposium on Biomedical Imaging: Macro to Nano, 2006. IEEE. pp 1172–1175. http://ieeexplore.ieee.org/lpdocs/epic03/wrapper.htm?arnumber=1625132.

Tosun D, Rettmann ME, Han X, Tao X, Xu C, Resnick SM, Pham DL, Prince JL (2004): Cortical surface segmentation and mapping. Neuroimage 23 Suppl 1:S108-18.

http://www.ncbi.nlm.nih.gov/pubmed/15501080.

Truwit CL, Barkovich AJ, Koch TK, Ferriero DM (1992): Cerebral palsy: MR findings in 40 patients. Am J Neuroradiol 13:67–78. http://www.ajnr.org/content/13/1/67.

Tustison NJ, Avants BB, Cook PA, Zheng Y, Egan A, Yushkevich PA, Gee JC (2010): N4ITK: improved N3 bias correction. IEEE Trans Med Imaging 29:1310–20. http://www.pubmedcentral.nih.gov/articlerender.fcgi?artid=3071855&tool=pmcentrez&rendertype=abstract.

Venkateswaran S, Shevell MI (2008): Comorbidities and clinical determinants of outcome in children with spastic quadriplegic cerebral palsy. Dev Med Child Neurol 50:216–22. http://www.ncbi.nlm.nih.gov/pubmed/18248493.

Villemagne VL, Burnham S, Bourgeat P, Brown B, Ellis K a, Salvado O, Szoeke C, Macaulay SL, Martins R, Maruff P, Ames D, Rowe CC, Masters CL (2013): Amyloid β deposition, neurodegeneration, and cognitive decline in sporadic Alzheimer's disease: a prospective cohort study. Lancet Neurol 12:357–67. http://www.ncbi.nlm.nih.gov/pubmed/23477989.

Volpe JJ (2009): Brain injury in premature infants: a complex amalgam of destructive and developmental disturbances. Lancet Neurol 8:110–124.

de Vries LS, Rademaker KJ, Groenendaal F, Eken P, van Haastert IC, Vandertop WP, Gooskens R, Meiners LC (1998): Correlation between neonatal cranial ultrasound, MRI in infancy and neurodevelopmental outcome in infants with a large intraventricular haemorrhage with or without unilateral parenchymal involvement. Neuropediatrics 29:180–8. http://europepmc.org/abstract/med/9762693.

de Vries LS, van Haastert IC, Benders MJNL, Groenendaal F (2011): Myth: Cerebral palsy cannot be predicted by neonatal brain imaging. Semin Fetal Neonatal Med 16:279–287. http://www.sciencedirect.com/science/article/pii/S1744165X11000291.

Vrooman HA, Cocosco CA, van der Lijn F, Stokking R, Ikram MA, Vernooij MW, Breteler MMB, Niessen WJ (2007): Multi-spectral brain tissue segmentation using automatically trained k-Nearest-Neighbor classification. Neuroimage 37:71–81. http://www.sciencedirect.com/science/article/pii/S1053811907004181.

Waber D (1976): Sex differences in cognition: a function of maturation rate? Science (80-) 192:572–574. http://science.sciencemag.org/content/192/4239/572.abstract.

Wahl M, Lauterbach-Soon B, Hattingen E, Jung P, Singer O, Volz S, Klein JC, Steinmetz H, Ziemann U (2007): Human motor corpus callosum: topography, somatotopy, and link between microstructure and function. J Neurosci 27:12132–8.

http://www.jneurosci.org/content/27/45/12132.abstract.

Ward NS (2005): Neural plasticity and recovery of function. Prog Brain Res 150:527–35. http://www.sciencedirect.com/science/article/pii/S0079612305500360.

Warfield S, Dengler J, Zaers J, Guttmann CR, Wells WM, Ettinger GJ, Hiller J, Kikinis R (1995): Automatic identification of gray matter structures from MRI to improve the segmentation of white matter lesions. J Image Guid Surg 1:326–38. http://www.ncbi.nlm.nih.gov/pubmed/9080353.

Warfield SK, Kaus M, Jolesz F a, Kikinis R (2000): Adaptive, template moderated, spatially varying statistical classification. Med Image Anal 4:43–55. http://www.ncbi.nlm.nih.gov/pubmed/10972320.

Watkins KE, Vargha-Khadem F, Ashburner J, Passingham RE, Connelly A, Friston KJ, Frackowiak RSJ, Mishkin M, Gadian DG (2002): MRI analysis of an inherited speech and language disorder: structural brain abnormalities. Brain 125:465–478. http://brain.oxfordjournals.org/content/125/3/465.full.

Wechsler D (1967): Wechsler preschool and primary scale of intelligence. Psychological Corporation New York.

Weisenfeld NI, Warfield SK (2009): Automatic segmentation of newborn brain MRI. Neuroimage 47:564–72. http://www.pubmedcentral.nih.gov/articlerender.fcgi?artid=2945911&tool=pmcentrez&rendertype=abstract.

Wells WM, Grimson WL, Kikinis R, Jolesz F a (1996): Adaptive segmentation of MRI data. IEEE Trans Med Imaging 15:429–42. http://www.ncbi.nlm.nih.gov/pubmed/18215925.

Van der Werf YD, Scheltens P, Lindeboom J, Witter MP, Uylings HBM, Jolles J (2003): Deficits of memory, executive functioning and attention following infarction in the thalamus; a study of 22 cases with localised lesions. Neuropsychologia 41:1330–1344. http://www.sciencedirect.com/science/article/pii/S0028393203000599.

White T, Andreasen NC, Nopoulos P, Magnotta V (2003): Gyrification abnormalities in childhood- and adolescent-onset schizophrenia. Biol Psychiatry 54:418–426. http://www.sciencedirect.com/science/article/pii/S0006322303000659.

Wolz R, Aljabar P, Hajnal J V., Hammers A, Rueckert D (2010): LEAP: Learning embeddings for atlas propagation. Neuroimage 49:1316–1325. http://www.sciencedirect.com/science/article/pii/S1053811909010684.

Wright IC, Sham P, Murray RM, Weinberger DR, Bullmore ET (2002): Genetic Contributions to

Regional Variability in Human Brain Structure: Methods and Preliminary Results. Neuroimage 17:256–271. http://linkinghub.elsevier.com/retrieve/pii/S1053811902911638.

Wu CS, Pedersen LH, Miller JE, Sun Y, Streja E, Uldall P, Olsen J (2013): Risk of cerebral palsy and childhood epilepsy related to infections before or during pregnancy. PLoS One 8:e57552. http://journals.plos.org/plosone/article?id=10.1371/journal.pone.0057552.

Wu Y, Warfield SK, Tan IL, Wells WM 3rd, Meier DS, van Schijndel RA, Barkhof F, Guttmann CRG (2006): Automated segmentation of multiple sclerosis lesion subtypes with multichannel MRI. Neuroimage 32:1205–1215. http://www.ncbi.nlm.nih.gov/pubmed/16797188.

Xu C, Pham DL, Rettmann ME, Yu DN, Prince JL (1999): Reconstruction of the human cerebral cortex from magnetic resonance images. IEEE Trans Med Imaging 18:467–80. http://www.ncbi.nlm.nih.gov/pubmed/10463126.

Xue H, Srinivasan L, Jiang S, Rutherford M, Edwards AD, Rueckert D, Hajnal J V (2007): Automatic segmentation and reconstruction of the cortex from neonatal MRI. Neuroimage 38:461–77. http://www.ncbi.nlm.nih.gov/pubmed/17888685.

Yezzi A (1998): Modified curvature motion for image smoothing and enhancement. IEEE Trans Image Process 7:345–352.

Yin R, Reddihough D, Ditchfield M, Collins K (2000): Magnetic resonance imaging findings in cerebral palsy. J Paediatr Child Health 36:139–144. http://onlinelibrary.wiley.com/doi/10.1046/j.1440-1754.2000.00484.x/abstract.

Yokochi K, Aiba K, Horie M, Inukai K, Fujimoto S, Kodama M, Kodama K (2008): Magnetic Resonance Imaging Children with Spastic Diplegia: Correlation with the Severity of their Motor and Mental Abnormality. Dev Med Child Neurol 33:18–25. http://doi.wiley.com/10.1111/j.1469-8749.1991.tb14781.x.

Yoshida S, Faria A V., Oishi K, Kanda T, Yamori Y, Yoshida N, Hirota H, Iwami M, Okano S, Hsu J, Li X, Jiang H, Li Y, Hayakawa K, Mori S (2013): Anatomical characterization of athetotic and spastic cerebral palsy using an atlas-based analysis. J Magn Reson Imaging 38:288–298. http://www.pubmedcentral.nih.gov/articlerender.fcgi?artid=3749241&tool=pmcentrez&rendertype=abstract.

Yu P, Grant PE, Qi Y, Han X, Ségonne F, Pienaar R, Busa E, Pacheco J, Makris N, Buckner RL, Golland P, Fischl B (2007): Cortical surface shape analysis based on spherical wavelets. IEEE Trans Med Imaging 26:582–97. http://www.ncbi.nlm.nih.gov/pubmed/17427744.

Zacharaki EI, Bezerianos A (2012): Abnormality Segmentation in Brain Images Via Distributed

Estimation. IEEE Trans Inf Technol Biomed 16:330–338. http://ieeexplore.ieee.org/ielx5/4233/6193253/06096414.pdf?tp=&arnumber=6096414&isnumber=6193253.

Zacharaki EI, Hogea CS, Shen D, Biros G, Davatzikos C (2009): Non-diffeomorphic registration of brain tumor images by simulating tissue loss and tumor growth. Neuroimage 46:762–774. http://www.sciencedirect.com/science/article/pii/S1053811909000755.

Zatorre RJ, Fields RD, Johansen-Berg H (2012): Plasticity in gray and white: neuroimaging changes in brain structure during learning. Nat Neurosci 15:528–36. http://www.nature.com/neuro/journal/v15/n4/pdf/nn.3045.pdf.

Zeng X, Staib LH, Schultz RT, Duncan JS (1999): Segmentation and measurement of the cortex from 3-D MR images using coupled-surfaces propagation. IEEE Trans Med Imaging 18:927–37. http://www.ncbi.nlm.nih.gov/pubmed/10628952.

Zhang Y, Brady M, Smith S (2001): Segmentation of brain MR images through a hidden Markov random field model and the expectation-maximization algorithm. IEEE Trans Med Imaging 20:45–57. http://www.ncbi.nlm.nih.gov/pubmed/11293691.

Zhang Y, Inder TE, Neil JJ, Dierker DL, Alexopoulos D, Anderson PJ, Van Essen DC (2015): Cortical structural abnormalities in very preterm children at 7 years of age. Neuroimage 109:469–79. http://www.sciencedirect.com/science/article/pii/S1053811915000087.

Zijdenbos AP, Forghani R, Evans AC (2002): Automatic “pipeline” analysis of 3-D MRI data for clinical trials: application to multiple sclerosis. IEEE Trans Med Imaging 21:1280–91. http://www.ncbi.nlm.nih.gov/pubmed/12585710.

Zou H, Hastie T (2005): Regularization and variable selection via the elastic net. J R Stat Soc Ser B (Statistical Methodol 67:301–320. http://doi.wiley.com/10.1111/j.1467-9868.2005.00503.x.

Appendices

A. Supplementary Material

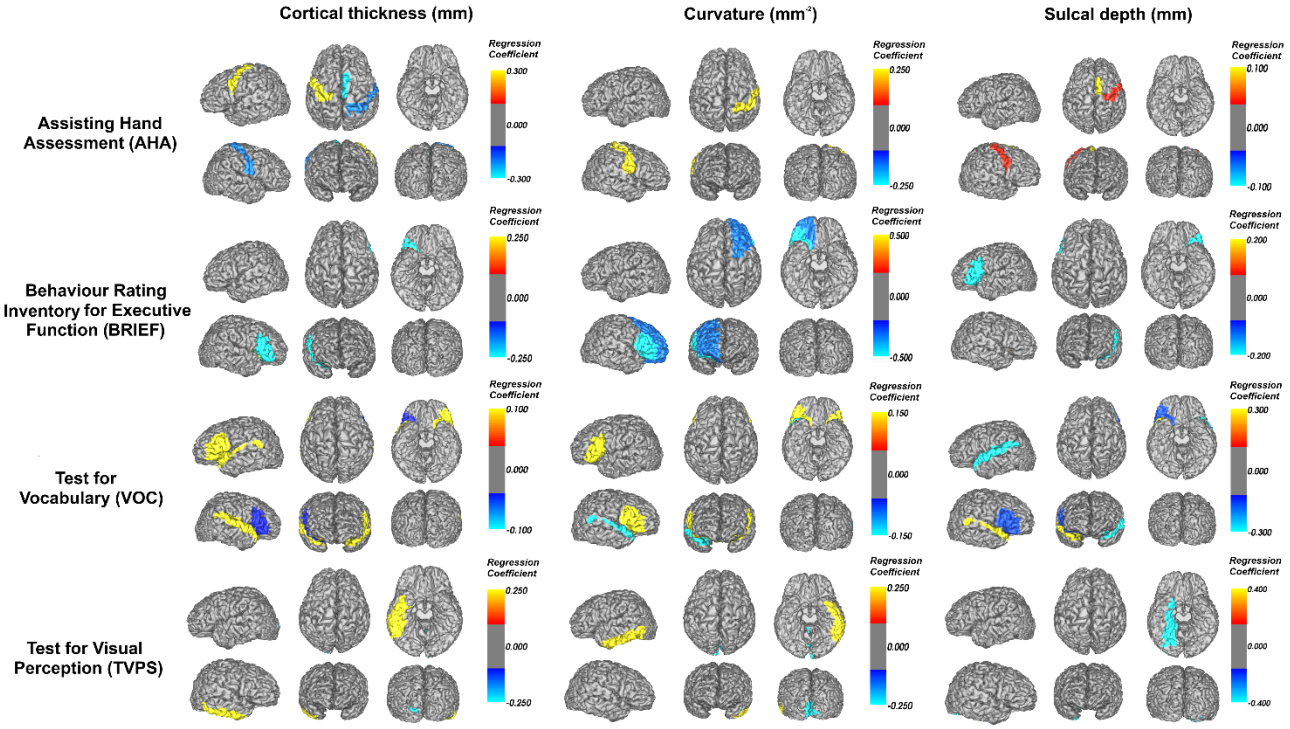

Supplementary Figure A.1 An illustration of the regression coefficients obtained using the methodology in Chapter 6, on the cortical regions retained after data-driven variable selection, for only those children with left side hemiplegia. Coloured regions can be interpreted as either an increase (if red to yellow) or decrease (if blue) in cortical z-score (relative to healthy) is associated with an improvement in the clinical score. Model results are displayed for each of the three cortical measures and four clinical scores. Patient age and gender were excluded.

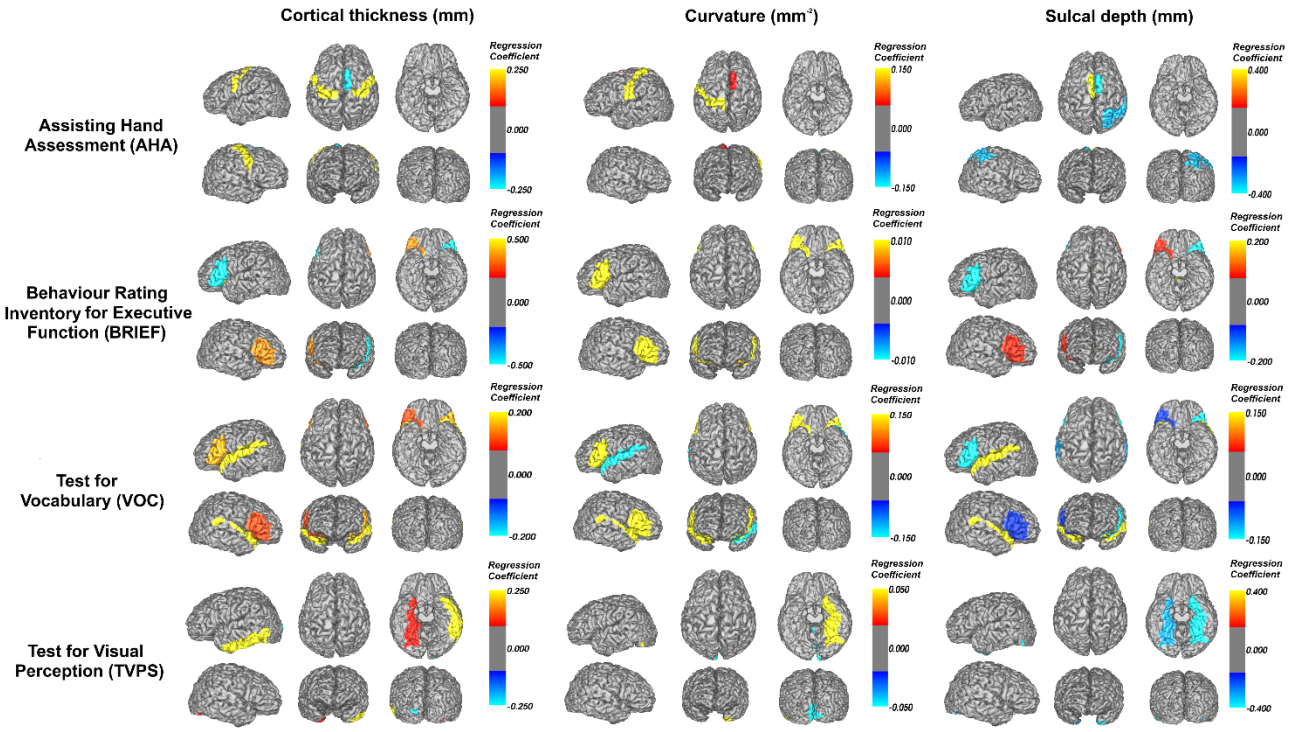

Supplementary Figure A.2 An illustration of the regression coefficients obtained using the methodology in Chapter 6, on the cortical regions retained after data-driven variable selection, for only those children with right side hemiplegia. Coloured regions can be interpreted as either an increase (if red to yellow) or decrease (if blue) in cortical z-score (relative to healthy) is associated with an improvement in the clinical score. Model results are displayed for each of the three cortical measures and four clinical scores. Patient age and gender were excluded.

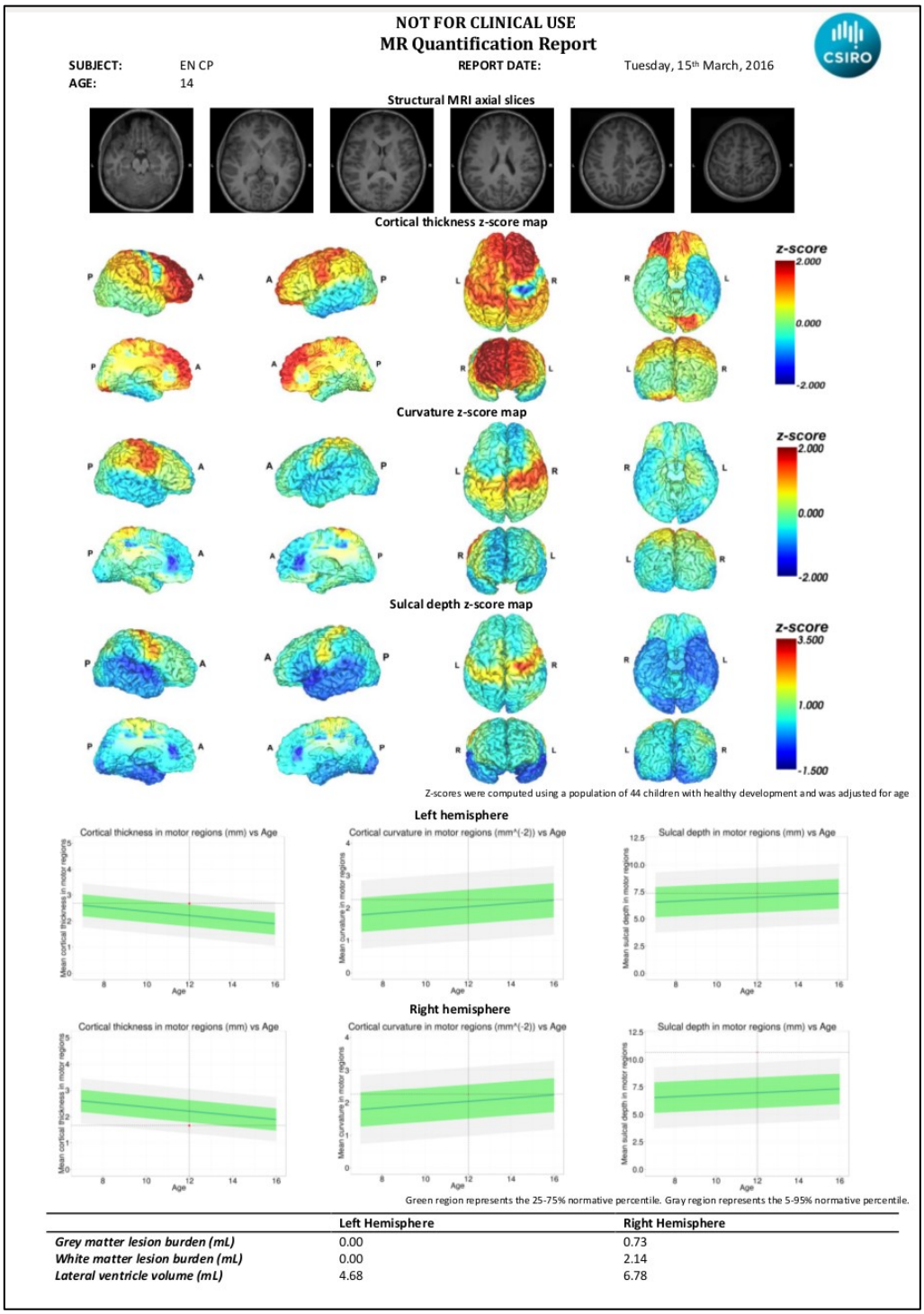

Supplementary Figure A.3 An example MR Quantification Report. Using the techniques developed throughout this thesis, this report provides patient name and age, six axial slices of the structural MRI, cortical z-scores of each cortical measure (relative to healthy cortical measures), and the cortical measures in the motor regions of the left and right hemisphere, plotted against the normative percentiles as a function of age. Additionally, WM and GM lesion burden, and lateral ventricle volume, is provided for both hemispheres.